August, 1978
Report No. Env. E. 59-78-2

Mathematical Model of the Fluidized Bed Biofilm Reactor

Leo T. Mulcahy
Enrique J. La Motta

Division of Water Pollution Control
Massachusetts Water Resources Commission
Contract Number MDWPC 76-10(1)

ENVIRONMENTAL ENGINEERING PROGRAM
DEPARTMENT OF CIVIL ENGINEERING
UNIVERSITY OF MASSACHUSETTS
AMHERST, MASSACHUSETTS 01003

MATHEMATICAL MODEL

OF THE

FLUIDIZED BED BIOFILM REACTOR

By

Leo T. Mulcahy
Research Assistant

Enrique J. La Motta
Assistant Professor of Civil Engineering

Division of Water Pollution Control
Massachusetts Water Resources Commission

Contract Number MDWPC 76-10(1)

Environmental Engineering Program
Department of Civil Engineering
University of Massachusetts
Amherst, Massachusetts 01003

August, 1978

ACKNOWLEDGEMENTS

This report is a reproduction of Dr. Leo T. Mulcahy's PhD dissertation, which was directed by Dr. Enrique J. La Motta, Chairman of the Dissertation Committee. The other members of this committee were Dr. E. E. Lindsey (Chemical Engineering and Civil Engineering Departments) and Dr. R. L. Laurence (Chemical Engineering Department).

This research was performed in part with support from the Department of Civil Engineering, which awarded teaching assistantships and associateships to L. T. Mulcahy, and in part with support from the Massachusetts Division of Water Pollution Control, Research and Demonstration Project No. 76-10(1).

ENGINEERING RELEVANCE

Although the fluidized bed biofilm reactor (FBBR) has been extensively used in fermentation engineering for several years, its application to wastewater treatment is recent, and it is still in the experimental stage. The potential offered by this novel technique is great: Pollutant removal can be achieved with high efficiency using hydraulic detention times which are a fraction of those commonly used in conventional units. This is obviously reflected on significant savings in initial plant costs, and on exceptional flexibility in plant expansions.

A rational design of the FBBR requires a thorough understanding of the phenomena taking place in the unit. Although there is abundant literature describing the behavior of gas-solid fluidized beds, liquid-solid systems have not been studied in such detail. Thus, there is a paucity of information regarding process behavior and process design equations.

Modeling the FBBR must include a mathematical description of the physical behavior of the unit, a model of the heterogeneous kinetics of the reaction, and a mathematical model linking both physical and biochemical phenomena. The study described in this report is a first attempt to tackle this complex problem. As such, it must include simplifications, such as using uniform particle size and constant pollutant loading, among others.

Once this first attempt is shown to successfully describe the process, the simplifications mentioned above will have to be eliminated

to obtain a more complex model, which will describe the performance of full scale units. It is hoped that the simplified model presented herein will provide a good basis for other researchers and engineers to attempt the more complex model of the FBBR.

Enrique J. La Motta, PhD
Assistant Professor of
Civil Engineering

ABSTRACT

Mathematical Model of the Fluidized Bed Biofilm Reactor

(June 1978)

Leo Thomas Mulcahy, B.E., Manhattan College

M.S., Ph.D., University of Massachusetts, Amherst

Directed by: Dr. Enrique LaMotta

The fluidized bed biofilm reactor is a novel biological wastewater treatment process. The use of small, fluidized particles in the reactor affords growth support surface an order of magnitude greater than conventional biofilms systems, while avoiding clogging problems which would be encountered under fixed bed operation. This allows retention of high biomass concentration within the reactor. This high biomass concentration, in turn, translates to substrate conversion efficiencies an order of magnitude greater than possible in conventional biological reactors.

The primary objective of this research has been the development of a mathematical model of the fluidized bed biofilm reactor. The mathematical model has two major subdivisions. The first predicts biomass holdup and biofilm thickness within the reactor using drag

coefficient and bed expansion correlations developed as part of this research. The second predicts mass transport-affected substrate conversion by biofilm covering individual support particles. The intrinsic kinetic coefficients and effective diffusivity for nitrate limited biofilm denitrification, used as input to this portion of the model, were determined in an independent study using a rotating disk biofilm reactor.

Biomass holdup, biofilm thickness, and nitrate profiles observed in a laboratory fluidized bed biofilm reactor were compared with simulated results obtained using the mathematical model. Good agreement between observed and simulated results was obtained, with closest agreement obtained for biofilm thicknesses under 300 microns.

It was found that the most significant parameter affecting substrate conversion efficiency in a FBBR is biofilm thickness. It was further determined that biofilm thickness, and thus FBBR performance, can be regulated through specification of five design parameters:

1) Expanded bed height, H_B;
2) Reactor area perpendicular to flow, A;
3) Support media density, ρ_m;
4) Support media diameter, d_m;
5) Total volume of support media in the reactor, V_m.

The mathematical model developed as part of this research furnishes a rational basis for selection of design parameters such that FBBR performance is optimized.

A chapter on engineering applications of the mathematical model has been included in the dissertation. This chapter provides background for the selection of an optimum biofilm thickness at which to operate a fluidized bed biofilm reactor. Figures are presented which allow graphical determination of FBBR design parameters such that a desired operating biofilm thickness is obtained. These figures are also used to assess the effect of changes in inflow rate on FBBR bed expansion. This information provides a rational basis for the determination of FBBR flow equalization requirements. In addition, reactor freeboard requirements may be assessed, graphically, using these figures.

TABLE OF CONTENTS

Table of Contents Continued...

Table of Contents Continued...

LIST OF TABLES

LIST OF FIGURES

List of Figures Continued...

List of Figures Continued...

List of Figures Continued...

NOMENCLATURE

A	=	reactor area perpendicular to flow
A_T	=	disk biofilm total surface area
B	=	dimensionless substrate concentration = $S_b/S_b\|_{Z=0}$
Bi	=	modified Biot number = $k_c\delta/D_{SB}$
Bo	=	Bodenstein number = $D_Z/H_B U$
c	=	tracer concentration
c_o	=	tracer concentration at reactor inlet
C	=	biofilm dimensionless substrate concentration = S/S_b
C_D	=	drag coefficient
C_t	=	reactor exit concentration
C_v	=	solids volume fraction
d_1, d_2	=	diameters defined in Eq. 3.41
d_a, d_b	=	diameters defined in Eq. 3.36
d_m	=	support medium diameter
d_p	=	bioparticle diameter
D	=	column diameter
D_{SB}	=	diffusivity of species S through biofilm B
D_{SL}	=	diffusivity of species S through liquid L
D_Z	=	axial dispersion coefficient
E_t	=	reactor exit age distribution
$f(\varepsilon)$	=	correction factor = F_D/F_{DI}
F_B	=	buoyancy force

F_D = drag force on a particle in a swarm

F_{DI} = drag force on an isolated particle

F_G = gravity force

g = gravity acceleration constant

$g(\varepsilon)$ = porosity correction factor

Ga = Galileo number = $d_P^3 \ (\rho_S - \rho_L) \ \rho_L \ g \ / \mu^2$

H_B = expanded bed height

k = maximum substrate reaction rate

k_c = mass transfer coefficient

$\hat{k}$ = zero order reaction rate

k' = k/K_S

K = coefficient in Eq. 3.22

K_1, K_2 = coefficients in Eq. 3.23

K_F = shape factor = $\pi/6 \ (d_a/d_b)^3$

K_S = Michaelis-Menten constant

K' = volume of solids plus immobilized fluid per unit solids volume

L = reactor length

n = bed expansion index

n_a = apparent bed expansion index

n_e = effective bed expansion index

N = number of tanks-in-series

N_Z = dispersive flux in the Z direction

N' = diffusional flux defined in Eq. 3.43

Pe = Peclet number = $d_p U_R / D_{SL}$

Pe_A = axial Peclet number = $d_p U / D_Z$

Q = volumetric flowrate

r = bioparticle radial coordinate

Re = Reynolds number = $d_p U \rho_L / \mu$

Re_{MF} = minimum fluidization Re = $d_p U_{MF} \rho_L / \mu$

Re_t = terminal Re = $d_p U_t \rho_L / \mu$

R_I = intrinsic reaction rate per unit biofilm volume

R_o = observed reaction rate per unit biofilm volume

R_v = reaction rate per unit reactor volume

$\bar{R}$ = reaction rate defined in Eq. 3.55

S = substrate concentration

Sc = Schmidt number = $\mu / D_{SL} \rho_L$

Sh = Sherwood number = $k_c d_p / D_{SL}$

St = Stanton number = $k_c \varepsilon / U$

S_1, S_2 = surface areas defined in Eq. 3.41

S_b = bulk-liquid substrate concentration

S_f = substrate feed concentration

S_p = projected particle area

S_s = substrate concentration at the liquid-biofilm interface

t = time

T = temperature

U = superficial liquid velocity = Q/A

U_i = velocity defined in Eq. 3.24

U_R = relative particle-liquid velocity

U_t = particle terminal velocity

V_B = total biomass volume in FBBR

V_M = total support media volume in FBBR

V_P = particle volume

V_S = total solids volume in FBBR

W = coefficient in Eq. 3.5

x = dimensionless bioparticle radial coordinate defined for Eq. 4.34

X = volatile solids concentration in FBBR

X_A = effective volatile solids concentration defined in Eq. 6.1

X_c = substrate conversion defined in Eq. 5.9

Y = dimensionless axial coordinate = Z/H_B

Z = axial coordinate

GREEK

γ = K_S/S_b

δ = biofilm thickness

ϵ = FBBR bed porosity

ϵ_a = apparent bed porosity defined in Eq. 3.38

ε_e = effective bed porosity defined in Eq. 3.39

η = effectiveness factor

η_I = intraphase effectiveness factor

η_o = overall effectiveness factor

μ = liquid viscosity

μ_ε = apparent suspension viscosity

ξ = $d_M/2\delta$

ρ_B = biofilm volatile solids density

ρ_{BW} = biofilm wet density

ρ_L = liquid density

ρ_S = particle density

σ^2 = variance of residence time distribution

τ = space time = reactor volume / Q

ϕ^2 = Thiele-type modulus defined for Eq. 4.34

ψ = particle sphericity

Ω = $K_S/S_b|_{Z=0}$

CHAPTER I

INTRODUCTION

A surface in contact with a nutrient medium containing micro-organisms, will eventually become biologically active. That is, the surface will, in time, become covered with biofilm due to the adhesion of micro-organisms from the bulk-fluid. This phenomenon forms the cornerstone of the industrially important processes which utilize biofilms. Examples include the trickling filter wastewater treatment process, the "quick" vinegar process (111), animal tissue culture (111), and bacterial leaching (136).

Growth support media within conventional biofilm reactors are fixed in space either by gravity or by direct mechanical attachment to the reactor shell.

In contrast, the reactor which is the topic of this study retains growth support media in suspension by drag forces exerted by the upward flow of the nutrient medium. Particles within such a reactor are said to be fluidized, and the reactor will be refered to as a fluidized bed biofilm reactor or FBBR. Particles within the FBBR are no longer fixed in space but free to move under the influence of the passing fluid.

The fluidized mode of operation allows use of small support particles while avoiding clogging problems which would be encountered under packed bed operation. The resultant available growth surface

within a FBBR is more than an order of magnitude greater than practical in a fixed bed reactor; this allows retention of high biomass concentrations within the fluidized reactor. Jeris and Owens (62) have reported volatile solids concentrations between 30,000 and 40,000 mg/l for pilot-scale wastewater treatment studies using FBBR's. These high biomass concentrations translate to substrate conversion efficiencies an order of magnitude greater than possible in conventional biological reactors (63).

While the potential of fluidization technology to biological process industries has been clearly demonstrated, application of this technology to full scale use remains in the developmental stage.

Development of the fluidized bed biofilm reactor can be aided by a mathematical model of the process, which incorporates significant features of the system's behavior. This model should be able to assess the combined effects of biochemical rate processes and physical phenomena, such as diffusion, on the performance of the system.

The primary objective of this research is the developemnt of a mathematical model of the fluidized bed biofilm reactor. The model, which will be presented in later sections of this dissertation, has two major subdivisions. The first, based on an analysis of FBBR fluidization mechanics, predicts biomass holdup (i.e. biomass concentration) within the reactor. Specifically, the model estimates

the equilibrium biofilm thickness and volumetric concentration of biologically active particles which corresponds to a given set of operating conditions. The second model subdivision calculates the rate of substrate conversion by individual biologically active particles within a FBBR. Limitations on reaction rate imposed by external and internal (to the biofilm) transport phenomena are included in this analysis.

In order to calculate the transport-affected rate of substrate conversion by a biologically active particle, it is first necessary that the effective diffusivity and the kinetic coefficients intrinsic to the system be specified. As a paucity of such data exists in the literature, it was necessary to determine these intrinsic parameters experimentally. A rotating disk reactor (RDR) was used for this purpose. This reactor configuration was selected because it offers a uniformly accessible reaction surface which allows a clearer differentiation of the major steps involved in substrate conversion by biofilms.

Finally, the reaction used in this study of the fluidized bed biofilm reactor was biological denitrification. This reaction was chosen for several reasons. First, biological denitrification is among the most efficient and economical methods for nitrate removal from wastewaters. Second, there is substantial evidence in the literature that biofilm denitrification is a feasible process (45, 124, 110, 67, 131), and more specifically, that biological denitrification

in fluidized bed biofilm reactors is feasible (62, 63). And third, the required apparatus is relatively simple when compared to that needed for biochemical reactions such as carbonaceous oxidation or nitrification, which require oxygenation.

CHAPTER II

RESEARCH OBJECTIVES

Based on the considerations outlined in the introductory chapter, the research described in this dissertation has the following objectives:

1. To develop a mathematical model which will allow prediction of biomass holdup and biofilm thickness within a fluidized bed biofilm reactor under a given set of operating conditions.
2. To develop a mathematical model for substrate conversion by biofilm which includes consideration of external and internal mass transport resistances.
3. To incorporate the models developed under the first two objectives in an axial dispersion model for flow through a FBBR which can be used to predict substrate conversion within the reactor.
4. To obtain the intrinsic kinetic constants and effective diffusivity for biofilm denitrification using a rotating disk reactor.

CHAPTER III

FLUIDIZED BED BIOFILM REACTOR - BACKGROUND

Weber, Hopkins and Bloom (142) state that "It is recognized generally that biological growths develop on carbon surfaces during treatment of wastewaters." For a fixed bed of activated carbon, this biological growth is considered a nuisance because of clogging and head-loss problems which necessitate frequent backwash. However, Weber, Hopkins and Bloom (142) recognized that for fluidized operation of an activated carbon bed, such biological activity ". . . appears to be a fortuitous circumstance. . .". These researchers go on to comment that, "The biological activity does not appear to hinder the adsorption process in any observable fashion, but it does seem to enhance the overall capacity for removal of organics, thus affording longer periods of effective operation than might be predicted."

Another interesting phenomenon observed by Weber, Hopkins and Bloom (142) was the reduction of nitrate in their carbon columns. Nitrate levels as high as 15 mg/l NO_3^- were reduced to an average of less than 0.5 mg/l during the "adsorption" stage. The authors conclude that, "The observed reduction in nitrate is most likely a result of biological activity in the carbon columns. This conclusion is substantiated at least partially by the fact that very little

nitrate removal occurred in the activated carbon system during the first day or two of operation, during which time biological activity was just beginning within the adsorption systems."

In a continuation of their study of expanded bed carbon adsorption systems, Weber, Hopkins and Bloom (143) examined more closely the development of biological films on the carbon particles. It was noted that biofilm development was accompanied by a relatively uniform increase in the degree of bed expansion. During the first five days of continuous operation, biofilm growth caused expanded bed height to increase from 150 cm to completely fill the 275 cm column.

To determine if biofilm development was related to the sorptive nature of activated carbon, Weber, Hopkins and Bloom (143) conducted parallel experiments using activated carbon in one column and non-sorptive bituminous coal in the other. It was observed that the bed of coal removed little TOC, and that little biological coating of the particles occurred. The authors concluded that their experiments confirmed that biofilm development around individual carbon particles in an expanded bed is related to the sorptive capacity of that carbon.

Beer (13) cited the observations of Weber, Hopkins and Bloom (142) in suggesting a biological fixed-film reactor in which "fluidized granular material - activated carbon, sand, glass beads - be

used as support surface for denitrifying biota." Beer claimed that the advantage of fluidized bed versus fixed bed operation of a biofilm reactor is related to the available support surface for growth in each reactor. Beer postulated that removal efficiency is proportional to available surface and therefore a fluidized biofilm reactor is advantageous because it allows the use of small support particles (high area-to-volume ratio) while avoiding the clogging problems which would be encountered if small particles were used in fixed-bed operation.

Research on denitrification, based on the fluidized bed biofilm reactor proposed by Beer, was initiatiated at Manhattan College under the direction of Dr. John Jeris. In this study both activated carbon and sand were used as support media for the growth of denitrifiers; a synthetic feed solution was used as a nutrient medium (61).

The results of this study were presented at the 44th Annual Conference of the Water Pollution Control Federation, October, 1971. Reporting on their results, Jeris, Beer and Mueller (61) state that they were unable to achieve significant biological growth on the sand particles. No explaination for this lack of growth was offered. Good biological growth and "excellent" nitrate reduction was obtained, however, on fresh activated carbon within two weeks of startup. Startup was achieved by recycling a mixture of raw wastewater and high strength synthetic feed through the carbon bed, at an upflow

velocity of 0.54 cm/sec (8 gpm/ft^2). The effect of temperature and upflow velocity on the rate of denitrification and on the rate of biological growth within fluidized beds of biologically active carbon was also examined. The data presented indicate an Arrhenius-type dependence of denitrification rate on temperature.

In general, increased upflow velocity was accompanied by nitrate removal that decreased on a percent removal basis, but increased on an absolute mass removed basis. This result is characteristic of a reaction rate either intrinsically dependent on substrate concentration or restricted by mass transport limitations. Because of the weak or nonexistant dependence of intrinsic denitrification rate on substrate concentration (137), the latter possibility is the more likely.

The effect of upflow velocity on the rate at which biofilm sloughed from the carbon support particles was also examined by Jeris et al. (61). The authors had hoped to achieve a steady state condition, with biomass growth balanced by biomass attrition through sloughing. However, a three-fold increase in upflow velocity "failed to affect the growth on the media, and the idea of achieving a balance was abandoned."

In their discussion, Jeris et al. (61) note that the detention time of 15 to 20 minutes required for denitrification in a FBBR is significantly less than possible in conventional biological denitrification systems (11).

These authors conclude "...that the fluidized biological bed concept has excellent potential for treatment of nitrified secondary effluents and for water and wastewater containing objectionable concentrations of nitrate or nitrite nitrogen. The fluidized biological bed has demonstrated the capacity to handle extremely high hydraulic and nitrogen loadings with correspondingly low detention times."

Jeris, Beer and Mueller were subsequently granted a patent (55) for the denitrification fluidized bed biofilm reactor.

At the 6th International Conference on Water Pollution Research, June 1972, Weber, Friedman and Bloom (144) presented a paper entitled "Biologically - Extended Physicochemical Treatment". This study, a continuation of the research of Weber, Hopkins and Bloom (142, 143), focused on the effects of biological activity within expanded bed adsorption systems.

Phase 1 of this study compared aerobic and anaerobic biological activity within the expanded bed adsorbers. The aerobic system was found to be capable of higher TOC removal than its anaerobic counterpart. In addition, the anaerobic adsorber effluent was reported to have had a pronounced H_2S odor while aerobic operation avoided this problem.

Phase 2 compared aerobic with combined anaerobic-aerobic operation of the expanded carbon beds. Again, higher TOC removals were exhibited by the aerobic system. No mention was made of H_2S evolution in the aerobic-anaerobic system.

Phase 3 of this investigation compared the effect of media sorptive capacity on biological activity within the expanded beds. Activiated carbon was used in one of the systems while a non-activated anthracite coal was used in parallel system. Although there was evidence of biological activity in both systems, higher TOC removals were observed in the bed containing activated carbon. The authors state that, "This demonstrates that the adsorber behavior is due both to the adsorptive nature of the activated carbon and to the bacterial action within the adsorbers. Presumably, the better sorbent adsorbs more organic substrate and therefore presents a more favorable environment for effective bacterial growth". They go on to conclude that, "the principal separations process operative in these systems is adsorption from solution onto the surfaces of the activated carbon." (144)

Encouraged by the results obtained by Jeris, Beer and Mueller (61), Jeris and Owens (62) conducted a pilot-scale investigation of biological denitrification using a fluidized bed biofilm reactor. Silica sand (diameter = 0.6 mm) was used as the fluidized support media for biological growth. A plexiglass column (0.46 x 4.72 m) was used as the experimental reactor. Expanded bed height was controlled by a rotary mixer at the top of the column. An open loop recycle system (1 part nitrified secondary effluent: 2 parts recycle) with an upflow velocity of 1.15 cm/sec was used to seed the sand particles during startup.

After the sand particles became seeded, recycle was discontinued and upflow velocity was adjusted to approximately 1.0 cm/sec. Inflow nitrate concentration was approximately 22 mg/l NO_3^- - N. Although the methanol: nitrate - N weight ratio for this study averaged 4.2:1, it was found that methanol to NO_3^- - N weight ratios in excess of 3:1 had no effect on nitrate removal efficiency. Under the described conditions, nitrate removals in excess of 99 percent were consistently achieved in the pilot-scale FBBR. The effect of high inflow rate on nitrate conversion was examined by operation of the FBBR at an upflow velocity of 1.63 cm/sec, corresponding to the maximum output of the feed pump. Again nitrate removals exceeded 99 percent. The authors note that because the pump was not capable of providing a greater flow, the limiting hydraulic load to the column was not reached.

The influence of high nitrate concentration on FBBR performance was also examined as part of this study. For a period of one week, NO_3^- - N concentration was increased from 20 mg/l to a maximum loading of 100 mg/l. Although the system was limited by methanol on the days of the highest influent nitrate concentrations, the authors concluded that the fluidized bed was capable of greater than 95 percent nitrate reduction even at nitrate loadings of 100 mg/l.

The effects of a prolonged shutdown of the system on process performance were also investigated. The feed pump to the FBBR was

restarted after a 17 hour shutdown and the system's response monitored. Although some biomass was sloughed from the support media by turbulence associated with restart (expanded bed height 330 cm versus 355 cm before shutdown) the shutdown had no apparent detrimental effect on nitrate removal efficiency.

Finally, the effects of diurnal flow variations were examined by increasing upflow velocity in the morning from 0.8 to 1.6 cm/sec and reducing it back to 0.8 cm/sec in the evening. Nitrate removals were consistantly found to be in excess of 99 percent during these variations.

In concluding, the authors state that the pilot-scale FBBR "consistantly produced greater than 99 percent removal of the influent nitrogen in less than 6.5 min (empty bed detention time) at a flux *rate of 15 gpm/ft^2 (1.0 cm/sec)*". *They further note* that "The operational routine was simple and trouble free.." (62).

The success of the FBBR for denitrification led Jeris and coworkers to apply this technology to aerobic wastewater treatment (63).

Pilot-scale aerobic fluidized bed reactors capable of either carbonaceous oxidation or nitrification were fabricated. The columnar reactors measured 0.6 x 4.6 m. Sand was used as the support media for biological growth. Excess growth was pumped from the reactor to a Sweco vibrating screen unit. This device separated the excess growth from the support media with the latter being returned to the reactor. Wastewater was oxygenated in an "aeration cone"

(see Reference 125)prior to entering the FBBR.

In studying carbonaceous oxidation, the authors found that removal rate was limited by an ability to transfer adequate amounts of oxygen into the primary effluent feed stream. Recycle of flow through the "aeration cone" was used to get more oxygen into the system. It was found that a recycle ratio of 1.5 (recycle flow / primary effluent flow) was adequate to obtain an effluent which meets secondary treatment requirements. It was noted that recycle could be reduced or eliminated and treatment time reduced, if either automatic controls were obtained to adjust the rate of oxygen gas feed throughout the day or an oxygen transfer system was devised to allow more oxygen gas to be dissolved in the influent wastewater.

In summarizing their experience with carbonaceous oxidation in a fluidized bed reactor, Jeris et al. (63) report an average reduction in BOD_5 of 84 percent across the reactor in an empty bed detention time of 16 min with a recycle ratio of 2.2:1. The average volatile solids concentration within the FBBR during this period was 14,200 mg/l.

Oxygen limitations were also encountered in the nitrification FBBR (63). Again, recycle was used to minimize this limitation. An additional limitation was imposed by insufficient alkalinity present in the secondary effluent. This problem was met by the addition of alkalinity to the reactor feed stream. In summary, ammonia - N conversions of 99 percent were obtained by the nitrification FBBR

in an empty bed detention time of 10.6 minutes with recycle at a ratio of 2.3:1. The volatile solids concentration in the nitrification FBBR averaged about 8500 mg/l.

Jeris was granted five additional patents for aerobic wastewater treatment processes using fluidized bed biofilm reactors (56, 57, 58, 59, 60).

The application of FBBR technology to the biochemical process industries has been suggested by Atkinson and Davies (5), who proposed the "completely mixed microbial film fermenter" (CMMFF) as a method of overcoming microbial washout in continuous fermentation.

Starting with the hypothesis that "any surface in contact with a nutrient medium which contains suspended microorganisms will, in time, become active due to the adhesion of microorganisms", Atkinson and Davies suggest the addition of small particles to biological reactors to provide support surfaces for microbial growth. They advance fluidization as a most efficient means of maintaining these support particles in suspension. These authors also postulate that the frequent particle-particle contacts which occur within a CMMFF would cause "the biological film to attain a dynamic steady state between the growth and attrition of the microbial mass." It should be noted here that for the microbial systems examined by Jeris et al. (61, 62, 63), growth consistently exceeded attrition, neces-

sitating a mechanical removal of excess growth.

Atkinson and Davies present a mathematical description of substrate uptake within a CMMFF. A Michaelis-Menten kinetic expression was used. The authors begin by assuming that no substrate or biomass concentration gradients exist within the reactor. They further assume negligible external mass transfer limitations and rectangular biofilm geometry. The mathematical analysis is subdivided according to biofilm thickness and bulk-fluid substrate concentration. For thin biofilms, the authors neglect internal concentration gradients to arrive at a rate equation linearly dependent on film thickness with a Michaelis-Menten dependence on bulk-fluid substrate concentration. For thick biofilms, internal gradients are considered but the Michaelis-Menten intrinsic rate expression is simplified to its zero and first order asymptotes. For large values of bulk-fluid substrate concentration (zero order approximation) a biofilm rate equation with linear dependence on film thickness is obtained (due to complete penetration of the biofilm). For small bulk-fluid substrate concentrations (first order approximation) the resultant rate equation is independent of film thickness but linearly dependent on bulk-fluid substrate concentration.

An investigation of CMMFF operating characteristics is reported by Atkinson and Knights (7). It is noted that any fermenter applicable to large scale processing must be capable of operating at a steady-state for prolonged periods and that this requires the amount

of biomass in the system to remain constant at a given flow rate. These authors claim that the completely mixed microbial film fermenter (CMMFF) proposed by Atkinson and Davies (5), "has the basic advantage that it contains a constant amount of biomass." This constant biomass is achieved by establishing an equilibrium between growth and mechanical attrition of the surface films. It is suggested that an equilibrium biofilm thickness, corresponding to an equilibrium biomass concentration can be achieved in a CMMFF through particle-particle abrasion. Atkinson and Knights (7) report that they were, in fact, able to achieve equilibrium conditions within their laboratory CMMFF. It should be noted, however, that the microbial system used by these investigators (anaerobic fermentation of Brewer's yeast) is characterized by an extremely low growth rate. The ability of a FBBR (CMMFF) to achieve steady-state would logically be highly dependent on the growth rate of the reactor's microbial population. This is illustrated by the fact that in the microbial systems used by Jeris and coworkers (61, 62, 63), biofilm growth consistantly exceeded sloughing brought about by particle-particle contacts. These investigators were, however, able to operate their systems in dynamic equilibrium by supplementing natural abrasive forces with other growth control devices (rotating mixer, vibrating screen, etc) (63).

In a recent study, Jennings (54) has proposed a mathematical model for biological activity in expanded bed adsorption systems. The model is based on an adaptation to spherical coordinates of

the biofilm model proposed by Williamson and McCarty (152). Substrate utilization by biofilms within the expanded bed is modeled as a process involving external mass transfer coupled with internal mass transfer and simultaneous Michaelis-Menten reaction. Ideal plug flow through the adsorber-reactor was assumed. Analytical solutions are presented for the zero and first order rate asymptotes. Jennings neglects the sorptive properties of the support media by specification of a no-flux boundary condition at the biofilm - support particle interface. A serious shortcoming of the model proposed by Jennings is that no rational attempt is made to link biofilm thickness, bed porosity and flow velocity through the reactor. Instead, a biofilm thickness is arbitrarily chosen and a bed porosity calculated by a solids balance. No consideration is given to the effect of upflow velocity on bed expansion, bed porosity or biofilm thickness.

3.1 Flow Models

Non-ideal flow in fluidized beds.

Ideal conditions within a flow reactor are described by either a plug flow reactor (PFR) model or a continuous flow stirred tank reactor (CFSTR) model.

The PFR is characterized by the fact that flow of fluid through the reactor is orderly with no element of fluid overtaking or mixing with any other element ahead or behind. Levenspiel (83) states that "The necessary and sufficient condition for plug flow is for the residence time in the reactor to be the same for all elements of fluid."

The CFSTR is a reactor in which the contents are well mixed and uniform throughout. Thus, the exit stream from this reactor has the same composition as the fluid within the reactor (83). While all molecules entering a PFR enjoy the same residence time within the reactor, there is an exponential distribution of residence times within a CFSTR (21).

Much attention has been given to the description of non-ideal flow conditions within a reactor. Figure 3.1 compares the responses of an ideal PFR, an ideal CFSTR and a non-ideal reactor to pulse inputs of a conservative material.

The need for an accurate description of non-ideal flow conditions within a reactor is highlighted by Levenspiel (83) who states that "The problems of non-ideal flow are intimately tied to those of scale-up because the question of whether to pilot-plant or not rests in large part on whether we are in control of all the major variables for the process. Often the uncontrolled factor in scale-up is the magnitude of the non-ideality of flow, and unfortunately this

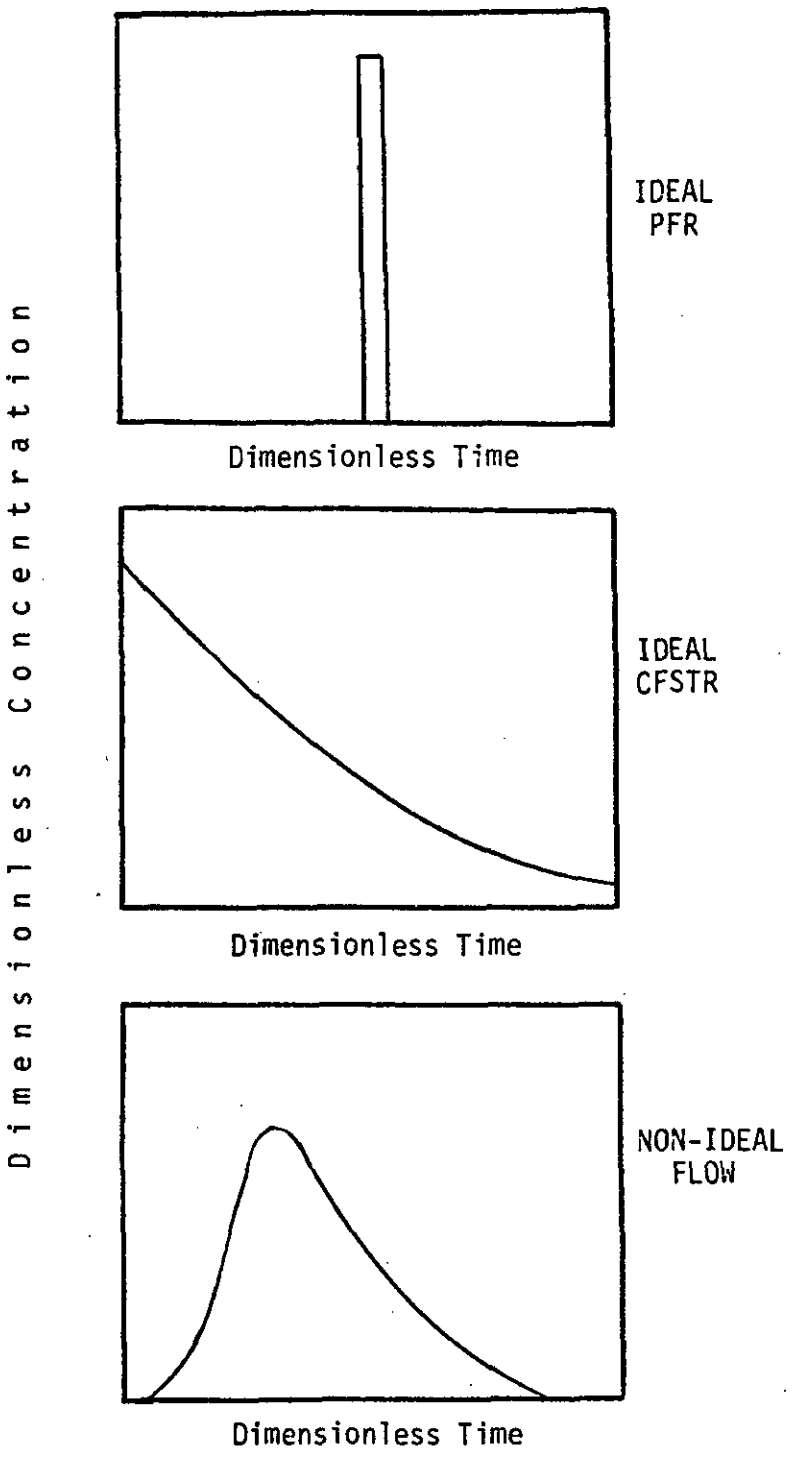

Figure 3.1 Reactor Response to Pulse Inputs of a Conservative Material.

very often differs widely between large and small units. Therefore ignoring this factor may lead to gross errors in design."

Models for non-ideal flow vary from simple one parameter models, such as the tanks-in-series model or the dispersion model, to highly sophisticated multiparameter models, which consider the real reactor to consist of different regions (plug, dispersed plug, mixed, deadwater) interconnected in various ways (bypass, recycle or crossflow).

A common one parameter reactor model used to describe non-ideal flow is the tanks-in-series model. Flow through the real reactor is viewed as flow through a series of equal-size ideal stirred tanks whose total volume sums to the volume of the real reactor. The one parameter of this model is the number of tanks in this chain, N. The magnitude of N indicates the degree of deviation from ideal plug flow conditions. In the extremes, $N = \infty$ corresponds to ideal plug flow conditions while $N = 1$ indicates perfect mixing conditions (i.e. ideal CFSTR) within the real reactor.

The parameter N can be experimentally determined using stimulus-response techniques. A tracer is introduced to a reactor (stimulus) and the time record of tracer leaving the reactor (response) is recorded. The distribution of tracer in the reactor effluent is called the exit age distribution E or the residence time distribution RTD of the fluid. For a pulse input, exit age distribution is given by the following expression:

$$E_t = \frac{C_t}{\sum_{o}^{\infty} C_t \, \Delta t} \qquad 3.1$$

where E_t is the exit age distribution and C_t is the exit concentration at time t. The number of reactors, N, is related to the variance of the distribution as follows (83):

$$N = \tau^2 / \sigma^2 \qquad 3.2$$

in which τ = reactor volume / volumetric flow rate,

σ^2 = variance of a tracer RTD.

An alternate means for describing non-ideal flow is the dispersion model. Deviation from ideal plug flow within a reactor is described by an axial dispersion term, analogous in development and application to Fick's first law. The axial dispersion term is expressed mathematically as follows:

$$N_Z = - D_Z \frac{dS_b}{dZ} \qquad 3.3$$

in which N_Z = dispersion flux of S_b in the Z direction

D_Z = axial dispersion coefficient

Z = axial spatial coordinate.

In this one parameter model, the magnitude of the axial dispersion coefficient indicates the degree of deviation from ideal plug flow. In the extremes, $D_Z = 0$ corresponds to ideal plug flow while $D_Z = \infty$ indicates perfect mixing of the reactor contents.

The experimental procedure used to evaluate the dispersion coefficient is identical to that used to evaluate the tanks-in-series parameter, N. For a closed vessel, Levenspiel (83) relates dispersion coefficient to the variance of the exit age distribution as follows:

$$\frac{\sigma^2}{\tau^2} = 2\,\frac{D_Z}{UL} - 2\,\frac{D_Z}{UL}\,(1 - e^{-UL/D_Z}) \qquad 3.4$$

in which U = average flow velocity

L = reactor length.

Several researchers have examined the axial mixing characteristics of liquid fluidized beds. In their book on reactor flow models, Wen and Fan (146) present a summary of these research efforts. Some of the more significant studies are discussed below.

Using a step function response technique, Cairns and Prausnitz (20) found axial dispersion to be strongly affected by the density and concentration of the particles in the fluidized beds. Kramers et al. (72) also used a step function response technique to study axial mixing in fluidized beds. They suggested that measured axial

dispersion coefficients were composed of one part due to eddies produced by individual particles, and a second part connected with the presence of local voidage fluctuations which could be seen to travel upwards through the beds.

Bruinzeel et al. (17) studied the effect of tube diameter and particle size on axial mixing using a technique similar to that used by Cairns and Prausnitz (20) and Kramers et al. (72). Bruinzeel et al. (17) represented the axial mixing phenomena by a tanks-in-series model. They found little influence of column diameter on the height of the mixing stage and the dispersion coefficient derived from the stage concept.

Chung and Wen (26) used sinusoidal and pulse response techniques to study axial mixing in fixed and fluidized beds. Parameters such as particle size, fluid velocity, voidage and particle density were varied. A generalized correlation based on 482 data points, obtained using both fixed and fluidized beds, was developed and is given here by Equation 3.5:

$$Pe_A = \frac{W}{\varepsilon} (0.20 + 0.011\ Re^{.48}) \qquad 3.5$$

in which $Pe_A = \frac{d_p U}{D_Z}$ = the axial Peclet number

$Re = \frac{d_p U \rho_L}{\mu}$ = the Reynolds number

d_p = particle diameter

ρ_L = fluid density

μ = fluid viscosity

W = 1 for fixed beds

W = Re_{MF} / Re for fluidized beds

Re_{MF} = minimum fluidization Reynolds number

ε = bed porosity = pore fluid volume/bed volume.

The minimum fluidization Reynolds number can be obtained using a correlation advanced by Wen and Yu (147):

$$Re_{MF} = (33.7^2 + 0.0408\ Ga)^{.5} - 33.7 \qquad 3.6$$

in which Ga, the Galileo number, is defined as follows:

$$Ga = \frac{d_p^3\ (\rho_S - \rho_L)\ \rho_L\ g}{\mu^2}$$

where ρ_S = particle density

g = gravity acceleration constant.

The standard deviation between the data and the correlation Equation 3.5 is 46 percent.

Boundary conditions on a fluidized bed reactor.

A recent paper by Choi and Perlmutter (24) scrutinized the inlet boundary condition for dispersive flow models. It was noted that although various assumptions have been used by previous researchers in developing inlet boundary conditions, the consensus (30, 105, 15, 145, 69)is that the proper condition at Z = 0 is:

$$UC^{+} - D_Z \frac{dC^{+}}{dZ} = UC_o \quad \text{at} \quad Z = 0^{+} . \qquad 3.7$$

in which C_o represents the concentration of the feed stream and the + symbol denotes conditions on the reactor-side of the inlet boundary. Choi and Perlmutter (24) proceed to furnish a detailed justification for the validity of Equation 3.7.

Krishnaswamy and Shemilt (73) have demonstrated that the less rigorous inlet boundary condition:

$$C^{+} = C_o \quad \text{at} \quad Z = 0^{+} \qquad 3.8$$

provides close agreement with results obtained using the more complex condition Equation 3.7.

With regard to the upper boundary of a fluidized bed, there is universal agreement that the following condition applies:

$$\frac{dC}{dZ} = 0 \quad \text{at} \quad Z = H_B \qquad 3.9$$

in which H_B = expanded bed height.

3.2 Fluidization Mechanics - Biomass Holdup

For a given set of operating conditions, an analysis of the mechanics of fluidization within a FBBR yields two critical pieces of information, the equilibrium biofilm thickness and bed porosity. This information can, in turn, be used to calculate biomass holdup within the reactor.

The concentration of particles which can exist in a fluidized bed reactor at steady-state is a function of particle-fluid velocity and other physical parameters which characterize the system such as particle surface, size, shape and density and fluid viscosity and density. Many experimental and theoretical studies have attempted to define a quantitative relationship linking these factors. The most common approach is to first define a relative velocity - physical parameter correlation for an isolated particle; then extend this isolated particle treatment to cover multiparticle systems through inclusion of a correction factor dependent on bed voidage. Therefore, the analysis of fluidization mechanics which follows will begin with a treatment of the isolated particle case.

Consider the isolated particle shown in Figure 3.2. Under conditions of dynamic equilibrium, the sum of the drag force on the isolated particle F_{DI} and the buoyancy force F_B must equal the gravitational force F_G. That is:

$$F_{DI} + F_B = F_G . \qquad 3.10$$

For a spherical particle these forces are defined as follows:

$$F_{DI} = \frac{\pi d_p^2 \rho_L U_R^2 C_D}{8} \qquad 3.11$$

$$F_B = \frac{\pi \rho_L g d_p^3}{6} \qquad 3.12$$

$$F_G = \frac{\pi \rho_s g d_p^3}{6} \qquad 3.13$$

in which C_D = drag coefficient

U_R = relative particle - liquid velocity.

The relationship among drag coefficient, relative velocity and a system's physical parameters has been the subject of extensive study. The consensus of these investigations (36) is presented in Figure 3.3. When the physical parameters which describe a system are known, Figure 3.3 can be used to calculate the equilibrium relative velocity (U_R = terminal velocity U_t) of a particle by

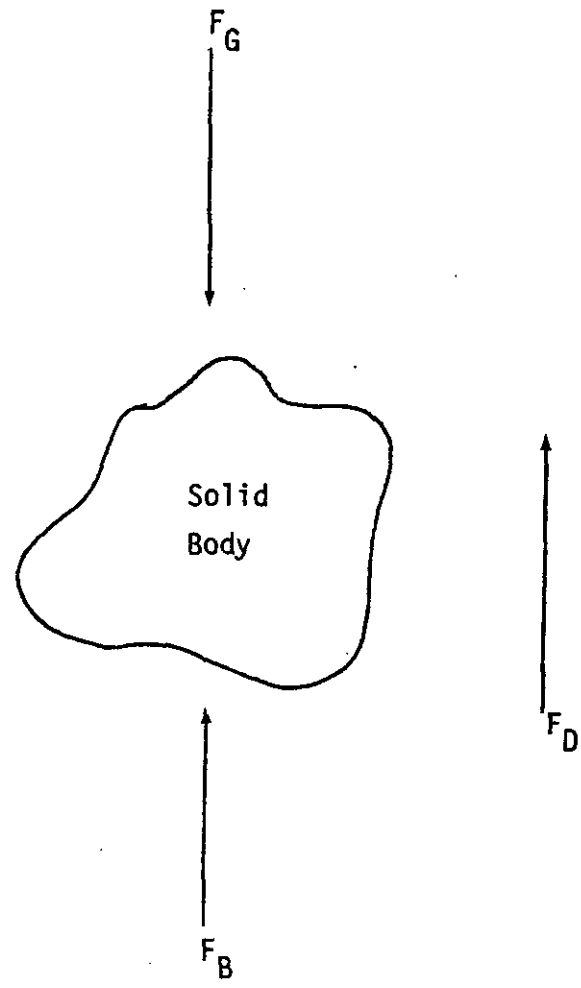

Figure 3.2 Forces Acting on a Fluidized Particle

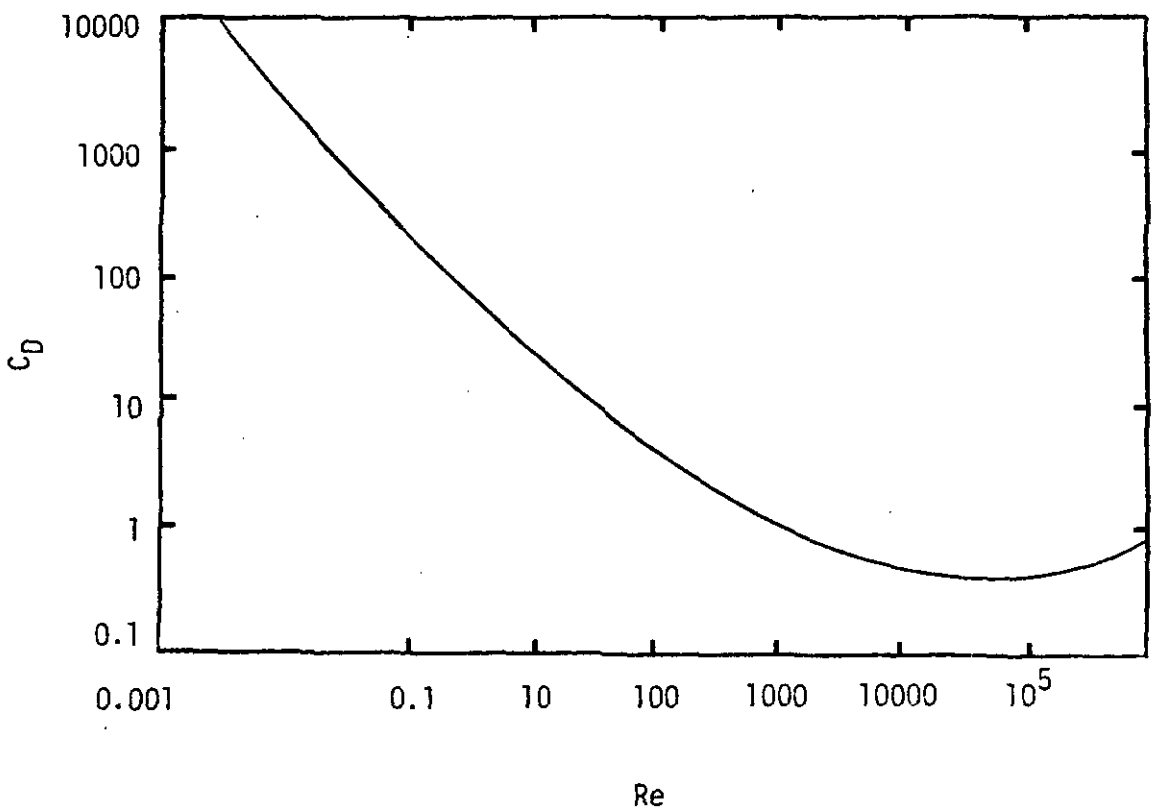

Figure 3.3 Correlation of Drag Coefficient vs. Reynolds Number for a Single Solid Sphere (After Foust (36)).

a trial and error procedure.

To avoid the tedium of a trail and error solution, Zenz (156) has proposed that the following demensionless groups be correlated:

$$(Re/C_D)^{1/3} = U_R \left[4g\mu \left[\frac{(\rho_s - \rho_L)}{3\,\rho_L^2} \right]^{-1/3} \right] \qquad 3.14$$

$$(Re^2\, C_D)^{1/3} = d_p \left[\frac{3\mu^2}{4g\rho_L\,(\rho_s - \rho_L)} \right]^{-1/3} \qquad 3.15$$

Wallis (140) has termed these quantities the dimensionless velocity and the dimensionless particle diameter, respectively. A plot of dimensionless velocity versus dimensionless particle diameter is reproduced in Figure 3.4.

For convenience in numerical calculation and particularly in computer-aided solution, mathematical descriptions of the graphs presented in Figures 3.3 or 3.4 are desirable.

In the Stokes' region of flow (approximately $Re < 1$) inertial forces are negligible. Therefore, an analytical solution of the simplified Navier-Stokes equations is possible and yields the following relationship for drag force on an isolated particle (36):

$$F_{DI} = 3\pi\mu d_p U_R \qquad 3.16$$

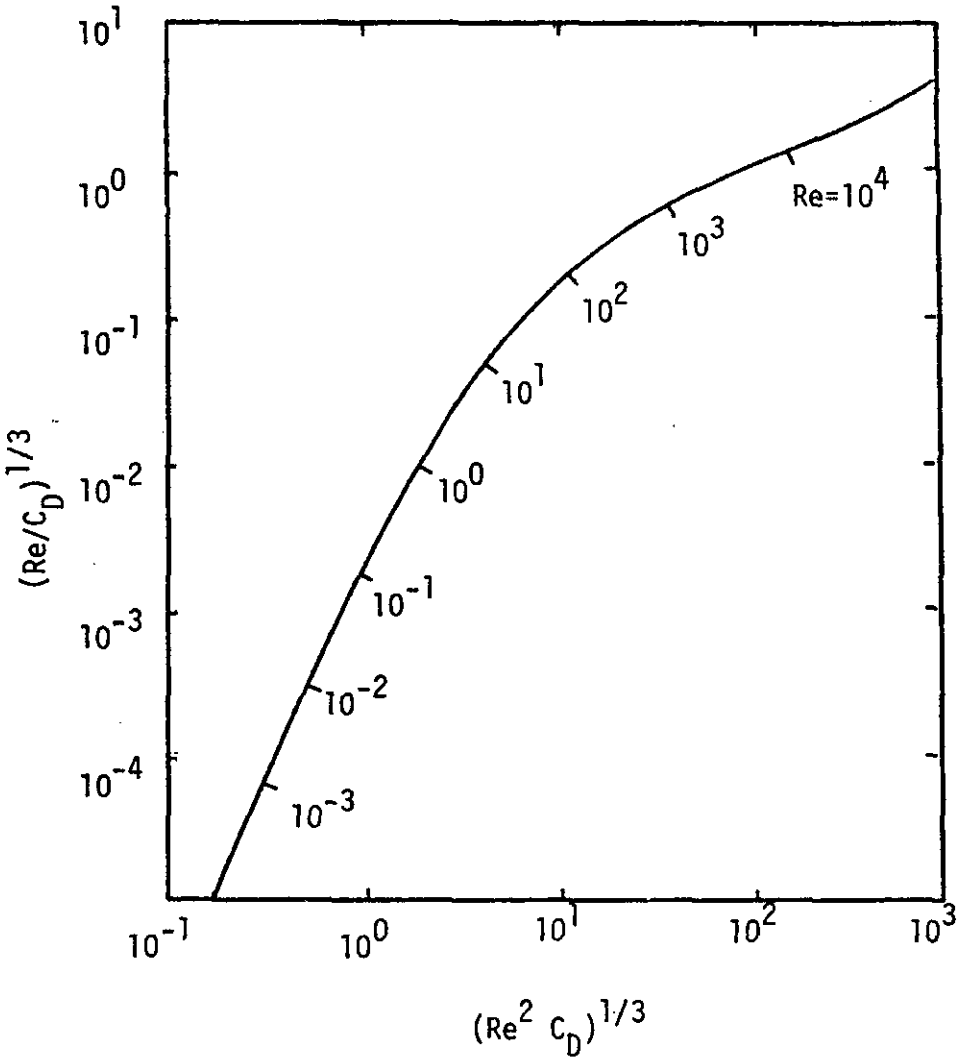

Figure 3.4 $\left(\frac{Re}{C_D}\right)^{1/3}$ vs. $(Re\ C_D)^{1/3}$ for a Single Solid Sphere (After (10)).

Using this result, Equation 3.11 can be solved for drag coefficient. The resultant expression can be written in terms of Reynolds number, as follows:

$$C_D = 24/Re \qquad 3.17$$

In the Newton's law region of flow (approximately 700 < Re < 20,000), viscous forces are negligible. Drag coefficient in this region is approximately constant and given by (36)

$$C_D = 0.44 \pm 0.04 \qquad 3.18$$

Several empirical C_D - Re correlations have been proposed for flow in the intermediate region between the Stokes and Newton regions. The following "very approximate" relationship has been cited by Bird et al. (14):

$$C_D = 18.5 / Re^{.6} . \qquad 3.19$$

For the entire regime of flow conditions, Dallavalle (28) has suggested the following approximate C_D - Re correlation:

$$C_D = \left(0.63 + 4.8 / Re\right)^2 \qquad 3.20$$

For an isolated particle, one of the C_D - Re correlations presented above can be used to develop an explicit expression linking relative velocity (terminal velocity) to the physical parameters describing the system.

For a multiparticle system however, relative velocity-physical parameter expressions must be modified to include the effects of bed porosity. The brief review that follows presents such modifications, which cover the spectrum from theoretical to purely empirical approaches.

Theoretical models of multiparticle systems.

Jackson (53) states that "...the motion of a system of particles suspended in a fluid is completely determined by the initial state of motion, the initial thermal state, the boundary conditions, the Navier-Stokes equations to be satisfied at each point of the fluid, together with the corresponding continuity equations and energy equations, and the Newtonian equations of motion of each particle, together with the heat conduction equations in its interior...When the system contains many particles, as in suspensions of engineering interest, the problem is far too complicated to permit direct solution when stated in these terms."

For practical purposes, therefore, all theoretical models attempting to describe the mechanics of multiparticle systems are based

on solution of the Navier-Stokes equations under particular sets of limiting assumptions. Simplifing assumptions commonly used include:

(i) limitation of analysis to the creeping flow region
(ii) zero slip velocity on only part of the solid surface
(iii) no collisions between particles
(iv) no aggregation of particles
(v) choice of a convenient spatial arrangement of the particles.

The most important theoretical models have been summarized by Barnea and Mizrahi (10). The models together with their limitations are presented in Table 3.1. Note that only the cell models are applicable beyond the range of creeping flow.

Semi-theoretical models of multiparticle systems.

Both theoretical and semi-theoretical models of multiparticle systems are based on solution of the Navier-Stokes equations under simplifing assumptions. Semi-theoretical models differ, however, in that they contain one or more empirical contants. Several of these models (153, 87, 16) are based on the adaption of fixed bed formulae to fluidized beds.

Brinkman (16), in studying pressure drop through packed towers, combined the Navier-Stokes equations for creeping flow with Darcy's

Table 3.1 Mathematical models and techniques used in attempts at the theoretical calculation of drag forces in multiparticle systems (after Barnea and Mizrahi (10)).

Name of the Method	Principle	Limitations
Reflections	Iterative approximation technique for successive correction of the perturbation resulting from solid surfaces	The solution converges only for relatively dilute suspensions
Point force technique	The disturbance produced by a submerged particle is replaced by a point force	Only for extremely dilute suspensions
Cell models	The Navier-Stokes equations are solved within a fluid cell encasing a representative particle. The ratio of the cell/particle volume is related to the suspension concentration	Different solutions may be obtained with different assumptions on cell configuration and boundary conditions
Multipole representation technique	Each object is approximated by a truncated series of multilobular disturbances. It has been claimed that this converges more rapidly than the reflection method, represents the desired boundaries more precisely than the point force technique, and may therefore be applied for more concentrated suspensions	This has been applied only to a limited number of particles

law (itself a solution of a particular case of the Navier-Stokes equations) and obtained the following expression for superficial velocity U:

$$\frac{U}{U_t} = 1 + \left[0.75 \left(5 - 2\varepsilon - 3\varepsilon^2\right)\right]^{1/2} \qquad 3.21$$

in which U_t is the terminal velocity of an isolated sphere. It has been noted that this equation does not provide a good fit to experimental data (10).

Several researchers (82, 92, 127) have suggested the adaption of the Carman-Kozeny equation to fluidized beds. Loeffler and Ruth (87) have modified the Carman equation so that it reduces to Stokes law as porosity approaches unity:

$$U/U_t = \left[\frac{1}{\varepsilon} + \frac{2K(1 - \varepsilon)}{\varepsilon^3}\right]^{-1} \qquad 3.22$$

in which K is an empirical constant.

Other investigators (102, 47, 115, 148, 75) have proposed the use of an apparent suspension viscosity μ_ε in developing correlations to describe the relationship among U, ε and a system's physical parameters. The following general relationship has been suggested (10, 95):

$$\mu_\varepsilon/\mu = \exp\left[\frac{K_1(1-\varepsilon)}{1-K_2(1-\varepsilon)}\right] \qquad 3.23$$

in which K_1 and K_2 are empirical constants.

Empirical models of multiparticle systems.

A number of researchers including Hancock (43), Steinour (127), Lewis et al. (86), Lewis and Bowerman (85) and Richardson and Zaki (114) have suggested the use of a log-log plot of porosity versus superficial velocity. For all but very dilute suspensions, a linear relation has been observed and is described by the following expression (114):

$$\frac{U}{U_i} = \varepsilon^n \qquad 3.24$$

in which $U_i = U_t$ for sedimentation

$\log U_i = \log U_t - d_p/D$ for fluidization

D = column diameter

n = empirical bed expansion index.

By dimensional analysis, Richardson and Zaki (114) have shown that, in general, the expansion index n is a function of an aspect ratio d_p/D and the particle terminal Reynolds number Re_t, defined by:

$$Re_t = \frac{d_p U_t \rho_L}{\mu}$$

However, at extreme values of Re_t ($Re_t < .2$ or $Re_t > 500$), the expansion index becomes independent of terminal Reynolds number.

The following empirical correlations have been developed for uniform spherical particles by Richardson and coworkers (113, 114):

$$n = 4.65 + 20\, d_p/D \qquad Re_t < 0.2 \qquad 3.25$$

$$n = (4.4 + 18\, d_p/D)\, Re_t^{-0.03} \qquad 0.2 < Re_t < 1 \qquad 3.26$$

$$n = (4.4 + 18\, d_p/D)\, Re_t^{-0.1} \qquad 1 < Re_t < 200 \qquad 3.27$$

$$n = 4.4\, Re_t^{-.1} \qquad 200 < Re_t < 500 \qquad 3.28$$

$$n = 2.4 \qquad Re_t > 500 \qquad 3.29$$

For the entire range of particle concentration, Barnea and Mizrahi (10) have assembled data from the literature to show that a hyperbolic function more accurately describes the log U - log ε re-

lationship. This confirms the observations of Happle (44) and Adler and Happle (1) who have suggested that Equation 3.24, underestimates the mutual interference of particles in very dilute systems giving values of superfical velocity which are too high in this region. However, for fluidized bed reactors of practical interest, an adequate description of the bed expansion characteristics is provided by the linear expression, Equation 3.24.

An interesting approach to the mechanistic description of particulate fluidization has been advanced by Wen and Yu (147). They consider the various forces acting on an isolated particle in dynamic equilibrium; then adjust this analysis to describe fluidization through inclusion of a correction factor which accounts for particle interactions within the fluidized bed. Thus, Equation 3.10 can be rewritten:

$$F_D + F_B = F_G \qquad 3.30$$

in which F_D is the drag force on a constituent particle within a fluidized bed.

Wen an Yu (147) relate the multiparticle drag force F_D to the familar isolated particle drag force F_{DI} through use of a correction factor dependent on bed porosity, ε. This correction factor $f(\varepsilon)$ can be written in terms of drag forces as follows:

$$f(\varepsilon) = F_D / F_{DI} . \qquad 3.31$$

Using this expression, the particle force balance, Equation 3.30, may be rewritten as:

$$f(\varepsilon) \cdot F_{DI} + F_B = F_G \,. \qquad 3.32$$

Substituting the individual force equations, Equations 3.11, 3.12 and 3.13, into the force balance equation, Equation 3.32, the following expression for correction factor is obtained:

$$f(\varepsilon) = \frac{4d_p (\rho_s - \rho_L) g}{3 C_D \rho_L U^2} \qquad 3.33$$

Drag coefficient can be linked to superficial velocity using one of the methods discussed earlier for the isolated particle case.

Wen and Yu (147) used Equation 3.33 to calculate $f(\varepsilon)$ for their own experimental data and also for data reported in the literature (86, 114, 150). The resultant $f(\varepsilon)$ values were plotted against the corresponding observed bed porosities and a linear relationship was found to exist. Wen and Yu suggest the following expression to correlate this data:

$$f(\varepsilon) = \varepsilon^{-4.7} \qquad 3.34$$

The data base for this correlation includes spherical particle systems with the following ranges of characteristics:

$$15 < d_p < 6350 \text{ microns}$$

$$1.06 < \rho_s < 11.25 \text{ g/cm}^3$$

$$0.818 < \rho_L < 1.135 \text{ g/cm}^3$$

$$1.0 < \mu < 15.01 \text{ cp}$$

$$0.00244 < d_p/D < 0.1$$

An expression which links bed porosity to superficial velocity and the physical parameters of a system is obtained by combining Equations 3.33 and 3.34.

It should be emphasized that all correlations presented thus far are directly applicable only to systems comprised at particles which are spherical or nearly so. The effect of particle shape on bed expansion will now be considered.

Effect of particle shape on bed expansion characteristics.

The terminal velocity of a particle of any shape is given by the following expression:

$$U_t = \left[\frac{2 V_p g (\rho_s - \rho_L)}{C_D \rho_L S_P} \right]^{1/2} \qquad 3.35$$

in which V_p and S_p are, respectively, the particle volume and projected area normal to flow. Note that C_D must be evaluated at the proper sphericity, ψ. Sphericity is defined as the ratio of the surface area of a sphere of volume equal to that of the particle, to the surface area of the particle (36).

McCabe and Smith (89) state that "A different C_D - Re relationship exists for each shape and orientation. The relationship must in general be determined experimentally...". The effect of sphericity on the empirical C_D - Re relationship is shown in Figure 3.5.

Previous research efforts have demonstrated that the expansion (or sedimentation) behavior of a bed of uniform, non-spherical particles is also described by a linear log U - log ε relationship such as Equation 3.24 (148, 114, 149, 35). These studies note, however,

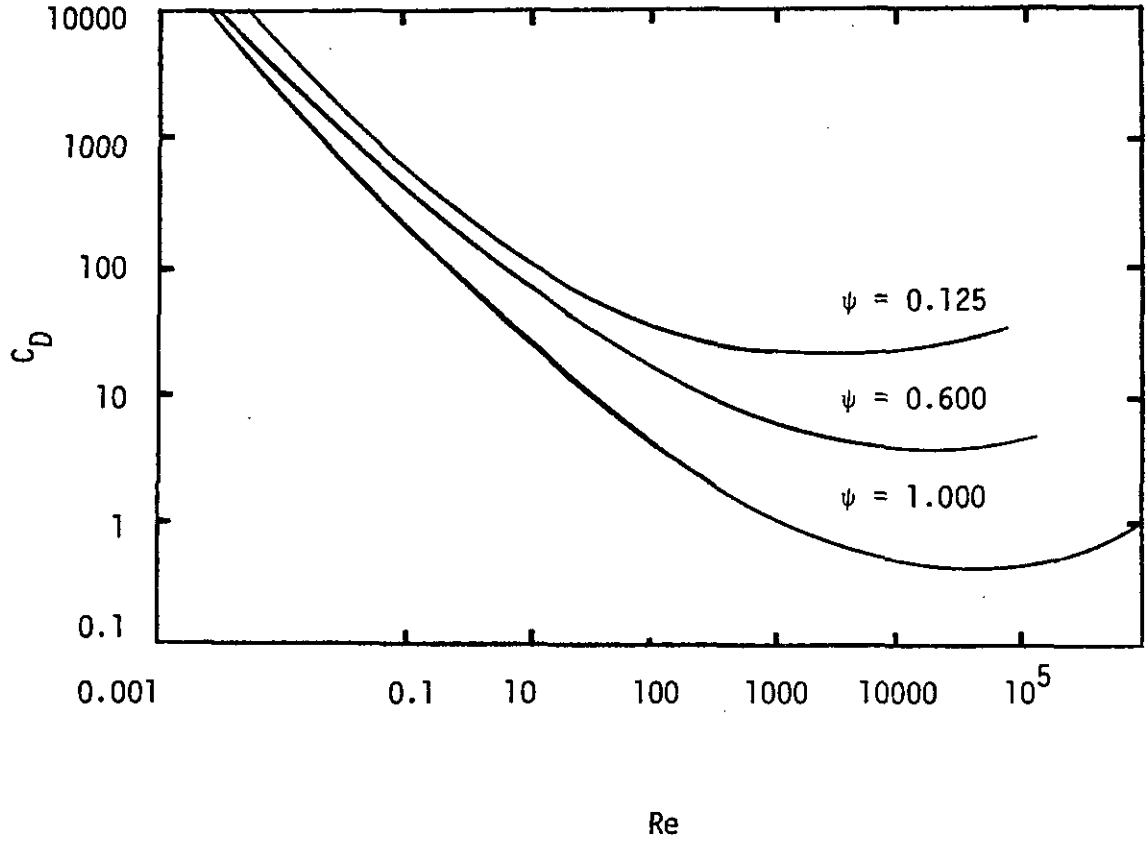

Figure 3.5 Drag Coefficient as a Function of Reynolds Number and Particle Sphericity ψ (After Foust (36)).

that larger values of the expansion index n are associated with non-spherical particles.

For particles with $Re_t > 500$, Richardson and Zaki (114) found that the expansion index can be expressed in terms of a shape factor, K_F, defined as follows:

$$K_F = \frac{\pi}{6}\left(\frac{d_a}{d_b}\right)^3 \qquad 3.36$$

in which d_a = the diameter of a sphere with the same surface area as the particle

d_b = the diameter of a circle of the same area as that projected by the particle when lying in its most stable position.

Richardson and Zaki (114) developed the following correlation for non-spherical particles with $Re_t > 500$:

$$n = 2.7\ K_F^{0.16} \qquad 3.37$$

For smaller, irregular particles, Whitmore (149) has reported n in the range 6.9 to 9.5.

In an interesting study by Edeline, Tesarik and Vostrcil (33)

on the fluidization of chemical and biological flocs, it was found that $n = 10.5$ for the "very irregular particles of aluminum powder" and $n = 12$ to 27 for the biological flocs.

The larger values of n observed for non-spherical particles have been attributed to "immobile fluid trapped with the solids due to particle agglomeration, occlusion in surface irregularities or simply increased volume of boundary layer relative to the particle volume" (35). Fouda and Capes (35) note that as a result of this trapped fluid, the particles have a larger effective diameter but lower density. Thus, a fluidized bed with an apparent porosity based on solids volume, defined as:

$$\varepsilon_a = (1 - C_v) \qquad 3.38$$

actually has an effective porosity with respect to fluidized volume which can be defined as:

$$\varepsilon_e = (1 - K' C_v) \qquad 3.39$$

where C_v is the solid volume fraction and K' is the volume of solids plus immobilized fluid per unit solid volume. Using the linear log u - log ε relationship, Equation 3.24, the apparent expansion index, n_a, can be linked to the effective expansion index, n_e as follows:

$$n_a = n_e \frac{\ln \varepsilon_e}{\ln \varepsilon_a} \qquad 3.40$$

Since non-spherical particles have significant quantities of bound water, $K' > 1$ and $\varepsilon_e < \varepsilon_a$; therefore, $n_a > n_e$. A hypothetical representation of this phenomenon is depicted in Figure 3.6.

Fouda and Capes (35) developed the following empirical correlation for K':

$$K' = \left[(d_2/d_1)\ (S_2/S_1) \right]^{0.284} \qquad 3.41$$

in which d_2 = diameter to encircle an average particle in its most stable position

d_1 = average particle diameter based on sieve analysis

S_2 = surface area of an average particle

S_1 = surface area of a sphere of equivalent volume.

The fluidization behavior of a bed of non-spherical particles can then be described by:

$$\frac{U}{U_t} = (1 - K'C)^n \qquad 3.42$$

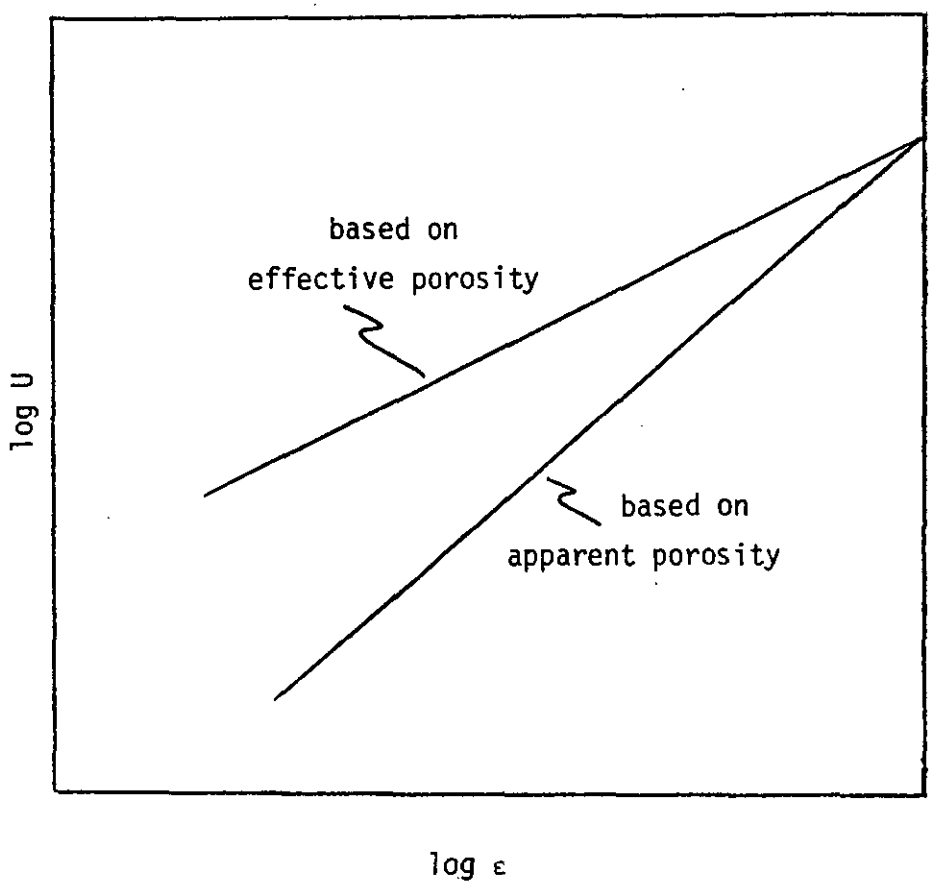

Figure 3.6 Hypothetical expansion curves based on apparent and effective porosities.

in which K' is calculated using Equation 3.41 and n is calculated using apparent particle properties and the correlations developed by Richardson and coworkers (113, 114), namely Equations 3.25 - 3.29.

3.3 Substrate Conversion by Biological Films

Microorganisms which mediate reactions of interest in the biochemical process industries rarely exist as individual cells dispersed in solution (99). Rather these microorganisms agglomerate to form gelatinous aggregates of bacteria and extracellular material. When fixed to solid support surfaces, the aggregates are commonly referred to as biological films or biofilms. Unsupported aggregates are referred to as biological floc particles.

Electron-microphotographs of biofilms taken by Jones et al. (66) show 0.5 to 1.0 micron diameter cells spaced approximately 1 to 4 microns apart within a matrix of extracellular material. This structure is conceptually similar to that of a porous catalyst in that both contain discrete reactive sites and inert diffusion zones.

For reaction to occur, reactant molecules must be transported from bulk-solution to reactive sites within a biofilm. Because more than one phase is involved, such reactions are referred to as heterogeneous.

Atkinson and Daoud (2) and LaMotta (76) have noted the analogy between substrate utilization by biofilms and heterogeneous catalytic

reactions. For heterogeneous catalytic reactions, Smith (123) lists the following sequence of steps for converting reactants to products:

1. Transport of reactants from the bulk-fluid to the fluid-solid interface
2. Intraparticle transport of reactants into the catalyst particle
3. Adsorption of reactants at interior sites of the catalyst particle
4. Chemical reaction of adsorbed reactants to adsorbed products
5. Desorption of adsorbed products
6. Transport of products from interior sites to the outer surface of the catalyst particle
7. Transport of products from the fluid-solid interface into the bulk-fluid stream.

It is common practice to simplify this general sequence so that only the most significant steps are included in subsequent analysis. LaMotta (76) has suggested the following sequence of steps as adequate for biofilm systems:

1. Transport of substrate (reactant) from the bulk-fluid to the fluid-biofilm interface (external mass transfer).

2. Transport of substrate within the biofilm (internal mass transfer)
3. Substrate consumption reaction within the biofilm.

Smith's (123) steps 3 - 5 are lumped together to yield LaMotta's (76) step 2. Smith's steps 6 and 7 are neglected by LaMotta who notes that product concentration will not affect the irreversible reaction rate unless allowed to build to such a level that poisoning occurs. Note that LaMotta's steps 2 and 3 take place simultaneously, while step 1. occurs in series with these steps.

The mass transport resistances, delineated by steps 1 and 2, act to establish concentration gradients within and around biofilms. This situation is depicted in Figure 3.7. For intrinsic reaction rates with a positive dependence on reactant concentration (Michaelis-Menten, first order, etc.), these gradients decrease the observed rate of reaction by lowering local reactant concentration. For intrinsic zero order kinetics, transport phenomena can decrease observed reaction rate by limiting the depth of reactant penetration within the biofilm.

3.3.1 External Mass Transfer

Fluid passing over a solid surface develops a boundary layer which offers resistance to the transport of reactant molecules from

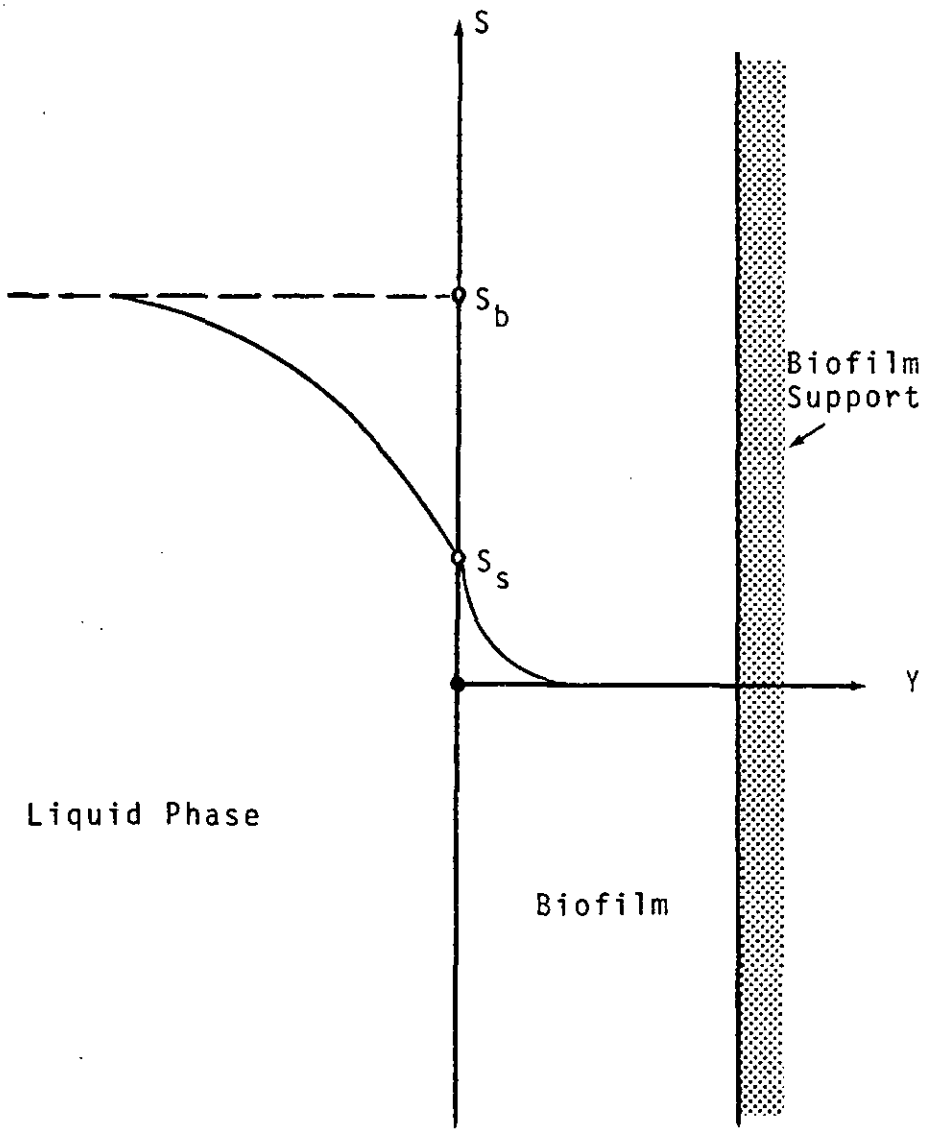

Figure 3.7 Sketch of a Biofilm Showing External and Internal Substrate Concentration Gradients.

the bulk-fluid to active sites on or within the solid.

A boundary layer is characterized by a drastic variation in fluid velocity over a very small distance normal to the solid surface. Satterfield (118) notes that "fluid velocity is zero at the solid surface but approaches the bulk-stream velocity at a plane not far (usually less than a millimeter) from the surface."

In studying transport phenomena associated with biofilm systems, Bungay, Whalen and Sanders (18) were able to experimentally verify the existance of a concentration boundary layer at the biofilm-liquid interface. Dissolved oxygen levels, measured with a microprobe electrode, were observed to decrease sharply across a 100 micron liquid layer at the interface.

Many other researchers in the field of biological wastewater treatment have considered the rate limiting effects of external mass transfer resistance (76, 98, 8, 130, 88, 71, 4, 3, 2, 6, 68, 42, 18).

Because of the complex nature of flow near immersed objects, it has been found necessary to develop semiempirical correlations of data on mass transfer between the phases (118). These data are commonly expressed in terms of an empirical mass transfer coefficient, k_c, which is related to the diffusional flux, N', at the solid surface by the following relationship:

$$N' = k_c (S_b - S_s) . \qquad 3.43$$

The concentrations S_b and S_S are defined in Figure 3.7.

An analytical solution for k_c is possible for the ideal case of a single sphere at rest in an infinite stagnant fluid. The mass transfer coefficient is then given by:

$$k_c = \frac{2D_{SL}}{d_p} \qquad 3.44$$

in which D_{SL} = molecular diffusion coefficient of species S through liquid L.

Any particle-fluid motion will increase k_c (118). For the general case of mass transfer between a moving fluid and a sphere, dimensional analysis leads to the following as a basis for correlation:

$$Sh = f(Re,Sc) \qquad 3.45$$

in which Sherwood number, $Sh = \frac{k_c d_p}{D_{SL}}$

Schmidt number, $Sc = \frac{\mu}{D_{SL}\,\rho_L}$.

For liquid flow past a single sphere, Rowe and Claxton (116) have used data from the literature to develop the following correlation:

$$Sh = 2.0 + 0.76 (Re)^{1/2} (Sc)^{1/3} \qquad 3.46$$

This correlation applies to Reynolds numbers in the range 20 to 2000.

Under extreme flow conditions, liquid-solid mass transfer is subject to analytical solution.

It has been noted (133) that for most systems of practical interest, the characteristic Peclet number ($Pe = d_P U_R / D_{SL}$) of the process is high ($Pe > 1000$). Restricting his analysis to this region, Levich (84) developed a solution for mass transfer to a single sphere falling through an infinite fluid. This solution can be expressed in terms of the Sherwood number as:

$$Sh = 0.997(Pe)^{1/3} . \qquad 3.47$$

For spherical particles in Stokes flow ($Re < 1$), Friedlander (37) developed the following approximate theoretical expression for mass transfer:

$$Sh = 0.991(Pe)^{1/3} \qquad 3.48$$

Tardos et al. (133) derived an expression for high Peclet number mass transfer to a sphere situated in a swarm of like particles. A porosity correction factor $g(\varepsilon)$ was introduced which accounts

for variations in velocity profile caused by the particle swarm. The correction factor is combined with the theoretical solution of Levich, Equation 3.47, to yield the following expression:

$$Sh = g(\varepsilon) \cdot 0.997 \, (\overline{Pe})^{1/3} \qquad 3.49$$

in which Peclet number is redefined in terms of superficial velocity U as:

$$\overline{Pe} = \frac{U \, d_p}{D_{SL}} \, . \qquad 3.50$$

Correlations which are directly applicable to interphase mass transfer in fluidized beds are reviewed by Beek (12). Beek notes that "a chaos of correlations, statements and conclusions is found in the literature due to the fact that an increase in fluidization velocity increases the bed expansion, which in many cases is not measured. The consequence is, that in the proposed correlations, not only the influence of U (superficial velocity) on the fluid to particle mass transfer coefficient k_c is hidden, but also that of ε (bed porosity) on k_c."

Of the correlations discussed by Beek, the one proposed by Snowdon and Turner (126) is of particular interest. This is due to the fact that this correlation is based on data covering a

similar Reynolds number range as that found in the FBBR. Snowdon and Turner state that their expermental data are well correlated by the following:

$$Sh = \frac{0.81}{\varepsilon} Re^{1/2} Sc^{1/3} . \qquad 3.51$$

in which Reynolds number is defined in terms of superficial velocity U as:

$$Re = \frac{U\rho_L d_p}{\mu} .$$

Beek (12) developed a more general correlation of liquid-particle mass transfer within a fluidized bed based on the data of several researchers (126, 107, 112, 92, 25, 38), including Snowdon and Turner. The correlation developed by Beek is as follows:

$$St \cdot Sc^{2/3} = (0.81 \pm 0.05) Re^{-1/2} \qquad 3.54$$

for $5 < Re < 500$

in which Stanton number, $St = k_c \varepsilon / U$

This correlation results in slightly lower values of k_c than does the correlation of Snowdon and Turner (126).

Although the correlation of Beek is founded on a broader data base than that of Snowdon and Turner, the latter will be used in subsequent sections of this dissertation to correlate k_c within a fluidized bed biofilm reactor. This choice is made because of the Reynolds number similarity mentioned earlier.

3.3.2 Internal Mass Transfer - FBBR

Internal mass transfer resistance acts to establish a concentration gradient within a biofilm. Thus, interior portions of the biofilm are exposed to lower substrate concentrations than exist in the bulk-fluid. This often results in observed reaction rates which are significantly lower than would occur if mass transport limitations were absent.

Analysis of this phenomenon is complex because internal mass transfer and reaction occur simultaneously, therefore, neither process can become limiting in the sense that it alone will determine the overall or observed reaction rate (83, 76, 118, 51).

Among the first to report on the rate limiting aspects of internal mass transfer were researchers in the biomedical field. Krough (74) in 1918, Warburg (141) in 1923, Fenn (34) in 1927, Hill (48) in 1929, and Gerard (40) in 1931 all considered the effect of internal diffusion on oxygen utilization by respiring tissue or cells.

This early research is typified by the work of Warburg (141)

Although the correlation of Beek is founded on a broader data base than that of Snowdon and Turner, the latter will be used in subsequent sections of this dissertation to correlate k_c within a fluidized bed biofilm reactor. This choice is made because of the Reynolds number similarity mentioned earlier.

3.3.2 Internal Mass Transfer - FBBR

Internal mass transfer resistance acts to establish a concentration gradient within a biofilm. Thus, interior portions of the biofilm are exposed to lower substrate concentrations than exist in the bulk-fluid. This often results in observed reaction rates which are significantly lower than would occur if mass transport limitations were absent.

Analysis of this phenomenon is complex because internal mass transfer and reaction occur simultaneously, therefore, neither process can become limiting in the sense that it alone will determine the overall or observed reaction rate (83, 76, 118, 51).

Among the first to report on the rate limiting aspects of internal mass transfer were researchers in the biomedical field. Krough (74) in 1918, Warburg (141) in 1923, Fenn (34) in 1927, Hill (48) in 1929, and Gerard (40) in 1931 all considered the effect of internal diffusion on oxygen utilization by respiring tissue or cells.

This early research is typified by the work of Warburg (141)

in which mass transfer, described by Fick's first law, and simultaneous zero order reaction are included in a mathematical description of oxygen utilization within muscle tissue slices. Warburg's analysis allowed calculation of the "Grenzschnittdicke" or limiting slice thickness such that just the center of the tissue slice was anoxic.

The effect of transport phenomena on observed reaction rate was next recognized by researchers in the field of heterogeneous catalysis. Independently, Thiele (134), Damkohler (29) and Zeldovitch (155) each developed quantitative descriptions of the factors that determine a porous catalyst effectiveness. Catalyst effectiveness was quantified by a parameter termed the effectiveness factor, n. Intraphase effectiveness factor can be defined as follows:

$$\eta_I = \left\{ \begin{array}{l} \text{Observed} \\ \text{reaction} \\ \text{rate} \end{array} \right\} \div \left\{ \begin{array}{l} \text{Reaction rate which would occur if the} \\ \text{entire catalyst particle were exposed to} \\ \text{reactant of the same concentration as ex-} \\ \text{ists at the outside surface of the catalyst.} \end{array} \right\}$$

Overall or interphase - intraphase effectiveness factor can be defined as:

$$\eta_o = \left\{\begin{array}{l}\text{Observed} \\ \text{reaction} \\ \text{rate}\end{array}\right\} \div \left\{\begin{array}{l}\text{Reaction rate which would occur if the} \\ \text{entire catalyst particle were exposed to} \\ \text{reactant of the same concentration as ex-} \\ \text{ists in the bulk-liquid.}\end{array}\right\}$$

In the absence of external mass transfer limitation, $\eta_I = \eta_o$.

In the absence of all mass transfer limitations intrinsic kinetics is observed with $\eta_I = \eta_o = 1$.

Significant mass transport limitations are associated with low values of effectiveness factors. Kobayashi and Laidler (70) and Satterfield (118) have suggested that $\eta_I = 0.95$, and $\eta_I = 0.6$ be used as criteria to indicate insignificant and significant internal mass transfer limitations, respectively.

Thiele presented the results of his analysis as plots of effectiveness factor versus a dimensionless quantity, since termed the Thiele modulus. This modulus lumps important system parameters such as reactant concentration driving force, reaction rate constant, effective diffusivity of reactant within the catalyst and catalyst particle size.

Among the first researchers in the wastewater treatment field to consider the effect of transport phenomena on observed substrate utilization rate was Pasveer (104). He postulated that the inverse relationship found to exist between observed rate and floc size was

due to oxygen transport limitations within the floc particles. Pasveer suggested intensification of turbulence within the aeration basin as a means of increasing treatment efficiency through reduction of floc size.

In other research related to biological wastewater treatment, Wuhrmann (154) used the theoretical analysis of Gerard (40) to compute the depth of penetration of oxygen in microbial aggregates. Using an assumed effective diffusivity of 5×10^{-6} cm/sec and a bulk-fluid oxygen concentration of 2 mg/l, Wuhrmann calculated that the center of a spherical floc particle would just be respiring at a critical oxygen tension of 0.1 mg/l when the floc particle diameter reached 500 microns. For fixed film systems with the same bulk-liquid oxygen concentration, Wuhrmann estimated the critical biofilm thickness to be 100 microns.

Mueller (98) examined mass transfer resistance related to the utilization of oxygen by pure culture Zoogloea ramigera floc particles. It was demonstrated that at low dissolved oxygen concentrations, the overall rate of oxygen utilization was significantly limited by internal mass transport resistances. The limiting dissolved oxygen levels for unblended floc particles were found to vary between 0.6 and 2.5 mg/l depending on temperature and floc size. For blended floc samples, the resultant dispersed cells and smaller floc particles exhibited markedly lower limiting dissolved oxygen concentrations of 0.1 to 0.4 mg/l.

Mueller (98) developed an anoxic core model (zero order kinetics) of a floc particle which was represented as a triangular prism. Using this model, oxygen diffusivity within the floc particle was determined to be about 8 percent of the corresponding value in water.

Baillod and Boyle (9) examined the effects of glucose transport within floc particles of Zoogloea ramigera on overall glucose utilization rate. They concluded that glucose diffusion through the floc matrix became rate limiting at low glucose concentrations. A zero order anoxic core model was used to calculate the effective diffusivity of glucose in the zoogloeal floc material. Calculated effective diffusivities ranged from about 7 to 9 percent of the corresponding values for glucose in water.

Sanders (117) observed the effects of biofilm thickness on film growth kinetics. Biofilm was allowed to develop on the inside wall of a continuous flow culture chamber. Mixing of the chamber contents was provided by a magnetic stirrer. A nutrient broth feed solution was used.

Sanders postulated that biofilm organisms exist in either reproductive or retarded stages of growth. He attributed retarded growth to limiting levels of oxygen or nutrients caused by diffusional resistances. The thickness of the "active" reproductive stage is referred to as the limiting film thickness.

Sanders observed that oxygen utilization rates increased with film thickness until the limiting film thickness (21.2 microns) was reached; beyond this point the rate of oxygen utilization remained constant.

Tomlinson and Snaddon (135) examined factors affecting the biological oxidation of sewage using an inclined rotating tube biofilm reactor. It was observed that carbon removals increased with film thickness until depths of approximately 120 microns were obtained. Beyond that thickness, removals remained constant. The anoxic core model developed by Warburg (141) was used to calculate the effective diffusivity of oxygen within the biological film. The value obtained was approximately 67 percent of the corresponding value in water.

Maier (88) used an inclined plane biofilm reactor to examine factors which affect the rate of glucose removal. Uniform biofilms were obtained by containing the films within a screen framework. Film thickness was controlled by scraping such that film thickness corresponded to screen thickness.

Maier observed that biofilm thickness had no effect on glucose removal. He therefore concluded that "the thickness of the slime layer is not an important variable." Baillod and Boyle (9) later pointed out that the film thicknesses used by Maier (480-1400 microns) were too great to allow observation of any change in uptake rate with thickness.

Kornegay and Andrews (71) studied biofilm substrate utilization kinetics using annular reactors. The reactors consisted of enclosed outer vessels which housed rotating drums. External mass transfer resistances were minimized by rotating the drums at 100 rpm. The substrate consisted of glucose and a mineral base. Dissolved oxygen was maintained at levels which exceeded limiting concentrations.

A mathematical model of substrate utilization was proposed based on the hypothesis "that the entire mass of attached microorganisms is not active in the removal of soluble organics" (71). Monod (Michaelis-Menten) kinetics was used to describe the model reaction term. Experimentally, Kornegay and Andrews (71) observed that substrate removal rate increased linearly with film thickness until the "active thickness" (80 microns) was exceeded. Greater film thicknesses resulted in no further increase in the rate of removal. A Lineweaver-Burk plot was used to determine the biological kinetic contants. The effect of internal mass transfer on such a plot was, however, not considered resulting in an unreasonably large Michaelis constant (K_S = 121 mg/l).

Atkinson and Daoud (3, 4) presented a theoretical analysis of substrate utilization by biological films. Their analysis draws on the analogy between biological reaction and heterogeneous catalysis. Specifically, a differential equation was developed which describes internal mass transfer of reactant and simultaneous biochemical reaction. A Michaelis-Menten kinetic expression was used. The re-

sultant differential equation is identical to one developed by Schneider and Mitschka (119) for transport and reaction (Langmuir-Hinshelwood kinetics) within a porous catalyst. Atkinson and Daoud (4) present the numerical solution of Schneider and Mitschka for the common differential equation.

Simplified solutions were also presented for asymptotic forms of the differential equation. For thick films, Atkinson and Daoud's asymptotic solution predicts that substrate uptake will by independent of film thickness. This result agrees with phenomena observed by previous researchers.

Bungay, Whalen and Sanders (18) utilized a microprobe electrode to examine oxygen profiles near the interface and within biological films. When low concentrations of substrate were fed to the biofilm reactor, a flat, high concentration oxygen profile was observed within the biofilm, indicating substrate limited respiration. More concentrated substrate feed solutions caused a significant internal oxygen gradient indicating oxygen limited respiration. The effective diffusivity of oxygen within the biofilm was calculated assuming zero order reaction kinetics. The resultant value was approximately 2 percent of the corresponding value in water.

Hoehn (49) examined the effects of thickness on the activity of bacterial films. A horizontal rotating cylinder was used as the growth support surface. A synthetic feed solution was used. Hoehn's observations agreed with previous researchers in that substrate

utilization rate increased with film thickness until a limiting value (100 microns) was reached. For thicker films a constant substrate utilization rate was observed. Hoehn attributed the leveling off of utilization rate to oxygen limitations within the biofilm imposed by diffusional resistances.

LaMotta (76) evaluated the external and internal diffusional resistances associated with substrate utilization by biological films. An annular reactor, similar to that used by Kornegay and Andrews (71) was used in the experimental portion of this study. The reactors differed, however, in that LaMotta held the inner drum stationary and rotated the outer cylinder. A glucose feed solution was used. Oxygen levels were maintained in excess of limiting concentrations.

LaMotta's experimental results were consistent with previous studies in that substrate removal increased with film thickness until a limiting thickness was reached. Beyond this limiting thickness, removal remained constant. LaMotta demonstrated that the limiting biofilm thickness increased with increased concentration of glucose in the feed stream. A mathematical model was developed which considered internal mass transfer and simultaneous zero order reaction. The average effective diffusivity of glucose within the biofilm was calculated to be approximately 44 percent of the corresponding value in water.

Williamson and McCarty (152) proposed a model of substrate utilization by bacterial films. The model is basically the same as

the model proposed by Atkinson and Daoud (3, 4). Both pairs of researchers describe substrate utilization as a process of molecular diffusion and simultaneous biochemical reaction with Michaelis-Menten (Monod) reaction kinetics.

The model of Williamson and McCarty is for a single rate-limiting species. Criteria are presented which allow a priori determination of whether rate is limited by electron donor or electron acceptor.

Biological rate constants were obtained using a suspended growth reactor. It was assumed that the constants so obtained were unaffected by diffusional limitations. However, recent study by Shieh (121) demonstrated that, in fact, significant diffusional limitations are possible in suspended growth reactors.

In Williamson and McCarty's investigation effective diffusivities within biofilms were obtained using an experimental apparatus designed especially for that purpose. An ersatz biofilm was created by filtering dispersed bacteria onto a support filter. The biofilm was made inactive by restricting a needed reactant. The species under study was allowed to diffuse through the biofilm and its concentration history recorded. This record was then used to calculate an effective diffusivity. The resultant effective diffusivities for ammonia, nitrite, nitrate and oxygen all were between 80 and 100 percent of the corresponding values in water.

Harremoes (44) has reported on the significance of internal mass transfer (pore diffusion) to filter denitrification. He arrives at

conclusions which are similar to those of LaMotta (76) and well known by analogy to heterogeneous catalysis, namely, that zero-order intrinsic kinetics result in zero-order observed kinetics only when reactants fully penetrate a biofilm. When a rectangular biofilm is only partially penetrated, zero-order intrinsic kinetics results in half-order observed kinetics. Harremoes presents concentration profiles for fixed film denitrification systems which substantiate the half-order concept.

3.3.3 Substrate Conversion Reaction

Common rate expressions used to describe substrate conversion by biological systems include Michaelis-Menten (Monod) kinetics, discontinuous linear kinetics and zero-order kinetics. Of these rate expressions, Michaelis-Menten kinetics offers the most general description of substrate conversion. That is, the Michaelis-Menten expression is applicable over the entire range of substrate concentrations.

Several researchers (71, 151, 19, 39, 41, 64, 80, 81, 78) in biological wastewater treatment and related fields have concluded that the consumption of both electron donors and electron acceptors follows Michaelis-Menten kinetics. For suspended growth systems the Michaelis-Menten rate expression can be mathematically formulated as follows:

$$\bar{R} = \frac{kXS}{K_S + S} \qquad 3.55$$

in which $\bar{R}$ = Substrate reaction rate, mol/l.sec

S = substrate concentration, mol/l

X = microbial concentration, mg/l

k = maximum substrate reaction rate, mol/mg·sec

K_S = Michaelis or half-velocity constant, mol/l.

Figure 3.8 is a graphical representation of Equation 3.57 which illustrates the meaning of the parameters k and K_S.

Discontinuous linear kinetics describes the asymptotic regions of the hyperbolic Michaelis-Menten curve. For $S << K_S$ the following expression describes substrate conversion kinetics:

$$\bar{R} = k'SX \qquad 3.56$$

in which $k' = k/K_S$

For $S >> K_S$ substrate conversion is described by the following equation:

$$\bar{R} = kX \qquad 3.57$$

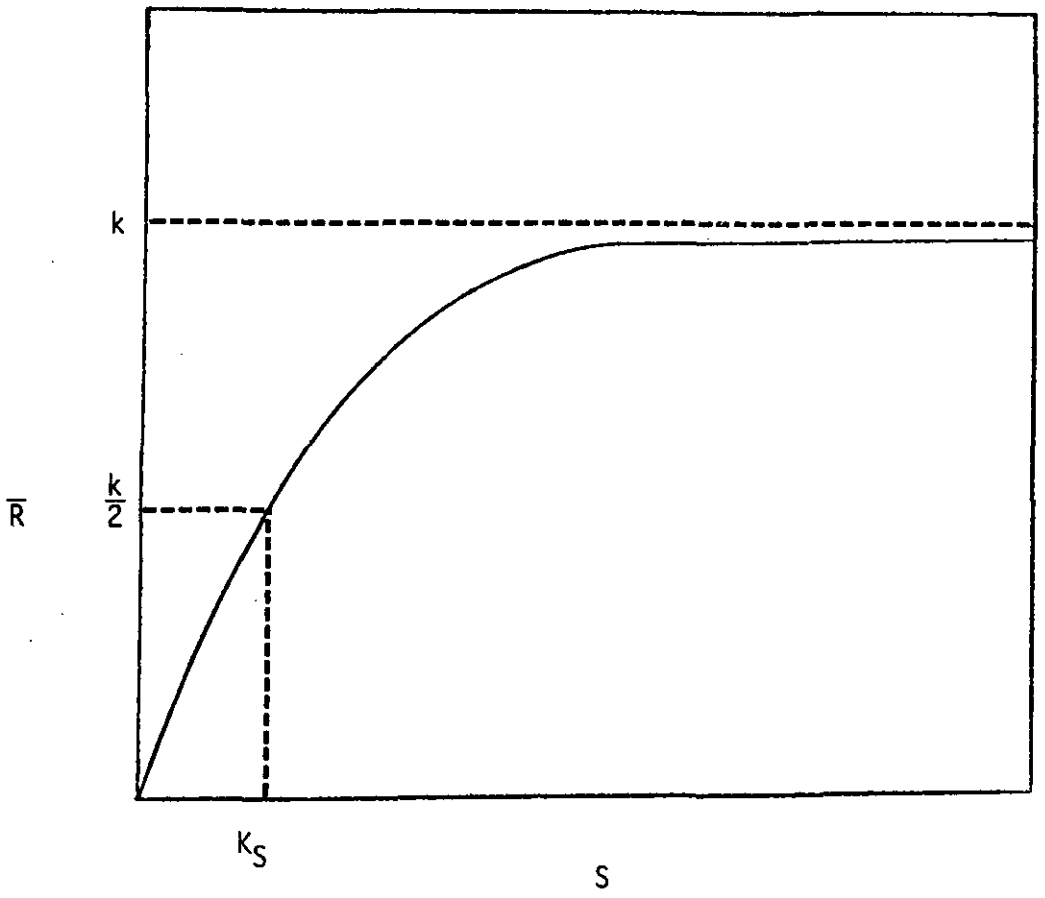

Figure 3.8 Reaction Rate Versus Substrate Concentration for Michaelis-Menten Kinetics.

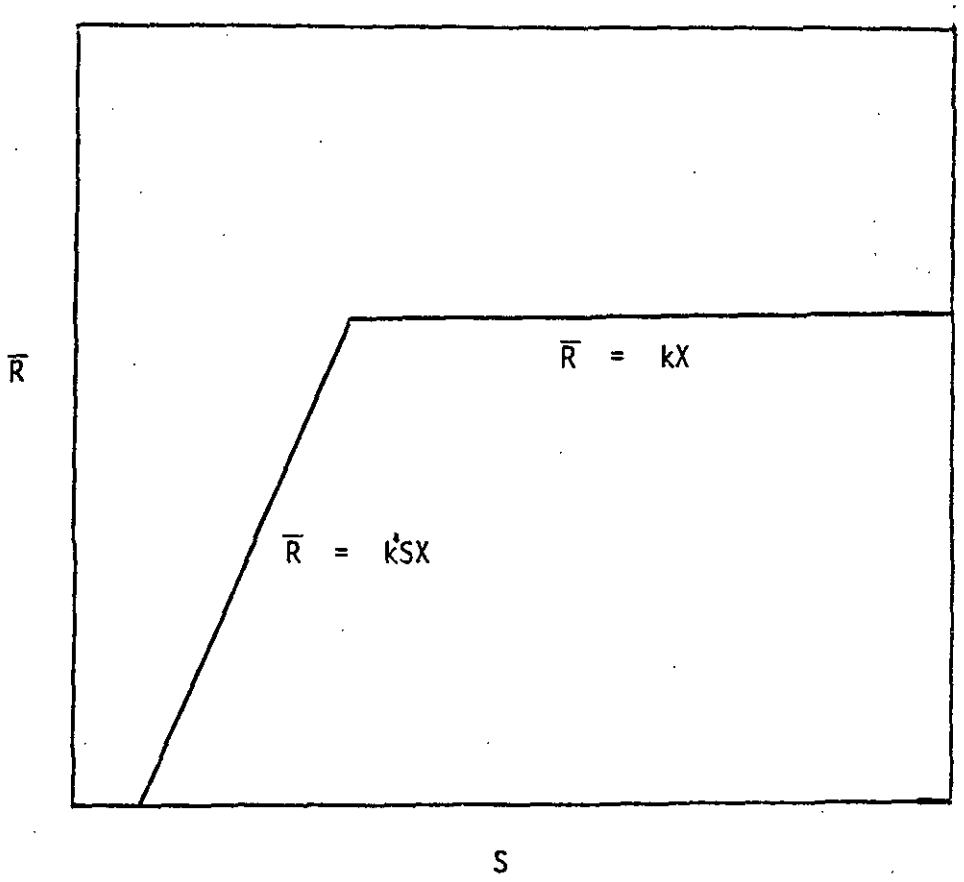

Figure 3.9 Reaction Rate Versus Substrate Concentration for Discontinuous Linear Kinetics.

Figure 3.9 depicts discontinuous linear kinetics. Obviously, the discontinuous linear approach is least accurate in the region of the discontinuity.

Simple zero-order kinetics is among the earliest expressions used to describe biological reaction rates. Stumm-Zollinger et al. (129) note that as early as 1892, zero-order kinetics was reported as applicable to the description of fermentation rates. These authors also note that substrate concentration dependence observed with mixed substrate-mixed population systems may in fact be due to superposition of many individual zero-order reactions. This argument is substantiated by the fact that several researchers have observed zero-order kinetics when dealing with single substrates or pure cultures (98, 9, 76). Further, there is evidence that reaction rates which appear to follow Michaelis-Menten kinetics may, in fact, be intrinsic zero-order reactions limited by diffusional resistances. LaMotta (76) has shown that a zero-order, transport limited biofilm model provides an excellent fit to the data of Kornegay and Andrews (71), which these authors had modeled with Michaelis-Menten kinetics (K_S = 121 mg/l).

One should, however, be mindful of the caution noted by Levenspiel (83) regarding zero-order kinetics. Levenspiel states that "as a rule reactions are of zero-order only in certain concentration ranges. If the concentration is lowered far enough we usually find that the reaction becomes concentration dependent."

In summary, it is noted that although simplified linear kinetic

expressions are often adequate in describing observed rates of reaction, the Michaelis-Menten equation offers a more general kinetic expression applicable over a broader range of substrate concentrations.

3.3.4 Biological Denitrification

The biochemical reaction of interest in this research is denitrification. Biological denitrification may be either assimilatory or dissimilatory (138). Assimilatory denitrification involves the reduction of nitrate-nitrogen to ammonia which is subsequently utilized by the microorganisms for cell synthesis. If ammonia is already present, assimilatory reduction of nitrate need not occur to meet cell growth requirements (137).

Dissimilatory denitrification is a process by which nitrate-nitrogen is reduced to a gaseous nitrogen species by heterotrophic microorganisms (i.e., microorganisms requiring an external organic carbon source. The gaseous product is primarily elemental nitrogen, however, trace amounts of nitrous of nitric oxide may also be formed (120).

A large number of bacteria are capable of dissimilatory nitrate reduction while a much smaller number appear capable of assimilatory reduction (103). That is, many organisms which denitrify require an external source of ammonia for cell synthesis.

Organisms able to assimilate nitrate include Neurospora, Achromobacter, Aspergillus, Lactobacillus, Escherichia coli and Azotobacter.

Those capable of dissimilating nitrate include Micrococcus, Pseudomonas, Denitrobacillus, Spirillum, Bacillus and Achromobacter (103).

It has been established that aerobic respiration (using molecular oxygen) and dissimilatory nitrate reduction are homologous processes i.e., the same electron-transfer pathways are followed in both reactions (132, 52, 101). The processes differ, however, at the terminal enzymes. For dissimilatory denitrification, a nitrate reductase replaces the aerobic process cytochrome oxidase as the terminal enzyme of the metabolic pathway (120).

Organisms which can utilize either oxygen or nitrate as terminal hydrogen acceptors are termed facultative organisms. Although facultative organisms have the capacity to obtain energy from both nitrate and oxygen reduction, the aerobic process is favored as indicated by the following: (a) generally microorganisms denitrify only under anoxic conditions and the presence of oxygen prevents the formation of nitrate-reducing enzymes, (b) cell yield is usually lower in bacteria dissimilating nitrate than in those grown aerobically (which may result from a lower formation of adenosine triphosphate during oxidation of carbohydrate by nitrate), and (c) even cells with active nitrate-reducing enzymes can readily use oxygen instead of nitrate as the terminal hydrogen acceptor (103).

In assessing the effect of oxygen on bacterial denitrification, a differentiation must be made between assimilatory and dissimilatory nitrate reduction. Although assimilatory nitrate reduction is

unaffected by the presence of oxygen, it is generally accepted that oxygen completely inhibits dissimilatory denitrification. While dissimilatory nitrate reduction has been observed in aerobic systems (50, 124), this denitrification has been attributed to mass transport limitations which result in portions of the biomass being anoxic and thus able to reduce nitrate (103, 50, 122).

Other important factors affecting biological denitrification are temperature, pH and carbon source. Dawson and Murphy (31) found that for a pure culture of Pseudomonas denitrificans, the dependence of denitrification rate on temperature can be described by an Arrhenius type relationship. Specifically, these researchers developed the following correlation between zero-order rate constant $\hat{k}$ (mg NO_3^--N/mg cells·hr) and temperature:

$$\hat{k} = 3.19 \exp - \frac{8455}{T(^\circ K)} \qquad 3.58$$

Similar dependence of denitrification rate on temperature has been observed in mixed culture biological denitrification (100). Stensel (128), however, found that the rate of denitrification at 30°C was the same or less than the rate at 20°C. He did observe that an Arrhenius expression fit his rate data over a temperature range of 15°C to 25°C.

The results of several researchers who examined the effects of pH on biological denitrification are presented in Figure 3.10. These results indicate an optimum pH in the range of 6.5 to 7.5. In reviewing literature denitrification data, Harremoes and Riemer (44) note that

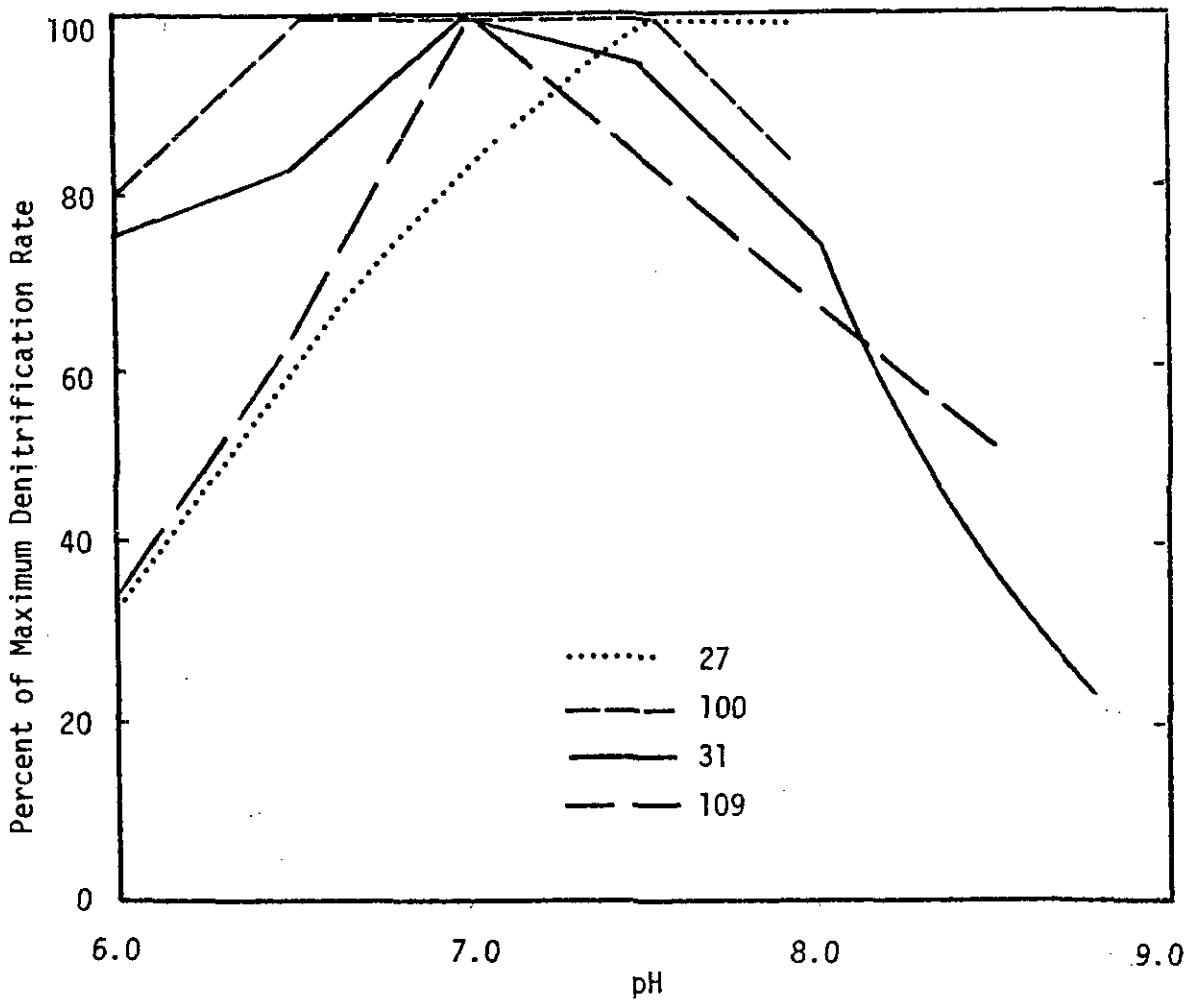

Figure 3.10 Effect pH on Denitrification Rate (after (137)).

optimum denitrification results when pH is between 7.0 and 8.2. Significantly reduced rates were noted at pH 6.0.

As mentioned earlier, the heterogeneous microorganisms which mediate dissimilatory denitrification require an external source of organic carbon. The most common organic compound used in denitrification is methanol. Other organic materials, ranging from sugar to brewery wastewater, have been examined as substitutes for methanol in denitrification (90, 91). Although several of these compounds were found to be satisfactory from a biokinetic standpoint, other problems such as cost or availability were noted.

C H A P T E R I V

FLUIDIZED BED BIOFILM REACTOR - MODEL DEVELOPMENT

4.1 An Overview of the Model

Reactor flow model.

The dispersion model will be used to describe flow conditions in the fluidized bed biofilm reactor. Development of the dispersion model proceeds under the following assumptions:

1. The liquid phase moves through the reactor by convection and axial dispersion.
2. No radial gradients exist.
3. Solid phase characteristics (film thickness, bed porosity) are independent of axial position.
4. Substrate uptake is solely by biologically active fluidized particles.
5. Steady-state conditions exist in the reactor.

A differential element within a FBBR is shown in Figure 4.1. A material balance on the differential element for any reactant can be written as follows:

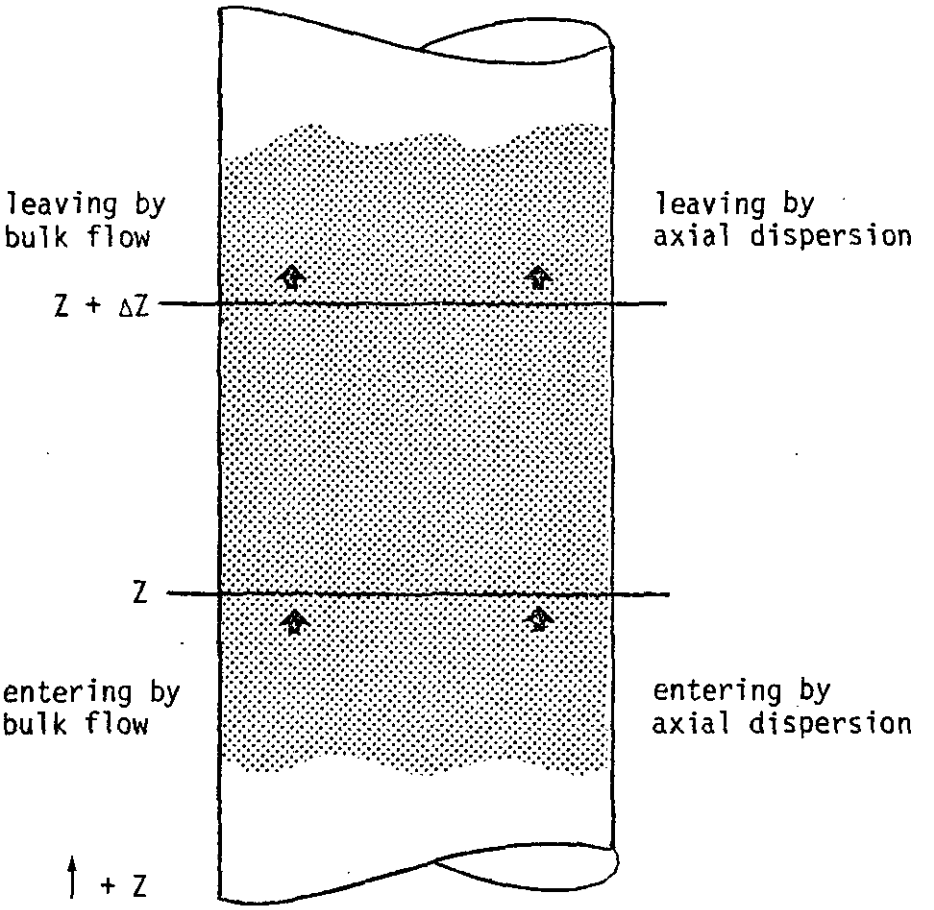

Figure 4.1 Differential Element Within a FBBR.

(output-input) + (output-input) +
bulk flow axial dispersion

disappearance + accumulation = 0 4.1
by reaction

In terms of bulk-liquid substrate concentration S_b the individual components can be expressed as;

entering by bulk flow = $UA \cdot S_b|_Z$

leaving by bulk flow = $UA \cdot S_b|_{Z + \Delta Z}$

entering by axial dispersion = $- D_Z A \frac{dS_b}{dZ}|_Z$

leaving by axial dispersion = $- D_Z A \frac{dS_b}{dZ}|_{Z + \Delta Z}$

disapperance by reaction = $(- R_v)\ A\ \Delta\ Z$

accumulation = 0 at steady-state.

where: U = superficial upflow velocity

A = reactor area perpendicular to flow

Z = axial coordinate

D_Z = axial dispersion coefficient

R_v = reaction rate in terms of reactor volume,

$$= \frac{\text{(mass substrate reacting)}}{\text{(time) (volume reactor)}}$$

Entering these terms in Equation 4.1 and dividing by A Δ Z yields:

$$U\left[\frac{S_b|_{Z+\Delta Z} - S_b|_Z}{\Delta Z}\right] - D_Z\left[\frac{\frac{dS_b}{dZ}|_{Z+\Delta Z} - \frac{dS_b}{dZ}|_Z}{\Delta Z}\right] + R_v = 0 \qquad 4.2$$

Taking the limit as $\Delta Z \rightarrow 0$, obtain:

$$U\frac{dS_b}{dZ} - D_Z\frac{d^2S_b}{dZ^2} + R_v = 0 \qquad 4.3$$

Boundary conditions for Equation 4.3 were discussed in Section 3.1 of this dissertation. The following conditions will be used:

$$S_b = S_b|_{Z=0} \quad \text{at} \quad Z = 0 \qquad 4.4$$

$$\frac{dS_b}{dZ} = 0 \quad \text{at} \quad Z = H_B \qquad 4.5$$

In dimensionless form Equation 4.3 may be written:

$$\frac{dB}{dY} - B_o \frac{d^2B}{dY^2} + \left(\frac{\tau}{S_b|_{Z=0}}\right) R_v = 0 \qquad 4.6$$

in which: $B = S_b / S_b|_{Z=0}$

$Y = Z / H_B$

H_B = expanded bed height

$\tau = H_B / U$

B_o = Bodenstein number = $\frac{D_Z}{H_B U}$

Dimensionless boundary conditions on Equation 4.6 are:

$$B = 1 \quad \text{at} \quad Y = 0 \qquad 4.7$$

$$\frac{dB}{dY} = 0 \quad \text{at} \quad Y = 1 \qquad 4.8$$

Reaction term.

The Michaelis-Menten rate expression discussed in Section 3.3.3, will be used to describe intrinsic (not limited by transport phenomena) reaction kinetics within the FBBR. For biofilm systems, intrinsic Michaelis-Menten kinetics may be written in terms of the bulk-liquid substrate concentration S_b as:

$$R_I = \frac{k \rho_B S_b}{K_S + S_b} \qquad 4.9$$

in which: R_I = $\frac{\text{mass substrate reacting}}{\text{(time) (volume biofilm)}}$

ρ_B = $\frac{\text{mass volatile solids}}{\text{volume biofilm}}$

k = $\frac{\text{mass substrate reacting}}{\text{(time)(mass volatile solids)}}$

The observed (mass transfer limited) rate of reaction within a FBBR can, in turn, be related to the intrinsic rate by an overall effectiveness factor η_o, introduced in Section 3.3.2. The observed rate R_o can be written as follows:

$$R_o = \eta_o R_I \qquad 4.10$$

Details of the procedure used to evaluate η_o are presented in Section 4.3 of this dissertation.

Biomass holdup

At any point in a FBBR, the observed rate of reaction on a per unit biofilm volume basis R_o is related to the reaction rate on a per unit expanded bed volume basis R_v by the following simple expression:

$$V_B \cdot R_o|_Z = H_B A \cdot R_v|_Z \qquad 4.11$$

in which the biomass volume V_B is uniformly distributed in the expanded bed volume $H_B A$. The expanded bed reaction term R_v can be written in terms of the bulk-liquid substrate concentration S_b by combining Equation 4.9, 4.10 and 4.11 as follows:

$$R_v = \frac{\eta_o V_B}{H_B A} \cdot \frac{k \rho_B S_b}{K_S + S_b} \qquad 4.12$$

The biomass holdup (V_B / $H_B A$) can be determined using an analysis of fluidization mechanics within the FBBR. Details of the procedure used in this determination are given in Section 4.2.

Basically, the fluidization analysis allows prediction of the equilibrium bed porosity and biofilm thickness corresponding to a given set of reactor operating conditions. Biomass holdup may, therefore, be conveniently expressed in terms of bed porosity ε, and the operating parameter, media volume V_m as:

$$\frac{V_B}{H_B A} = 1 - \varepsilon - \frac{V_m}{H_B A} \; . \qquad 4.13$$

Axial dispersion coefficient

The axial dispersion coefficient correlation developed by Chung and Wen (26), Equation 3.5, was incorporated in the FBBR model.

$$Pe_A = \frac{Ud_P}{D_Z} = \frac{Re_{MF}}{\epsilon\, Re} \left[0.20 + 0.011\, Re^{.48}\right] \qquad 3.5$$

The Bodenstein number is then written:

$$Bo = d_p / (H_B \cdot Pe_A)$$

The minimum fluidization Reynolds number Re_{MF} was calculated using the following correlation, developed by Wen and Yu (147):

$$Re_{MF} = \left[(33.7)^2 + 0.0408\, Ga \right]^{\frac{1}{2}} - 33.7 \qquad 3.6$$

in which the Galileo number Ga is defined as follows:

$$Ga = \frac{d_P^3\ \rho_L\ (\rho_S - \rho_L)\ g}{\mu^2}$$

Comprehensive FBBR model.

Equations 4.12 and 4.13 were used to eliminate the reaction term R_V from Equation 4.3. The resultant expression is:

$$U \frac{dS_b}{dZ} - D_Z \frac{d^2S_b}{dZ^2} + \eta_o \left[1 - \varepsilon - \frac{V_m}{H_B A} \right] \left[\frac{k \rho_B S_b}{K_S + S_b} \right] = 0 \quad 4.14$$

Equation 4.14 may be rewritten in terms of dimensionless quantities as:

$$\frac{dB}{dY} - Bo \frac{d^2B}{dY^2} + \eta_o \left[1 - \varepsilon - \frac{V_m}{H_B A} \right] \left[\frac{\tau k \rho_B}{S_b|_{Z=0}} \right] \left[\frac{B}{\Omega + B} \right] = 0 \quad 4.15$$

in which: $\Omega = K_S / S_b|_{Z=0}$.

Bioparticle effectiveness factor η_o is dependent on bulk-liquid substrate concentration S_b (or B). This necessitates simultaneous solution of Equation 4.14 (or 4.15) with an equation which expresses the functional dependence of η_o on S_b. Such an expression is developed in Section 4.3 of this dissertation.

Section 4.2 presents details of the procedure used to predict bed porosity ε and biofilm thickness δ as functions of operating conditions within a fluidized bed biofilm reactor.

4.2 Fluidization - Bed Porosity and Biofilm Thickness.

An algorithm has been developed for calculating the equilibrium biofilm thickness δ and bed porosity ε which correspond to a given set of FBBR operating conditions. At the core of this algorithm is the empirical bed expansion expression, Equation 3.24, discussed

in Section 3.2 of this dissertation. The algorithm is presented in flow chart format in Figure 4.2.

Basically, the bed expansion corresponding to a trial biofilm thickness δ is calculated using the bed expansion expression Equation 3.24. Iteration continues on δ until the calculated expanded bed height $\hat{H}_B$ coincides with some specified bed height H_B.

In order to use Equation 3.24, two parameters specific to the system must first be determined. These parameters are the particle terminal velocity U_t and the expansion index, n. Correlations for these parameters, specific to the fluidized bed biofilm reactor, have been developed as part of this research (see Section 5.2 and 5.3).

A step by step description of the fluidization algorithm follows.

1. Guess a biofilm thickness δ.
2. Calculate the diameter of the biofilm-support medium composite particle (or bioparticle):

$$d_p = d_m + 2\,\delta \qquad 4.16$$

in which d_m = support particle diameter.

3. Calculate the biofilm volatile solids density and wet density corresponding to δ. It has been reported in the

Figure 4.2 Flow Chart of the Bed Fluidization Algorithm

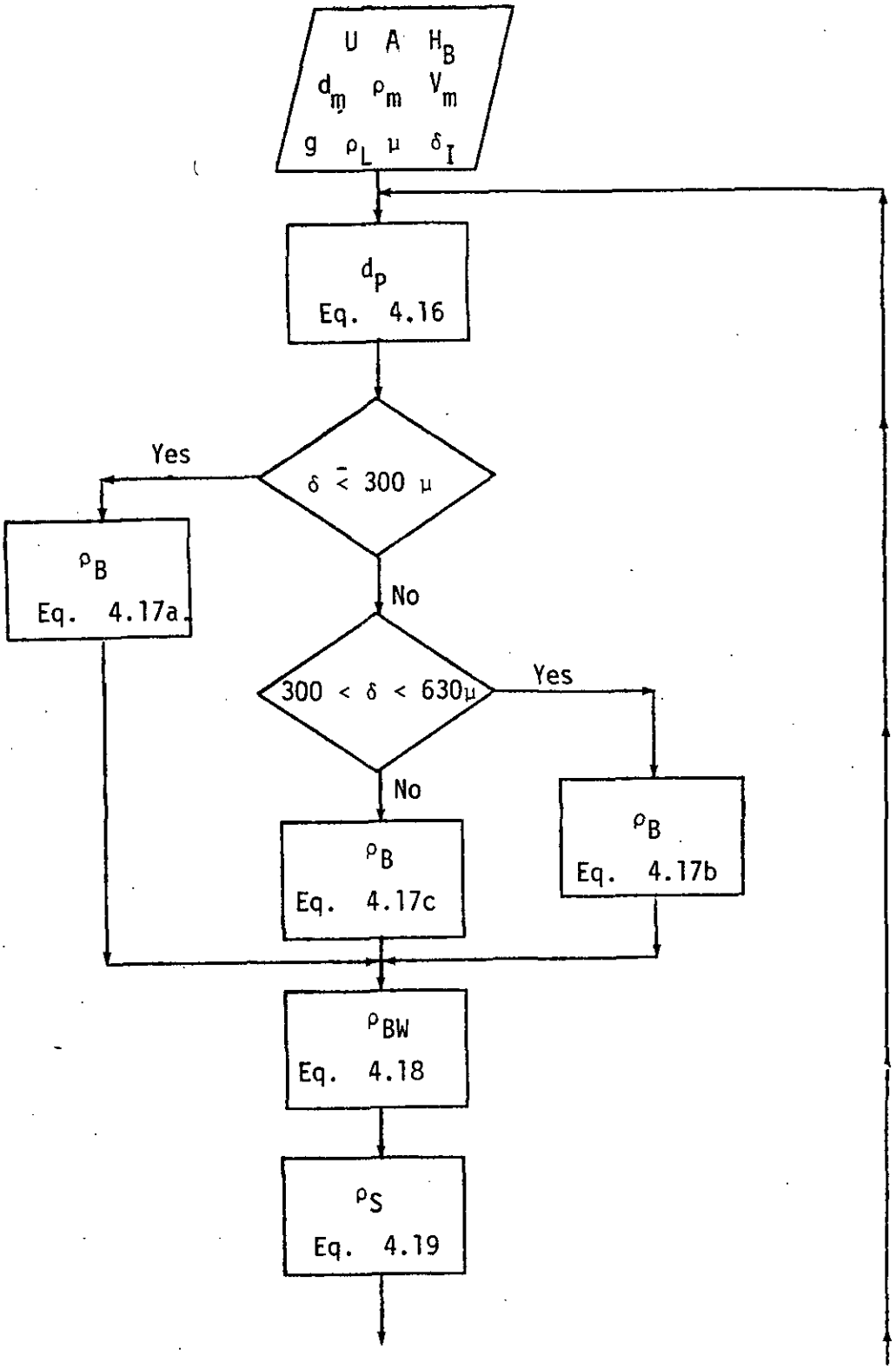

Figure 4.2 (con't)

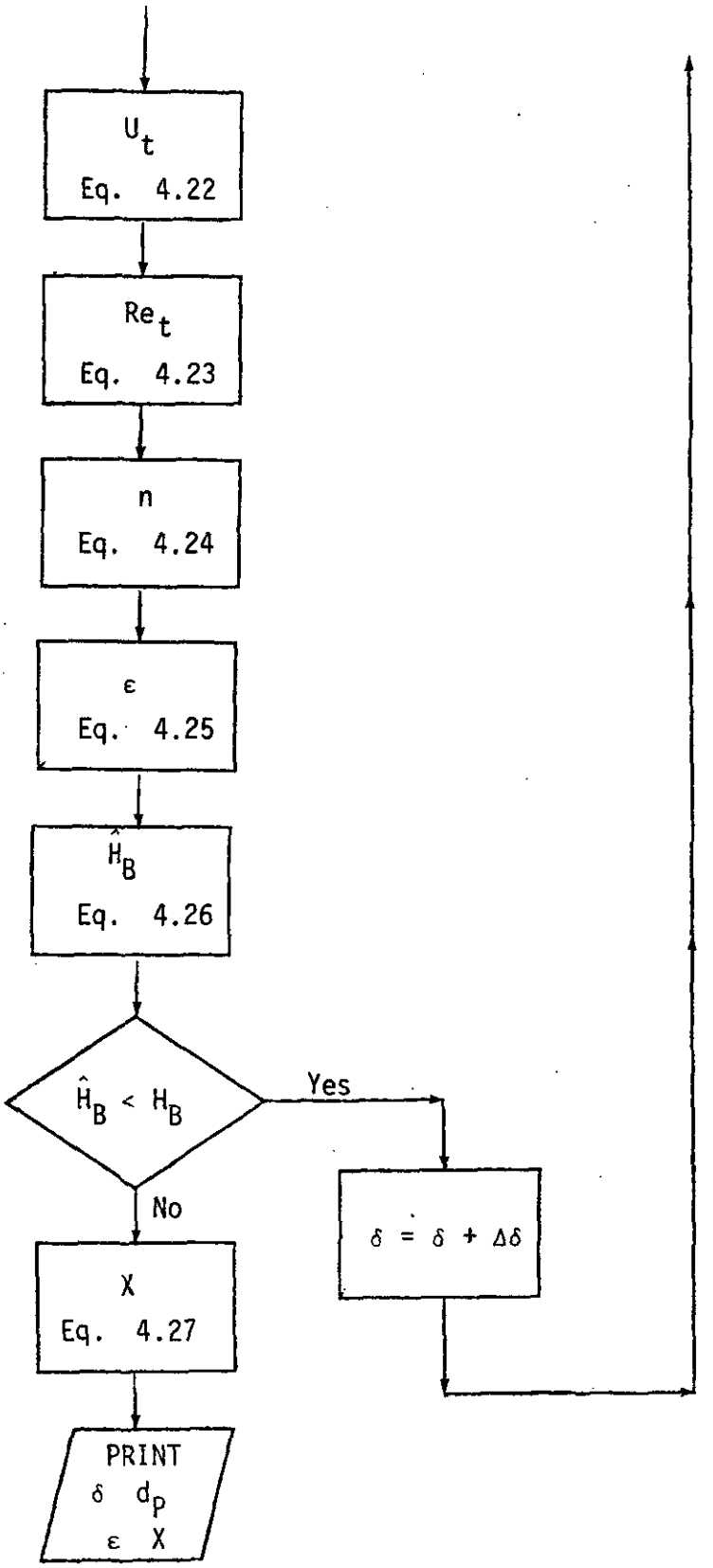

literature (49) that biofilm volatile solids density is a function of biofilm thickness. A decrease in volatile solids density with film thickness was observed in this research, however, the decrease was apparent only for relatively thick ($\delta > 300$) biofilms. Volatile solids - biofilm thickness data for the experimental FBBR are presented in Figure 5.13. The biofilm density-biofilm thickness relationship is incorporated in the fluidization algorithm through simple linear functions which roughly correlate the data of Figure 5.13. The correlation equations are given as follows:

$$\rho_B = 65 \frac{\text{mg V.S.}}{\text{cm}^3} , \qquad 0 < \delta \leq 300 \text{ microns} \qquad 4.17a$$

$$\rho_B = \left(\frac{-35 \text{ mg V.S.}}{330 \text{ micron} \cdot \text{cm}^3} \right) \delta + 96.8 \frac{\text{mg V.S.}}{\text{cm}^3} , \qquad 300 < \delta \leq 630 \text{ microns} \qquad 4.17b$$

$$\rho_B = 30 \frac{\text{mg V.S.}}{\text{cm}^3} , \qquad \delta > 630 \text{ microns} \qquad 4.17c$$

Both biofilm volatile and total solids density were measured in the experimental phase of this research. The ratio of volatile to total biofilm solids was found to be approximately constant at 0.8. Using this ratio, the biofilm wet density can be calculated by the following approximate relationship:

$$\rho_{BW} = \rho_L + \rho_B / 0.8 \qquad 4.18$$

4. Calculate the composite wet density ρ_S of the bioparticle:

$$\rho_S = \rho_{BW} + (\rho_m - \rho_{BW}) \quad (d_m / d_p)^3 \qquad 4.19$$

in which ρ_m is the support media density.

5. Calculate the terminal velocity U_t of the bioparticle. For smooth, spherical particles, terminal velocity may be calculated using Newton's law, Equation 4.20 (36):

$$U_t = \left(\frac{4(\rho_S - \rho_L)\ g\ d_p}{3\ C_D\ \rho_L} \right)^{\frac{1}{2}} \qquad 4.20$$

Equation 4.20 is applied here to the calculation of terminal velocities for the irregular bioparticles. The effect of particle shape and surface on terminal velocity is introduced through the C_D - Re correlation:

$$C_D = 36.66\ Re^{-2/3} \qquad 4.21$$

which has been developed specifically for bioparticles as part of this research. The experimental basis for the

correlation is described in Section 5.3.

Equations 4.20 and 4.21 are combined to yield the following explicit expression for bioparticle terminal velocity:

$$U_t = \left(\frac{(\rho_S - \rho_L)\ g\ d_P^{5/3}}{27.5\ \rho_L^{1/3}\ \mu^{2/3}} \right)^{3/4} \qquad 4.22$$

6. Calculate the bioparticle terminal Reynolds number Re_t

$$Re_t = \frac{U_t\ \rho_L\ d_P}{\mu} \qquad 4.23$$

7. Calculate the expansion index n which corresponds to this bioparticle terminal Reynolds number. The following empirical correlation is used:

$$n = 10.35\ Re_t^{-0.18} \qquad 4.24$$

This correlation is specific for bioparticle fluidization and has been developed as part of this research. The experimentation backing this correlation is described in Section 5.2 of this dissertation.

8. Specify a superficial velocity U.
9. Calculate the resultant equilibrium bed porosity ε using Equation 3.24 with $U_i = U_t$.

$$\varepsilon = \left(\frac{U}{U_t}\right)^{1/n} \qquad 4.25$$

10. Specify the total volume of support media in the reactor V_m.
11. Calculate the resultant trial expanded bed height $\hat{H}_B$ using a volume balance on solids within the reactor:

$$\hat{H}_B = \frac{V_m}{A\,(1-\varepsilon)} \left(\frac{d_p}{d_m}\right)^3 \qquad 4.26$$

12. Compare the calculated bed height $\hat{H}_B$ with the specified bed height H_B. If unacceptable, return to step 1 and repeat the procedure.

As an aside, biomass holdup (actually volatile solids concentration per unit expanded bed volume) X may be calculated as follows:

$$X = \frac{V_m\ \rho_B}{A\ H_B}\left[\left(\frac{d_p}{d_m}\right)^3 - 1\right] \qquad 4.27$$

4.3 Substrate Conversion - Biofilm Effectiveness

As presented in Section 3.3, the rate of substrate conversion by biological film is controlled by three major processes.

1. Transport of substrate from the bulk-liquid to the liquid-biofilm interface (external mass transfer).
2. Transport of substrate within the biofilm (internal mass transfer).
3. Substrate consumption reaction within the biofilm.

Mathematical description of substrate uptake by biological film proceeds under the following assumptions.

1. Homogeneous biofilm of uniform thickness.
2. Mass transfer described by Fick's first law.
3. Single-substrate biochemical reaction described by Michaelis-Menten kinetics.
4. Steady-state conditions.

Consider the idealized bioparticle depicted in Figure 4.3. Under the listed assumptions, a material balance on a differential shell within the biofilm can be written as follows:

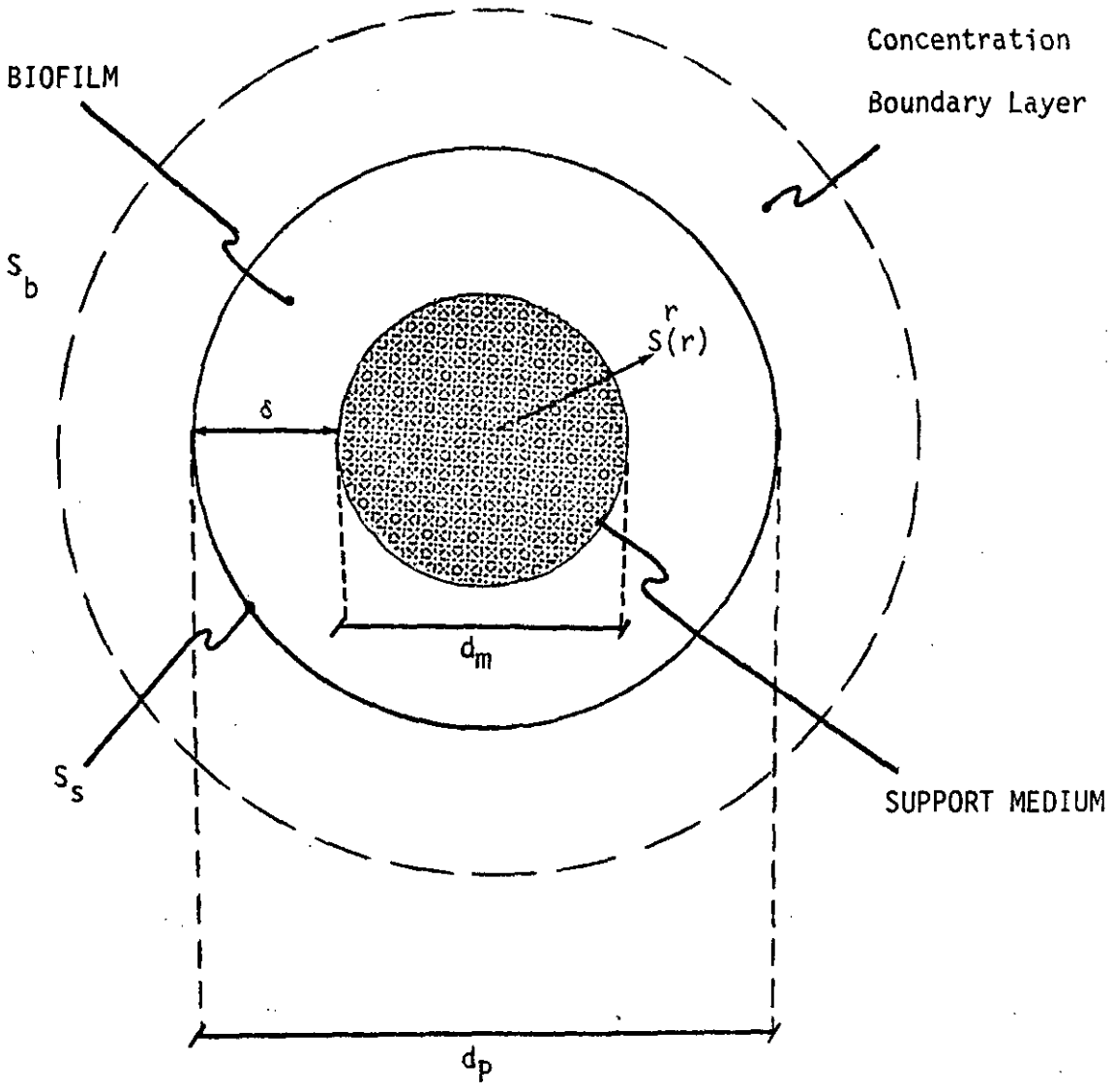

Figure 4.3 Schematic of Bioparticle.

$$\begin{matrix}\text{(output-input)} \\ \text{internal} \\ \text{mass transfer}\end{matrix} + \begin{matrix}\text{disappearance} \\ \text{by reaction}\end{matrix} + \text{accumulation} = 0 \qquad 4.28$$

In terms of local substrate concentration S the individual components of Equation 4.28 may be expressed as:

$$\text{input by internal mass transfer} = -4\pi D_{SB} \left(r^2 \frac{dS}{dr} \right)_{r + \Delta r}$$

$$\text{output by internal mass transfer} = -4\pi D_{SB} \left(r^2 \frac{dS}{dr} \right)_{r}$$

$$\text{disappearing by reaction} = -(4\pi r^2 \Delta r) \frac{k \rho_B S}{K_S + S}$$

$$\text{accumulation} = 0 \quad \text{at steady-state}$$

in which D_{SB} is the effective diffusivity of the substrate in the biofilm.

Entering these terms in Equation 4.28 and dividing through by $4\pi \Delta r$ yields:

$$D_{SB} \left[\frac{\left(r^2 \frac{dS}{dr} \right)_{r+\Delta r} - \left(r^2 \frac{dS}{dr} \right)_{r}}{\Delta r} \right] - r^2 \frac{k \rho_B S}{K_S + S} = 0 \qquad 4.29$$

Taking the limit as $\Delta r \rightarrow 0$:

$$D_{SB} \frac{d}{dr} \left(r^2 \frac{dS}{dr} \right) - r^2 \frac{k \rho_B S}{K_S + S} = 0 \qquad 4.30$$

The effect of external mass transport or the rate of substrate conversion is included in this analysis through the boundary condition at the liquid-biofilm interface.

As discussed in Section 3.3.1, flux across this boundary may be expressed in terms of an empirical mass transfer coefficient k_c:

$$N' = -k_c (S_b - S) \quad \text{at } r = d_p / 2 \qquad 4.31$$

This flux can, in turn, be related to biofilm-side concentration gradient at the interface as follows:

$$D_{SB} \frac{dS}{dr} = k_c (S_b - S) \quad \text{at } r = d_p / 2 \qquad 4.32$$

The procedure used to evaluate the mass transfer coefficient k_c is outlined at the end of this section.

At the biofilm-support particle interface, a no-flux boundary condition applies. Thus:

$$\frac{dS}{dr} = 0 \quad \text{at} \quad r = d_m / 2 \qquad 4.33$$

Equation 4.30 and the accompanying boundary conditions, Equations 4.32 and 4.33, may be expressed in dimensionless form as:

$$\frac{1}{(X + \xi)^2} \quad \frac{d}{dX}\left[(X + \xi)^3 \ \frac{dC}{dX}\right] - \phi^2 \ \frac{C}{\gamma + C} = 0 \qquad 4.34$$

$$\frac{dC}{dX} = Bi\ (1 - C) \quad \text{at} \quad X = 1 \qquad 4.35$$

$$\frac{dC}{dX} = 0 \qquad \text{at} \quad X = 0 \qquad 4.36$$

in which:

$$C = S/S_b$$

$$X = r/\delta - d_m/2\delta$$

$$\xi = d_m/2\delta$$

$$\gamma = K_S/S_b$$

$$\phi^2 = \frac{k\ \rho_B\ \delta^2}{S_b\ D_{SB}} \quad \text{, a Thiele-type modulus}$$

$$Bi = \frac{k_C \delta}{D_{SB}}$$, a modified Biot number.

Equation 4.30 or 4.34 may be integrated numerically to yield the substrate concentration profile within a bioparticle. Details of the numerical integration procedure are presented in Appendix 1.

The biofilm substrate concentration profile can, in turn, be integrated to yield observed reaction rate, R_o, as follows:

$$R_o = \frac{\int_{d_m/2}^{d_p/2} \frac{k \rho_B S}{K_S + S} 4\pi r^2 dr}{\frac{\pi}{6}(d_p^3 - d_m^3)} \qquad 4.37$$

Overall effectiveness factor, η_o, is obtained by combining Equations 4.9, 4.10 and 4.37 to yield the following expression:

$$\eta_o = \frac{24 (K_S + S_b)}{S_b (d_p^3 - d_m^3)} \int_{d_m/2}^{d_p/2} \frac{S}{K_S + S} r^2 dr \qquad 4.38$$

In dimensionless terms, Equation 4.38 may be written:

$$\eta_o = \frac{1 + \gamma}{\xi^2 + \xi + 1/3} \int_0^1 \frac{C}{\gamma + C} (x + \xi)^2 \, dx \qquad 4.39$$

Details of the procedure for numerical integration of Equation 4.39 are included in Appendix 1.

External mass transfer coefficient k_C

Integration of the biofilm substrate conservation expressions, Equations 4.30 or 4.34 requires a knowledge of the external mass transfer coefficient, k_C. As pointed out in Section 3.3.1, this coefficient can be related to conditions existing within a fluidized bed biofilm reactor by the expression proposed by Snowdon and Turner (126):

$$Sh = \frac{k_C \, d_P}{D_{SL}} = \frac{0.81}{\varepsilon} \, Re^{1/2} \, Sc^{1/3} \qquad 3.53$$

This correlation was developed for fluidized beds operating under the same Reynolds number range as is common to fluidized bed biofilm reactors.

4.4 A Summary of the Model

Prediction of substrate conversion within a fluidized bed biofilm reactor requires simultaneous solution of the reactor flow equation, Equation 4.15 and the biofilm effectiveness equations, Equationons 4.34 and 4.39.

Solution of these equations is possible, however, only after the parameters bed porosity, ε, and biofilm thickness, δ, have been specified. An algorithm, described in Section 4.2, is proposed as a means of predicting these parameters.

To predict substrate conversion within a FBBR using the mathematical models developed thus far, a total of thirteen system parameters and six empirical correlations must be specified.

The required parameters and correlations are presented in Table 4.1. System parameters are subdivided into fixed parameters (not readily controllable by a designer) and design parameters.

Figure 4.4 further subdivides the parameters and correlations as inputs to the appropriate segments of the overall FBBR model. Details of the numerical solution of the FBBR model are presented in Appendix 2. A computer program for such a numerical solution is included in this appendix.

Table 4.1. FBBR MODEL INPUT PARAMETERS AND CORRELATIONS.

Fixed Parameters

Liquid Phase Parameters:

diffusivity of species S in the liquid, D_{SL}

liquid density, ρ_L

liquid viscosity, μ

Biofilm Parameters:

diffusivity of species S in the biofilm, D_{SB}

maximum rate constant, k

Michaelis constant, K_S

System Dependent Parameters:

inflow concentration of species S, $S_b|_{Z=0}$

inflow rate, Q

Design Parameters

Reactor Parameters:

horizontal area, A

expanded bed height, H_B

Support Media Parameters:

media density, ρ_m

media diameter, d_m

total volume of media, V_m

Table 4.1 (con't)

Empirical Correlations

1) Biofilm density - biofilm thickness correlation, Equation 4.17.
2) Drag coefficient - Reynolds number correlation, Equation 4.21.
3) Expansion index - terminal Reynolds number correlation, Equation 4.24.
4) External mass transfer coefficient correlation, Equation 3.53.
5) Axial dispersion coefficient correlation, Equation 3.5.
6) Minimum fluidization Reynolds number correlation, Equation 3.6.

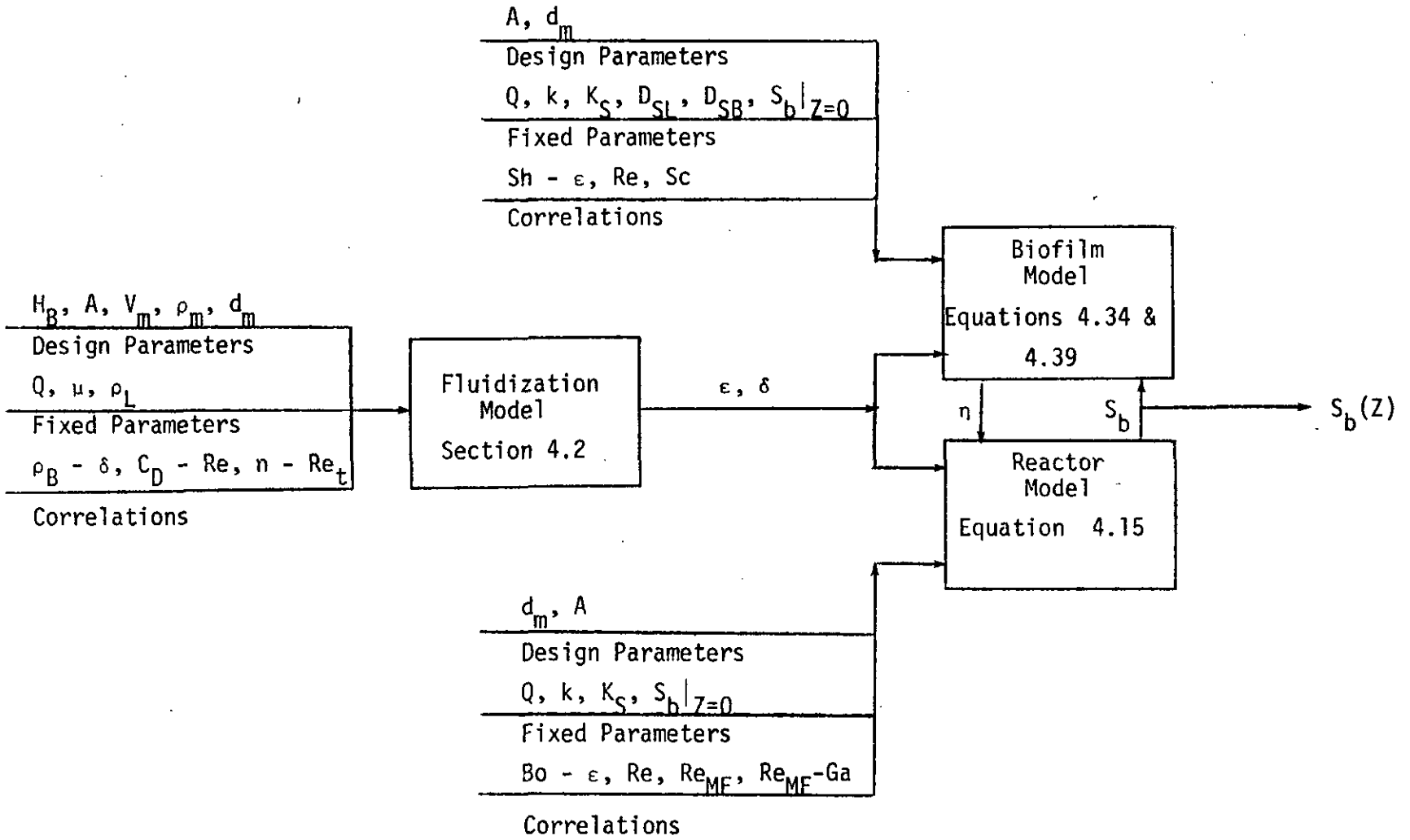

Figure 4.4 Block Diagram of the FBBR Model

CHAPTER V

EXPERIMENTAL PROGRAM

The basic objectives of the experimental portion of this research were:

1. To obtain parameters and correlations needed as input to the FBBR mathematical model.
2. To obtain FBBR performance data which can be used to evaluate the mathematical model.

Input information derived in this chapter includes the nitrate-biofilm effective diffusivity D_{SB} and the intrinsic rate constants for biofilm denitrification, k and K_S. These parameters were determined using a rotating disk biofilm reactor. In addition, expressions relating biofilm density to biofilm thickness, drag coefficient to Reynolds number and expansion index to terminal Reynolds number were determined experimentally using a laboratory scale fluidized bed biofilm reactor.

Fluidized bed experimentation included the measurement of nitrate-nitrogen profiles through the laboratory reactor. These observed profiles were compared with nitrate profiles predicted by the mathematical model.

5.1 Rotating Disk Reactor

Biofilm Intrinsic Rate Constants and Effective Diffusivity

The reaction of interest in this research was nitrate-limited biofilm denitrification. Intrinsic reaction kinetics were described in terms of a Michaelis-Menten rate expression. The rate constants appropriate to nitrate-limited biofilm denitrification were determined using a bench-scale biofilm reactor.

5.1.1. Materials and Methods

The Biofilm Reactor. The prime concern in selecting an experimental reactor was that the reactor allowed a clear differentiation among the steps involved in heterogeneous reaction i.e., among external mass transfer, internal mass transfer and simultaneous biochemical reaction.

One of the first reactors used in the environmental engineering area to study biofilm reaction kinetics was the inclined plane reactor (130, 88, 6, 68, 18). Substrate was allowed to trickle down a biofilm covered inclined plane and factors affecting substrate consumption were investigated. La Motta (76) notes, however, that such reactors are unsatisfactory for rigorous examination of biofilm reaction kinetics because the thickness of the external diffusional boundary layer varies along the length of the planar reactor. Specifically,

the thickness of this boundary layer starts at zero at the leading edge of the plane and increases with the square root of distance along the axis of flow. Chambre and Acrivos (22) have shown that at the leading edge of the reactor reaction kinetics controls conversion; at the end of the reactor external diffusion controls; while between these extremes, conversion is influenced by both reaction kinetics and diffusional limitations. Because of this variation in diffusional resistance, a clear differentiation between the reaction and transport steps is difficult. Another problem encountered with the inclined plane reactor is a tendency to develop biofilm with non-uniform thickness. Maier (88) and Atkinson and co-workers (2,6) tried to eliminate this difficulty by developing biofilm within a support grid. The biofilm thickness was controlled by manually scraping the surface of the grid. This technique limited their studies to relatively thick biofilms.

More sophisticated biofilm reactors were used by Kornegay (71) and La Motta (76) in their studies of biofilm kinetics. The reactors were concentric cylinders with one fixed, the other capable of rotation. Biofilm of uniform thickness developed on the cylinder walls. External diffusional limitation was eliminated by high-speed rotation of one of the cylinders. By measuring substrate removal rate as a function of biofilm thickness the effect of internal diffusional resistance was separated from intrinsic kinetics.

An experimental reactor configuration which allowed an even clearer differentiation among heterogeneous reaction steps was the

rotating disk reactor (RDR) used by Gulevich (42) in his biofilm study. A clearer differentiation among steps was possible because the rotating disk provides a uniformly accessible surface for interphase mass transfer. A mathematical description of this phenomenon is provided by Levich (84).

Because it offers a relatively simple, yet rigorous means for examining factors affecting biofilm kinetics, the rotating disk reactor was selected for use in this investigation.

A schematic of the plexiglass experimental RDR used in this study, with appropriate dimensions, is presented in Figure 5.1. A photograph of the experimental apparatus is given in Figure 5.2.

As dissolved oxygen concentration is a critical parameter in biological denitrification, DO within the rotating disk reactor was continuously monitored using a YSI DO meter and probe (models 54 and 5739, respectively). The reactor was fitted with a cover to aid in maintaining anoxic conditions. In addition, nitrogen gas was continuously fed to the RDR to strip out trace amounts of dissolved oxygen which entered with the liquid feed. This gas was vented through the disk shaft bearing in the reactor cover, preventing backflow of atmospheric oxygen through this opening. The RDR effluent line was looped to provide a liquid barrier against oxygen intrusion via this route.

A schematic of a growth support disk is shown in Figure 5.3; again dimensions are indicated. To facilitate measurement of biofilm thickness, each plexiglass disk was fitted with four removable slides.

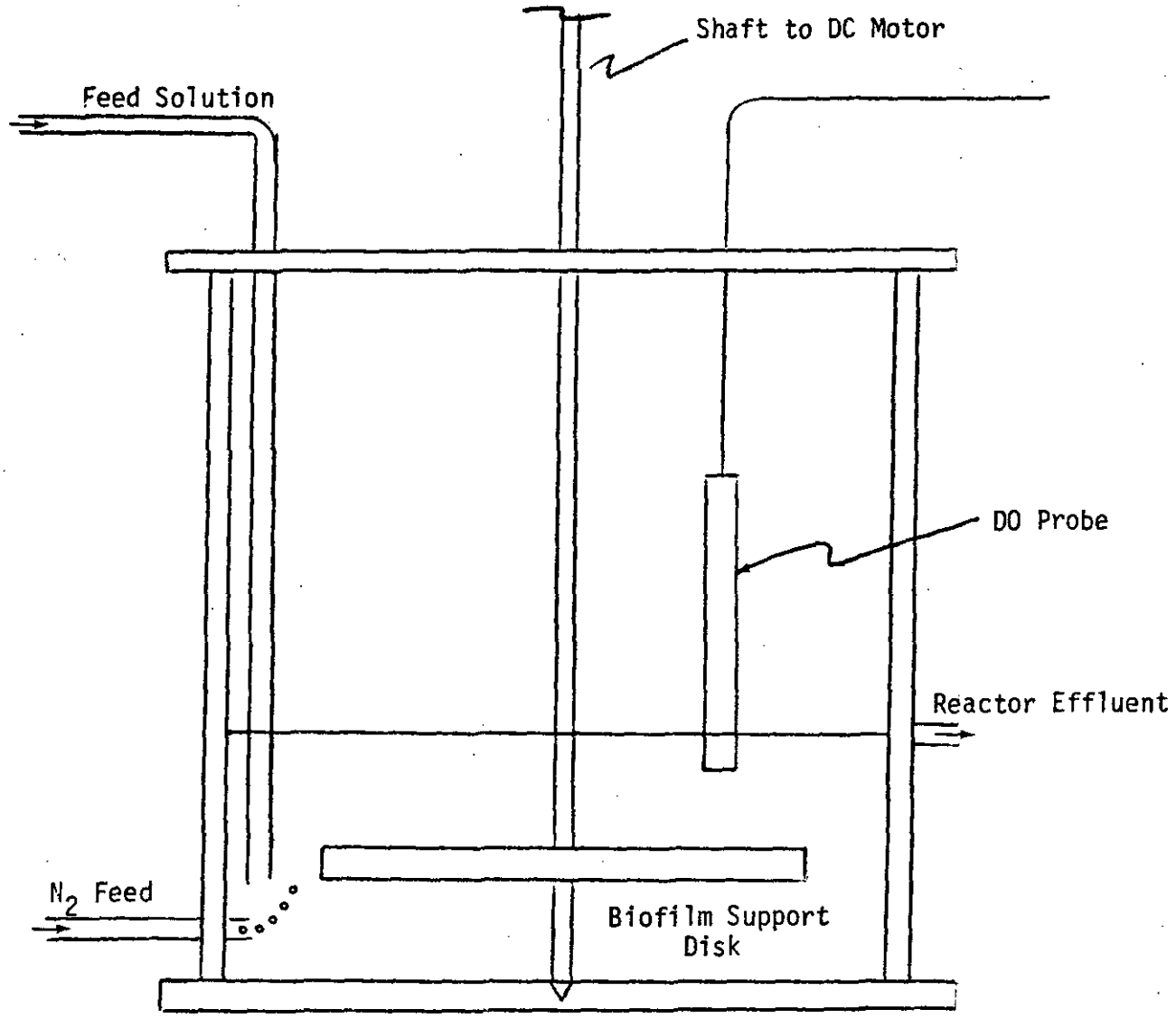

Figure 5.1 Schematic of the Laboratory Rotating Disk Reactor (scale 1/2" = 1").

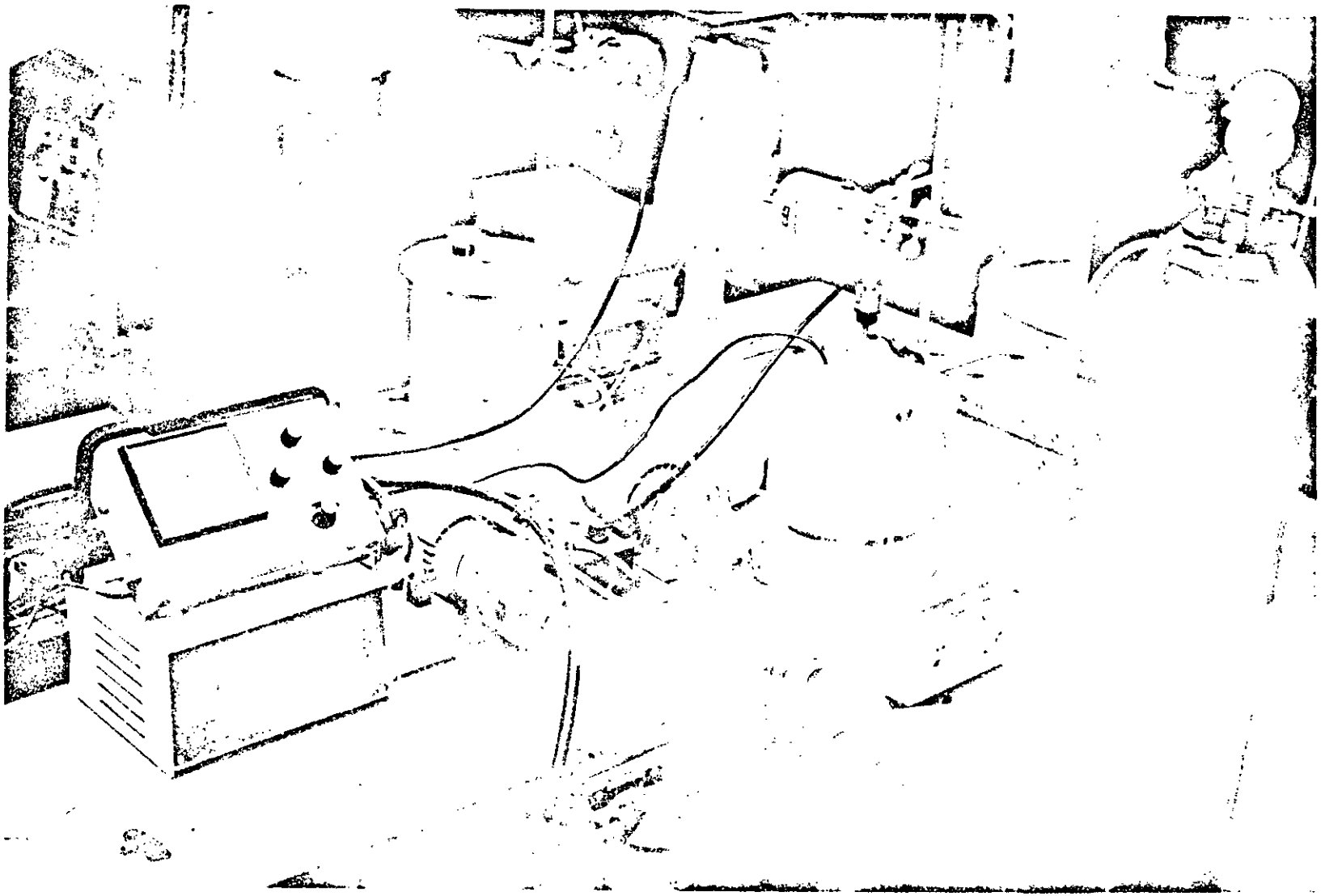

Figure 5.2 Photograph of the laboratory rotating disk reactor.

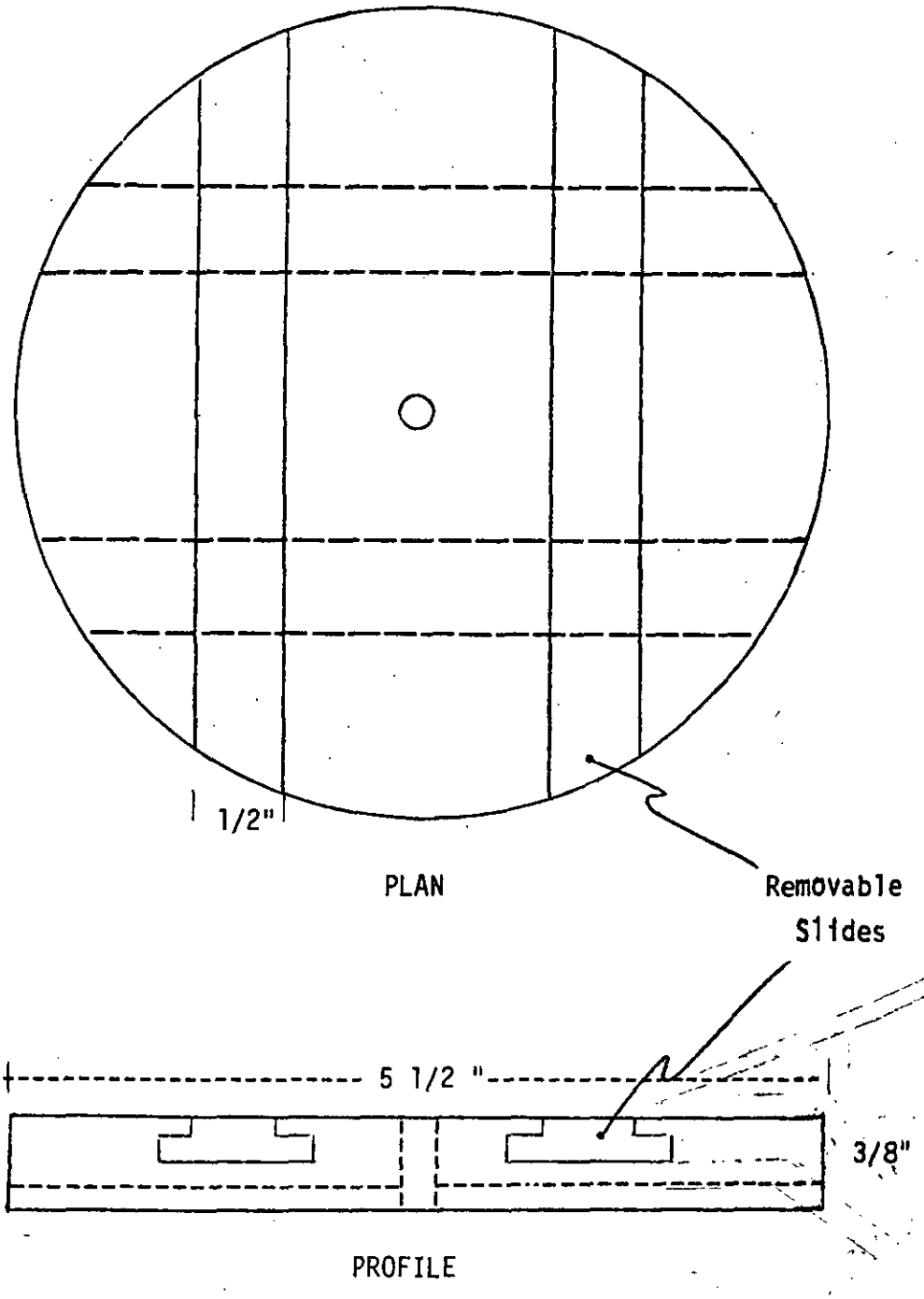

Figure 5.3 Schematic of the rotating growth-support disk.

The slides, also of plexiglass, were machined so that they formed an integral part of the disk surface. The disk was rotated by a Fisher Stedi-Speed stirrer. The disk shaft passed through a ball bearing in the reactor cover; a brass point bearing was used to seat the shaft at the reactor floor.

Two Masterflex pumps were used to supply liquid feed to the rotating disk reactor. The pump which supplied the bulk of the inflow fed nitrified effluentfrom one of the extended aeration units (Davco Package Plant Model 6DA7S) of the University of Massachusetts Wastewater Pilot Plant. The other pump supplied methanol and supplemental nitrate ($NaNO_3$). To insure that methanol did not limit the biological process, weight ratios of at least 6:1 methanol to nitrate-nitrogen were maintained at the reactor inlet. The discharge lines of the two feed pumps were joined at a Y connector, the reactor was fed the resultant mixture.

The extended aeration unit effluent was used as feed only after attempts at sustaining denitrifying biofilm with various synthetic substrates had failed. Synthetic substrates used by Moore and Schroeder (96), Requa and Schroeder (110) and Stensel (128) were all tried without success. Biofilm grown originally on the disk using extended aeration effluent as growth medium, sloughed off and was eventually replaced by a milky, weak (sloughed easily) biofilm which did not denitrify. In all cases, make-up water was activated carbon-filtered Amherst tap

water. In an attempt to encourage growth, the organic carbon source was switched from methanol to glucose; again without success. To expedite this research effort, extended aeration unit effluent with methanol and supplemental nitrate added was used as feed during the kinetic experimentation. Vigorous denitrifying biofilm development resulted.

Next, problems with non-uniform growth were encountered when disks were stored for long periods of time (more than a day) in a horizontal position, as was the case in the RDR. Specifically, it was noted that significantly thinner biofilm developed on the underside of the disk. To eliminate differences in biofilm thickness between disk surfaces, disks were stored, in a vertical position, outside the RDR between experimental runs. The FBBR feed vessel-clarifier, depicted in Figure 5.10, offered a convenient location for vertical disk storage. Since extended aeration effluent, methanol and nitrate were also fed to this unit, the environmental conditions which existed there were similar to those in the RDR.

Experimental Procedure. For all experimentation, volumetric flowrate into the RDR was controlled at approximately 50 cm^3/min. The volumetric composition of the inflow was maintained, throughout, at an approximate ratio of ten parts extended aeration effluent to one part methanol -nitrate solution. Determination of Michaelis-Menten coefficients

required that reaction rates corresponding to a range of substrate concentrations be obtained. Therefore, nitrate-nitrogen feed concentrations of approximately 25, 50 and 100 mg/l were used in the RDR experimentation. Feed concentration was varied by changing the concentration of the methanol-nitrate feed solution.

An experimental run was initiated by filling a clean (no wall growth) reactor with a ten-to-one mixture of extended aeration effluent and methanol-nitrate solution. Nitrogen gas was then fed to the reactor at a relatively high rate to eliminate any oxygen contamination incurred during the filling operation. A biofilm covered disk was removed from the FBBR feed vessel-clarifier and its edge scraped so that only horizontal disk surfaces were biofilm covered. The biofilm was gently rinsed with extended aeration effluent to remove any loosely bound material. The disk was then placed in the reactor and the reactor covered. The reactor was again purged of oxygen by a brief high rate injection of nitrogen gas. When the DO meter indicated that anoxic conditions had been achieved, the gas flow rate was adjusted to the minimum level needed to maintain those conditions.

Inflow pumps were then turned on and adjusted to yield desired inflow rates and concentrations. Because nitrate levels in the extended aeration unit effluent were subject to fluctuation, inflow nitrate concentration to the RDR was monitored during operation by means of an Orion nitrate electrode (Model 92-07). It was observed

that for most runs, little or no variation in nitrate concentration occurred over the 3 or 4 hour period of experimentation. When the magnitude of variation did exceed 5 percent of the total nitrate conversion across the reactor, the data were discarded.

A Fisher Stedi-Speed stirrer was used to rotate the biofilm covered disk. Disk rotation was used as a means of eliminating external mass transfer limitation on observed reaction rate. In preliminary experimentation, it was determined that external transport effects were negligible for rotational speeds in the neighborhood of 150 rpm. The experimental backing for this is given in Section 5.1.3. Disk rotation was controlled at 150 rpm for subsequent experimentation.

The rotating disk reactor was operated, as described above, until steady-state was achieved. To determine when steady-state conditions had been attained within the RDR, reactor effluent nitrate concentration was measured intermittently. When no significant variation in concentration was observed between successive samples, the reactor was assumed to be at steady-state. Steady-state was normally realized in 3 to 5 reactor detention times.

In addition to nitrate concentration measurement, the DO, pH and temperature of the RDR contents were monitored during experimentation. Anoxic conditions were maintained within the reactor through control of the nitrogen gas flow rate. Although no direct control

was exercised over reactor pH and temperature, both parameters were observed to be approximately constant at values of 6.9 ± 0.1 and 22°C ± 1°C, respectively, during experimentation. Because rate kinetics are particularly sensitive to temperature, data were discarded when temperature variation during an experimental run exceeded 1°C.

To account for any nitrate conversion within the reactor, not attributable to the disk biofilm, a preliminary study was conducted in which the RDR was operated both with, and without, the growth-covered disk. After the RDR with disk had attained steady state, the disk was removed and the reactor allowed to again reach steady state. It was found that no nitrate reduction took place in the diskless reactor. It was, therefore assumed in subsequent experimentation, that all nitrate reduction observed in the RDR was due to the disk-supported biofilm.

In order to measure the thickness of biofilm developed on the disk surfaces, samples were taken by means of the removable slides previously mentioned. The film thickness was then measured using a microscope equipped with a stage micrometer. The procedure used is described as follows. A pencil mark was made on the slide surface (i.e., at the bottom of the biofilm). A mark was also made on a sliver of cover glass (approximately 1 x 5 mm). The cover glass was then placed mark down, crosswise, over the mark on the slide. The microscope was focused first on the slide mark, then on the cover glass mark. The difference in the micrometer readings provided the

thickness of the biofilm plus the marks. To correct for the thickness of the marks, the procedure was repeated on a bare portion of the slide; the thickness of the pencil marks was subtracted from the total thickness measured to yield the net biofilm thickness.

At least five measurements of biofilm thickness were made on each slide. For the relatively thin biofilms used in this study (δ < 350 microns) good film uniformity was observed, with the thickness usually varying less than 10 percent across the length of the slide. The RDR study was limited to these thin biofilms because of sloughing problems encountered for thicker biofilms under the turbulent conditions caused by disk rotation.

In addition to its thickness, the biofilm total and volatile solids content were also determined. This was accomplished by performing the appropriate analyses on a measured volume of biofilm which had been scraped from the disk surface.

5.1.2 Theoretical Analysis.

A theoretical analysis of substrate conversion by biofilm provides the basis for the determination of nitrate-biofilm effective diffusivity. This analysis is also useful for assessing the effect of variation in parameters such as bulk-liquid substrate concentration or biofilm thickness on substrate conversion rate.

Consider the differential biofilm element shown in Figure 5.4. A general substrate mass balance was given earlier by Equation 4.28. Specific terms for this balance equation, which apply to the RDR biofilm, are as follows:

$$\text{mass entering by intraphase transport} = 1/2\ A_T\ D_{SB}\ \left.\frac{dS}{dY}\right|_Y$$

$$\text{mass leaving by intraphase transport} = 1/2\ A_T\ D_{SB}\ \left.\frac{dS}{dY}\right|_{Y\ +\ \Delta Y}$$

$$\text{mass disappearing by reaction} = -\ 1/2\ A_T\ \Delta Y\ \frac{k\ \rho_B\ S}{K_S + S}$$

In which A_T = total biofilm surface area

accumulation = 0 at steady-state.

Entering these terms in Equation 4.28 and dividing by $1/2\ A_T\ \Delta Y$ yields:

$$D_{SB}\left[\frac{\left.\frac{dS}{dY}\right|_{Y+\Delta Y} - \left.\frac{dS}{dY}\right|_Y}{\Delta Y}\right] - \frac{k\ \rho_B\ S}{K_S + S} = 0 \qquad 5.1$$

Taking the limit as $\Delta Y \rightarrow 0$ gives

$$D_{SB}\ \frac{d^2S}{dY^2} - \frac{k\ \rho_B\ S}{K_S + S} = 0 \qquad 5.2$$

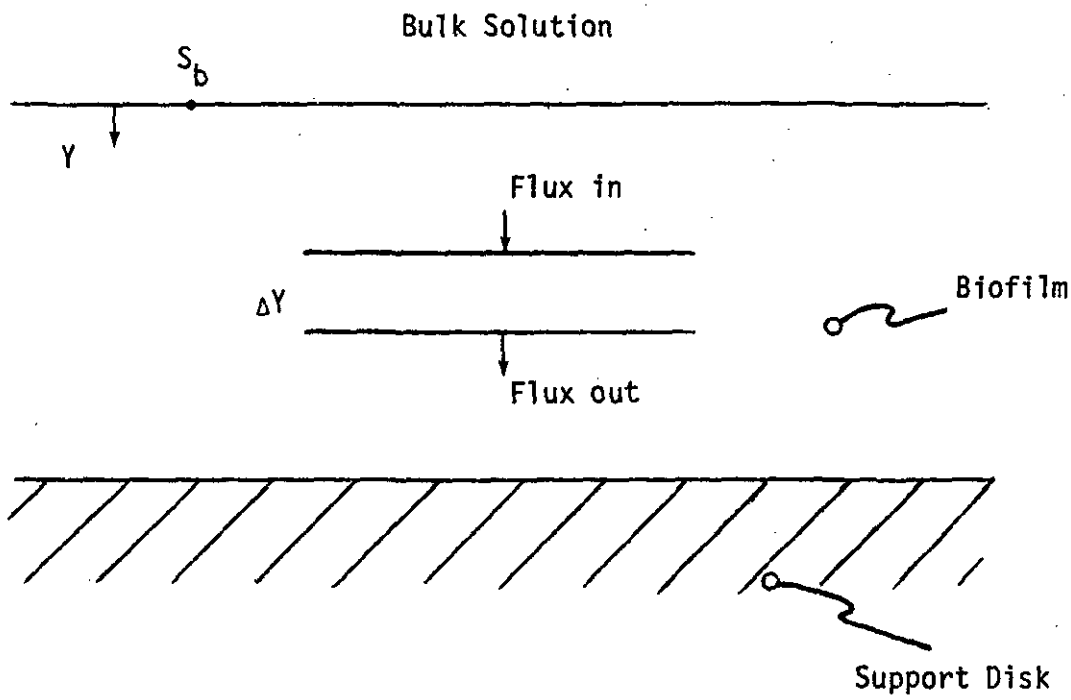

Figure 5.4 Differential Biofilm Element.

Because the disk is rotated to eliminate interphase mass transfer limitations, the boundary condition at the liquid-biofilm interface may be written:

$$S = S_b \quad \text{at} \quad Y = 0 \tag{5.3}$$

At the disk-biofilm interface, a no-flux boundary condition applies, thus:

$$\frac{dS}{dY} = 0 \quad \text{at} \quad Y = \delta. \tag{5.4}$$

where δ = biofilm thickness.

Equation 5.2 may be numerically integrated to yield the substrate concentration profile within a biofilm. Details of the numerical integration procedure are given in Appendix 3. The substrate concentration profile can, in turn, be integrated to determine the biofilm overall effectiveness factor η_o, defined for Michaelis-Menten kinetics and rectangular geometry as:

$$\eta_o = \eta_I = \frac{K_S + S_b}{\delta S_b} \int_0^{\delta} \frac{S}{K_S + S} \, dY. \tag{5.5}$$

Details of the procedure for numerical integration of Equation 5.5 are included in Appendix 3.

If the intrinsic Michaelis-Menten parameters k and K_S are known, Equations 5.2 and 5.5 can be used to calculate the effective diffusivity corresponding to an observed rate of reaction. The procedure used in this calculation is outlined below.

Under steady-state conditions, a substrate mass balance on the RDR may be written as follows:

$$Q\ (S_f - S_b) = A_T\ \delta\ R_o \qquad 5.6$$

in which Q = volumetric flow rate

S_f = substrate feed concentration

R_o = observed rate of reaction.

For kinetics described by the Michaelis-Menten rate expression, Equation 5.6 may be combined with Equation 4.9 and 4.10 to yield the following expression:

$$Q\ (S_f - S_b) - A_T\ \delta\ \eta_o\ \frac{k\ \rho_B\ S_b}{K_S + S_b} = 0 \qquad 5.7$$

Equation 5.7 is rearranged so that the overall effectiveness factor η_o may be written in terms of observable quantities.

$$\eta_o = \frac{Q\,(S_f - S_b)\,(K_S + S_b)}{A_T\,\delta\,\rho_B\,k\,S_b} \qquad 5.8$$

For a given RDR experimental run, all quantities to the right of the equality in Equation 5.8 are either measured or known; therefore η_o can be calculated. The effective diffusivity for the given run may be calculated as follows:

1. Calculate η_o using Equation 5.8
2. Assume a trial value for effectiveness diffusivity, $\hat{D}_{SB}$
3. Calculate a trial effectiveness factor $\hat{\eta}$ by numerical integration of Equation 5.2 and 5.5 using:
   (a) trial effective diffusivity, $\hat{D}_{SB}$.
   (b) known Michaelis-Menten parameters, k and K_S.
   (c) measured bulk-liquid substrate concentration, S_b, and measured biofilm thickness, δ.
4. Compare the trial effectiveness factor (step 3) with the observed effectiveness factor (step 1). If unacceptable, return to step 2 and repeat the procedure.

If a system's intrinsic Michaelis-Menten parameters and effective diffusivity are known, Equation 5.2 and 5.5 can be used to predict substrate conversion in the RDR. For a given set of operating conditions, Q and S_f, if the disk biofilm thickness is known, the reactor effluent

concentration, S_b, can be calculated by an iterative procedure as follows.

1. Specify: Biofilm parameters k, K_S, D_{SB}, ρ_B, operational parameters Q, So, A_T; biofilm thickness δ.
2. Assume a trial bulk-liquid (i.e., effluent) substrate concentration $\hat{S}_b$.
3. Calculate a trial biofilm effectiveness factor $\hat{\eta}_o$ by using $\hat{S}_b$ in the reactor substrate balance expression, Equation 5.8.
4. Calculate an independent (of step 3) trial biofilm effectiveness factor $\bar{\eta}_o$ by numerical solution of Equation 5.2 and 5.5 i.e., by a substrate mass balance on the biofilm.
5. Compare the effectiveness factors determined in steps 3 and 4. If unacceptable return to step 2.
6. Calculate substrate conversion X_C in the RDR as:

$$X_C = \frac{S_f - S_b}{S_f} \qquad 5.9$$

5.1.3 Results and Discussion

Michaelis-Menten Constants. A substrate mass balance on the rotating disk reactor resulted in Equation 5.2. Equation 5.2 as presented,

however, is not well suited for estimation of the Michaelis-Menten rate constants k and K_S. For this purpose it is useful to rearrange Equation 5.2 to the Lineweaver-Burk format as:

$$\frac{A_T \delta \rho_B}{Q (S_f - S_b)} = \frac{K_S}{\eta_o k} \cdot \frac{1}{Sb} + \frac{1}{\eta_o k} \qquad 5.10$$

To evaluate the intrinsic Michaelis-Menten coefficients, it is necessary that external and internal diffusional limitations be eliminated, i.e., that the overall effectiveness factor, η_o, be unity. External diffusional limitation can be controlled by rotation of the biofilm support disk. The rotational speed required to eliminate external diffusional limitation is determined experimentally by holding all conditions constant within a RDR except disk rotational speed. When an increase in rotational speed does not result in an increase in substrate conversion rate, external diffusional limitation has been eliminated.

Using a rotating disk reactor identical to that used in this study, LaMotta (77) examined the effect of disk rotational speed on substrate conversion rate. The results of LaMotta's study, shown in Figure 5.5, indicate that external mass transfer limitation is appreciable for rotational speeds under 70 rpm. To verify these results, the effect of rotational speed on substrate conversion rate was examined as part of this research. The results of this study are also shown in Figure

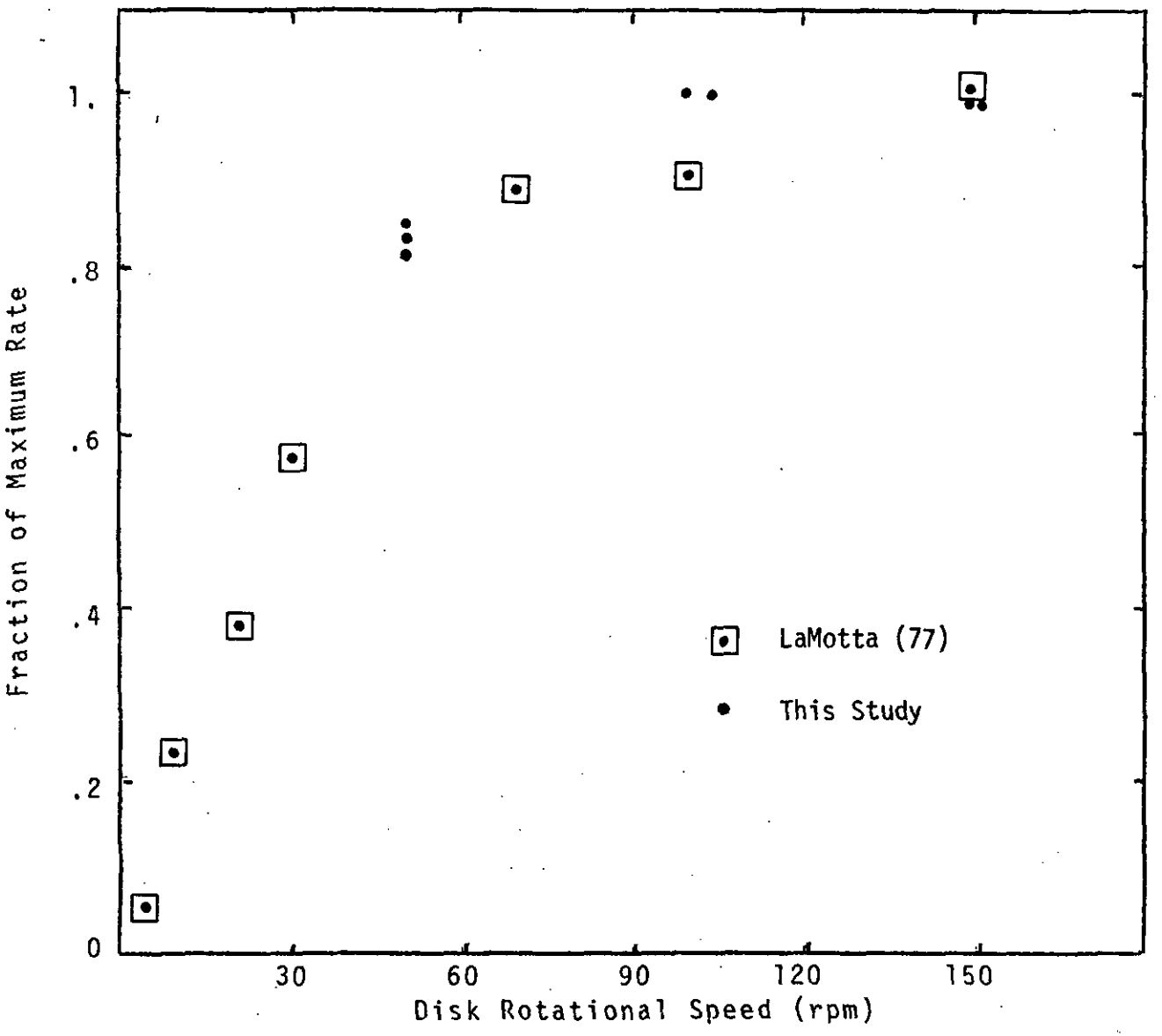

Figure 5.5 The Effect of Disk Rotational Speed on External Mass Transfer Limitations.

5.5. Raw data for this experimentation is included in Appendix 4. Based on the information presented in Figure 5.5 it was concluded that external mass transfer limitations are negligible when disk rotational speed is in the 150 rpm range. Rotational speed was controlled at 150 rpm for subsequent experimentation.

To evaluate internal diffusional resistance, researchers in the field of heterogeneous catalysis commonly reduce the size or thickness of a catalyst and observe the effect of this reduction on observed rate. When a decrease in catalyst dimension is not accompanied by an increase in observed rate, it is assumed that internal mass transfer resistance is negligible and that the observed rate is, in fact, intrinsic.

A similar approach was used in this research. For a given set of operating conditions, the effect of biofilm thickness on observed reaction rate was examined. When a decrease in biofilm thickness was not accompanied by an increase in reaction rate, it was assumed that the kinetics observed were intrinsic.

To obtain the intrinsic data necessary to construct a Lineweaver-Burk plot, reaction rates corresponding to a range of bulk-liquid substrate concentrations must be determined. Toward this end, RDR feed concentrations of approximately 25, 50 and 100 mg/l NO_3^- - N were used. For each feed concentration, experimental runs were conducted at various

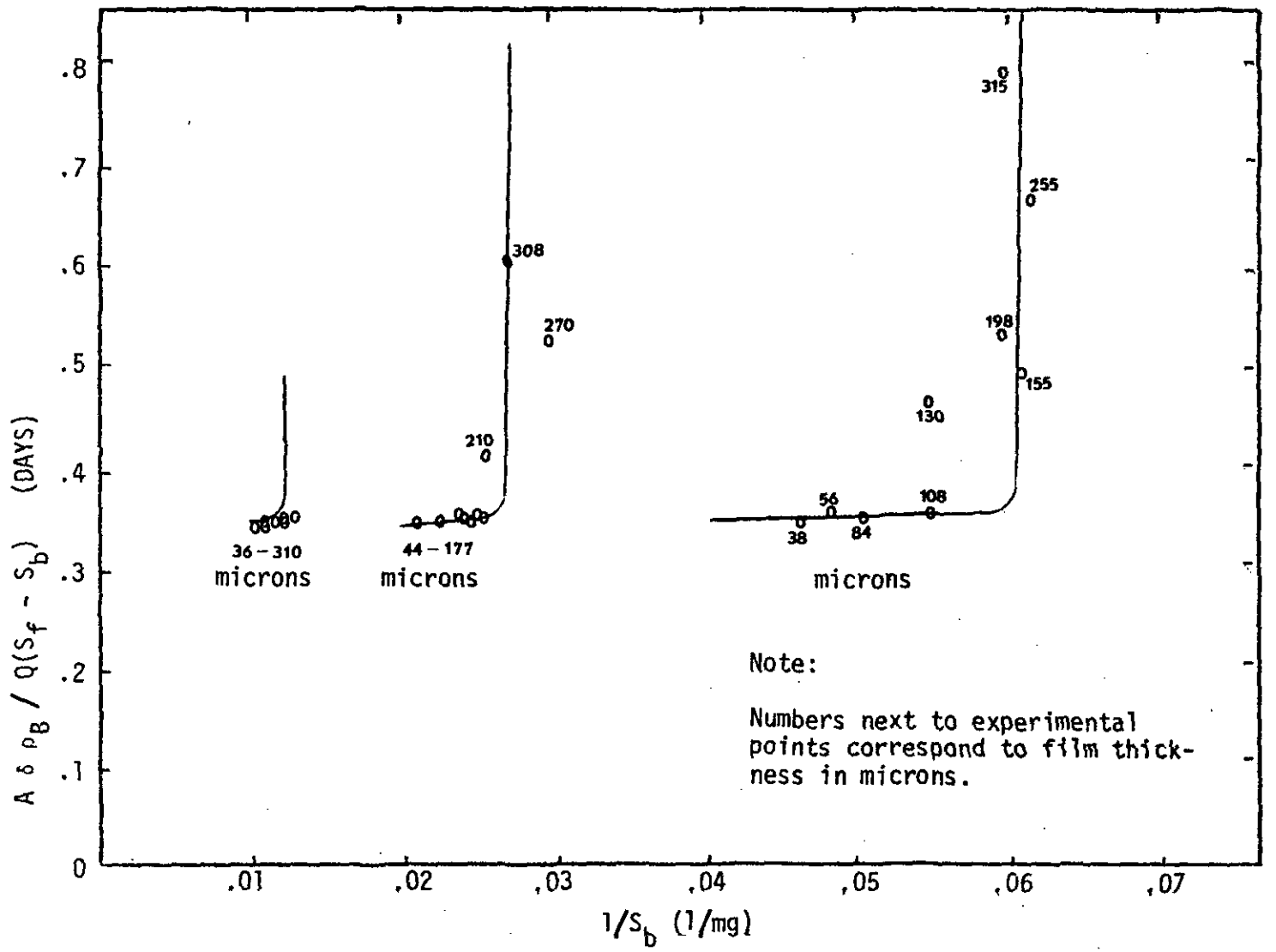

Figure 5.6. Lineweaver-Burk Plot of the RDR Data.

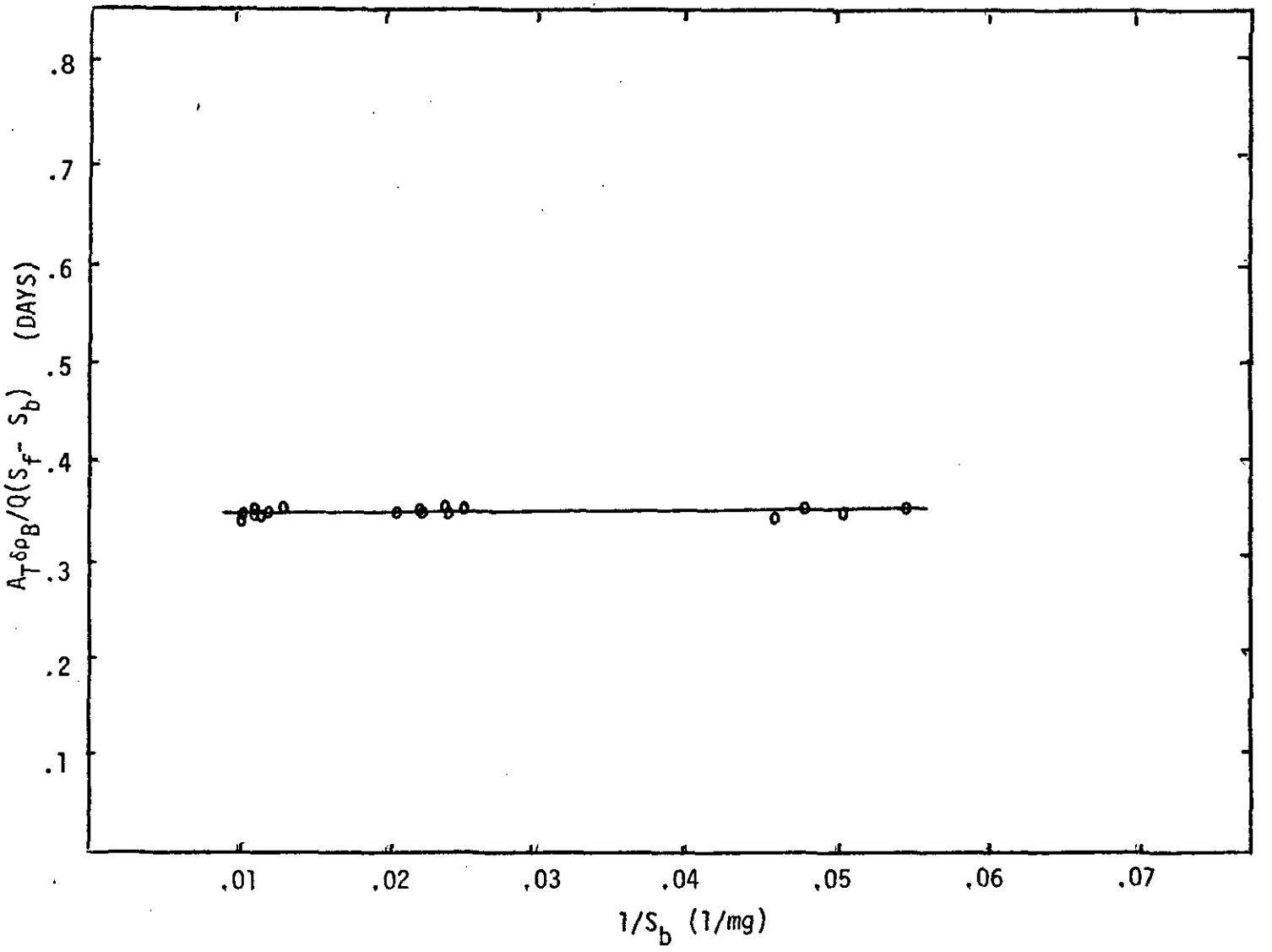

Figure 5.7. Lineweaver-Burk Plot of the Intrinsic RDR Data.

biofilm thicknesses. It was observed that for each feed concentration, a critical biofilm thickness existed, beyond which observed rate, on a per unit biomass basis, decreased sharply. This phenomenon is clearly evident in the Lineweaver-Burk plot of the RDR data, Figure 5.6. The reaction rates obtained for experimental runs in which the biofilm thickness was less than the critical value were used to determine the intrinsic Michaelis-Menten constants, k and K_S. These intrinsic data have been replotted in Figure 5.7. Using the data shown in Figure 5.7, the least squares best estimate of the Michaelis-Menten constants are as follows:

$$k = 2.875 \ \frac{\text{mg } NO_3^- - N}{(\text{mg V.S.})(\text{DAY})}$$

$$K_S = 0.0607 \text{ mg/l } NO_3^- - N.$$

The 95 percent confidence intervals for the estimates are:

$$2.873 \leq k \leq 2.878 \ \frac{\text{mg } NO_3^- - N}{(\text{mg V.S.})(\text{DAY})}$$

$$0 \leq K_S \leq 0.3077 \text{ mg/l } NO_3^- - N$$

for pH = 6.9 ± 0.1 and temperature = 22°C ± 1°C.

Effective Diffusivity. Having obtained the Michaelis-Menten constants k and K_S, the RDR data were analyzed using the theoretical approach for effective diffusivity presented in Section 5.1.2. This analysis yielded a value for effective diffusivity for each of the RDR experimental runs. The resultant 95 percent confidence internal estimate for the mean nitrate effective diffusivity in biofilm is:

$$D_{SB} = (0.815 \pm 0.617) \times 10^{-5} \text{ cm}^2/\text{sec}$$

for $T = 22^{\circ}C \pm 1^{\circ}C$.

This value is approximately 50 percent of the diffusivity of nitrate in an aqueous solution at the same temperature (106).

The values of D_{SB}, k and K_S obtained for denitrifying biofilm were used as input data to the theoretical analysis for substrate conversion by biofilm presented in Section 5.1.2. For a given feed substrate concentration, biofilm thickness was specified and the resultant effluent concentration and substrate conversion rate were calculated. By varying biofilm thickness and repeating the theoretical analysis, the solid curves shown on Figure 5.6 were generated. These theoretical curves provide a good fit to the observed data.

It is of interest to compare the rate constants with denitrification constants reported in the literature. Table 5.1 presents zero-order rate constants (approximately equal to the parameter, k,

Table 5.1 Literature Zero Order Denitrification Rate Data.

Organism	Temperature °C	Zero Order Denitrification Rate Data mg NO_3^- - N/(mg V.S.)(DAY)	Reference
Micrococcus denitrificans	37	1,42	23
Micrococcus denitrificans	32	1,34	108
Activated Sludge	20	,02-,03	32
Activated Sludge	20	,01-22	65
Spirillum (Undula?)	25	2,88	94
Activated Sludge	20	,85	96
Activated Sludge	8	,03	100
	11	,02-34	
	25	,33-,58	
Activated Sludge	20	,04	11
Pseudomonas denitrificans	5	,32-42	31
	20	1,57-1,72	
	27	3,94-4,32	
Biofilm	27	,05-1,3	124
Biofilm	25	,21-,31	110

used in this research) reported by various investigators of biological denitrification. The low values reported for denitrification with activated sludge can be attributed to the fact that only a fraction of the biomass measured as volatile solids are actually active in denitrification. The low values reported for biofilm denitrification rate are likely the result of diffusional limitation which mask intrinsic kinetics.

5.2 Fluidized Bed Biofilm Reactor - Bed Expansion

The purpose of the bed expansion study was to develop a correlation for expansion index, n, applicable to the FBBR. Basically, this experimentation involved varying the superficial velocity through the laboratory FBBR and observing the effect of this variation on bed porosity for an range of film thicknesses. The expansion index n corresponding to a given biofilm thickness (more specifically to a given terminal Reynolds number) was obtained as the slope of the resulting log U - log ε plot. Background information for this study was given in Sections 3.2 and 4.2.

5.2.1 Materials and Methods

The Experimental FBBR. A schematic of the laboratory FBBR is given in Figure 5.8. A photograph of the apparatus is shown in Figure 5.9. The reactor was fabricated from 3.8 cm I.D. plexiglass column. Screened sampling plots were provided along the column length which allowed exclusion of gross reactor solids from liquid samples. Separate sampling ports were provided for solids removal. Approximately 12 cm of pea gravel was used at the reactor inlet to provide even flow distribution and prevent backflow of support media.

A Masterflex pump was used to deliver feed solution to the FBBR.

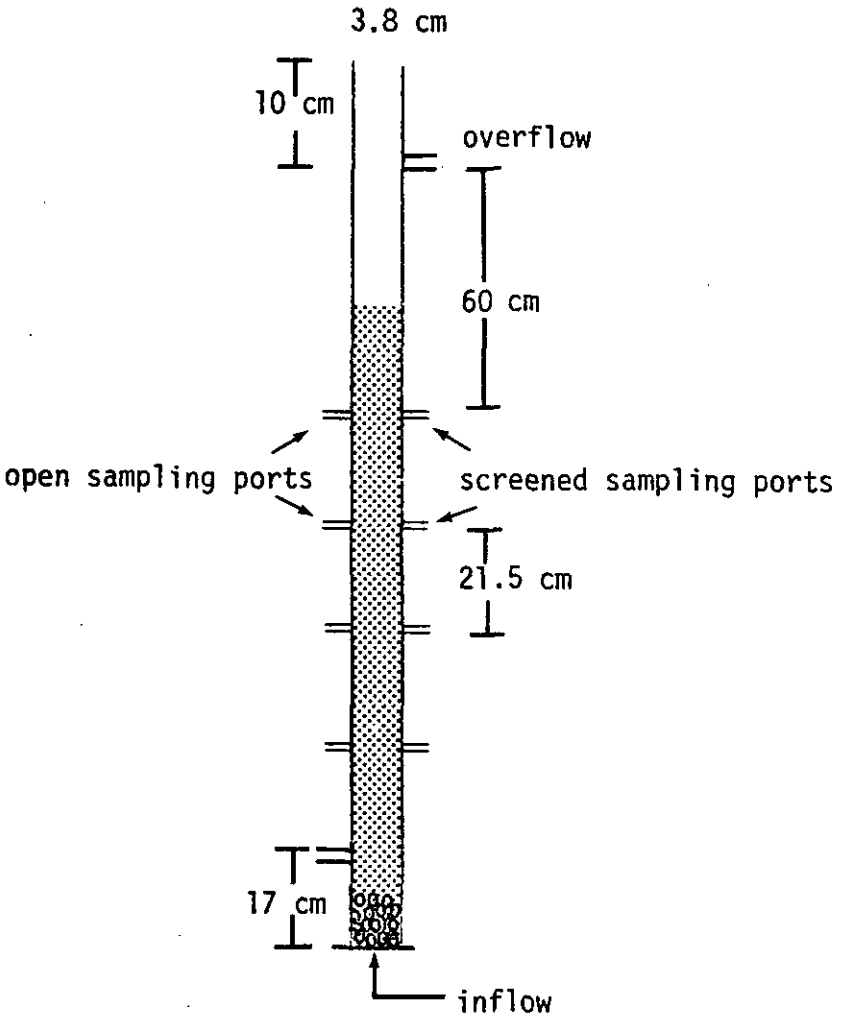

Figure 5.8 Schematic of the laboratory FBBR.

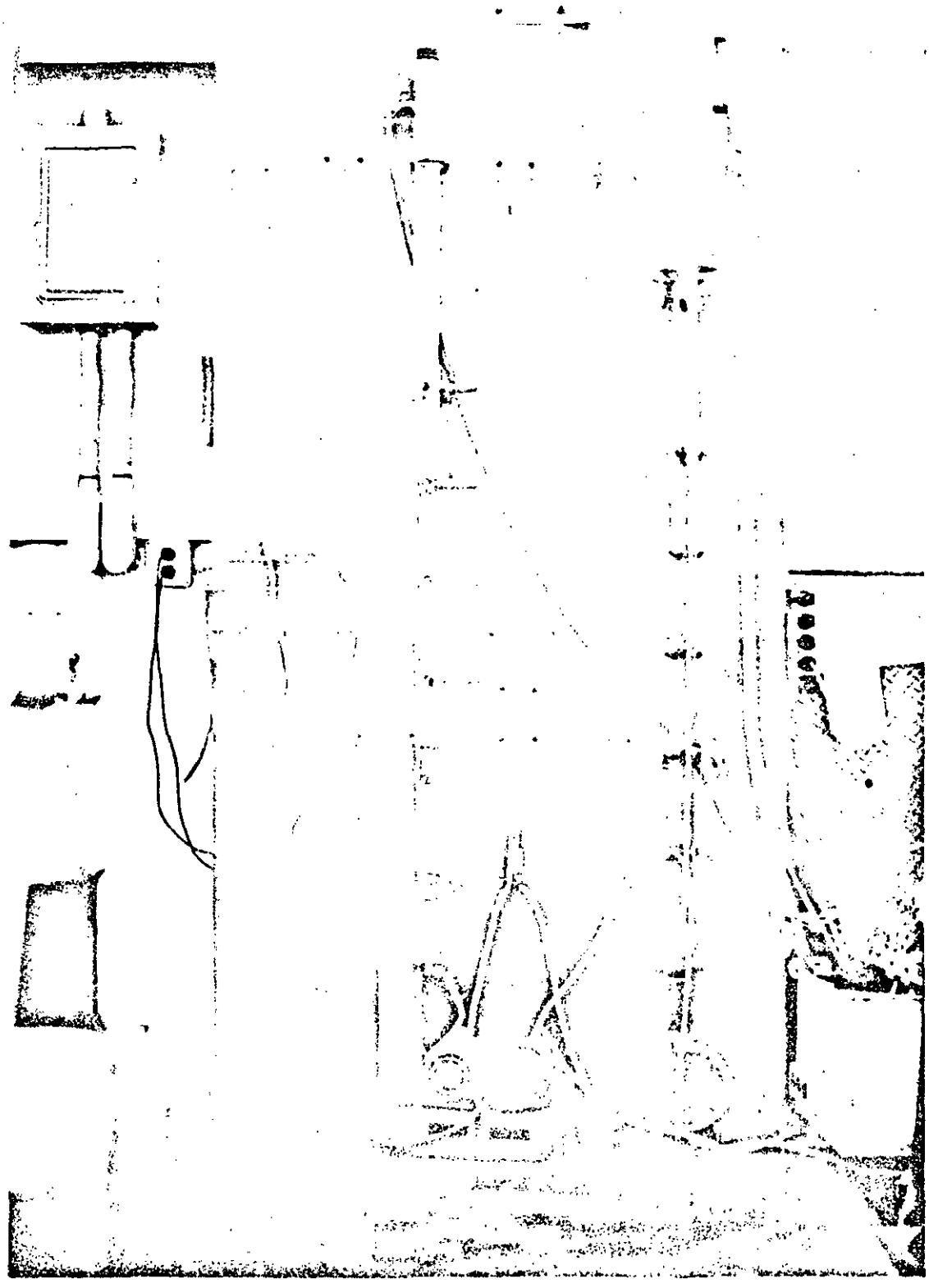

Figure 5.9 Photograph of the laboratory FBBR

The reactor feed consisted of clarified effluent from an extended aeration unit at the University of Massachusetts Wastewater Pilot Plant; methanol and supplemental nitrate ($NaNO_3$) were added. To insure that methanol did not limit the biological process, weight ratios of at least 6:1,methanol to nitrate-nitrogen were supplied. As was the case with the RDR, the mixture of extended aeration unit effluent and methanol nitrate solution was used as feed to the FBBR only after attempts at sustaining denitrifying biofilm on various synthetic substrates (see Section 5.1) had failed. The extended aeration unit effluent was pumped into the pilot plant building by a centrifugal pump situated over the extended aeration unit clarifier. This pump delivered effluent to a feed vessel (a 750 ml flask) housed in the FBBR clarifier as depicted in Figure 5.10. The solution of methanol and nitrate was pumped at a rate of approximately 5 cm^3/min to the feed vessel by a Masterflex pump. The intake of the FBBR feed pump was also located in the feed vessel (hence its name). Because the inflow rate to the feed vessel was at least 50 percent greater than the outflow rate due to the FBBR feed pump, the contents of the feed vessel were not diluted by the bulk-clarifier contents. However, in the event that extended aeration unit effluent flow to the feed vessel was interrupted, the FBBR would continue to operate in a closed loop with the bulk-clarifier contents supplying the feed vessel.

The biofilm growth support media used in this study were 25-30 mesh (590-710 micron) spherical glass microbeads.

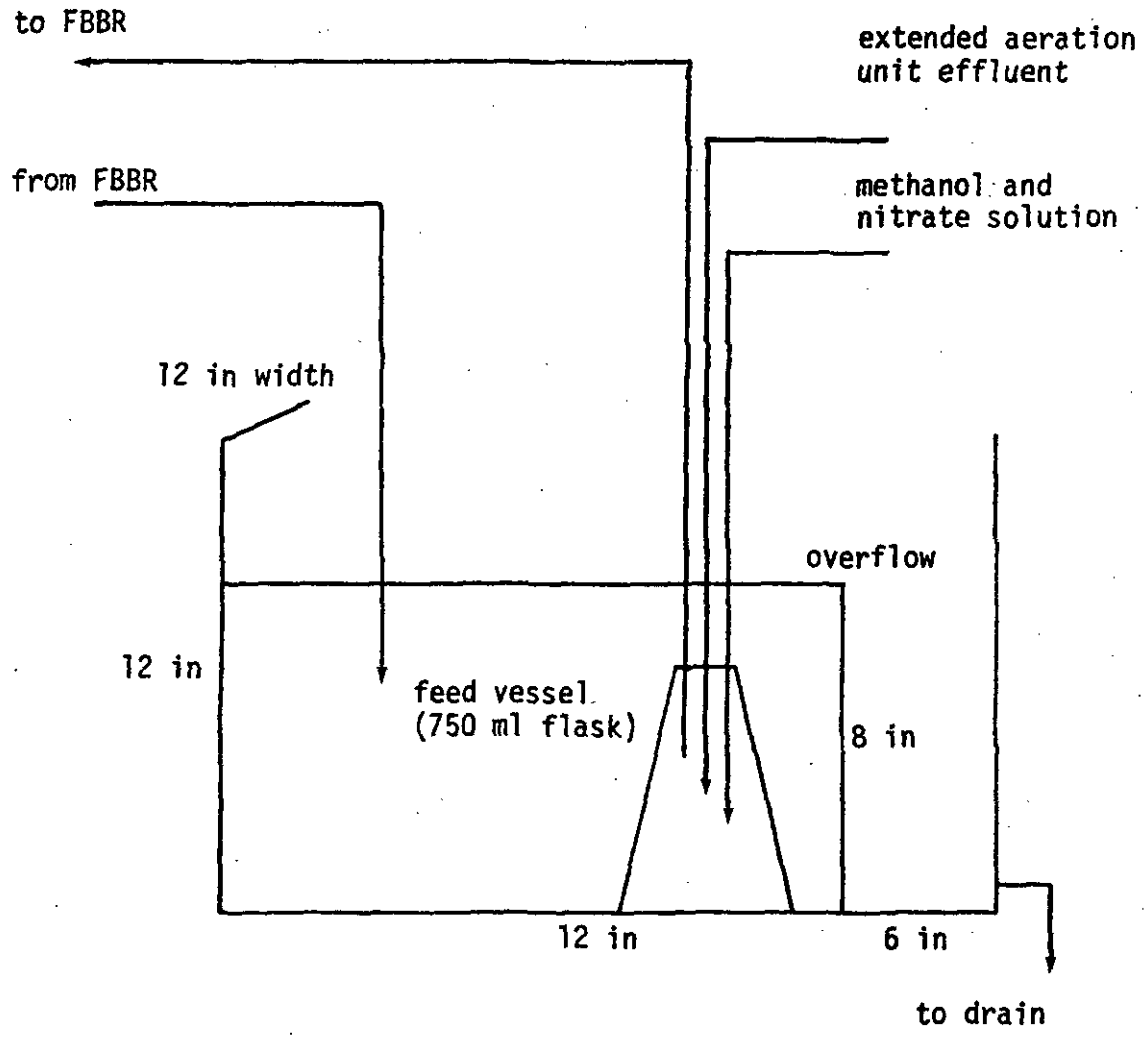

Figure 5.10 FBBR feed vessel and clarifier.

To provide a more accurate description of media size than is provided by sieve analysis, the diameters of a sample (N = 100) of the microbeads were measured using a microscope with ocular micrometer. The result is expressed in terms of a volume surface mean or Sauter mean diameter which has particular application in mass transfer or catalytic reaction studies (36). It was found that:

$$\text{Sauter } \bar{d}_m = 682.15 \text{ microns}$$

Seeding of the FBBR was accomplished by expanding the media bed with feed solution at a superfical velocity of approximately 0.7 cm/sec. A growth interface, which separated clean from biofilm covered support media, was observed to propagate downward through the expanded bed. When the bed was allowed to expand, unchecked, large (4-5 mm) balloon-like bioparticles collected at the top of the bed. This situation was remedied by regularly (twice a day) agitating the bed with a steel rod. This prevented build up of outsized particles and resulted in uniform biofilm thickness throughout the bed.

At the start of an expansion run, superficial upflow velocity was increased to approximately 1.5 cm/sec and a portion of the growth covered media was removed through sampling ports at the top and bottom of the expanded bed. This removal further eliminated biofilm thickness variation at the bed extremes, assuring an even more uniform biofilm thickness throughout the reactor. In addition, the interface

between seeded and unseeded media near the bottom of the bed, which served as a datum for all FBBR experimentation, was made more distinct by this removal. For each experimental run, before superficial velocity variation was begun, it was necessary to establish the basis for calculation of bed porosity in terms of the easily observable parameter, bed height. By the definition of porosity, the following may be written:

$$\varepsilon = 1 - \frac{V_S}{H_B A} \qquad 5.11$$

in which V_S = total solids (biofilm + media) volume in $H_B A$.

Thus, if the total solids volume in the expanded bed is known, bed porosity and bed height are related by the simple expression, Equation 5.11. In this study, V_S was determined as follows.

Bioparticles were removed from the laboratory FBBR by carefully lowering a vial into the expanded bed and allowing it to fill with growth covered particles. Great care was taken during this operation to avoid any shearing of biomass from the support particles. An average bioparticle diameter d_p (and thus biofilm thickness δ) was determined by direct measurement of at least 50 particles using a microscope with ocular micrometer. After determining bioparticle diameter, superficial velocity was measured (bucket and stopwatch tech-

nique) and the corresponding expanded bed height $H_B|_1$ recorded. A volume of solids was then withdrawn from the reactor through a sampling port and the new expanded bed height $H_B|_2$ noted. The total and volatile solids concentration of the withdrawn sample was determined. The support media was separated from the ash which remained after volatile solids ignition, rinsed, dried and weighed. The number of bioparticles in $\Delta H_B = H_B|_1 - H_B|_2$ could then be calculated using the media density and average diameter as follows:

$$\begin{matrix}\#\ \text{particles} \\ \text{in}\ \Delta H_B\end{matrix} = \frac{\text{mass of media in}\ \Delta H_B}{(\rho_m)\left(\frac{\pi}{6}\ d_m^{\,3}\right)} \qquad 5.12$$

The total volume of solids remaining in the growth covered portion of the expanded bed could then be calculated as:

$$V_S = \frac{H_B|_2}{\Delta H_B}\left[\left(\begin{matrix}\#\ \text{Particles in} \\ \Delta H_B\end{matrix}\right)\left(\frac{\pi}{6}\ d_p^{\,3}\right)\right] \qquad 5.13$$

Thus, bed porosity could be related directly to measured bed height by Equation 5.11.

During an expansion run, superficial velocity was decreased, the resultant bed height measured and the bed porosity calculated using Equation 5.11. Superficial velocity was decreased rather than increased during expansion runs after it was observed that the increase in turbulence associated with the latter procedure caused significant sloughing of biofilm which resulted in non-linear log U - log ε plots.

Examples of FBBR expansion plots are given in Figure 5.11. The expansion index, n, is the slope of the log U - log ε plot.

The procedure outlined above was repeated for several different biofilm thicknesses i.e., for several d_p's. Biofilm thickness was varied by varying the amount of support media within the FBBR. In general, the more media used, the thinner were the resultant equilibrium biofilms.

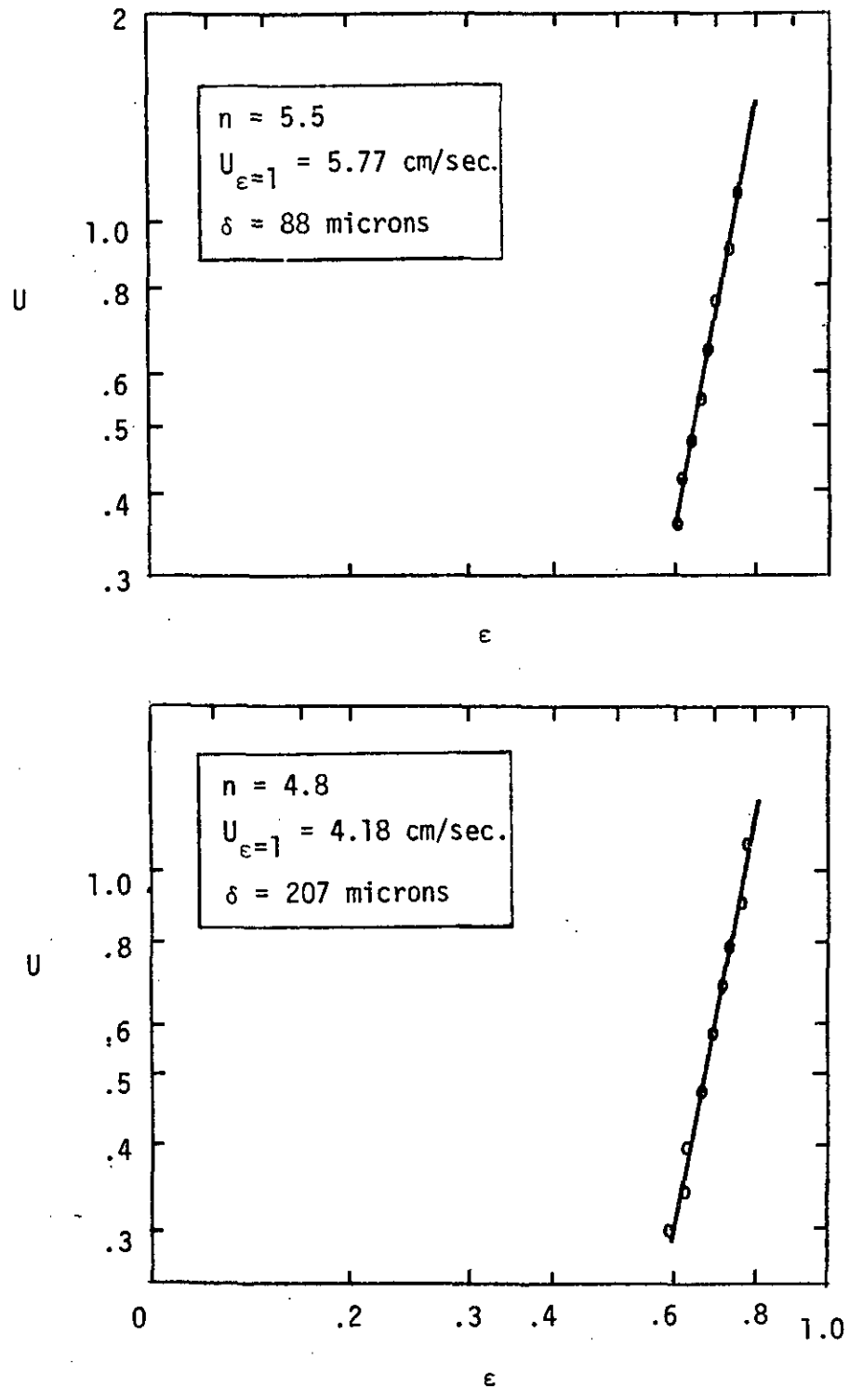

Figure 5.11 Typical FBBR Bed Expansion Data

5.2.2 Results and Discussion

The results of the FBBR bed expansion study are tabulated in Appendix 4. Each set of data was analyzed by the least squares technique to obtain "best fit" values for the expansion index n and the extrapolated superficial velocity intercept at $\varepsilon = 1$, U_i. For nineteen of the twenty sets of data, correlation coefficients in excess .99 were obtained. This indicates that the linear expression, Equation 3.24, provides an excellent description for FBBR bed expansion.

The values obtained by the least squares analysis are included in Appendix 4. In attempting to correlate the expansion data, dimensional analysis leads to the conclusion that the expansion index n is likely a function of terminal Reynolds number Re_t. This dependence of n on Re_t was experimentally verified by Richardson and Zaki (114) as indicated by their expansion index correlation, Equation 3.25-3.29. Specifically, these researchers found a linear relationship to exist between log n and log Re_t. Based on this experience, FBBR bed expansion behavior was correlated by a linear log n - log Re_t expression. A log n versus log Re_t plot is presented in Figure 5.12. The numbers beside each data point represent biofilm thicknesses. Details of the procedure used to determine Re_t are presented in Section 5.3 of this dissertation.

A least squares analysis of the data presented in Figure 5.12 was used to obtain the following correlation for expansion index n:

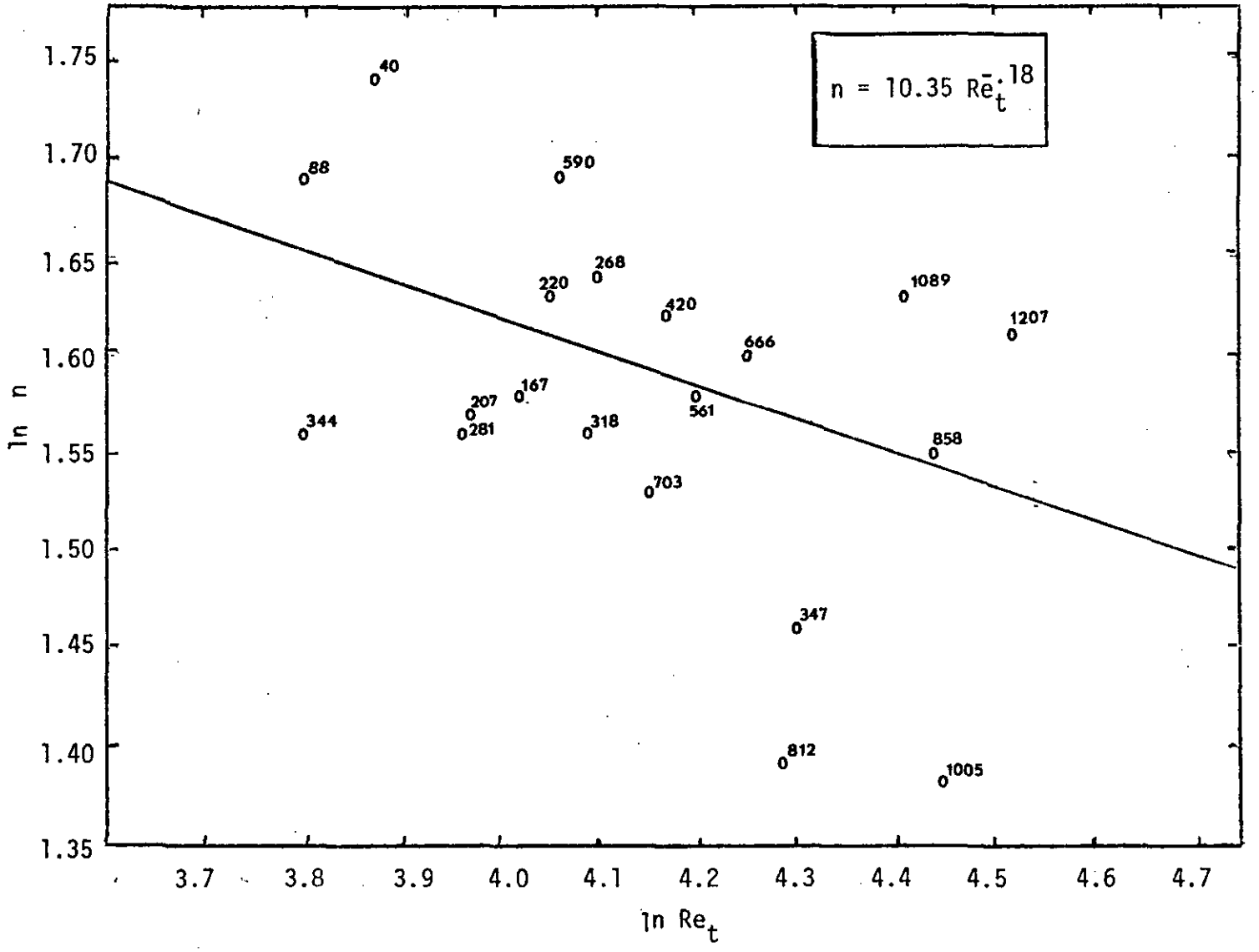

Figure 5.12. Expansion index versus Reynolds number; a log-log plot.

$$n = 10.35\ Re_t^{-.18} \qquad 5.14$$

It is noted that the correlation coefficient for this equation is only -.43. Because of this low correlation coefficient, a statitistical test for independence was performed on these data. The null hypothesis, Ho : $\rho = 0$, was rejected at the 10 percent level of significance indicating statistically significant correlation of n with Re_t. Although this low correlation coefficient indicates significant differences between observed and predicted (by the correlation) values of expansion index, it can be shown that the bed porosity-superficial velocity relationship is rather insensitive to these differences.

Consider the δ = 1005 micron data point of Figure 5.12 which lies far from the best fit line. The expansion observed for this film thickness was 4.01; that calculated by the correlation equation is 4.64. The error in the predicted value is approximately 16 percent. Now, assuming a typical superficial velocity of 0.8 cm/sec and using the observed intercept velocity of 2.69 cm/sec, bed porosities are calculated below using both the observed and the correlation expansion indices:

$$\text{observed, } n = 4.01: \qquad \varepsilon = \left[\frac{.8}{2.69}\right]^{1/4.01} = .74$$

$$\text{correlation, } n = 4.64 \qquad \varepsilon = \left[\frac{.8}{2.69}\right]^{1/4.64} = .77$$

a difference of only 4 percent.

For comparison sake, the correlation developed by Richardson and coworkers (113, 114) for rigid spheresin similar Re_t range is presented here. By assuming the aspect ratio d_p/D to be negligible, the correlation developed by these researchers may be written as:

$$n = 4.4\ Re_t^{-.1} \qquad 1 < Re_t < 500 \qquad 5.15$$

It is noted that, as expected, expansion indices observed in the FBBR are uniformly higher than predicted by the Richardson-Zaki correlation, Equation 5.1. In addition, the correlation developed here indicates a stronger dependence of expansion index n on Re_t than observed with rigid spheres. And finally, the expansion behavior of a FBBR appears to be less "quantifiable" than possible with rigid particles. This is evidenced by the significant scatter of data shown in Figure 5.12.

As mentioned in Section 4.2, it has been reported in the literature (49) that biofilm volatile solids density ρ_B is a function of biofilm thickness δ. Although clear evidence of this dependence was not observed in the RDR portion of this study (which was limited to relatively thin biofilms), a pronounced dependence of density on film thickness was observed in the FBBR. This is indicated in Figure 5.13. The solid lines shown in Figure 5.13 were drawn by eye and are described, mathematically by Equations 4.17 a, b and c.

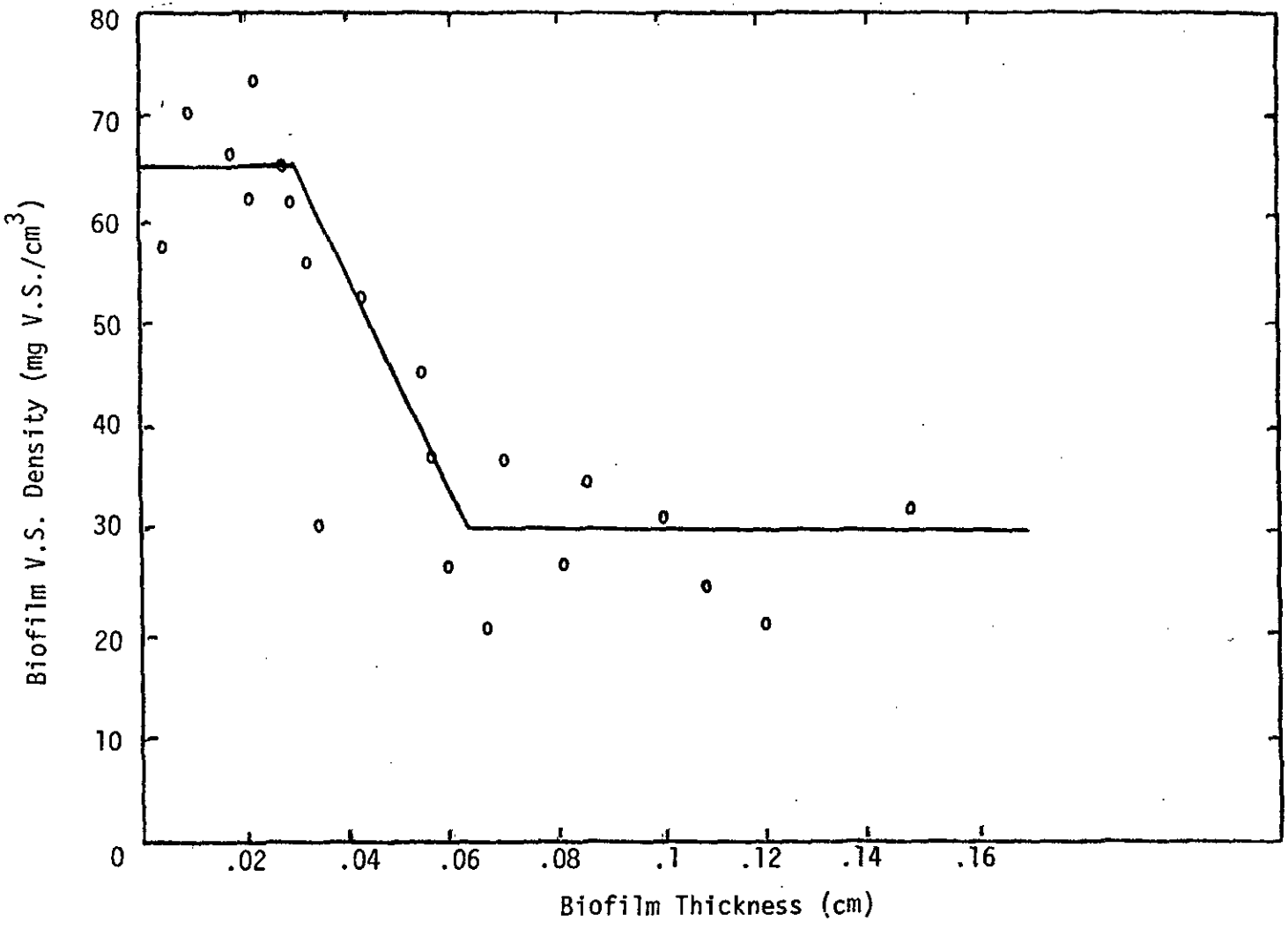

Figure 5.13. Biofilm V.S. density versus biofilm thickness.

5.3 Fluidized Bed Biofilm Reactor - Bioparticle Terminal Velocity

The objective of this segment of the experimentation was to develop a drag coefficient-Reynolds number correlation which could be used, with Equation 4.20, to predict the terminal velocity of a bioparticle.

The bioparticle terminal velocity determination served a dual purpose in that it provided a basis for prediction of the expansion curve superficial velocity intercepts at $\varepsilon = 1$, U_i and it provided the terminal Reynolds numbers needed in developing the expansion index - terminal Reynolds number correlation presented in Section 5.2.

5.3.1 Materials and Methods

Equation 4.20 can be rearranged so that drag coefficient can be expressed in terms of observable quantities as:

$$C_D = \frac{4\ (\rho_S - \rho_L)\ g\ d_p}{3\ \rho_L\ U_t^2} \qquad 4.20$$

For a given experimental run, the average bioparticle diameter d_p, was determined as described in Section 5.2. Also determined in Section 5.2 were the total solids, volatile solids, mass of support media and number of support particles in the sampled segment of the FBBR. Thus,

bioparticle density, ρ_S, could be calculated as outlined in the fluidization algorithm of Section 4.2.

As described in Section 5.2, during each experimental run a bioparticle sample was carefully removed from the expanded bed and a portion of the sample used to determine an average bioparticle diameter. The remainder of the sample was allowed to settle through a 14 cm ID x 195 cm water filled plexiglass column. By timing particle descent through a 120 cm segment of the column, terminal velocity was determined. At least fifty individual settlements were conducted for each biofilm thickness. The individual measurements were averaged to obtain the terminal velocity representative of the given biofilm thickness.

The properties of the fluid phase, ρ_L and μ, were determined by relating tabulated values (106) to the water temperature measured in the settling column.

The information needed to calculate drag coefficient using Equation 4.20 was, therefore, available.

The corresponding terminal Reynolds number was, in turn, calculated using Equation 4.23.

By repeating the procedure outlined above for FBBR experimental runs with different equilibrium biofilm thicknesses, a data base for the drag coefficient-Reynolds number correlation was obtained.

5.3.2 Results and Discussion

For each of the twenty FBBR experimental runs, terminal Reynolds number and the corresponding drag coefficient were determined, as described in Section 5.3.1. A log-log plot of these data is given in Figure 5.14. A least squares analysis was used to obtain the best fit line shown in this figure. The resultant drag coefficient-Reynolds number correlation, which is specific for FBBR bioparticles, was presented in Chapter 4 as:

$$C_D = 36.66\ Re^{-2/3} \qquad 4.21$$

The correlation coefficient for the expression is -.74.

Combining this correlation equation with Newton's law, Equation 4.20, an explicit expression for bioparticle terminal velocity is obtained. This expression was also presented in Chapter 4 as Equation 4.22.

$$U_t = \left[\frac{(\rho_S - \rho_L)\ g\ d_P^{5/3}}{27.5\ \rho_L^{1/3}\ \mu^{2/3}} \right]^{3/4} \qquad 4.22$$

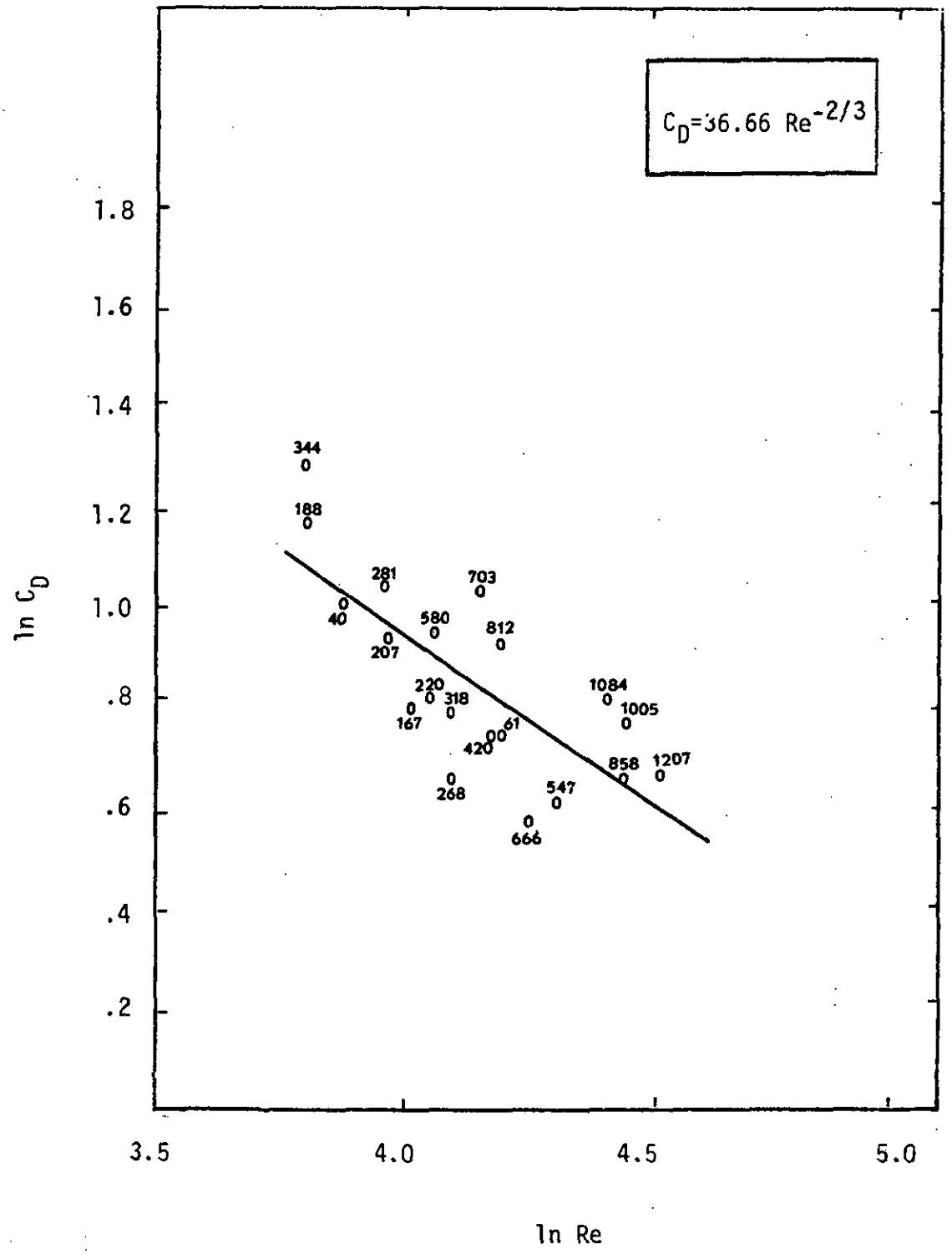

Figure 5.14 Log-log Plot of Drag Coefficient vs. Reynolds Number.

5.4 Fluidized Bed Biofilm Reactor - Biomass Holdup and Nitrate Profiles.

In this section, biomass holdup and nitrate profiles measured in the laboratory FBBR are compared with values predicted by the FBBR are compared with values predicted by the FBBR mathematical model. Input parameters to the FBBR model include the nitrate effective diffusivity and intrinsic Michaelis-Menten coefficients determined in the RDR experimentation. Input correlations to the FBBR model, developed as part of this research, relate biofilm volatile solids density to biofilm thickness, drag coefficient to Reynolds number and expansion index to terminal Reynolds number.

5.4.1 Materials and Methods

The laboratory FBBR and its operation were described in Section 5.2. Nitrate profiles through the reactor were obtained by the following procedure. During each bed expansion run (cf. Section 5.2) flow variation was interrupted to allow the nitrate concentration distribution throughout the bed to be measured. To avoid any transients which result from altered upflow velocity and concentration, at least one half hour (roughly ten detention times) was allowed to elapse between a flow variation and a nitrate profile measurement. After this period, several nitrate profiles were taken to assure that steady-state had been realized. Steady-state was assumed when no

significant variation in nitrate concentration was noted between successive profiles.

Nitrate-nitrogen profiles were obtained by withdrawing liquid samples from five screened sampling ports along the length of the reactor. Additional samples were obtained at the reactor inlet and overflow. Samples were withdrawn in order of largest to smallest space time, $\tau = ZA/Q$. To minimize hydraulic upset of the expanded bed, the rate of liquid sample withdrawal was kept below two percent of the upflow rate.

Samples were analysed for nitrate-nitrogen using an Orion specific ion meter Model 407A with an Orion specific ion electrode Model 93-07.

In addition to nitrate measurements, dissolved oxygen, pH and temperature were also monitored during FBBR experimentation.

Dissolved oxygen levels in the FBBR influent were under 0.2 mg/l for all runs. Effluent dissolved oxygen concentrations, measured by lowering the DO probe directly into the experimental reactor were consistantly zero.

Influent pH was found to be 6.9 ± .1. Hydroxide ion produced during biological reduction of nitrate caused an increase in pH across the FBBR of up to one unit.

The liquid temperature during all experimental runs was 21°C ± 2°C.

To predict biomass holdup and substrate conversion in the laboratory reactor using the FBBR model, a total of thirteen parameters and

six correlations must be specified. Numerical values for the parameters used in generating the predicted values presented in this section are given in Table 5.2.

5.4.2 Results and Discussion

For each of the twenty biofilm thicknesses examined in this research, a nitrate profile through the laboratory FBBR was measured. Typical plots showing observed and predicted values for biofilm thickness, total volatile solids concentration and nitrate profiles are presented in Figures 5.15, 5.16 and 5.17. Data for the other experimental runs is presented in Appendix 4.

In general, there was good agreement between conditions observed in the laboratory FBBR and those predicted by the mathematical model. It was observed, however, that as biofilm thickness increased beyond 300 microns, the ability of the model to accurately predict nitrate reduction decreased significantly. This phenomenon is probably linked to the decreasing biofilm volatile solids density observed in this film thickness region. A possible explanation for this is that the biofilm parameters k, K_S and D_{SB} may not be independent of biofilm density as assumed in development of the model. It seems especially unlikely that the effective diffusivity D_{SB} would be unaffected by variation in biofilm density. Unfortunately, detailed study of this phenomenon was not possible in the rotating disk reactor due to the limitation to relatively thin biofilms imposed by the turbulent conditions within the RDR.

Table 5.2 FBBR Model - Numerical Values for Input Parameters.

D_{SL}	=	1.67 E-5 cm^2/sec
ρ_L	=	.998 g/cm^3
μ	=	.009548 g/cm·sec
D_{SB}	=	.815 E-5 cm^2/sec
k	=	3.32 E-5 /sec
K_S	=	6.06 E-8 g/cm^3
$S_b\|_{Z=0}$	=	specify for each run
Q	=	specify for each run
A	=	11.4 cm^2
H_B	=	specify for each run
ρ_m	=	2.42 g/cm^3
d_m	=	682 E-4 cm
V_m	=	specify for each run

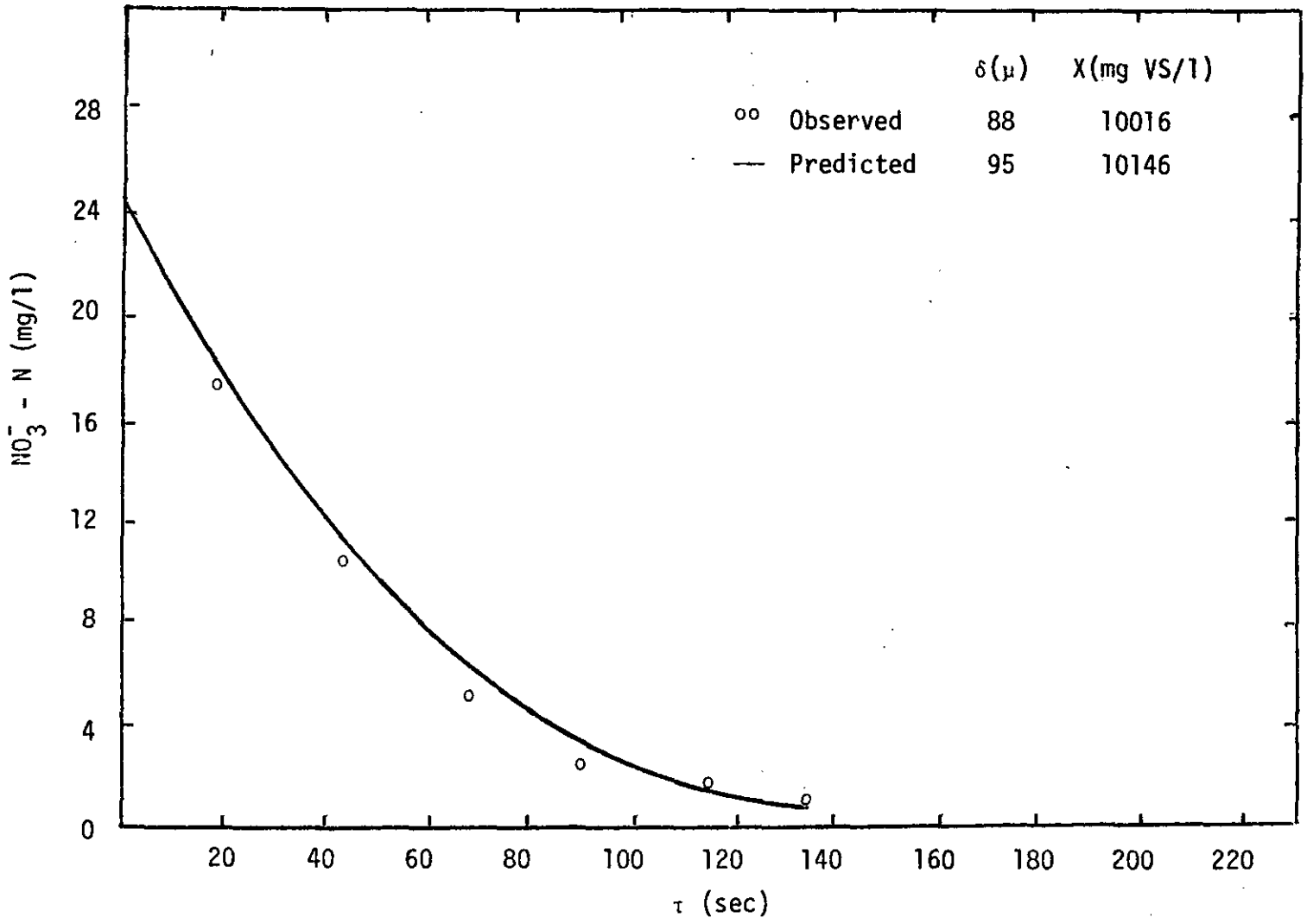

Figure 5.15 Observed and predicted nitrate profiles for the laboratory FBBR.

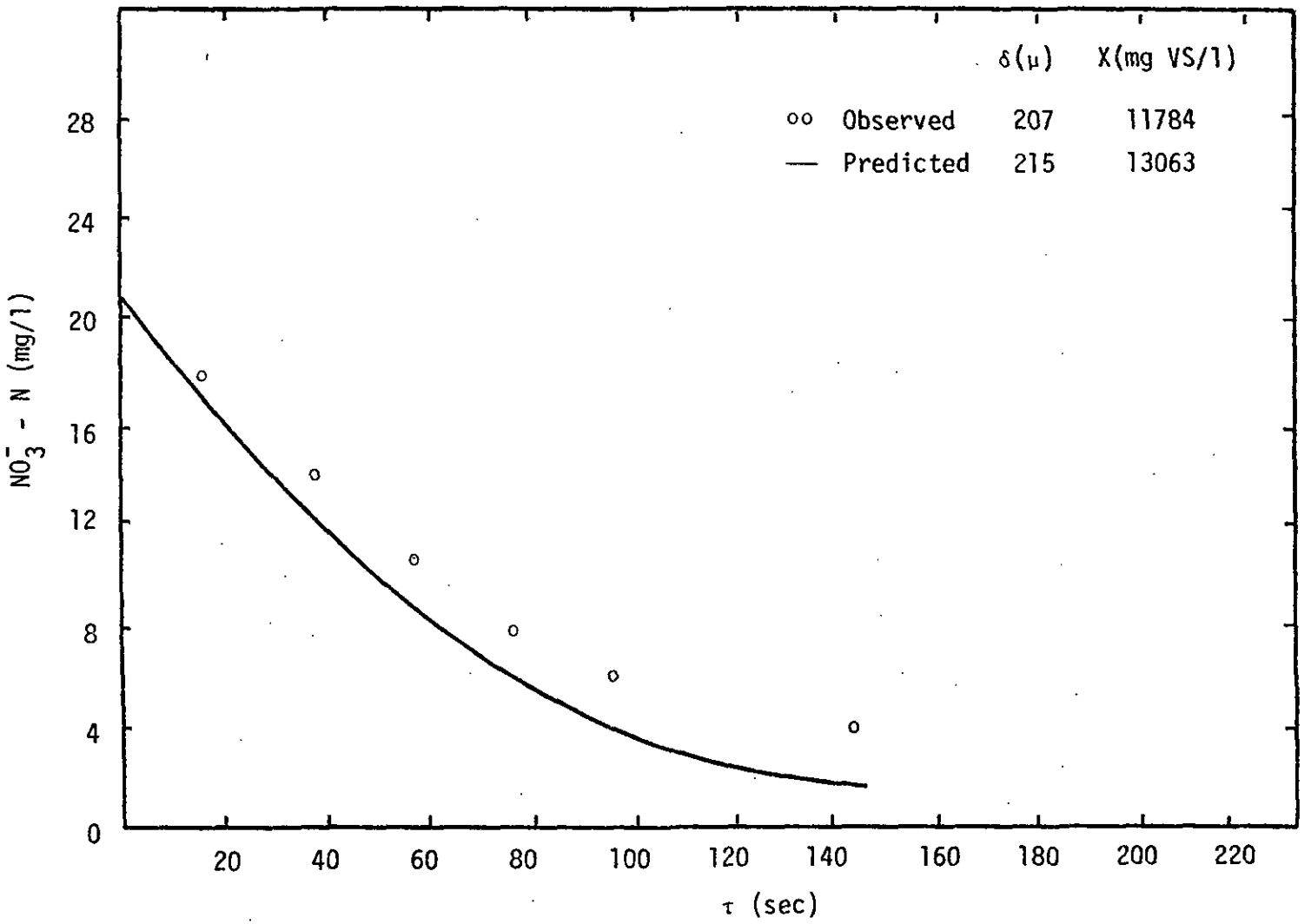

Figure 5.16 Observed and predicted nitrate profiles for the laboratory FBBR

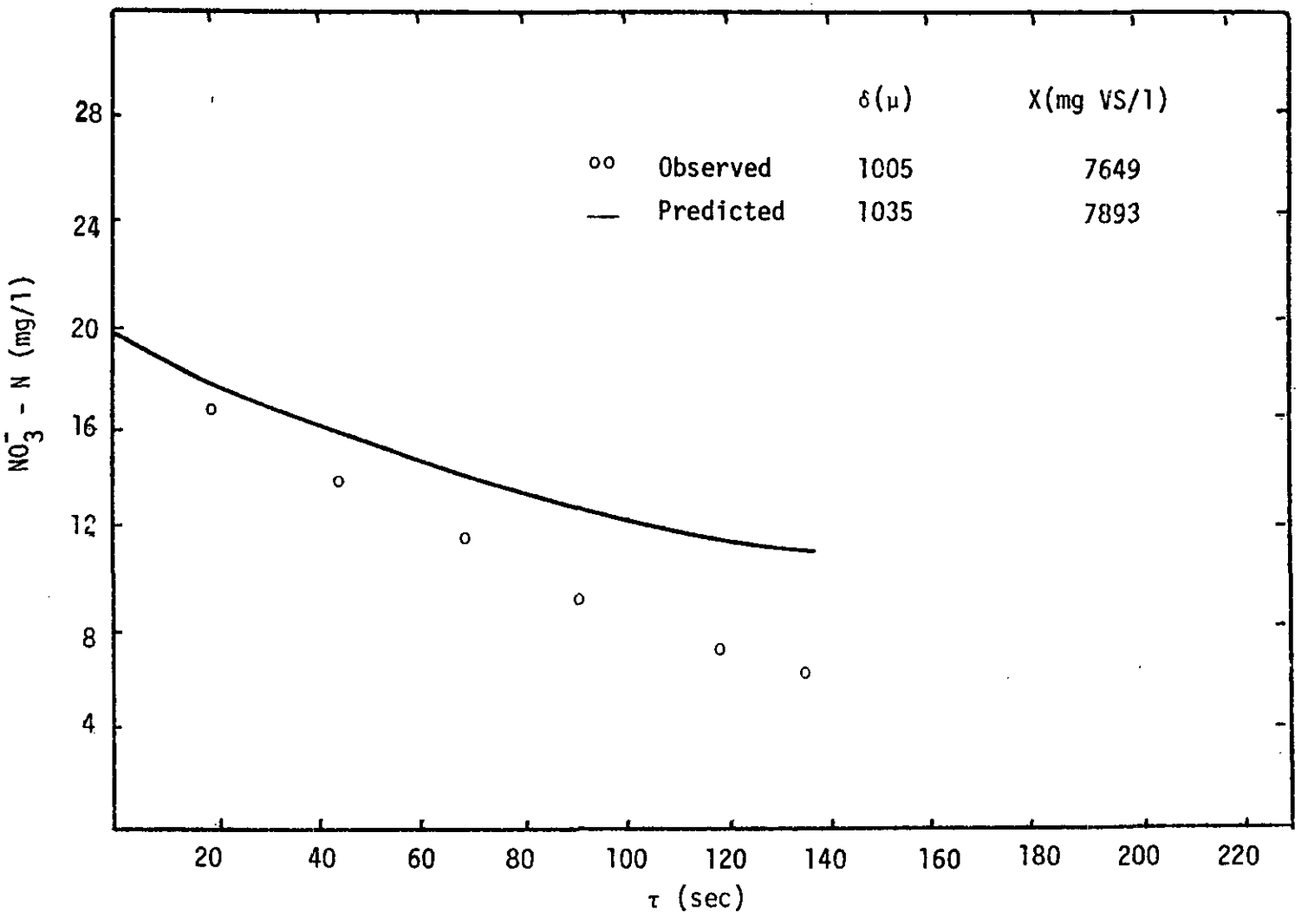

Figure 5.17 Observed and predicted nitrate profiles for the laboratory FBBR.

C H A P T E R V I

ENGINEERING APPLICATIONS

As developed in the fourth chapter of this dissertation, fluidized bed biofilm reactor performance is affected by five parameters which are under the direct control of the design engineer. These parameters are listed below:

1) Expanded bed height, H_B;
2) Reactor area perpendicular to flow, A;
3) Support media density, ρ_m;
4) Support media diameter, d_m;
5) Support media volume, V_m.

A parameter which is indirectly controllable by the design engineer is the equilibrium biofilm thickness, δ. For a given media (d_m and ρ_m), equilibrium biofilm thickness is dependent on superficial upflow velocity, expanded bed height and support media volume. Biofilm thickness is, in turn, the single most important parameter affecting biomass effectiveness and hence the overall performance of a FBBR.

A concept which aids in understanding the performance characteristics of a FBBR is that of effective biomass (actually effective

volatile solids) concentration within the reactor. The effective V.S. concentration is less than total biomass concentration because of diffusional limitations; it is defined here as the product of effectiveness factor and the reactor total volatile solids concentration. Effective V.S. concentration, X_A, may therefore be written as:

$$X_A = \eta_o X = \eta_o \rho_B \cdot \frac{\text{volume of biomass}}{\text{volume of expanded bed}} . \qquad 6.1$$

Effective V.S. concentration is, in turn, related to the overall reaction term R_v of Equation 4.3 as follows:

$$R_v = X_A \frac{k S_b}{K_S + S_b} \qquad 6.2$$

Thus, the rate of reaction at any point in a FBBR is directly proportional to the effective V.S. concentration at that point. Maximization of effective V.S. concentration will therefore maximize the overall rate of substrate conversion in the FBBR. Optimization of FBBR performance is, however, not a straightforward process because effectiveness factor, and hence effective V.S. concentration, will vary with bulk substrate concentration through the reactor.

As background to an understanding of this phenomenon, the relationship between total volatile solids concentration and equilibrium biofilm thickness must be determined. The fluidization algorithm of

Section 4.2, with modifications, serves as the basis for this determination. The required modifications are as follows:

Step 1. Specify a biofilm thickness, δ.

Step 10. Calculate the total volatile solids concentration X as:

$$X = \rho_B (1 - \varepsilon) \left[1 - (d_m / d_p) 3 \right] \qquad 6.3$$

Step 11 and 12. delete

The modified algorithm was used to develop the total volatile solids versus biofilm thickness curves of Figure 6.1. Additional information needed to generate these curves was provided earlier in Table 5.1. Note that these curves are specific to the given upflow velocities and media characteristics. The rather abrupt slope changes around biofilm thicknesses of 0.03 and 0.063 cm. are due to the abrupt slope changes in the ρ_B - δ correlation at these points (cf. Equation 4.17).

If the objective were simply to maximize total volatile solids concentration for the given media characteristics, the FBBR should be operated so as to control biofilm thickness at approximately 0.03 cm. Because of diffusional limitations, however, this simplistic approach may not optimize overall performance of the FBBR. To examine this

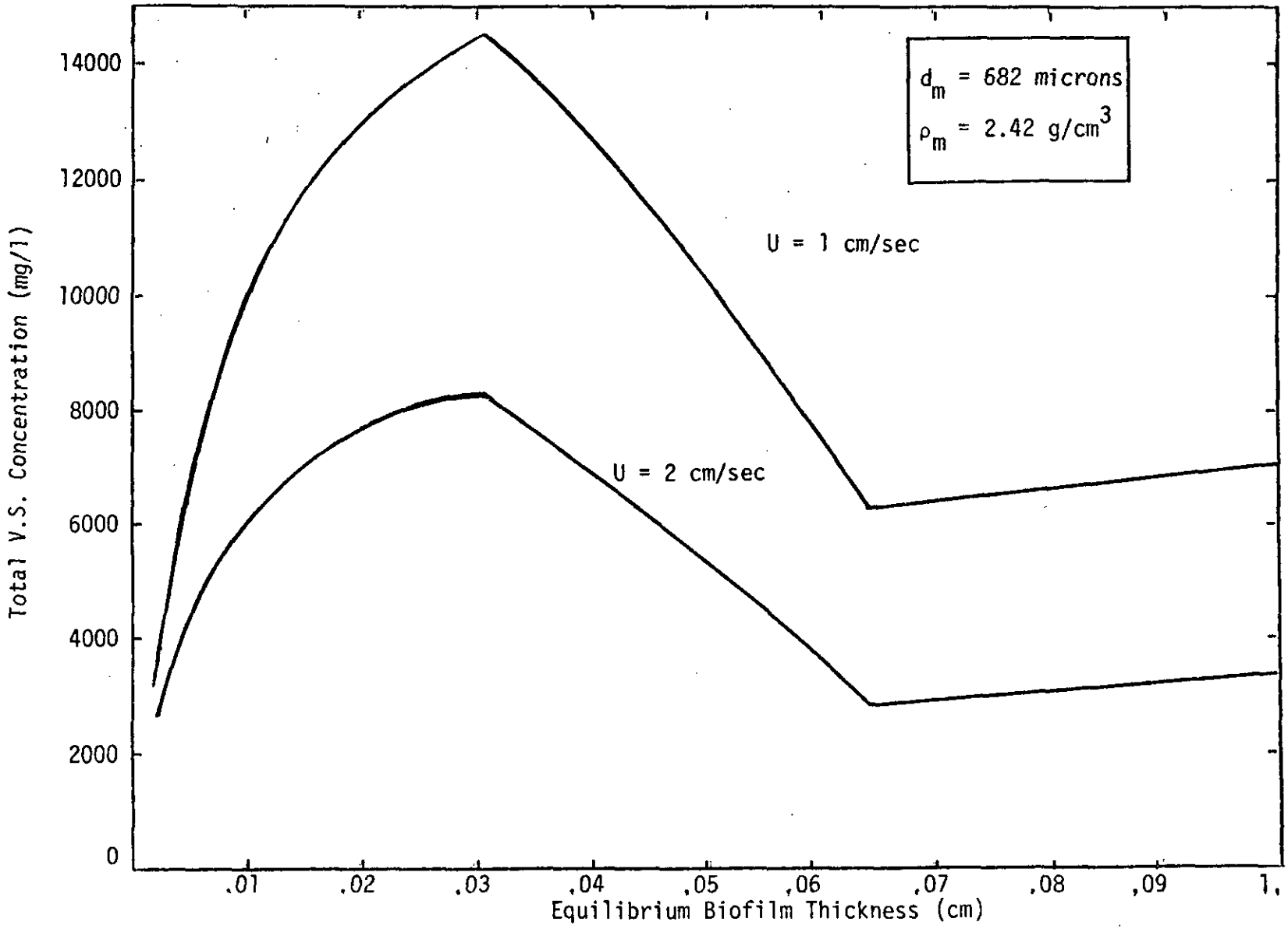

Figure 6.1 The Effect of Equilibrium Biofilm Thickness and Superficial Velocity on FBBR Total Volatile Solids Concentration.

possibility, it is necessary to determine the effect of biofilm thickness on the biofilm effectiveness factor. The mathematical background for this determination is developed in Section 4.3.

For a single bulk substrate concentration (in this case S_b = 20 mg/l NO_3 - N), numerical solutions of Equations 4.34 and 4.39 yield the effectiveness factor versus biofilm thickness plot shown in Figure 6.2.

The rather strange (as compared to catalysis) shape of this curve over the interval $0.03 < \delta < 0.063$ cm is due to the variable volatile solids density ρ_B in this region. In Section 4.3, it is shown that biofilm effectiveness factor is dependent on a Thiele-type *modulus given as:*

$$\phi^2 = \frac{k \rho_B \delta^2}{S_b D_{SB}} .$$

As the modulus increases in magnitude, the effectiveness factor decreases. In the biofilm thickness region mentioned above, the impact of increases in film thickness on the modulus and hence the effectiveness factor are countered by decreases in biofilm volatile solids density. This competitive phenomenon causes the effectiveness factor curve to level in this region and, in fact, show a slight upward trend in the neighborhood of δ = 0.063 cm.

Superimposed on the effectiveness factor curve is the total volatile solids concentration versus biofilm thickness plot of Figure

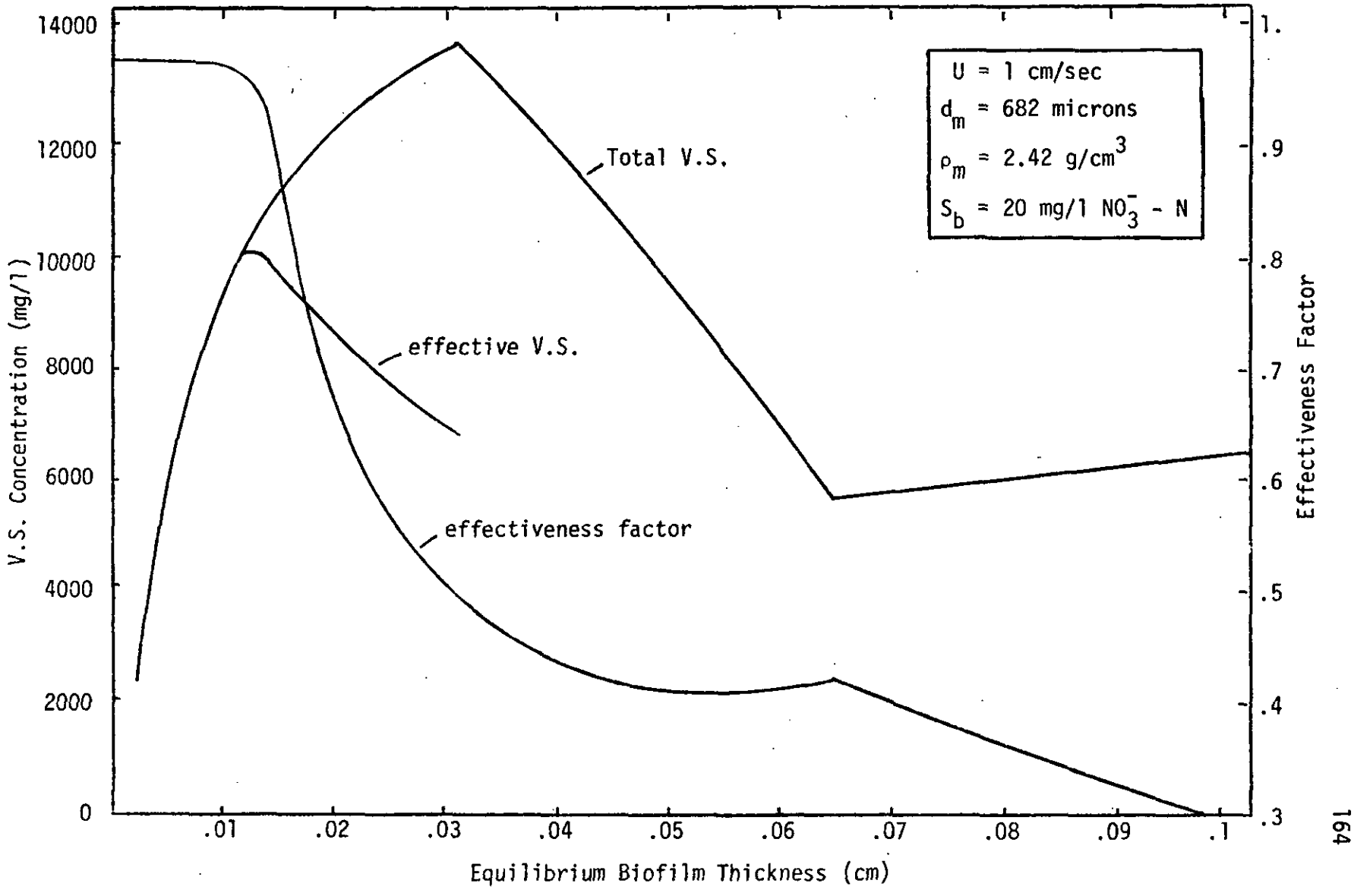

Figure 6.2 The Effect of Biofilm Thickness on Effective Volatile Solids Concentration.

6.1 for a superficial upflow velocity of 1.0 cm/sec. Information given by these two curves is used to calculate the effective volatile solids concentration curve, also shown in Figure 6.2.

Observe that although total volatile solids concentration is maximized by controlling biofilm thickness at approximately 0.03 cm, the effective volatile solids concentration for the listed conditions is a maximum at a biofilm thickness of approximately 0.012 cm. In fact, for the given case, the effective volatile solids concentration at a biofilm thickness of 0.03 cm is approximately 25 percent less than its maximum value.

For a constant bulk substrate concentration, selection of an optimum biofilm thickness at which to operate the reactor is a relatively straightforward matter. However in a real FBBR, bulk substrate concentration, and therefore, effectiveness factor and effective biomass concentration, vary with space time through the reactor. To illustrate this phenomenon, effectiveness factor versus biofilm thickness curves for several bulk substrate concentrations are presented in Figure 6.3. Note that as S_b decreases, the biofilm thickness which maximizes X_A also decreases.

To more clearly show the effect of variations in bulk substrate concentration on effective V.S. concentration, the data of Figure 6.3 are reworked to yield the plots shown in Figure 6.4. For each of the curves of Figure 6.4, effective V.S. concentration approaches total V.S. concentration (from Figure 6.1) as effectiveness factor approaches unity.

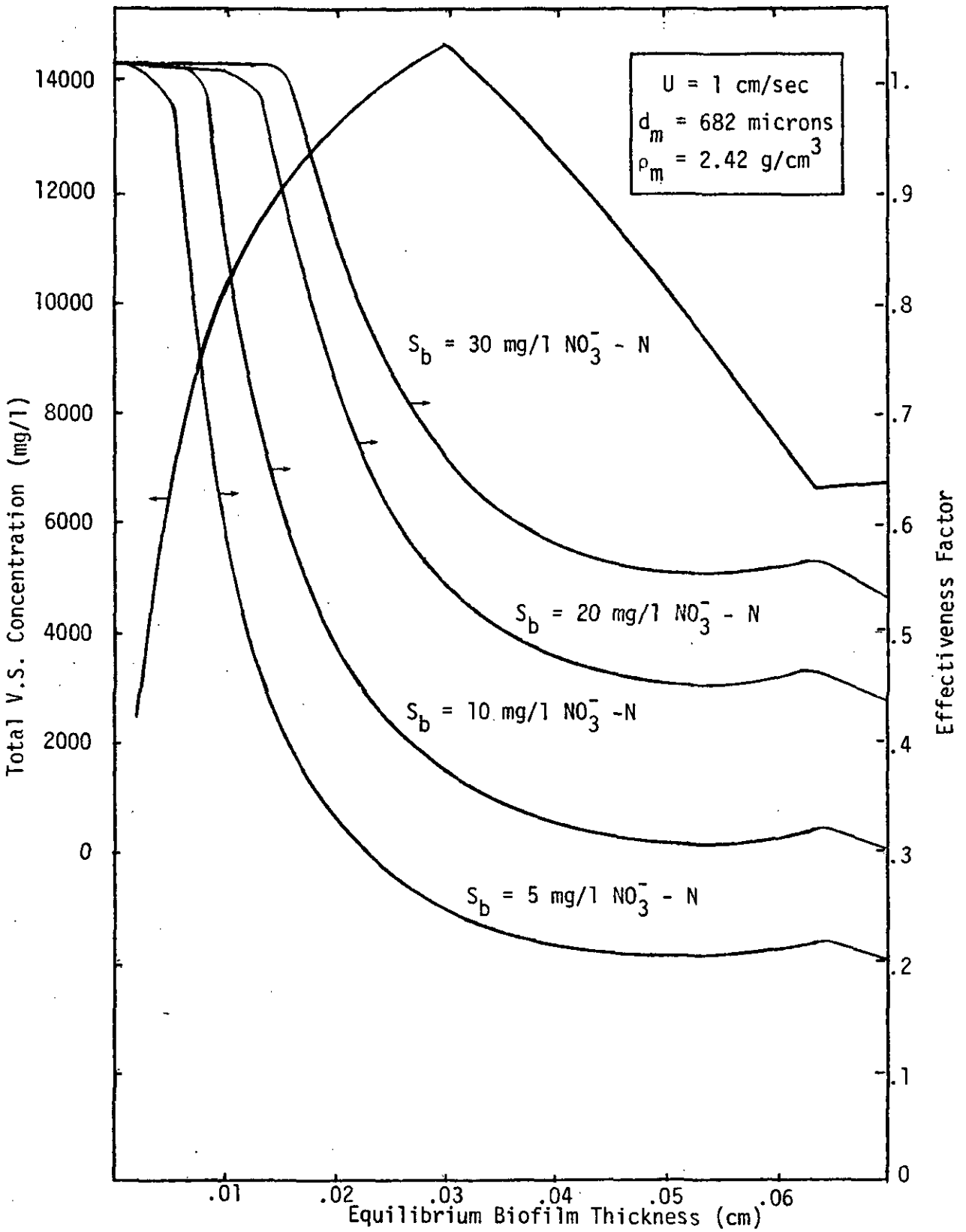

Figure 6.3 The Effect of Equilibrium Biofilm Thickness on FBBR Total V.S. and Effectiveness Factor.

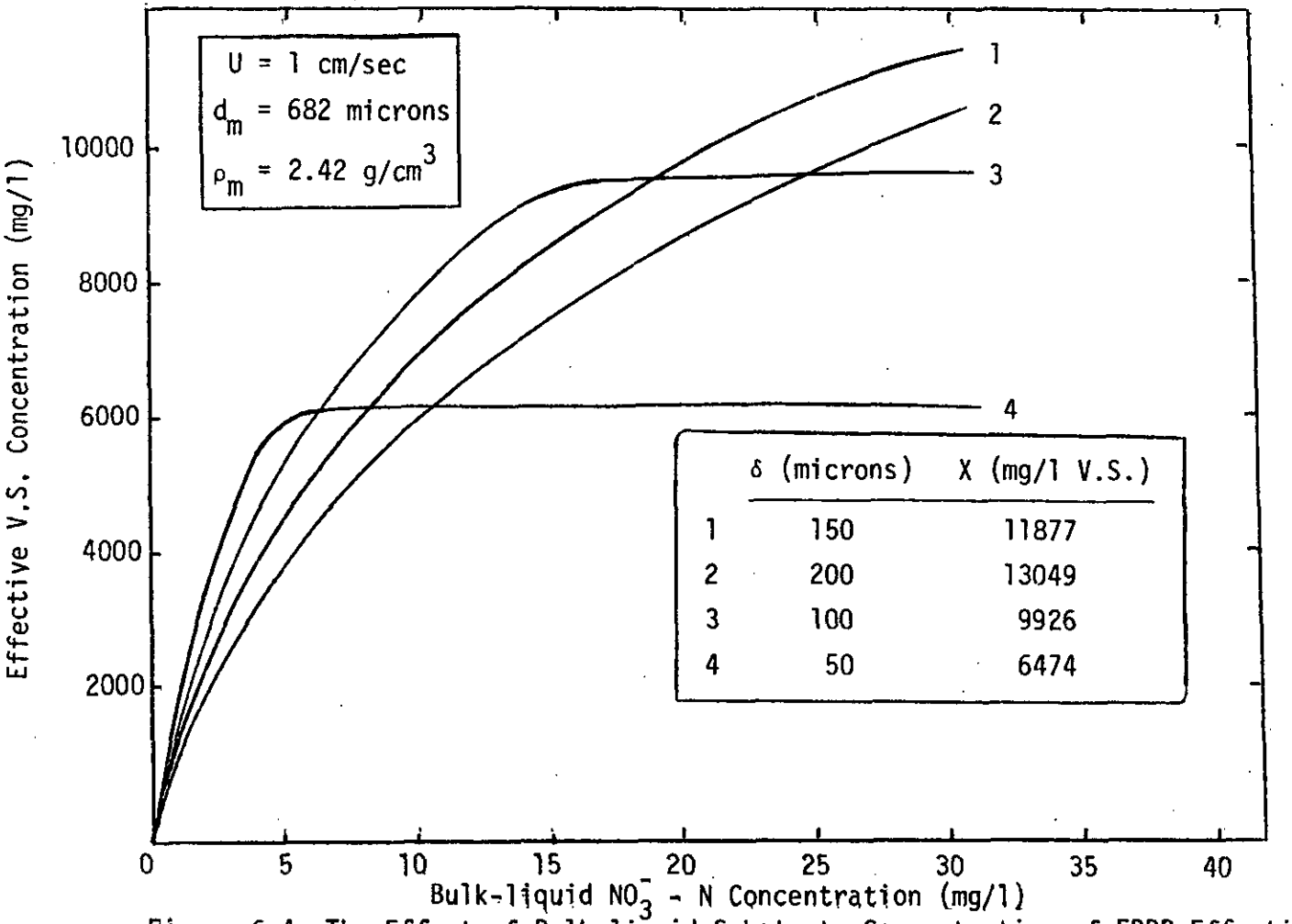

Figure 6.4 The Effect of Bulk-liquid Substrate Concentration of FBBR Effective Volitile Solids Concentration.

The relative importance of effectiveness factor and total V.S. concentration in determining the effective V.S. concentration can be brought into focus by examining specific regions of the X_A - S_b plots of Figure 6.4. For the listed flow and media characteristics, consider the objective to be selection of an optimum biofilm thickness for the reduction of nitrate-nitrogen concentration from 30 to 25 mg/l. It is apparent that effective V.S. concentration over this region is maximized by operation of the FBBR to maintain biofilm thickness in the 150 micron range. Both the 50 and 100 micron biofilms have effectiveness factors which approach unity in the given S_b range; however, both effective V.S. concentrations are limited by the corresponding, relatively low, total V.S. concentrations. In contrast, the 200 micron biofilm has the highest total V.S. concentration of the biofilms examined, but the effective V.S. concentration is limited by biofilm effectiveness factor. The 150 micron biofilm maximizes effective V.S. concentration over the given S_b range because it has an optimum combination of total V.S. concentration and effectiveness factor.

As bulk substrate concentration decreases, the importance of diffusional limitations increases. This is illustrated by focusing on the 0 to 5 mg/l NO_3 - N region of Figure 6.4. It can be seen that although the 50 micron biofilm has the lowest total V.S. concentration of the thicknesses examined, it has the highest effective V.S. concentration over this region. This is due to the fact that the

thicker biofilms are severely limited by transport resistances at low bulk substrate concentrations.

The impact of biofilm thickness on nitrate-nitrogen concentration profiles generated using the FBBR mathematical model is illustrated by Figure 6.5. This figure shows clearly that to optimize substrate conversion the FBBR should not be operated to maximize total V.S. concentration (200 micron biofilm) or to maximize effectiveness factor (50 micron biofilm) but rather to maximize the product of these parameters throughout the reactor.

Thus far in this chapter, an attempt has been made to demonstrate the utility of being able to exercise control of biofilm thickness within a FBBR. The mathematical model for biofilm bed fluidization developed as part of this research is advanced as a rational basis for selection of design parameters to yield a desired biofilm thickness.

Consider the following examples.

EXAMPLE 1. For a given reactor and inflow, determine the volume of a specified support media which will yield an equilibrium biofilm thickness of approximately 100 microns.

GIVEN:

H_B = 200 cm

A = 100 cm^2

Q = 100 cm^3/sec

ρ_m = 2.42 g/cm^3

d_m = 682 microns

δ_{eq} = 100 microns

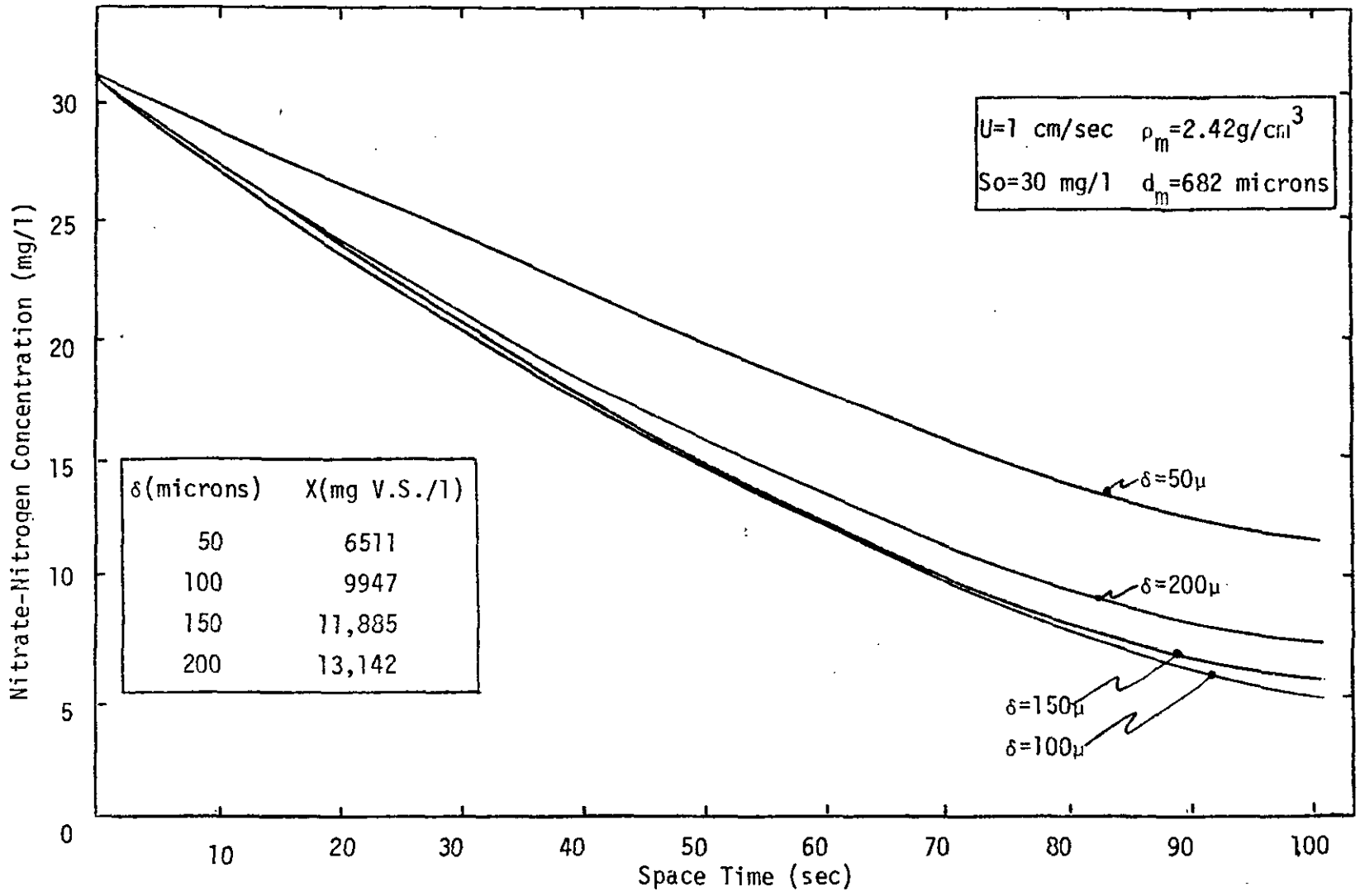

Figure 6.5 The Effect of Biofilm Thickness on Nitrate Conversion in a FBBR as predicted by the FBBR Mathematical Model.

FIND: V_m.

SOLUTION:

Equation 4.16	d_p = 882 microns
Equations 4.17, 4.18 and 4.19	ρ_s = 1.70 g/cm^3
Equation 4.22	U_t = 5.50 cm/sec
Equation 4.23	Re_t = 50.7
Equation 4.24	n = 5.1
Equation 4.25	ε = .716

$$V_m = H_B A (1 - \varepsilon) (d_m / d_p)^3$$

$$V_m = (200 \text{ cm}) (100 \text{ cm}^2) (1 - .716) (682 \mu/882\mu)^3$$

$$V_m = 2626 \text{ cm}^3$$

The solution scheme used in the preceeding example was used to develop Figure 6.6. The following is an alternate solution procedure for Example 1, which utilizes Figure 6.6.

SOLUTION: From the 100 micron curve of Figure 6.6;

at U = 1. cm/sec:

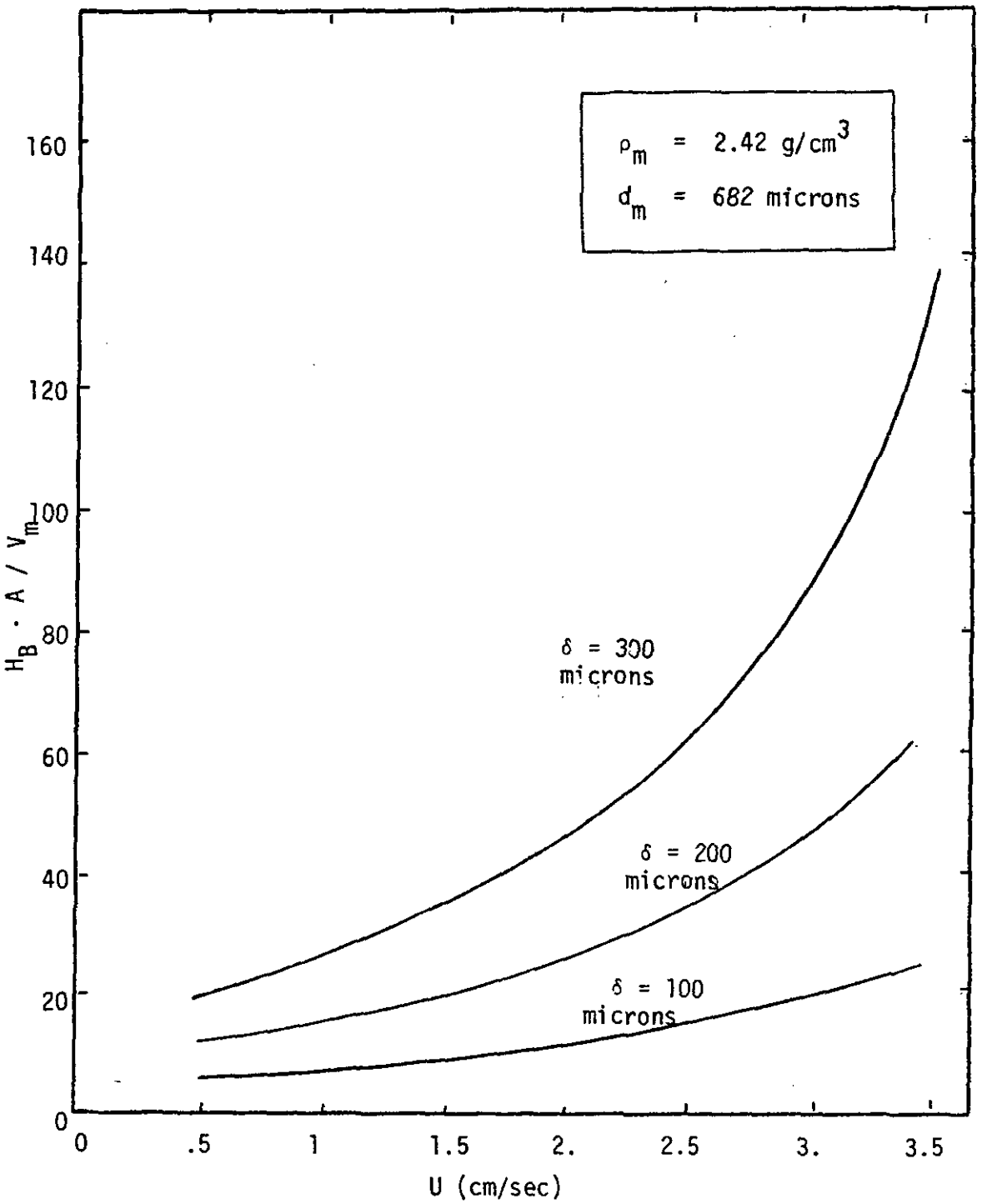

Figure 6.6 The Effect of Biofilm Thickness on FBBR Bed Expansion.

$$\frac{H_B A}{V_m} = 7.62$$

$$V_m = \frac{(200\ \text{cm})\ (100\ \text{cm}^2)}{7.62}$$

$$\underline{V_m = 2625\ \text{cm}^3}$$

Figure 6.6 is also useful in assessing the effect of hydraulic load variation on FBBR bed expansion. This is illustrated by the following example.

EXAMPLE 2. For the reactor of Example 1., find the percent increase in bed height which accompanies a 50 percent increase in inflow.

GIVEN: $V_m = 2626\ \text{cm}^3$ $A = 100\ \text{cm}^2$

$\rho_m = 2.42\ \text{g/cm}^3$ $\delta_{eq} = 100$ microns

$d_m = 682$ microns

FIND: H_B at $Q = 100\ \text{cm}^3/\text{sec}$

H_B at $Q = 150\ \text{cm}^3/\text{sec}$

SOLUTION: From Example 1., at Q = 100 cm^3, H_B = 200 cm.

From the 100 micron curve of Figure 6.6; at U = 1.5 cm/sec:

$$\frac{H_B\ A}{V_m} = 9.62$$

$$H_B = \frac{(9.62)\ (2626\ cm^3)}{100\ cm^2}$$

$$\underline{H_B = 252.6\ cm}$$

The percent increase in H_B which accompanies this 50 percent increase in inflow is:

$$\Delta H_B = 26.3 \text{ percent}$$

As discussed earlier, thin biofilm tends to maximize effectiveness factor. Figure 6.6 shows that thin biofilm in a FBBR is also advantageous from the standpoint of bed stability against hydraulic load variation. This is shown in the example below.

EXAMPLE 3. For the reactor and media of Examples 1 and 2, find the percent increase in bed expansion which accompanies a 50 percent increase in upflow velocity (1. to 1.5 cm/sec) for a biofilm thickness of 300 microns.

GIVEN: $V_m = 2626\ cm^3$ $\quad A = 100\ cm^2$

$\rho_m = 2.42\ g/cm^3$ $\quad \delta_{eq} = 300$ microns

$d_m = 682$ microns

FIND: H_B at $Q = 100\ cm^3/sec$

H_B at $Q = 150\ cm^3/sec$

SOLUTION: From the 300 micron curve of Figure 6.6; at U = 1.0 cm/sec

$$\frac{H_B A}{V_m} = 25.6$$

$$H_B = \frac{(25.6)\ (2626\ cm^3)}{100\ cm^2}$$

$$H_B = 672\ cm$$

At U = 1.5 cm/sec

$$\frac{H_B A}{V_m} = 33.7$$

$$H_B = \frac{(33.7)\ (2626\ cm^3)}{100\ cm^2}$$

$$H_B = 885 \text{ cm}$$

The percent increase in H_B which accompanies this 50 percent increase in inflow is:

$$\Delta H_B = 31.7 \text{ percent}$$

Even more significant than the percent increase in bed height is the actual magnitude of the bed height increase. For the 100 micron biofilm, the 50 percent increase in inflow causes a 52.6 cm increase in bed height. For the 300 micron biofilm, the same increase in inflow results in a bed height increase of 213 cm.

The previous examples have focused on the bed expansion-biomass holdup portion of the FBBR mathematical model. The following example more fully utilizes the comprehensive biomass holdup and substrate conversion capabilities of the model.

EXAMPLE 4. Design a FBBR which will reduce influent nitrate-nitrogen concentration from 30 to 3 mg/l. The reactor is to utilize the media of the previous examples and operate at a biofilm thickness of approximately 100 microns and a superficial velocity of 1 cm/sec. Specifically, determine the combination of V_m and H_B which will result in an effluent nitrate-nitrogen concentration of 3 mg/l under the stated conditions.

GIVEN: $Q = 100\ cm^3/sec$ $\quad \delta_{eq} = 100$ microns

$A = 100\ cm^2$ $\quad S_b|_{Z=0} = 30$ mg/l

$d_m = 682$ microns $\quad S_b|_{Z=H_B} = 3$ mg/l

$\rho_m = 2.42\ g/cm^3$

FIND: V_m and H_B

SOLUTION: Computer solution of this problem involves a slight modification of the fluidization portion of the FBBR model. Rather than specifying V_m and H_B and calculating biofilm thickness, V_m and δ are specified and the resultant H_B calculated. For the given biofilm thickness, V_m is varied until $S_b = 3$ mg/l at $Z = H_B$. The computer solution to this example is presented in Table 6.1.

The effect of support media characteristics on FBBR performance, as predicted by the FBBR mathematical model, will be examined briefly. Figures 6.7 and 6.8 present effective V.S. concentration as a function of superficial velocity and biofilm thickness for a range of support media characteristics. A bulk substrate concentration of 10 mg/l nitrate-nitrogen was used in developing these figures.

It is apparent that decrements in superficial velocity or increments in either support media density or size, increases effective V.S. concentration. In general, the computer simulations of this study indicate that substrate conversion is maximized when bed poro-

```
190 Q=100.
220 XA=100.
230 HB=117.3
270 VM=1540.
200 SO=30.E-6
RNH

DEL=     .01000
DP=      .08820
EP=      .71603
XVS=  .00992450

BI=     6.62736
```

model input

Z	TAU	NO3-N	ETA
0.	0.	.0000300	.9989077
5.8650000	5.8650000	.0000261	.9986959
11.7300000	11.7300000	.0000262	.9984138
17.5950000	17.5950000	.0000243	.9980236
23.4600000	23.4600000	.0000224	.9974619
29.3250000	29.3250000	.0000205	.9966028
35.1900000	35.1900000	.0000186	.9951644
41.0550000	41.0550000	.0000168	.9923694
46.9200000	46.9200000	.0000151	.9849935
52.7850000	52.7850000	.0000134	.9558897
58.6500000	58.6500000	.0000119	.9019762
64.5150000	64.5150000	.0000104	.8447467
70.3800000	70.3800000	.0000091	.7869991
76.2450000	76.2450000	.0000079	.7291665
82.1100000	82.1100000	.0000068	.6717472
87.9750000	87.9750000	.0000058	.6153268
93.8400000	93.8400000	.0000049	.5609046
99.7050000	99.7050000	.0000042	.5100013
105.5700000	105.5700000	.0000036	.4653947
111.4350000	111.4350000	.0000032	.4319402
117.3000000	117.3000000	.0000030	.4180686

```
 END.

SRU      66.349 UNTS.

RUN COMPLETE.
```

Table 6.1 FBBR model computer output (see Appendix 11 for a description of program nomenclature).

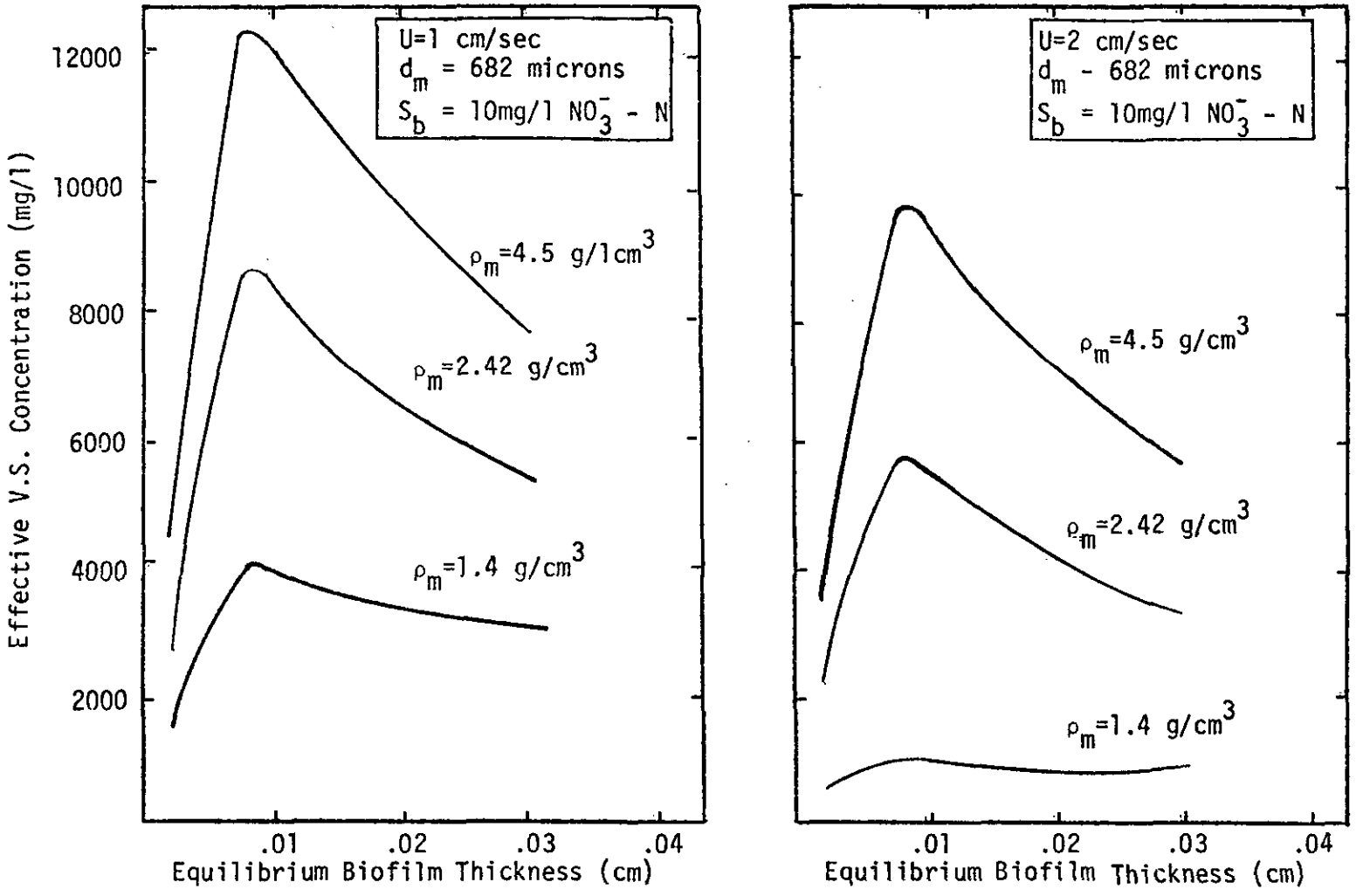

Figure 6.7 Effect of Support Media Density on Effective Volatile Solids Concentration.

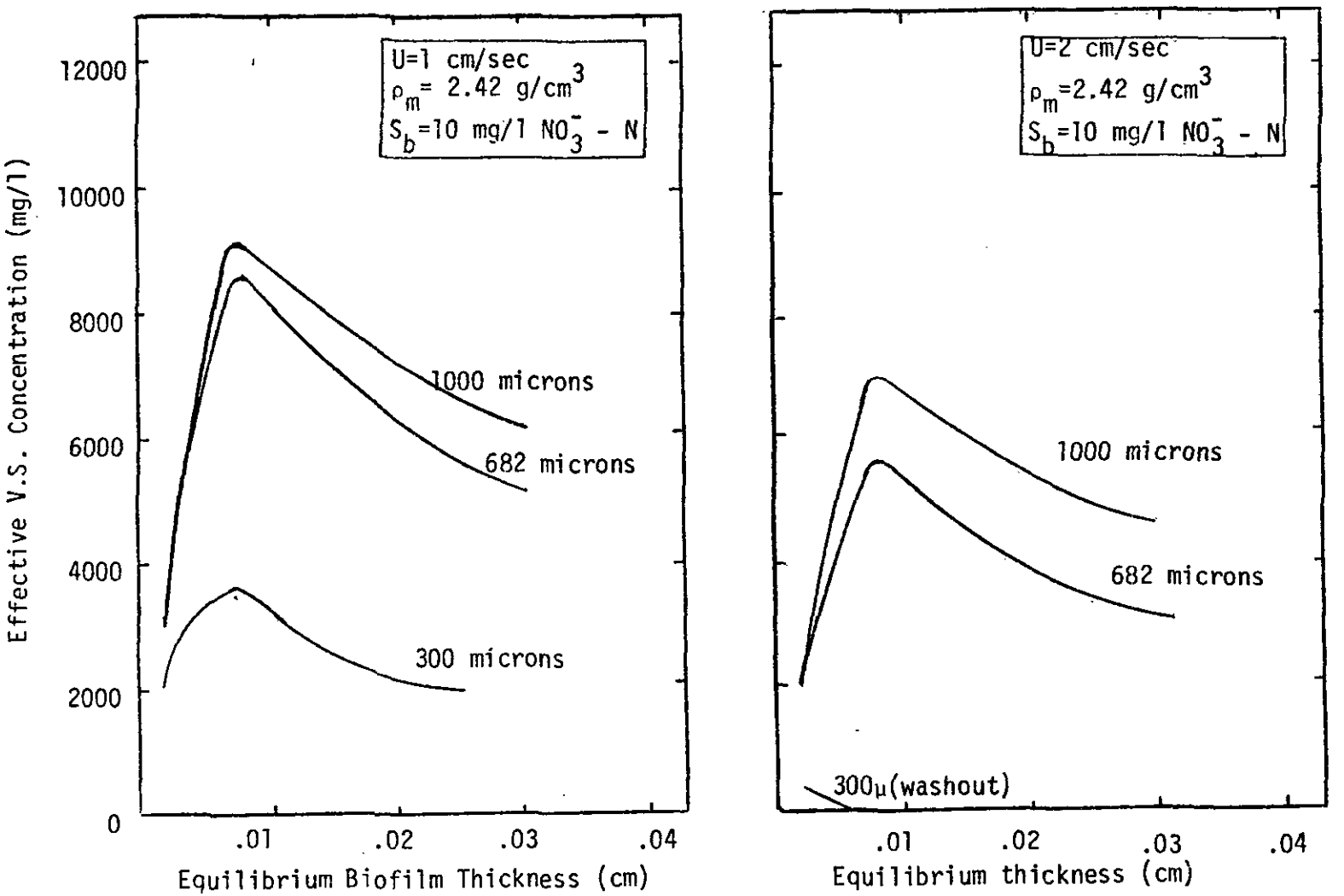

Figure 6.8 Effect of Support Media Diameter on Effective Volitile Solids Concentration.

sity is minimized.

The effect of support media characteristics on FBBR bed expansion is presented, graphically, in Figures 6.9 and 6.10. These figures show that FBBR bed height stability to variations in superficial velocity, increases with increased media size or density. This is extremely important with regard to flow equilization requirements for a system utilizing a fluidized bed reactor.

In summary, it appears that the use of larger or denser support media in a fluidized bed biofilm reactor offers advantages, as discussed above. Any such advantage, however, must be weighed against the higher energy requirements for fluidization of these media. In addition, problems such as bed clogging, particle-particle bridging and gas entrapment may accompany low porosity operation of a FBBR using larger or denser support media.

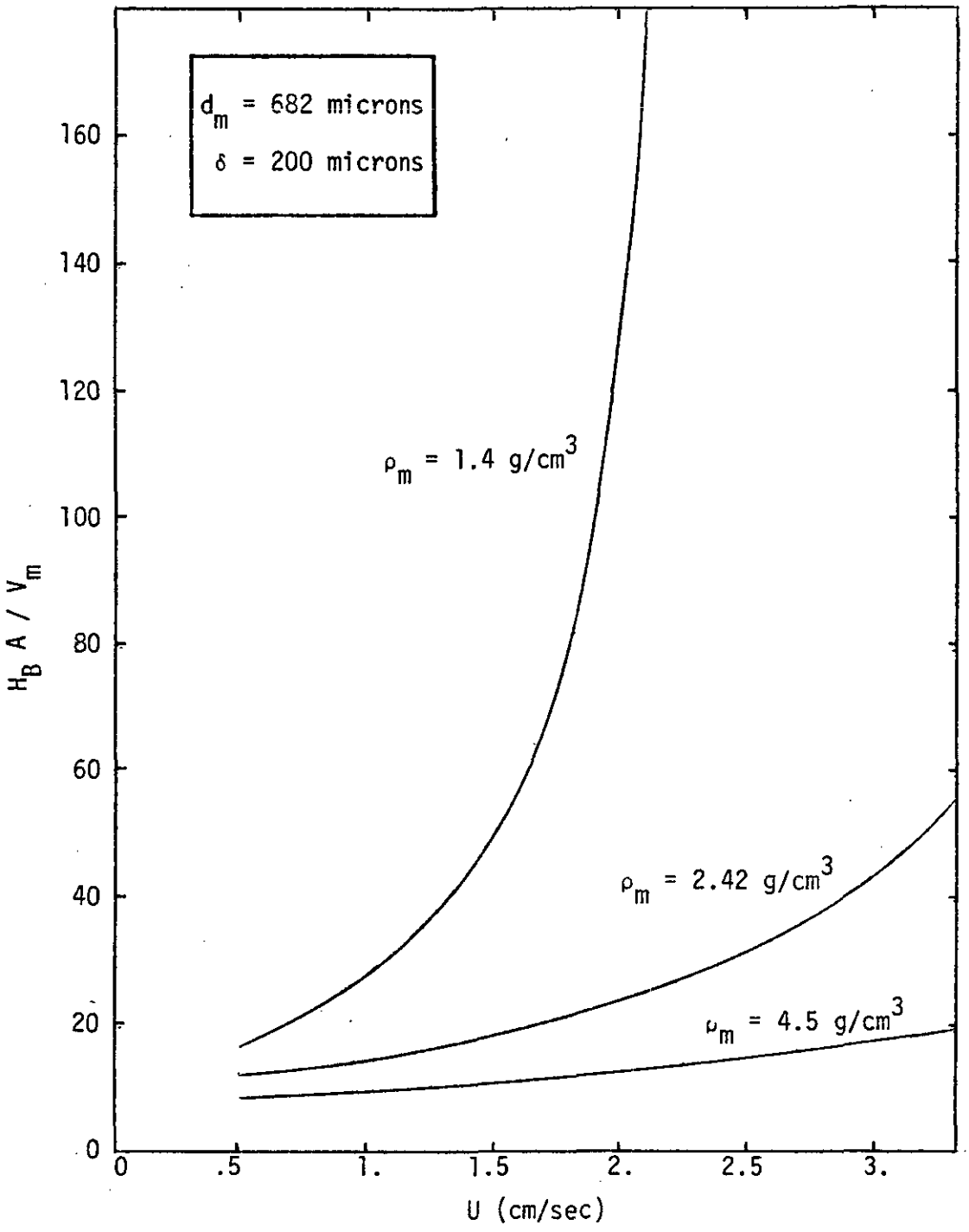

Figure 6.9 Effect of Support Media Density on FBBR Bed Expansion

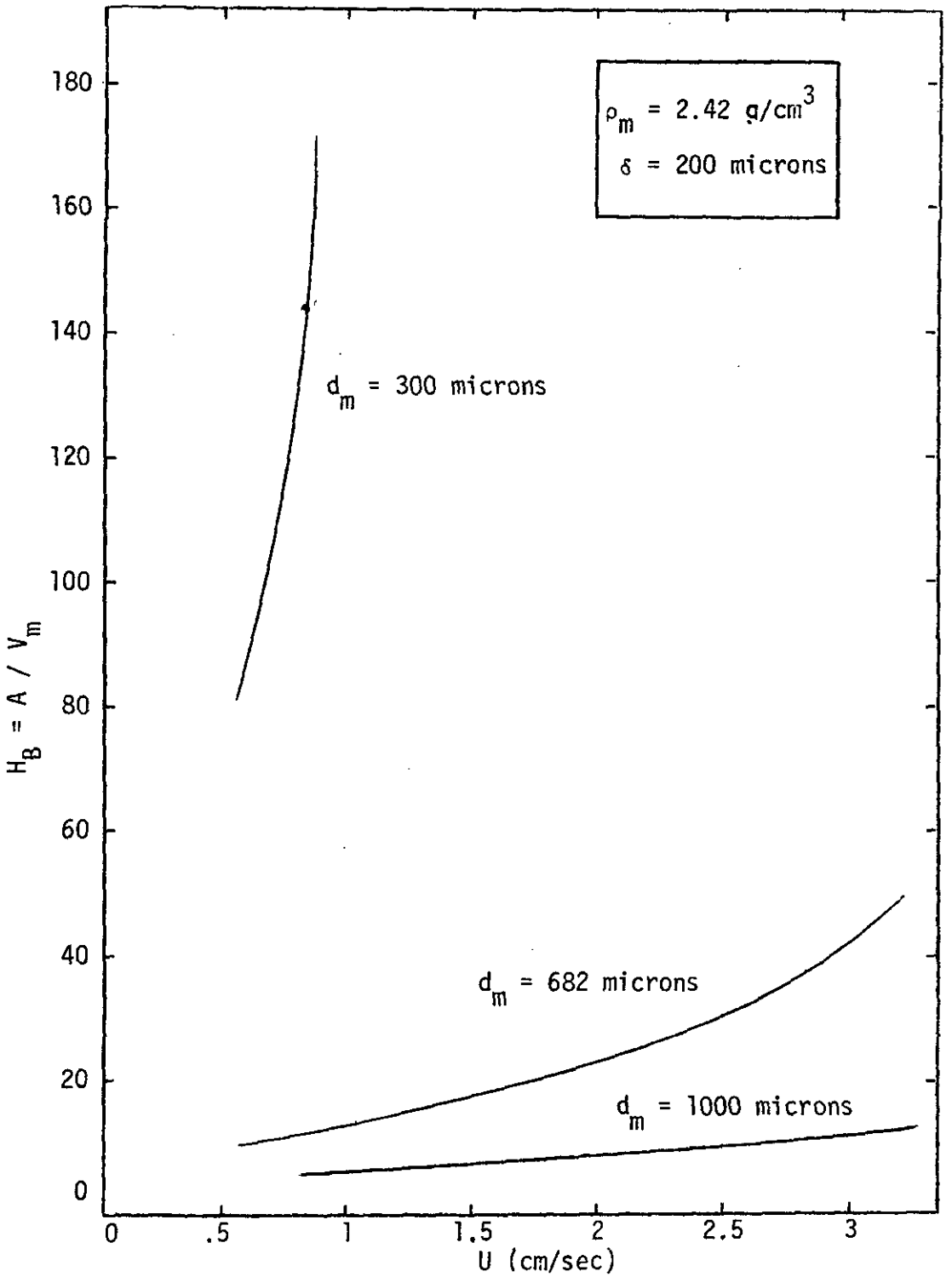

Figure 6.10 Effect of Support Media Diameter on FBBR Bed Expansion.

CHAPTER VII

SUMMARY, CONCLUSIONS AND RECOMMENDATIONS

Summary

The fluidized bed biofilm reactor is a novel biological wastewater treatment process. The use of small, fluidized particles in the reactor affords growth support surface an order of magnitude greater than conventional biofilms systems, while avoiding clogging problems which would be encountered under fixed bed operation. This allows retention of high biomass concentration within the reactor. This high biomass concentration, in turn, translate to substrate conversion efficiencies an order of magnitude greater than possible in conventional biological reactors.

The primary objective of this research has been the development of a mathematical model of the fluidized bed biofilm reactor. This model identifies five controllable parameters (A, H_B, V_m, ρ_m, d_m) which effect reactor performance and thus, provides a rational basis for reactor design. The mathematical model has two major subdivisions. The first predicts biomass holdup within the reactor using drag coefficient and bed expansion correlations developed as part of this research. The second predicts mass transport-affected substrate conversion by biofilm covering individual support particles.

Intrinsic kinetic coefficients and effective diffusivity for biofilm denitrification, used in this segment of the model, were determined in an independent study using a rotating disk biofilm reactor.

Conclusions

1. The FBBR model adequately predicts nitrate-limited denitrification within a fluidized bed biofilm reactor, especially for biofilm thickness under 300 microns.
2. The most significant parameter affecting substrate conversion efficiency in a fluidized bed biofilm reactor is biofilm thickness.
3. Biofilm thickness, and thus FBBR performance can be controlled through specification of the following design parameters:

   Expanded bed height, H_B;

   Reactor horizontal area, A

   Support media density, ρ_m;

   Support media diameter, d_m;

   Support media total volume, V_m.
4. The FBBR model provides a rational basis for selection of design parameters.
5. The biofilm denitrification parameters D_{SB}, k and K_S obtained in the rotating disk reactor study are applicable to denitrification in a fluidized bed reactor for similar biofilm thicknesses.

6. From the rotating disk reactor study, the following 95 percent confidence intervals were determined for the denitrifying biofilm parameters D_{SB}, k and K_S:

$$0.198 \times 10^{-5} \leq D_{SB}\ (\text{nitrate}) \leq 1.432 \times 10^{-5}\ \text{cm}^2/\text{sec}$$

$$2.873 \leq k \leq 2.878\ \text{day}^{-1}$$

$$0 \leq K_S \leq 0.3077\ \frac{\text{mg}}{\text{l}}\ NO_3^- - N$$

for pH = 6.92 $\pm$ .1, temperature = 22°C $\pm$ 1°C and biofilm thickness < 300 microns.

7. Biofilm volatile solids density was found to decrease with biofilm thickness between roughly 300 and 630 microns.
8. For the support media and substrate concentration range used in this study, the FBBR model predicts optimum denitrification when biofilm thickness is controlled at approximately 100 microns. Larger or denser support media or higher substrate concentration will shift this optimum toward thicker biofilm.
9. The FBBR model predicts maximum denitrification per unit reactor volume when design parameters are specified which minimize bed porosity while controlling biofilm thickness near its optimum. Bed porosity is minimized by large or dense support media and large reactor horizontal area.

Recommendations

The following are recommendations for future research:

1. That the FBBR model be verified using a pilot-scale denitrification fluidized bed reactor.
2. That the data base for the FBBR drag coefficient and bed expansion index correlations be extended by examining a wide range of support media of various densities and sizes.
3. That a biofilm model be developed which describes reaction under multiple or sequential substrate control.
4. That the effect of biofilm volatile solids density on effective diffusivity and the Michaelis-Menten constants be examined.
5. That a more rational parameter that volatile solids density be used in analysing for effective diffusivity and rate constants; adenosine triphosphate concentration (ATP) is suggested.
6. That the effect of environmental conditions such as pH and temperature on the biofilm denitrification parameters D_{SB}, k and K_S be examined.
7. That the effect of these environmental conditions be incorporated in the FBBR model.
8. That the FBBR model be extended to biochemical systems other than denitrification.

Bibliography

1. Adler, I.L., and Happel, J., "Fluidization of uniform spheres in liquid media." Chem. Eng. Prog., Symp. Ser. 58, 98 (1962).

2. Atkinson, B. and Daoud, I.S., "The analogy between microbial reactions and heterogeneous catalysis." Trans., Inst. Chem. Engrs. 46, T19 (1968).

3. Atkinson, B. and Daoud, I.S., "Diffusion effects within microbial films." Trans., Inst. Chem. Engrs. 48, T245 (1970).

4. Atkinson, B., Daoud, I.S., and Williams, D.A., "A theory for the biological film reactor," Trans., Inst. Chem. Engrs. 46, T245 (1968).

5. Atkinson, B., and Davies, I.J., "Overall rate of substrate uptake by microbial films. I. Biological rate equation." Trans., Inst. Chem. Engrs. 52, 248 (1974).

6. Atkinson, B., and How, S.Y., "The overall rate of substrate uptake by microbial films; Part II. Effect of concentration and thickners." Trans., Inst. Chem. Engrs. 52, 384 (1974).

7. Atkinson, B., and Knights, A.J., "Microbial film fermenters: their present and future applications." Biotech. Bioeng. 17, 1245 (1975).

8. Baillod, C.R., "Mass Transfer of Glucose through Bacterial Floc," Ph.D. Dissertation, University of Wisconsin (1968).

9. Baillod, C.R., and Boyle, W.C., "Mass transfer limitations in substrate removal." Jour. San. Eng. Div., A.S.C.E. 96, 525 (1970).

10. Barnea, E., and Mizrahi, J., "A generalized approach to the fluid dynamics of particulate systems. Part 1. General correlation for fluidization and sedimentation in solid multiparticle systems." Chem. Eng. Jour. 5, 171 (1973).

11. Barth, E.F., Brenner, R.C., and Lewis, R.F., "Chemical-biological control of nitrogen and phosphorous in wastewater effluent." Jour. Water Poll. Contr. Fed. 40, 2040 (1968).

12. Beek, W.J., "Mass transfer in fluidized beds." in Fluidization, eds, J.F. Davidson and D. Harrison, Academic Press, London and New York, (1971).

13. Beer, C., "Evaluation of Anaerobic Denitrification Processes." Jour. San. Eng. Div., A.S.C.E. 96, 1452 (1970).

14. Bird, R.B., Stewart, W.E., and Lightfoot, E.N., Transport Phenomena, John Wiley and Sons, New York (1960).

15. Bischoff, K.B., "A Note on Boundary Conditions for Flow Reactors." Chem. Eng. Sci. 16, 131 (1961).

16. Brinkman, H.C., "Theory of liquids", Physica 7, 747 (1940).

17. Bruinzeel, C., Reman, G.H., and van der Laan, E.T., "The Interactions Between Fluids and Particles." Third Congress of the European Fed. of Chem. Engrs. p 120 (1962).

18. Bungay, H.R., Whalen, W.J., and Sanders, W.M., "Microprobe Techniques for Determining Diffusivities and Respiration Rates in Microbial Slime Systems," Biotech. and Bioeng. 11, 765 (1969).

19. Button, D.K., and Garver, J.C., "Continuous Culture of Torulopsis utilis: A Kinetic Study of Oxygen Limited Growth." Journal of General Microbiology 45, 195 (1966).

20. Cairns, E.J., and Prausnitz, J.M., "Longitudinal mixing in packed beds" Chem. Eng. Sci., 12, p 20 (1960).

21. Carberry, J.J., Chemical and Catalytic Reaction Engineering, McGraw Hill, New York (1976).

22. Chambre, P.L., and Acrivos, A., "On Chemical Surface Reactions in Laminar Boundary-Layer Flow." Jour. Applied Physics 27, 1322 (1956).

23. Chang, J.P., and Morris, J.E., "Studies on the utilization of nitrate by Micrococcus denitrificans." Jour. Gen. Microb. 29, 301 (1962).

24. Choi, C.Y., and Perlmutter, D.D., "A unified treatment of the inlet-boundary condition for dispersive flow Models." Chem. Eng. Sci. 31, 250 (1976).

25. Chu, J.C., Kailil, J. and Wetteroth, W.A., "Mass Transfer in a Fluidized Bed." Chem. Eng. Prog. 49, 141 (1953).

26. Chung, S.F., and Wen, C.Y., "Longitudinal Dispersion of Liquid Flowing Through Fixed and Fluidized Beds." Amer. Inst. of Chem. Eng., Jour. 14, 857 (1968).

27. Clayfield, G.W., "Respiration and Denitrification Studies on Laboratory and Works Activated Sludges." Water Poll. Contr., London 73, 51 (1974).

28. Dallavalle, J.M., Micromeritics, 2nd ed., Pitman, London, (1948).

29. Damkohler, G., "The influence of flow, diffusion and heat transfer on the performance of reaction furnaces." Z. Elektrochem. 42, 846 (1936).

30. Danckwerts, P.V., "Continuous flow systems: Distribution of residence times." Chem. Eng. Sci. 2, 1 (1953).

31. Dawson, R.N., and Murphy, K.L., "Factors Affecting Biological Denitrification in Wastewater." In Advances in Water Pollution Research, S.H. Jenkins, Ed., Oxford, England, Pergamon Press (1973).

32. Eckenfelder, W.W., and Balkrishnan, S., "Kinetics of biological nitrification and denitrification." Center for Research in Water Resources, University of Texas (1968).

33. Edeline, F., Tesarik, I., and Vostricil, J., "Fluidization of Flocs Produced in Chemical or Biological Treatment Plants." Proc. Fifth Int. Conf. on Water Poll. Res. (1968).

34. Fenn, W.O., "The Oxygen Consumption of Frog Nerve During Stimulation." Jour. Gen. Physiology 10, 767 (1927).

35. Fouda, A.W., and Capes, C.E., "Hydrodynamic Particle Volume and Fluidized Bed Expansion." Can. Jour. Chem. Eng. 55, 386 (1977).

36. Foust, A.S., Wenzel, L.A., Clump, C.W., Maus, L. and Anderson, L.B., Principles of Unit Operations, John Wiley and Sons, New York (1960).

37. Friedlander, S.K., "A Note on Transport to Spheres in Stokes Flow." Amer. Inst. Chem. Eng., Jour. 7, 347 (1961).

38. Gamson, B.W., Thodos, G. and Hougen, D.A., "Heat, Mass and Momentum Transfer in the Flow of Gases Through Granular Solids." rans., Amer. Inst. Chem. Eng. 39, 1 (1943).

39. Gaudy, A.F., and Gaudy, E.T., "Biological Concepts for Design and Operation of the Activated Sludge Process." Water Pollution Control Research Series, 17090 FQJ 09/71 (1971).

40. Gerard, R.W., "Oxygen Diffusion into Cells." Bio. Bulletin, 60, 245 (1931).

41. Ghosh, S., "Kinetics of Aerobic Utilization of Mixed Sugars by Heterogeneous Microbial Populations." Ph.S. Dissertation, Georia Institute of Technology (1969).

42. Gulevich, W., "The Role of Diffusion in Biological Waste Treatment." Ph.D. Dissertation, The Johns Hopkins University (1967).

43. Hancock, R.T., "The law of motion of particles in a fluid." Trans. Inst. Mining Engrs. (London) 94, 114 (1937).

44. Happel, J. "Viscous Flow in Multiparticle Systems: Slow Motion of fluids Relative to Beds of Spherical Particles." Amer. Inst. Chem. Eng., Jour. 4, 197 (1958).

45. Harremoes, P. and Riemer, M., "Report on pilot experiments on down-flow filter denitrification." Rept. 75-1, Dept. of Sanitary Engineering, Technical Univ. of Denmark, Lyngby (1975).

46. Haug, R.T., and McCarty, P.L., "Nitrification with the Submerged Filter", Tech. Rept. No. 149, Civil Eng. Dept., Stamford Univ. (1971).

47. Hawksley, P.G.W., "The physics of particle-size measurement. I. Fluid dynamics and the Stokes diameter." Bull. Brit. Coal Util. Res. Assoc. 15, 105 (1951).

48. Hill, A.V., "The Diffusion of Oxygen and Lactic Acid Through Tissues." Proc. Royal Soc. London B104, 39 (1929).

49. Hoehn, D.C., "The Effects of Thickness on the Structure and Metabolism of Bacterial films." Ph.D. Dissertation, Univ. of Missouri (1970).

50. Horstkotte, G.A., Niles, D.G., Parker, D.S., and Caldwell, D.H., "Full-Scale Testin- of a Water Reclamation System." Jour. Water Poll. Cont. Fed. 46, 181 (1974).

51. Horvath, C., and Engasser, J., "External and Internal Diffusion in Heterogeneous Enzyme Systems." Biotech and Bioeng. 16, 909 (1974).

52. Itagaki, E., Fujita, T., and Sato, R., "Nitrate Reduction Interaction in a Solubilized System from E. coli." Biochem. Biophys. Acta 51, 390 (1961).

53. Jackson, R., "Fluid Mechanical Theory." In Fluidization, eds. J.F. Davidson and D. Harrison, Academic Press, London and New York (1971).

54. Jennings P.A., "A Mathematical Model for Biological Acitivity in Expanded Bed Adsorption Columns." Ph.D. Dissertation, University of Illinois (1974).

55. Jeris, J.S., Beer, C., and Mueller, J.A., U.S. Patent no 3846289 (1972).

56. Jeris, J.S., U.S. Patent no. 4,009,098 (1973).

57. Jeris, J.S., U.S. Patent no. 4,009,105 (1974).

58. Jeris, J.S., U.S. Patent no. 4,009,104 (1975).

59. Jeris, J.S., U.S. Patent no. 4,009,099 (1976).

60. Jeris, J.S., Beer, C., and Mueller, J.A., U.S. Patent no. 3,956, 129 (1974).

61. Jeris, J.S., Beer, C., and Mueller, J.A., "High Rate Biological Denitrification Using A Granular Fluidized Bed." Jour. Water Poll. Contr. Fed. 46, 2118 (1974).

62. Jeris, J.S., and Owens, R.W., "Pilot-Scale, High-Rate Biological Denitrification." Jour. Water Poll. Contr. Fed. 47, 2043 (1975).

63. Jeris, J.S., Owens, R.W., Hickey, R., and Flood, F., "Biological fluidized-bed treatment for BOD and nitrogen removal." Jour. Water Poll. Contr. Fed. vol 49, 816 (1977).

64. Johnson, M.J., "Aerobic Microbial Growth at Low Oxygen Concentration." Jour. of Bact. 94, 101 (1967).

65. Johnson, W.K., and Schroepfer, G.L., "Nitrogen removal by nitrification and denitrification." Jour. Water Poll. Contr. Fed. 36, 1015 (1964).

66. Jones, H.C., "Electron microscope study of a slime layer." Jour. of Bact. 99, 316 (1969).

67. Jones, J.R., "Denitrification by Anaerobic Filters and Ponds-Phase II." Rept. to Water Quality Office, U.S.E.P.A. (1971).

68. Kehrberger, G.J., and Busch, A.W., "Mass Transfer Effects in Maintaining Aerobic Conditions in Film-Flow Reactors." Jour. Water Poll. Contr. Fed. 43, 1514 (1971).

69. Kershenbaum, L., and Perkins, I.D., "The boundary conditions for a tubular vessel with well-mixed entrance region." Chem. Eng. Sci. 29, 624 (1974).

70. Kobayashi, T., and Laidler, K., "Kinetic Analysis for Solid Supported Enzymes." Biochem. Biophys Acta. 1, 302 (1973).

71. Kornegay, B.H., and Andrews J.F., "Characteristics and Kinetics of Biological Film Reactors." Federal Water Pollution Control Administration, Final Report, Research Grant WP-01181, Dept. of Environmental Systems Engineering, Clemson Univ. (1969).

72. Kramers, H., Westerman, M.D., de Groot, J.H., and Dupont, F.A.A., "The Interactions Between Fluids and Particles." Third Congress of the European Fed. of Chem. Engrs., p 114 (1962).

73. Krishnaswamy, P.R., and Shemilt, L.W., "Frequency Response in Liquid Fluidized Systems. Part 1. Effect of Particle Density and Size." Can. Jour. Chem. Eng. 51, 680 (1973).

74. Krogh, A., "The rate of diffusion of gases through animal tissues, with some remarks on the coefficient of invasion." J. Physiol. 52, 391 (1919).

75. Kynch, G.J., "The effective viscosity of suspensions of spherical particles." Proc. Roy. Soc. (London) A237, 90 (1956).

76. La Motta,E.J., "Evaluation of Diffusional Resistances in Substrate Utilization by Biological Films." Ph.D. Dissertation, University of North Carolina (1974).

77. La Motta,E.J., Personal Communication, University of Massachusetts, Amherst (1978).

78. Langmuir, I.S., "Respiration Rate of Bacteria as a Function of Oxygen Concentration." Biochem. Jour. 57, 81 (1954).

79. Lapple, C.E., and Shepherd, C.B., "Calculation of Particle Trajectories." Ind. Eng. Chem. 32, 605 (1940).

80. Lawrence, A.W., and McCarty, P.L., "Kinetics of Methane Fermentation in Aerobic Treatment." Jour. Water Poll. Contr. Fed. 41, R1 (1969).

81. Lawrence, A.W., McCarty, P.L., "Unified Basis for Biological Treatment Design and Operation." Jour. San. Eng. Div., A.S. C.E. SA3, 757 (1970).

82. Leva, M., Grummer, M., Weintraub, M., and Pollchik, M., "Introduction to Fluidization." Chem. Eng. Prog. 44, 511 (1948).

83. Levenspiel, O., Chemical Reaction Engineering, John Wiley and Sons, New York (1972).

84. Levich, V.G., Physicochemical Hydrodynamics, Translated by Scripta Technica, Inc., Prentice Hall, Englewood Cliffs, N.J., (1962).

85. Lewis, E.W., and Bowerman, E.W., "Fluidization of Solid Particles in Liquid." Chem. Eng. Prog. 48, 605 (1952).

86. Lewis, E.W., Gilliland, E.R. and Bauer, W.C., "Characteristics of Fluidized Particles." Ind. Eng. Chem. 41, 1104 (1949).

87. Loeffler, A.L., Jr., and Ruth, B.F., "Particulate Fluidization and Sedimentation of Spheres." Amer. Inst. of Chem. Eng., Jour. 5, 310 (1959).

88. Maier, W.J., Behn, V.C., and Gates, C.D., "Simulation of the Trickling Filter Process." Jour. San. Eng. Div., A.S.C.E. 93. 91 (1967).

89. McCabe, W.L., and Smith, J.C., Unit Operation of Chemical Engineering, 3rd ed., McGraw Hill, New York (1976).

90. McCarty, P.L., Beck, L., and St. Amant, P., "Biological Denitrification of Wastewaters by Addition of Organic Materials." Proc. 24th Industrial Waste Conference, Purdue Univ., Lafayette, Ind. (1969).

91. McCarty, P.L., "Nitrification-Denitrification by Biological Treatment." Correspondence Conference on Denitrification of Municipal Wastes, Univ. of Mass., Amherst (1973).

92. McCune, L.K., and Wilhelm, R.H., "Mass and Momentum Transfer in Solid-Liquid System-Fixed and Fluidized Beds." Ind. Eng. Chem. 41, 1124 (1949).

93. Mehta, D.S., Davis, H.H., and Kinsbury, R.P., "Oxygen Theory in Biological Treatment Plant Design." Jour. San. Eng. Div., A.S. C.E. 98, 471 (1972).

94. Meschner, K., and Wuhrmann, K., "Beitrag Zur Kenntnis der Microbiellen Denitrifikation." Path. Microbiol. 26, 579 (1963).

95. Mooney, M., "The viscosity of a concentrated suspension of spherical particles." J. Colloid. Sci. 6, 162 (1951).

96. Moore, S.F., and Schroeder, E.D., "The Effect of Nitrate Feed Rate on Denitrification." Water Res. 5, 445, (1971).

97. Morse, R.D., "Fluidization of Granular Solids." Ind. Eng. Chem. 41, 1117 (1949).

98. Mueller, J.A., "Oxygen Diffusion through a Pure Culture Floc of Zooglea ramigera. Ph.D. Dissertation, Universtiy of Wisconsin (1966).

99. Mueller, J.A., "Mass Transfer in Biological Systems, Phase 1. State of the Art." A report issued by the Environmental Eng. and Sci. Program, Civil Eng. Dept., Manhattan College (1974).

100. Mulbarber, M.C., "The Three Sludge System for Nitrogen and Phosphorus Removal." Presented at the 44th Annual Conference of the Water Pollution Control Federation, San Francisco, Calif. October (1971).

101. Nicholas, D.J.D., "The Metabolism of Inorganic Nitrogen and its Compounds in Microorganisms." Biol. Rev. 38, 530 (1963).

102. Oliver, D.R., "The Sedimentation of Suspensions of Closely-Sized Sphere Particles." Chem. Eng. Sci. 15, 230 (1961).

103. Painter, H.A., "A Review of Literature on Inorganic Nitrogen Metabolism in Microorganisms." Water Res. 4, 393 (1970).

104. Pasveer, H., "Distribution of Osygen in Activated Sludge Floc." Sewage and Ind. Wastes 26, 28 (1954).

105. Pearson, J.R.A.,"A note on the Danckwerts boundary conditions for continuous flow reactors." Chem. Eng. Sci. 10, 281 (1959).

106. Perry, J.H., Editor, Chemical Engineers' Handbook, 4th Edition, McGraw Hill, New York, pp.14-25 (1963).

107. Petrovic, J.J., and Thodos, G., "Effectiveness Factors for Heat Transfer in Fluidized Beds." Can. Jour. of Chem. Eng. 46, 114 (1968).

108. Pichinoty, F., and D'Ornano, L., "Sur le mechanisme de l'inhibitien par l'oxygine del la denitrification bacterienne." Biochem. Biophys. Acta 52, 386 (1961).

109. Renner, E.D., and Becker, G.E., "Production of Nitric Oxide and Nitrous Oxide During Denitrification by Coryebacterium nephridii." Jour. Bacteriol. 101, 821 (1970).

110. Requa, D.A., and Schroeder, E.D., "Kinetics of packed bed denitrification." Jour. Water Poll. Cont. Fed. 45, 1696 (1973).

111. Rhodes, A., Fletcher, D.L., Principles of Industrial Microbiology, Permagon Press, London (1971).

112. Ricetti, R.E. and Thodos, G., "Mass Transfer in the Flow of Gases Through Fluidized Beds." Amer. Inst. of Chem. Eng., Jour. 7, 442 (1961).

113. Richardson, J.F., and Meikle, R.A., "Sedimentation and Fluidization-Part IV: Drag Force on Individual Particles in an Assemblage." Trans. Inst. Chem. Eng. 39, 357 (1961).

114. Richardson, J.F., and Zaki, W.N.,"Sedimentation and Fluidization: Part I." Trans. Inst. Chem. Eng. 32, 35 (1954).

115. Robinson, C.S., "Some Factors Influencing Sedimentation." Ind. Eng. Chem. 18, 869 (1926).

116. Rowe, P.N., and Claxton, K.T., "Heat and Mass Transfer from a Single Sphere to Fluid Moving Through an Array." Trans. Inst. Chem. Eng. 43, T321 (1965).

117. Sanders, W.M., "Oxygen Utilization by Slime Organisms in Continous Culture." Air and Water Poll., Int. Jour. 10, 253 (1966).

118. Satterfield, C.N., Mass Transfer in Heterogeneous Catalysis., MIT Press, Cambridge, Mass. (1968).

119. Schneider, P., and Mitschka, P., "Effect of Internal Diffusion on Catalytic Reactions, III." Collection of Czechoslovak Chemical Communications 31, 1205 (1966).

120. Schroeder, E.D., and Busch, A.W., "The Role of Nitrate Nitrogen in Bio-oxidation." Jour. Water Poll. Contr. Fed. 40, R445 (1968).

121. Shieh, W.K., "Kinetics of Simultaneous Diffusion and Reaction for the Nitrification Process in Suspended Growth Systems." Ph.D. Dissertation, University of Massachusetts, Amherst (1978).

122. Skerman, V.B.D., and I.C. MacRae, "The Influence of Oxygen Availability on the Degree of Nitrate Reduction by Pseudomonas Denitrificans." Can. J. Microbiology 3, 505 (1957).

123. Smith, J.M., Chemical Engineering Kinetics, 2nd Edition, McGraw Hill, New York (1970).

124. Smith, J.M., Masse, A.N., Feige, W.A., and Kamphake, L.J., "Nitrogen Removal from Municipal Waste Water by Columnar Denitrification." Env. Sci. Tech. 6, 260 (1972).

125. Speece, R.E., "Downflow Bubble Contact Aeration." San. Eng. Div., A.S.C.E. SA4, 433 (1971).

126. Snowdon, C.B., and Turner, J.C.R., "Mass transfer in liquid-fluidized beds of ion exchange resin beads." in Proc. of the International Symposium on Fluidization, Eindhoven, A.A.H. Drinkenburg, ed. pp 599-608 (1967)

127. Steinour, J.H., "Rate of Sedimentation. Non-flocculent Suspensions of Uniform Spheres." Ind. Eng. Chem. 36, 618 (1944).

128. Stensel, H.D., "Biological Kinetics of the Suspended Growth Denitrification Process." Ph.D. Dissertation, Cornell Univ., (1971).

129. Stumm-Zollinger, E., Busch, P.L., and Stunm, W., discussion of "Kinetics of Aerobic Removal of Organic Wastes." by Keshavan, et al., Jour. San. Eng. Div. A.S.C.E. 90, No. SA4, 107 (1964).

130. Swilley, E.L., "Transport Phenomena and Rate Control in Trickling Filter Flow Models." Ph.D. Dissertation, Rice Univ. (1965).

131. Tamblyn, T.A., and Sword, B.R., "The Anaerobic Filter for the Denitrification fo Agricultural Subsurface Drainage." Proc. 24th Ind. Waste Conf., Purdue University, Part I, 263 (1969).

132. Taniguchi, S., Sato, R., and Egami, F., "The Enzymatic Mechanisms of Nitrate and Nitrite Metabolism in Bacteria." In Inorganic Nitrogen Metabolism, W.D. McElroy and B. Glass, Eds., Johns Hopkins Press, Baltimore, Md. (1956).

133. Tardos, G.I., Gutfinger, C., and Abuaf, N., "High Peclet Number Mass Transfer to a Sphere in a Fixed or Fluidized Bed." Amer. Inst. of Chem. Eng., Jour. 22, 1147 (1976).

134. Thiele, E.W., "Relation between Catalytic Activity and Size of Particle." Ind. Eng. Chem. 31, 916 (1939).

135. Tomlinson, T.G., and Snaddon, D.H.M., "Biological Oxidation of Sewage by Films of Microorganisms." Air and Water Poll., Int. Jour. 10, 865 (1966).

136. Trawinski, H., "Heat transfer between fluidized beds and container wall." Chem. Ing.-Tech. 24, 444 (1952).

137. U.S. Environmental Protection Agency Technology Transfer, Process Design Manual for Nitrogen Control, (1975).

138. Verhoven, W., In Inorganic Nitrogen Metabolism, W.D. McElroy and B. Glass, Eds., Johns Hopkins Press, Baltimore (1956).

139. Von Rosenburg, D.U., Methods for the Numerical Solution of Partial Differential Equations, Elsevier, New York (1969).

140. Wallis, G.B., One-Dimensional Two-Phase Flow, McGraw Hill, New York (1969).

141. Warburg, O., "Physical chemistry of cell respiration." Biochem. Z. 119, 134 (1921).

142. Weber, W.J., Jr., Hopkins, C.B. and Bloom, R., Jr., "Physicochemical treatment of wastewater." Jour. Water Poll. Contr. Fed. 42, 83 (1970).

143. Weber, W.J., Jr., Hopkins, C.B., and Bloom, R., Jr., "Expanded bed adsorption systems for treatment of sewage effluents." AIChE Symposium Series, Water 1970.

144. Weber, W.J., Jr., Friedman, L.D., and Bloom, R., Jr., "Biologically-Extended Physicochemical Treatment." Proc., Sixth Int. Conf. on Water Poll. Res., 18-23 June, 1972.

145. Wehner, I.F., and Wilhelm, R.H., "Boundary conditions on flow reactor." Chem. Eng. Sci. 6, 89 (1956).

146. Wen, C.Y., and Fan, L.T., Models for Flow Systems and Chemical Reactors, Marcel Dekker, New York (1975).

147. Wen, C.Y., and Yu, Y.H., "Mechanics of Fluidization." Chem. Eng. Prog. Symp. Ser. No. 62, 100 (1966).

148. Whitehead, A.B., and Dent, D.C., Proc. of the Internat. Symp. on Fluidization, Netherlands Univ. Press, Amsterdam (1967).

149. Whitmore, R.L., "The Relationship of the Viscosity to the Settling Rate of Slurries." Jour. Inst. Fuel 30, 238 (1957).

150. Wilhelm, R.H., and Kwauk, M., "Fluidization of Solid Particles." Chem. Eng. Prog. 44, 201 (1948).

151. Williamson, K., "The Kinetics of Substrate Utilization by Bacterial Films." Ph.D. Dissertation, Stanford Univ. (1973).

152. Williamson, K.J., and McCarty, P.L., "A Model of Substrate Utilization by Bacterial Films." Jour. Water Poll. Contr. Fed. 48, 9 (1976).

153. Wilson, B.W., "The sedimentation of dense suspensions of microscopic spheres." Austral. Jour. Appl. Sci. 4, 274 (1953).

154. Wuhrman, K., "Microbial Aspects of Water Pollution Control," Advances in Applied Microbiology 6, 119 (1964).

155. Zeldovich, Y.B., "The theory of reactions on powders and porous substances." Acta Physicochim. U.R.S.S. 10, 583 (1939).

156. Zenz, F.A., "Fluidcatalyst design data. I. How solid catalysts behave." Petrol. Refiner 36, 173 (1957).

A P P E N D I X I

NUMERICAL SOLUTION FOR BIOFILM EFFECTIVENESS; SPHERICAL COORDINATES

In Section 4.3, the differential equation describing substrate transport and reaction within a spherical biofilm was developed. The equation was expressed in dimensionless form as follows:

$$\frac{d^2C}{dx^2} + \frac{2}{(x + \xi)} \frac{dC}{dx} - \phi^2 \frac{C}{\gamma + C} = 0 \qquad 4.34$$

The appropriate boundary conditions on Equation 4.34 were shown to be:

$$\frac{dC}{dx} = Bi \ (1 - C) \text{ at } x = 1 \qquad 4.35$$

$$\frac{dC}{dx} = 0 \qquad \text{at } x = 0 \qquad 4.36$$

These differential equations may be converted to finite difference equations through use of the following second order correct analogs:

$$\left.\frac{d^2C}{dx^2}\right|_i = \frac{C_{i+1} - 2C_i + C_{i-1}}{(\Delta x)^2} \qquad A1.1$$

$$\left.\frac{dC}{dx}\right|_i = \frac{C_{i+1} - C_{i-1}}{2(\Delta x)} \qquad \text{A1.2}$$

Using these difference analogs, Equation 4.34 may be approximated as follows:

$$\frac{C_{i+1} - 2C_i + C_{i-1}}{(\Delta x)^2} + \frac{2}{\xi + i\,(\Delta x)}\left\{\frac{C_{i+1} - C_{i-1}}{2(\Delta x)}\right\} - \phi^2\left\{\frac{C_i}{\gamma + C_i}\right\} = 0 \qquad \text{A1.3}$$

Equation A1.3 is non-linear expression due to the presence of the quanity $(\gamma + C_i)$ in the denominator of the final term. Thus, direct solution of the equation is not possible. Instead, an interative solution procedure is employed in which the dependent variable in this quantity, C_i, is approximated by an assumed value $\hat{C}_i$. Equation A1.3 can then be solved and the computed values C_i compared with the assumed values $\hat{C}_i$. If the comparison is unsatisfactory, the computed C_i values are used to replace the assumed $\hat{C}_i$ values for the next trial solution. Thus, a linearized form of Equation A1.3 may be written as follows, with i = Z at x = 0:

$$\left(\frac{1}{(\Delta x)^2} - \frac{1}{(\Delta x)\;\xi + (i-2)(\Delta x)}\right) C_{i-1} + \left(\frac{-2}{(\Delta x)^2} - \frac{\phi^2}{(\gamma + \hat{C}_i)}\right) C_i +$$

$$\left(\frac{1}{(\Delta x)^2} + \frac{1}{(\Delta x)\;\xi + (i-2)(\Delta x)}\right) C_{i+1} = 0 \qquad \text{A1.4}$$

For convenience, Equation A1.4 may be rewritten as:

$$AP_i\ C_{i-1} + BP_i\ C_i + FP_i\ C_{i+1} = DP_i \qquad A1.5$$

The boundary conditions, Equation 4.35 and 4.36 may be expressed in finite difference form as follows:

$$\frac{C_{i+1} - C_{i-1}}{2(\Delta x)} = B_i\ (1 - C_i) \quad \text{at} \quad i = R + 2 \qquad A1.6$$

$$\frac{C_{i+1} - C_{i-1}}{2(\Delta x)} = 0 \quad \text{at} \quad i = 2 \qquad A1.7$$

where R is the number of increments in the interval between x = 0 and x = 1.

Equation A1.5 may then be written for the R + 1 nodes which correspond to the R biofilm increments i.e., $2 \leq i \leq R + 2$. The resultant tridiagonal matrix of equations is conveniently solved by computer using an algorithm developed by Thomas (139). This algorithm has been found to be stable to round-off errors for finite difference equations of this type (139).

The algorithm is as follows:

First, compute $BB_i = BP_i - \frac{AP_i\ FP_{i-1}}{BB_{i-1}}$ with $BB_2 = BP_2$ A1.8

$$\text{and} \quad GG_i = \frac{DP_i - AP_i\ GG_{i-1}}{BB_i} \quad \text{with } GG_2 = \frac{DP_2}{BP_2} \ . \qquad \text{A1.9}$$

The values of the dependent variable are than computed from:

$$C_{R+2} = GG_{R+2} \qquad \text{A1.10}$$

and

$$C_i = GG_i - \frac{FP_i\ C_{i+1}}{BB_i} \qquad \text{A1.11}$$

The substrate concentration profile obtained by the method outlined above may then be used to compute the biofilm overall effectiveness factor η_o, defined in Section 4.3 as:

$$\eta_o = \frac{1 + \gamma}{\xi^2 + \xi + 1/3} \int_0^1 \frac{C}{\gamma + C} (x + \xi)^2\, dx. \qquad 4.39$$

Equation 4.39 may be approximated by the following difference equation:

$$\eta_o = \frac{(1+\gamma)\ \Delta x}{8(\xi^2 + \xi + 1/3)} \sum_{i=2}^{R+1} \left[\frac{C_i}{\gamma + C_i} + \frac{C_{i+1}}{\gamma + C_{i+1}} \right] (x_i + x_{i+1} + 2\xi)^2 \qquad \text{A1.12}$$

A P P E N D I X I I

NUMERICAL SOLUTION OF THE FBBR FLOW EQUATION

In Section 4.1, the differential equation describing substrate transport and reaction within a fluidized bed biofilm reactor was developed, in dimensionless form, this equation was expressed as follows:

$$\frac{dB}{dY} - Bo\ \frac{d^2B}{dY^2} + \eta_o\left[1-\varepsilon - \frac{V_m}{H_B A}\right]\frac{\tau\ k\ \rho_B}{S_b|_{Z=0}}\ \frac{B}{\Omega + B} = 0 \qquad 4.15$$

Boundary conditions on Equation 4.15 were given as:

$$B = 1 \quad at \quad Y = 0 \qquad 4.7$$

$$\frac{dB}{dY} = 0 \quad at \quad Y = 1 \qquad 4.8$$

The following second order correct analogs may be used to convert these differential equations to finite difference equations:

$$\left.\frac{d^2B}{dY^2}\right|_i = \frac{B_{i+1} - 2B_i + B_{i-1}}{(\Delta Y)^2} \qquad A2.1$$

$$\left.\frac{dB}{dY}\right|_i = \frac{B_{i+1} - B_{i-1}}{2(\Delta Y)} \qquad \text{A2.2}$$

Equation 4.15 may then be approximated as follows:

$$\frac{B_{i+1} - B_{i-1}}{2(\Delta x)} - Bo\left(\frac{B_{i+1} - 2B_i + B_{i-1}}{(\Delta Y)^2}\right) + \eta_o\left(1-\varepsilon - \frac{V_m}{H_B A}\right)$$

$$\frac{\tau\, k\, \rho_B}{S_b}\bigg|_{Z=0} \frac{B_i}{\Omega + B_i} = 0 \qquad \text{A2.3}$$

A non-linearity is encountered in Equation A2.3 due to the $(\Omega + B_i)$ term. This necessitates an iterative solution procedure in which Equation A2.3 is linearized by replacing the dependent variable in this term B_i with a trial value $\hat{B}_i$. Equation A2.3 can then be solved and the computed values B_i compared with the trial values $\hat{B}_i$. If the comparison is unsatisfactory, the computed B_i values are used to replace the assumed $\hat{B}_i$ values for the next trial solution. With this linearization, Equation A2.3 may be rewritten as follows:

$$\left(-\frac{1}{2(\Delta Y)} - \frac{Bo}{(\Delta Y^2)}\right) B_{i-1} + \left(\frac{2Bo}{(\Delta Y)^2} + \frac{\eta_o\, EPH}{\Omega + \hat{B}_i}\right) B_i +$$

$$\left(\frac{1}{2(\Delta Y)} - \frac{Bo}{(\Delta Y)^2}\right) B_{i+1} = 0 \qquad \text{A2.4}$$

in which

$$EPH = \left\{ 1-\varepsilon - \frac{V_m}{H_B A} \right\} \cdot \frac{\tau \; k \; \rho_B}{S_b|_{Z=0}} \qquad A2.5$$

For convenience, Equation A2.4 may be rewritten as:

$$AR_i \; B_{i-1} + BR_i \; B_i + FR_i \; B_{i+1} = DR_i \qquad A2.6$$

The boundary condition equations may be expressed in finite difference form as follows:

$$B_i = 1 \quad \text{at} \quad i = 1 \qquad A2.7$$

$$\frac{B_{i+1} - B_{i-1}}{2(\Delta Y)} = 0 \quad \text{at} \quad i = IA + 1 \qquad A2.8$$

in which IA is the number of increments in the interval between Y = 0 and Y = 1 i.e., between Z = 0 and Z = H_B.

A tridiagonal matrix of equations results when Equation A2.6 is written for the IA + 1 nodes which correspond to the IA increments within the expanded bed. The algorithm developed by Thomas (139) can be used to solve this tridiagonal matrix as follows:

$$BBB_i = BR_i - \frac{AR_i\ FR_{i-1}}{BBB_{i-1}} \qquad \text{with } BBB_2 = BR_2 \qquad \text{A2.9}$$

then

$$GGG_i = \frac{DR_i - AR_i GGG_{i-1}}{BBB_i} \qquad \text{with } GGG_2 = \frac{DR_2}{BR_2} \qquad \text{A2.10}$$

The values of the dependent variable, dimensionless bulk-substrate concentration, are then computed as follows:

$$B_{IA+1} = GGG_{IA+1} \qquad \text{A2.11}$$

$$B_i = GGG_i - \frac{FR_i\ B_{i+1}}{BBB_i} \qquad \text{A2.12}$$

FBBR MODEL - COMPUTER PROGRAM NOMENCLATURE

DSL	=	D_{SL}
RL	=	ρ_L
VIS	=	μ
DSB	=	D_{SB}
XK	=	k
XKS	=	K_S
Q	=	Q
SO	=	$S_b\|_{Z=0}$
XA	=	A
HB	=	H_B
RM	=	ρ_m
DM	=	d_m
VM	=	V_m
G	=	g
U	=	U
DEL	=	δ
DP	=	d_p
XM, X_B	=	coefficients in Eq. 4.17
RB	=	ρ_B
RBW	=	ρ_{BW}
RS	=	ρ_S
UT	=	U_t

RET = Re_t

XN = n

EP = ϵ

HBH = $\hat{H}_B$

P = ξ

EPH = defined by program statement 582

PTHS = defined by program statement 583

OM = Ω

XVS = X

BI = Bi

GA = Ga

REMF = Re_{MF}

RE = Re

PEA = Pe_A

BO = Bo

IA = number of reactor increments

DY = length of a reactor increment

B(I) = B_i

BH(I) = $\hat{B}_i$ = trial value of B_i

AR(I), BR(I), FR(I), DR(I) = reactor coefficient matrix defined by program statements 810, 820, 830, 835

BBB(I), GGG(I) = variables in Thomas' algorithm

TRO = dummy variable used as a marker

EROK = allowable error

PER = fractional error

DS(I) = Z

TA(I) = τ

TAU = τ

NO3-N = Nitrate-nitrogen concentration

ETA = η

IR = number of biofilm increments

DX = length of a biofilm increment

C(I) = C_i

CH(I) = $\hat{C}_i$ = trial value of C_i

GM(I) = γ_i

THS(I) = ϕ_i^2

AP(I), BP(I), FP(I), DP(I) = biofilm coefficient matrix defined by program statements 2270, 2280, 2290, 2300

BB(I), GG(I) = variables in Thomas' algorithm

TOO = dummy variable used as a marker

PE = fractional error

ALER = allowable error

ET = differential effectiveness factor

```
10 PROGRAM FBBR(INPUT,OUTPUT)
20 DIMENSION B(110),BH(110),ETA(110),AR(110),BR(110),
30+FR(110),BS(110),TA(110),DR(110),BBB(110),GGG(110)
95C   ### CGS UNITS USED THROUGHOUT ###
100C   ***LIQUID PHASE PARAMETERS  ***
110 DSL=1.67E-5
120 RL=.998
130 VIS=.009548
140C *** BFILM PARAMETERS ***
150 DSB=.815E-5
160 XK=3.32E-5
170 XKS=6.06E-8
180C *** SYSTEM DEP PARAMETERS ***
190 Q=11.4
200 SO=30.E-6
210C *** REACTOR PARAMETERS ***
220 XA=11.4
230 HB=94.
240C *** SUPPORT MEDIA PARAMETERS ***
250 RM=2.42
260 DM=6.82E-2
270 VM=50.
280C ************
290 G=980.62
300 U=Q/XA
310C ### BED FLUIDIZATION ALGORITHM ###
320 DEL=0.0
325 325 CONTINUE
330 DP=2.*DEL+DM
335C *** BIOFILM DENSITY-DEL CORRELATION ***
340 IF(DEL.LE.0.03)350,380
350 350 XM=0.0
360 XB=.065
370 GO TO 440
380 380 IF(DEL.LE.0.063)390,420
390 390 XM=-.035/.033
400 XB=.0968
410 GO TO 440
420 420 XM=0.0
430 XB=.03
440 440 RB=XM*DEL+XB
450 RBW=RL+RB/.8
460 RS=RBW+(RM-RBW)*(DM/DP)**3
470C *** PARTICLE TERMINAL VELOCITY ***
480 UT=((RS-RL)*G*DP**(5./3.)/(27.5*RL**(1./3.)
485+*VIS**(2./3.)))**(3./4.)
490 RET=UT*RL*DP/VIS
500C *** EXPANSION INDEX CORRELATION ***
510 XN=10.35*RET**(-.18)
```

```
520C *** CALC BED VOIDAGE ***
530 EP=(U/UT)**(1./XN)
540C *** CALC TRIAL BED HEIGHT ***
550 HBH=VM/(XA*(1.-EP))*(DP/DM)**3
560 IF(HBH.LT.HB)565,580
565 565 DEL=DEL+5.E-4
570 GO TO 325
580 580 CONTINUE
581 P=DM/(2.*DEL)
582 EPH=((1.-EP)-VM/(HB*XA))*(HB*XK*RB/(SO*U))
583 PTHS=XK*RB*DEL**2/DSB
584 OM=XKS/SO
585C *** CALC REACTOR VS ***
590 XVS=VM*RB/(XA*HB)*((DP/DM)**3-1.)
600 PRINT 610,DEL,DP,EP,XVS
610 610 FORMAT(4HDEL=,F10.5,/,3HDP=,F10.5,/,3HEP=,
615+ F10.5,/,4HXVS=,F10.8,/)
620C ##############
625C
630C *** BIOT NUMBER CORRELATION ***
635C *** BFILM EXTERNAL MASS TRANSFER ***
640 BI=(.81/EP)*(DSL/DSB)*(DEL/DP)*(U*RL*DP/VIS)**
645+ (1./2.)*(VIS/(RL*DSL))**(1./3.)
650 PRINT 660,BI
660 660 FORMAT(3HBI=,F10.5,/)
665C ##############
670C *** AXIAL DISPERSION CORRELATION ***
680 GA=(RS-RL)*RL*G*DP**3/VIS**2
690C *** MIN.FLUID. REYNOLDS NO ***
700 REMF=(33.7**2+.0408*GA)**(1./2.)-33.7
710 RE=U*RL*DP/VIS
720 PEA=REMF/(EP*RE)*(.2+.011*RE**(.48))
722 BO=DP/(HB*PEA)
725C   ###   NUMBER OF REACTOR SEGMENTS = IA   ###
730 IA=100
735 IAP=IA+1
737 IAM=IA-1
740 DY=1./FLOAT(IA)
745C   ###   DEFINE TRIAL PROFILE   ###
747 B(1)=1.
750 DO 770 IT=1,IAP
760 BH(IT)=1.
770 770 CONTINUE
775 775 CONTINUE
780 CALL BFILM(BH,BI,SO,XKS,PTHS,P,IA,ETA)
790C   ###   DEFINE COEFFICIENT MATRIX   ###
800 DO 840 I=1,IAP
810 AR(I)=-1./(2.*DY)-BO/DY**2
820 BR(I)=2.*BO/DY**2+EPH*ETA(I)/(OM+BH(I))
830 FR(I)=1./(2.*DY)-BO/DY**2
835 DR(I)=0.0
```

```
840 840 CONTINUE
850C   $$$   ENTRANCE BC   $$$
860 DR(2)=DR(2)-AR(2)
870 AR(2)=0.0
880C   $$$   EXIT BC   $$$
890 AR(IAP)=AR(IAP)+FR(IAP)
900 FR(IAP)=0.0
910C   #$#$#$   REACTOR THOMAS ALGORITHM   #$#$#$
920 BBB(2)=BR(2)
930 GGG(2)=DR(2)/BR(2)
940 DO 960 I=3,IAP
950 IM=I-1
960 BBB(I)=BR(I)-AR(I)*FR(IM)/BBB(IM)
970 GGG(I)=(DR(I)-AR(I)*GGG(IM))/BBB(I)
980 980 CONTINUE
990 B(IAP)=GGG(IAP)
1000 DO 1030 JJJ=1,IAM
1010 I=IAP-JJJ
1015 IP=I+1
1020 B(I)=GGG(I)-FR(I)*B(IP)/BBB(I)
1030 1030 CONTINUE
1040C   @@@@   COMPARE B & BH   @@@@
1050 TRO=0.0
1060 EROK=.01
1070 DO 1120 I=2,IAP
1080 PER=ABS((BH(I)-B(I))/B(I))
1090 IF(PER.GT.EROK)1100,1110
1100 1100 TRO=1.
1110 1110 CONTINUE
1115 BH(I)=B(I)
1120 1120 CONTINUE
1130 IF(TRO.EQ.1.)GO TO 775
1140 DO 1160 I=1,IAP
1142 IM=I-1
1144 DS(I)=DY*HB*FLOAT(IM)
1146 TA(I)=DS(I)/U
1150 B(I)=B(I)*SO
1160 1160 CONTINUE
1170 PRINT 1180
1180 1180 FORMAT(7X,1HZ,14X,3HTAU,14X,5HNO3-N,8X,3HETA,/)
1200 PRINT 1300,(DS(I),TA(I),B(I),ETA(I),I=1,IAP,5)
1300 1300 FORMAT(4F15.7)
1500 END
2000 SUBROUTINE BFILM(BH,BI,SO,XKS,PTHS,P,IA,ETA)
2015 DIMENSION CH(110),AP(110),BP(110),FP(110),DP(110),C(110),BB(110),GG(110)
2017+,GH(110),THS(110),ETA(110),BH(110)
2020 IR=100
2030 IRP=IR+1
2040 IRPP=IR+2
2050 IR3P=IR+3
2060 DX=1./FLOAT(IR)
```

```
2070 DO 2090 ICH=2,IRPP
2080 CH(ICH)=1.
2090 2090 CONTINUE
2100 IAP=IA+1
2140 DO 2690 KR=1,IAP
2150 GM(KR)=XKS/(BH(KR)*SO)
2155 THS(KR)=PTHS/(BH(KR)*SO)
2160 2160 CONTINUE
2165C
2170C   ***   DEFINE COEFFICIENT MATRIX   ***
2180 DO 2240 I=2,IRPP
2190 X2=FLOAT(I-2)
2200 AP(I)=1./DX**2-1./(DX*(P+X2*DX))
2210 BP(I)=-2./DX**2-THS(KR)/(GM(KR)+CH(I))
2220 FP(I)=1./DX**2+1./(DX*(P+X2*DX))
2230 DP(I)=0.0
2240 2240 CONTINUE
2250C
2260C   ***   BFILM EXTERIOR BC   ***
2270 AP(IRPP)=AP(IRPP)+FP(IRPP)
2280 BP(IRPP)=BP(IRPP)-2.*DX*BI*FP(IRPP)
2290 DP(IRPP)=-FP(IRPP)*2.*DX*BI
2300 FP(IRPP)=0.0
2310C
2320C   ***   BFILM INTERIOR BC   ***
2330 FP(2)=FP(2)+AP(2)
2340 AP(2)=0.0
2350C
2360C   ####   BFILM THOMAS ALGORITHM   ####
2370 BB(2)=BP(2)
2380 GG(2)=DP(2)/BP(2)
2390 DO 2430 I=3,IRPP
2400 IM=I-1
2410 BB(I)=BP(I)-AP(I)*FP(IM)/BB(IM)
2420 GG(I)=(DP(I)-AP(I)*GG(IM))/BB(I)
2430 2430 CONTINUE
2440 C(IRPP)=GG(IRPP)
2450 DO 2490 JJJ=2,IRP
2460 I=IR3P-JJJ
2470 IP=I+1
2480 C(I)=GG(I)-FP(I)*C(IP)/BB(I)
2490 2490 CONTINUE
2500 TOO=0.0
2510 DO 2570 I=2,IRPP
2520 PE=ABS(CH(I)-C(I))/C(I)
2530 ALER=0.001
2540 IF(PE.GT.ALER)2550,2560
2550 2550 TOO=1.
2560 2560 CH(I)=C(I)
2570 2570 CONTINUE
2580 IF(TOO.EQ.1.)GO TO 2160
```

```
2590 ET=0.0
2600 DO 2650 I=2,IRP
2610 IP=I+1
2620 X2=FLOAT(I-2)
2630 X1=FLOAT(I-1)
2640 ET=ET+(C(I)/(GM(KR)+C(I))+C(IP)/(GM(KR)+C(IP)))*((P+X2*DX)+(P+X1*DX
2645+))**2
2650 2650 CONTINUE
2660 ETA(KR)=ET*DX*(1.+GM(KR))/(8.*(P**2+P+1./3.))
2690 2690 CONTINUE
2695 RETURN
2700 END
READY.
```

A P P E N D I X I I I

NUMERICAL SOLUTION FOR BIOFILM EFFECTIVENESS; RECTANGULAR COORDINATES

In Section 5.1, the following differential equation for substrate transport and Michaelis-Menten reaction within a rectangular biofilm was developed:

$$D_{SB} \frac{d^2S}{dY^2} - \frac{k\rho_B S}{k_S+S} = 0 \qquad 5.2$$

The appropriate boundary conditions on Equation 5.2 are:

$$S = S_b \qquad \text{at} \qquad Y = 0 \qquad 5.3$$

$$\frac{dS}{dY} = 0 \qquad \text{at} \qquad Y = \delta \qquad 5.4$$

Using second order correct finite difference analogs the above equations may be rewritten as follows:

$$\left(\frac{1}{(dY)^2}\right) S_i - 1 + \left(-\frac{2}{(dY)^2} - \frac{k\rho_B / D_{SB}}{k_S + \hat{S}_i}\right) S_i + \left(\frac{1}{(dY)^2}\right) S_i + 1 = 0$$

A3.1

$$S_i = S_b \quad \text{at} \quad i = 1 \qquad \text{A3.2}$$

$$\frac{S_{i+1} - S_{i-1}}{2(dY)} = 0 \quad \text{at} \quad i = R + 1 \qquad \text{A3.3}$$

Equation A3.1 is made linear through introduction of the approximate term $\hat{S}_i$. See Appendix I for details of this approximation.

For convenience, Equation A3.1 was rewritten:

$$AD_i \; S_{i-1} + BD_i \; S_i + FD_i \; S_{i-1} = DD_i \qquad \text{A3.4}$$

Equation A3.4 may then be written for the R+1 nodes corresponding to the R biofilm increments in δ. As in Appendix I, Thomas' algorithm can then be used to solve the resultant tridiagonal matrix.

The substrate concentration profile, obtained as outlined above, may then be used to compute the biofilm overall effectiveness factor n_o defined in Section 5.1 as:

$$n_o = \frac{K_S + S_b}{\delta \; S_b} \int_0^{\delta} \frac{S}{k_S + S} \; dY \qquad 5.5$$

which is approximated by the following difference equation:

A P P E N D I X I V

EXPERIMENTAL DATA

Table 1.

RDR - Experimental Data; Rotational Speed Study

RPM	δ (μm)	ρ_B (mgVS/l)	T ^{0}C	pH	Q (ml/min)	S_f	S_b ($mgNO_3^-$-N/l)
50	42	60.8	22	6.9	49.	98.8	96.1
50	59	62.7	22	6.9	52.3	101.3	97.6
50	47	66.1	21.5	7.	51.3	102.1	99.
100	38	59.4	21.	6.9	48.6	98.4	95.5
100	61	65.8	21.5	6.8	49.4	97.3	92.3
150	36	61.1	21.5	6.8	49.1	100.2	97.4

Table 2.

RDR - EXPERIMENTAL DATA

δ	ρ_B	ρ_T	T	pH	Q	S_f	S_b
(μm)	($mgVS/cm^3$)	($mgTS/cm^3$)	^0C		(ml/min)	($mgNO_3^-$-N/l)	
38	54.5	72.7	21.	6.9	51.4	24.2	21.7
56	68.2	82.3	21.5	7.	47.8	24.7	19.8
84	63.4	79.3	21.	6.8	50.3	27.1	20.7
108	55.	61.1	22.	6.9	50.9	25.3	18.2
130	69.4	99.1	21.5	6.9	51.2	24.	16.4
155	71.5	89.4	22.	6.9	51.4	28.1	18.2
198	59.2	84.6	23.	6.9	49.	26.3	16.7
255	63.	70.	23.	7.	49.3	25.4	16.6
315	53.6	60.1	21.	6.9	50.4	27.	16.2
44	65.7	83.	23.	6.9	50.3	51.4	47.9
49	59.8	73.2	21.5	6.9	51.	47.8	44.3
68	68.3	84.3	22.	7.	49.3	50.3	44.5
97	72.4	91.5	21.5	6.9	45.2	50.9	41.4
112	60.1	74.1	22.	6.8	49.1	49.1	40.7
137	54.1	66.8	22.	6.8	54.3	48.	39.7
140	63.5	79.1	22.	6.9	49.1	52.8	41.9
177	63.8	79.4	21.	6.9	48.2	51.1	39.
210	53.6	68.	22.	6.9	54.3	52.6	40.
270	57.	71.5	21.5	6.9	52.	47.3	36.9
308	58.9	73.6	22.	7.	50.6	48.	33.5

Table 2. continued....

δ	ρ_B	ρ_T	T	pH	Q	S_f	S_b
36	61.1	76.2	22.	6.9	49.1	100.2	97.4
49	68.	84.	21.	6.9	50.6	99.8	95.7
93	58.	73.4	21.	6.8	52.3	96.	89.7
134	65.1	81.4	22.	6.8	48.3	102.3	91.3
136	63.4	78.5	23.	6.8	48.4	101.4	90.5
158	54.3	67.9	22.	7.	51.3	96.8	86.6
175	59.7	74.5	22.	6.9	47.6	103.1	89.7
210	62.	77.4	21.5	6.9	50.8	98.	82.4
258	59.3	74.4	21.5	7.	49.	102.	83.
310	56.4	71.3	22.	7.	52.2	97.5	77.2

Table 3.

FBBR - Bed Expansion

40 μm		88 μm		167 μm		207 μm	
U(cm/sec)	ε	U(cm/sec)	ε	U(cm/sec)	ε	U(cm/sec)	ε
.361	.609	.35	.605	.380	.56	.30	.577
.440	.625	.406	.607	.43	.589	.341	.604
.50	.640	.463	.631	.494	.598	.391	.607
.566	.659	.537	.651	.60	.629	.484	.641
.66	.670	.635	.660	.681	.641	.579	.662
.76	.691	.760	.690	.779	.659	.681	.687
.97	.720	.908	.715	.89	.673	.770	.706
1.3	.76	1.13	.740	1.0	.690	.881	.730
				1.14	.714	1.08	.750
				1.46	.745		

Table 3 Continued...

220 μm		268 μm		281 μm		318 μm	
U(cm/sec)	ε	U(cm/sec)	ε	U(cm/sec)	ε	U(cm/sec)	ε
.376	.615	.394	.631	.336	.581	.431	.619
.466	.635	.460	.654	.391	.605	.475	.621
.571	.669	.514	.670	.438	.620	.533	.642
.692	.680	.618	.680	.514	.639	.615	.655
.781	.709	.671	.701	.619	.661	.718	.688
.850	.710	.760	.719	.738	.691	.790	.695
.939	.736	.829	.720	.845	.708	.908	.720
1.13	.759	.960	.755	.990	.731	1.12	.749
		1.11	.770	1.18	.76	1.37	.780

Table 3 Continued...

344 μm		420 μm		547 μm		561 μm	
U(cm/sec)	ε	U(cm/sec)	ε	U(cm/sec)	ε	U(cm/sec)	ε
.385	.651	.379	.619	.307	.555	.375	.595
.424	.677	.405	.639	.332	.56	.313	.611
.460	.679	.525	.661	.372	.596	.360	.621
.539	.705	.610	.682	.426	.600	.431	.645
.600	.719	.720	.686	.459	.618	.531	.675
.679	.740	.822	.725	.520	.635	.672	.710
.810	.760	.949	.740	.610	.651	.789	.724
.922	.791	1.01	.751	.738	.688	.890	.758
1.04	.805	1.24	.79	.850	.701	.955	.762
				.938	.719	1.16	.80
				1.27	.777		

Table 3 Continued...

590 μm		666 μm		703 μm		812 μm	
U(cm/sec)	ε	U(cm/sec)	ε	U(cm/sec)	ε	U(cm/sec)	ε
.302	.637	.285	.589	.306	.629	.284	.591
.361	.668	.316	.611	.345	.639	.361	.600
.426	.679	.350	.630	.406	.662	.402	.621
.506	.702	.416	.638	.489	.700	.450	.669
.590	.729	.499	.665	.570	.722	.522	.680
.681	.750	.560	.679	.658	.750	.612	.705
.759	.768	.615	.692	.779	.761	.690	.718
.861	.779	.719	.710	.835	.779	.839	.759
.979	.801	.846	.740	.94	.795	.980	.780
1.23	.819	.975	.759	1.19	.839	1.14	.818
		1.23	.80				

Table 3 Continued...

858 μm		1005 μm		1089 μm		1207 μm	
U(cm/sec)	ε	U(cm/sec)	ε	U(cm/sec)	ε	U(cm/sec)	ε
.461	.658	.429	.630	.369	.659	.416	.655
.512	.660	.482	.655	.418	.661	.471	.678
.579	.685	.565	.680	.477	.685	.541	.691
.671	.702	.674	.712	.561	.710	.659	.720
.759	.725	.772	.735	.638	.721	.732	.734
.890	.750	.880	.750	.710	.739	.810	.751
1.09	.780	.975	.779	.789	.76	.916	.762
				.965	.785	1.05	.795

Table 4

Bioparticle Terminal Velocity

δ (microns)	ρ_B (mg VS/cm^3)	ρ_T (mg TS/cm^3)	U_t (cm/sec)
40	57.6	71.8	6.17
88	70.6	88.0	5.15
167	66.8	84.0	5.41
207	62.1	77.2	4.75
220	73.6	91.4	5.02
268	32.6	41.1	4.87
281	62.0	77.5	4.16
318	56.1	71.1	4.50
344	30.8	38.8	3.24
420	52.9	66.3	4.23
547	45.7	57.3	4.12
561	37.0	46.0	3.67
590	26.6	33.7	3.09
666	20.8	26.4	3.45
703	36.6	45.8	3.03
812	26.8	33.5	2.89

Table 4 continued. . .

δ (microns)	ρ_B (mg VS/cm^3)	ρ_T (mg TS/cm^3)	U_t (cm/sec)
858	34.7	43.6	3.50
1005	31.1	38.9	3.17
1089	24.7	31.2	2.87
1207	21.1	26.0	2.95

Settling column water temperature = 20°

Table 5

FBBR Experimental Data

δ = 40 microns

X = 5054 mg VS/l

U = 0.76 cm/sec

Influent pH = 6.8

Effluent pH = 7.8

Effluent Temp. = 22°C

τ (sec)	NO_3^--N (mg/l)
0	22.6
21.7	17.9
50.0	12.3
78.3	7.1
106.6	3.3
134.9	1.1
180.3	0.9

Table 5 continued. . .

δ = 88 microns

X = 10016 mg VS/l

U = 0.908 cm/sec

Influent pH = 6.9

Effluent pH = 7.8

Effluent Temp. = 21°C

τ (sec)	NO_3^--N (mg/l)
0	24.5
19.8	17.7
43.5	10.4
67.2	5.1
90.9	2.3
114.55	1.8
133.8	1.1

Table 5 continued. . .

δ = 167 microns

X = 15214 mg VS/l

U = 0.89 cm/sec

Influent pH = 6.9

Effluent pH = 7.9

Effluent Temp. = 22°C

τ (sec)	NO_3^--N (mg/l)
0	30.5
19.7	22.0
43.8	13.5
67.95	7.4
92.1	3.6
110.6	2.0

Table 5 continued. . .

δ = 207 microns

X = 11784 mg VS/l

U = 1.07 cm/sec

Influent pH = 7.0

Effluent pH = 7.6

Effluent Temp. = 22°C

τ (sec)	NO_3^--N (mg/l)
0	21.0
15.75	17.8
36.61	13.9
56.53	10.7
76.46	8.0
96.39	6.1
142.73	4.4

Table 5 continued. . .

δ = 220 microns

X = 16551 mg VS/l

U = 0.85 cm/sec

Influent pH = 6.8

Effluent pH = 7.8

Effluent Temp. = 19.5°C

τ (sec)	NO_3^--N (mg/l)
0	21.4
21.2	15.0
46.5	9.0
71.76	4.9
97.1	2.6
122.4	1.8
162.9	1.5

Table 5 continued. . .

δ = 268 microns

X = 6182 mg VS/l

U = 1.1 cm/sec

Influent pH = 6.9

Effluent pH = 7.4

Effluent Temp. = 21°C

τ (sec)	NO_3^--N (mg/l)
0	21.8
17.3	17.6
36.8	14.9
56.4	12.6
75.9	9.9
95.5	7.6
108.2	6.8

Table 5 continued. . .

δ = 281 microns

X = 10357 mg VS/l

U = 1.59 cm/sec

Influent pH = 6.8

Effluent pH = 7.4

Effluent Temp. = 20°C

τ (sec)	NO_3^--N (mg/l)
0	21.3
11.7	18.6
25.2	16.0
38.7	13.3
52.3	11.2
65.8	9.7
72.7	8.9

Table 5 continued. . .

δ = 318 microns

X = 12807 mg VS/l

U = 1.03 cm/sec

Influent pH = 7.0

Effluent pH = 7.3

Effluent Temp. = 21°C

τ (sec)	NO_3^--N (mg/l)
0	22.1
17.1	17.4
38.5	12.7
58.9	9.3
79.9	6.4
91.6	4.8

Table 5 continued. . .

δ = 344 microns

X = 5400 mg VS/l

U = 1.0 cm/sec

Influent pH = 6.8

Effluent pH = 7.4

Effluent Temp. = 22°C

τ (sec)	NO_3^--N (mg/l)
0	24.4
21.5	20.0
43.0	17.4
64.5	14.7
86.0	11.8
107.5	9.1
124.5	7.9

Table 5 *continued. . .*

δ = 420 microns

X = 8184 mg VS/l

U = 1.8 cm/sec

Influent pH = 6.8

Effluent pH = 7.3

Effluent Temp. = 19°C

τ (sec)	NO_3^--N (mg/l)
0	20.7
10.0	19.3
22.2	17.7
33.9	16.3
45.9	14.8
57.8	13.5
68.4	12.5

Table 5 continued. . .

δ = 547 microns

X = 10778 mg VS/l

U = 1.14 cm/sec

Influent pH = 7.0

Effluent pH = 7.6

Effluent Temp. = 22°C

τ (sec)	NO_3^--N (mg/l)
0	16.0
16.7	13.5
35.5	10.9
54.4	8.5
73.2	6.6
92.1	5.0
119.3	3.9

Table 5 continued. . .

δ = 561 microns

X = 7875 mg VS/l

U = 1.04 cm/sec

Influent pH = 6.8

Effluent pH = 7.8

Effluent Temp. = 20°C

τ (sec)	NO_3^--N (mg/l)
0	57.0
17.9	51.6
38.6	45.5
59.4	39.5
76.8	34.9

Table 5 continued. . .

δ = 590 microns

X = 5059 mg VS/l

U = 0.98 cm/sec

Influent pH = 6.9

Effluent pH = 7.7

Effluent Temp. = 22°C

τ (sec)	NO_3^--N (mg/l)
0	35.3
19.4	31.8
41.3	28.1
63.3	24.6
85.2	21.9
99.5	20.2

Table 5 continued. . .

δ = 666 microns

X = 6398 mg VS/l

U = 0.56 cm/sec

Influent pH = 7.0

Effluent pH = 7.6

Effluent Temp. = 20°C

τ (sec)	NO_3^--N (mg/l)
0	27.1
33.1	22.3
71.5	16.1
109.9	11.5
148.3	8.6
186.7	6.8
206.4	6.2

Table 5 continued. . .

δ = 703 microns

X = 8125 mg VS/l

U = 0.82 cm/sec

Influent pH = 7.0

Effluent pH = 8.0

Effluent Temp. = 23°C

τ (sec)	NO_3^--N (mg/l)
0	30.1
20.8	25.0
47.2	18.7
73.5	13.6
99.9	9.5
126.3	6.5
133.6	5.5

Table 5 continued. . .

δ = 812 microns

X = 5744 mg VS/l

U = 0.98 cm/sec

Influent pH = 6.8

Effluent pH = 7.5

Effluent Temp. = 22°C

τ (sec)	NO_3^--N (mg/l)
0	24.1
17.4	21.4
39.3	18.6
61.2	16.4
83.2	14.5
105.0	12.8
151.0	10.8

Table 5 continued. . .

δ = 858 microns

X = 10171 mg VS/l

U = 0.67 cm/sec

Influent pH = 6.9

Effluent pH = 7.9

Effluent Temp. = 21°C

τ (sec)	NO_3^--N (mg/l)
0	23.3
26.1	19.6
58.2	15.7
90.3	12.2
122.4	9.4
154.4	7.1
200.7	5.4

Table 5 continued. . .

δ = 1005 microns

X = 7649 mg VS/l

U = 0.88 cm/sec

Influent pH = 6.9

Effluent pH = 7.6

Effluent Temp. = 22°C

τ (sec)	NO_3^--N (mg/l)
0	19.2
19.3	16.7
43.8	13.9
68.2	11.3
92.6	9.0
117.1	7.0
134.1	5.9

Table 5 continued. . .

δ = 1089 microns

X = 6091 mg VS/l

U = 0.76 cm/sec

Influent pH = 6.8

Effluent pH = 7.8

Effluent Temp. = 23°C

τ (sec)	NO_3^--N (mg/l)
0	24.0
24.9	19.2
53.1	14.4
81.2	10.5
109.4	8.0
137.6	6.1
148.1	5.7

Table 5 continued. . .

δ = 1207 microns

X = 5845 mg VS/l

U = 0.66 cm/sec

Influent pH = 7.0

Effluent pH = 7.5

Effluent Temp. = 19°C

τ (sec)	NO_3^--N (mg/l)
0	18.3
28.0	15.8
60.6	13.3
93.2	11.0
125.8	8.7
158.4	7.2
203.2	5.4

Figures A1 to A10. Comparisons of nitrate profiles, biomass holdups and biofilm thicknesses observed in the laboratory FBBR and predicted by the FBBR model for each of the twenty experimental runs.

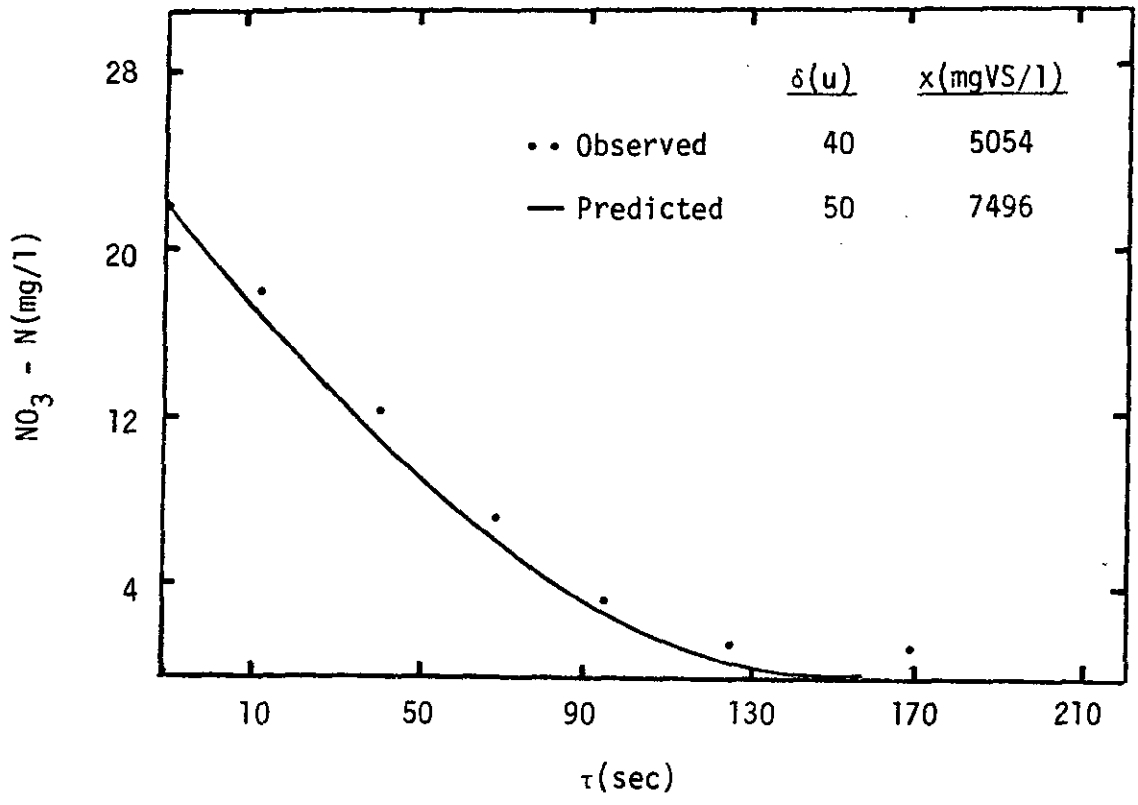
δ(u)
x(mgVS/l)
•• Observed
40
5054
— Predicted
50
7496
28
20
12
4
NO_3 - N(mg/l)
10
50
90
130
170
210
τ(sec)

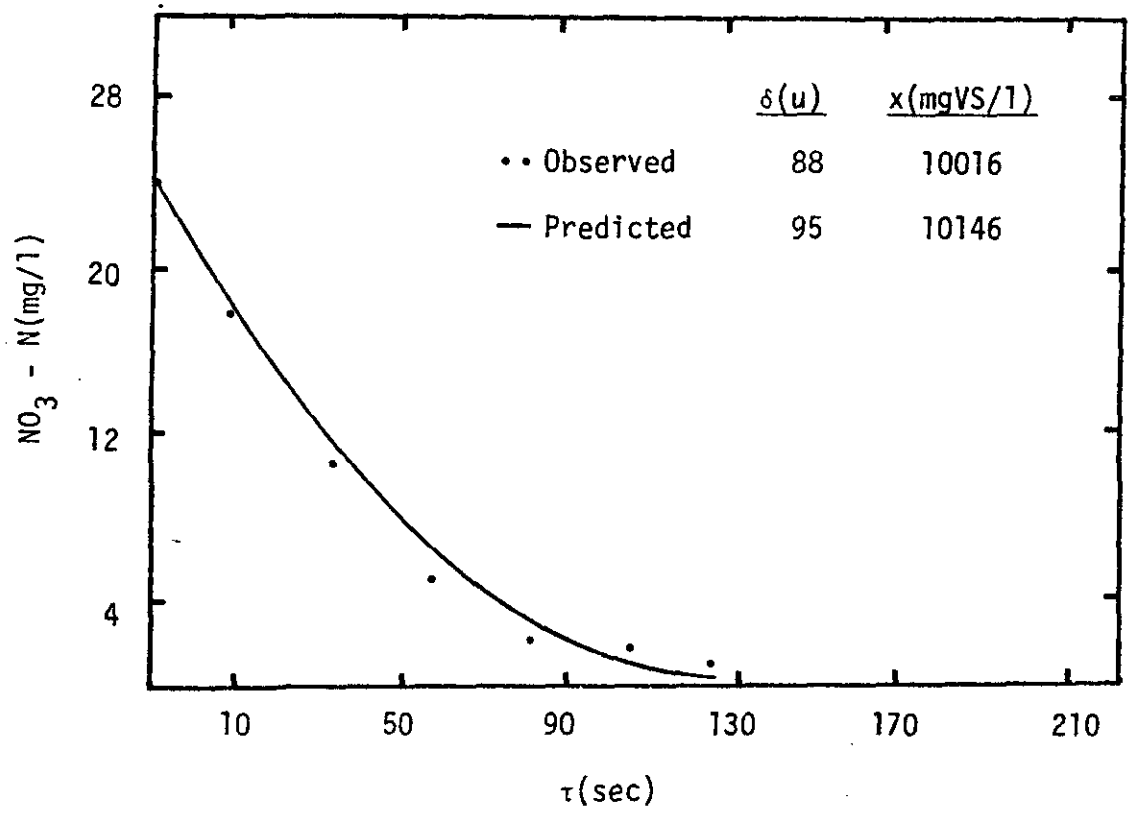
δ(u)
x(mgVS/l)
•• Observed
88
10016
— Predicted
95
10146
28
20
12
4
NO_3 - N(mg/l)
10
50
90
130
170
210
τ(sec)

Figure A1.

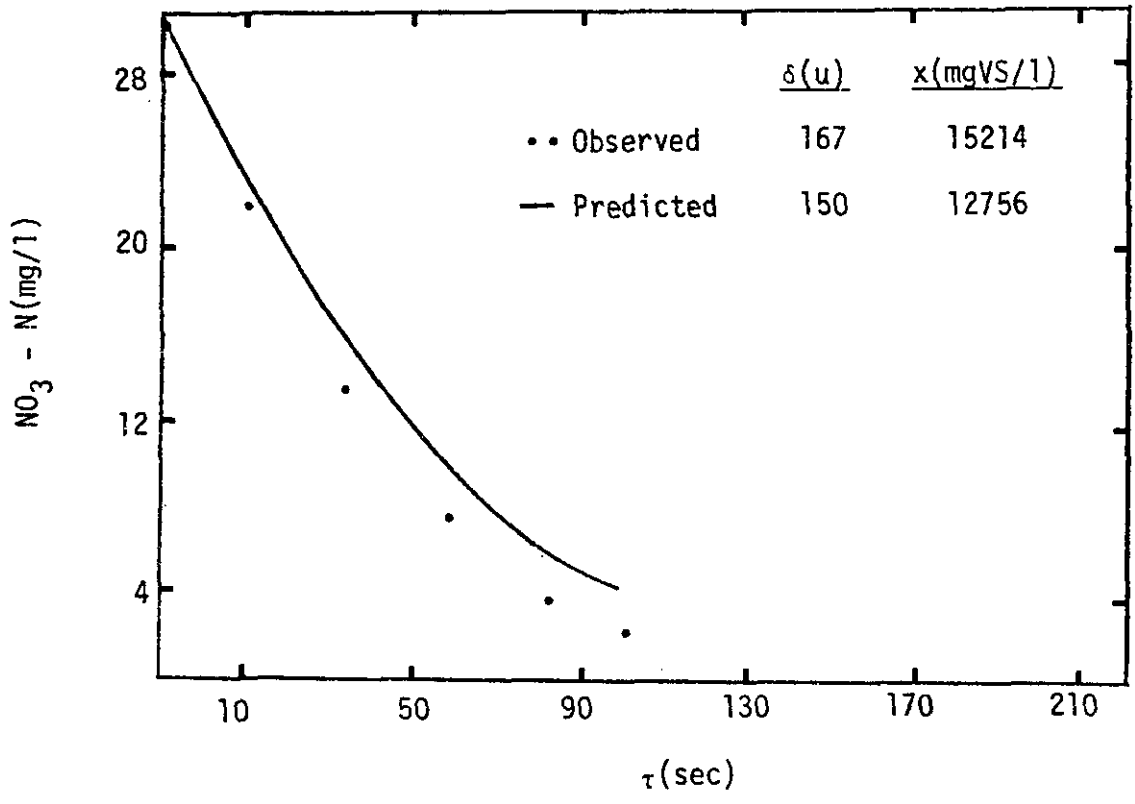
δ(u)
x(mgVS/1)
•• Observed
167
15214
— Predicted
150
12756
28
20
12
4
NO_3 - N(mg/1)
10
50
90
130
170
210
τ(sec)

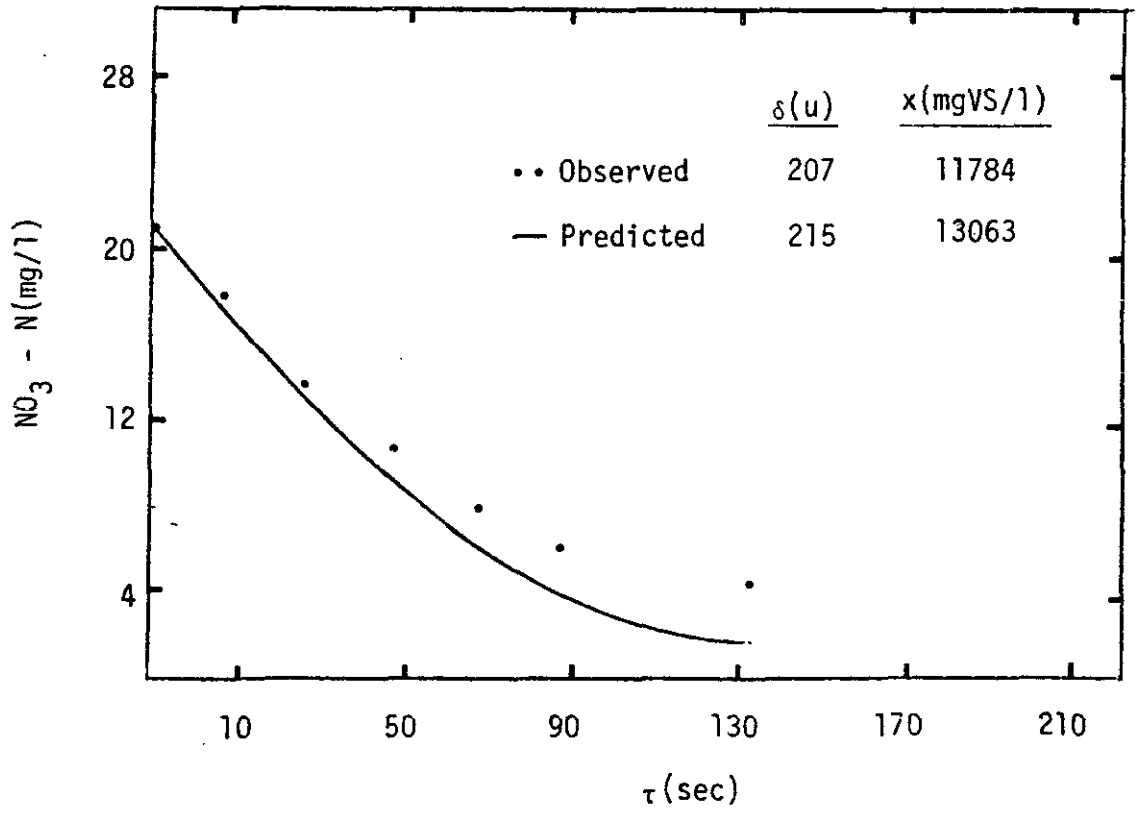
δ(u)
x(mgVS/1)
•• Observed
207
11784
— Predicted
215
13063
28
20
12
4
NO_3 - N(mg/1)
10
50
90
130
170
210
τ(sec)

Figure A2.

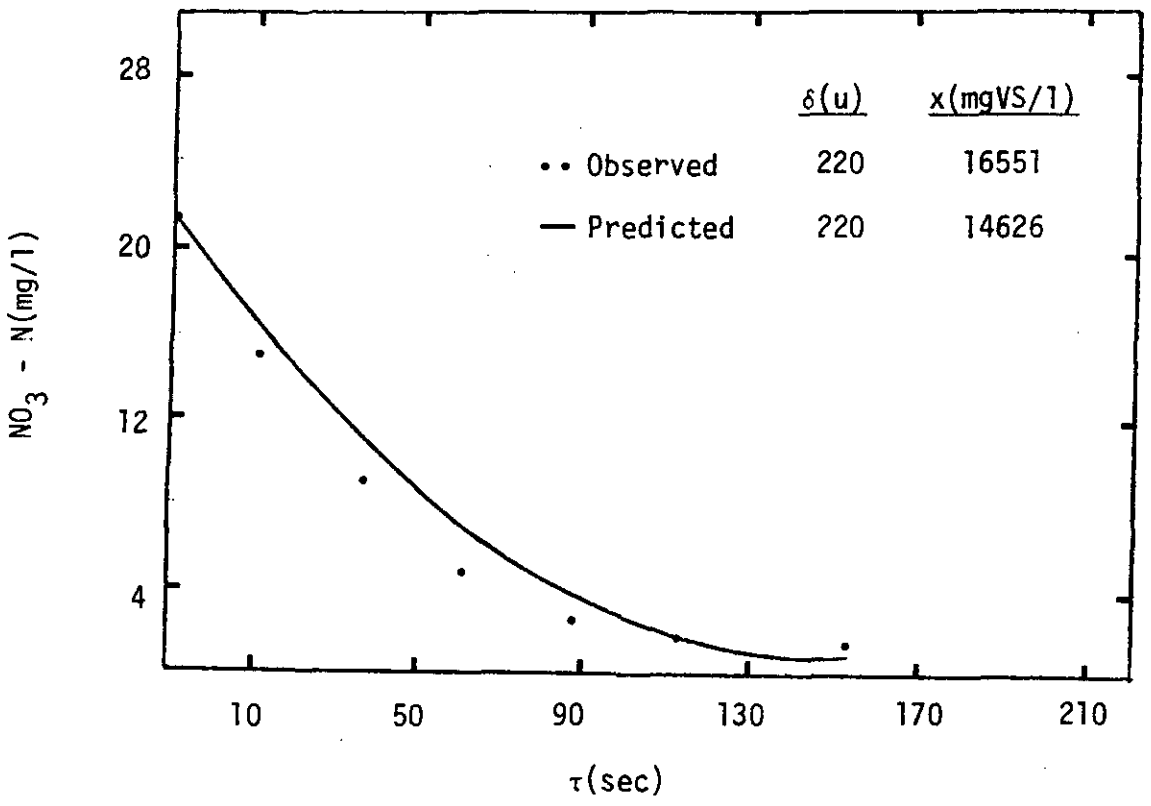
28
20
12
4
NO_3 - N(mg/l)
δ(u)
x(mgVS/l)
•• Observed
220
16551
— Predicted
220
14626
10
50
90
130
170
210
τ(sec)

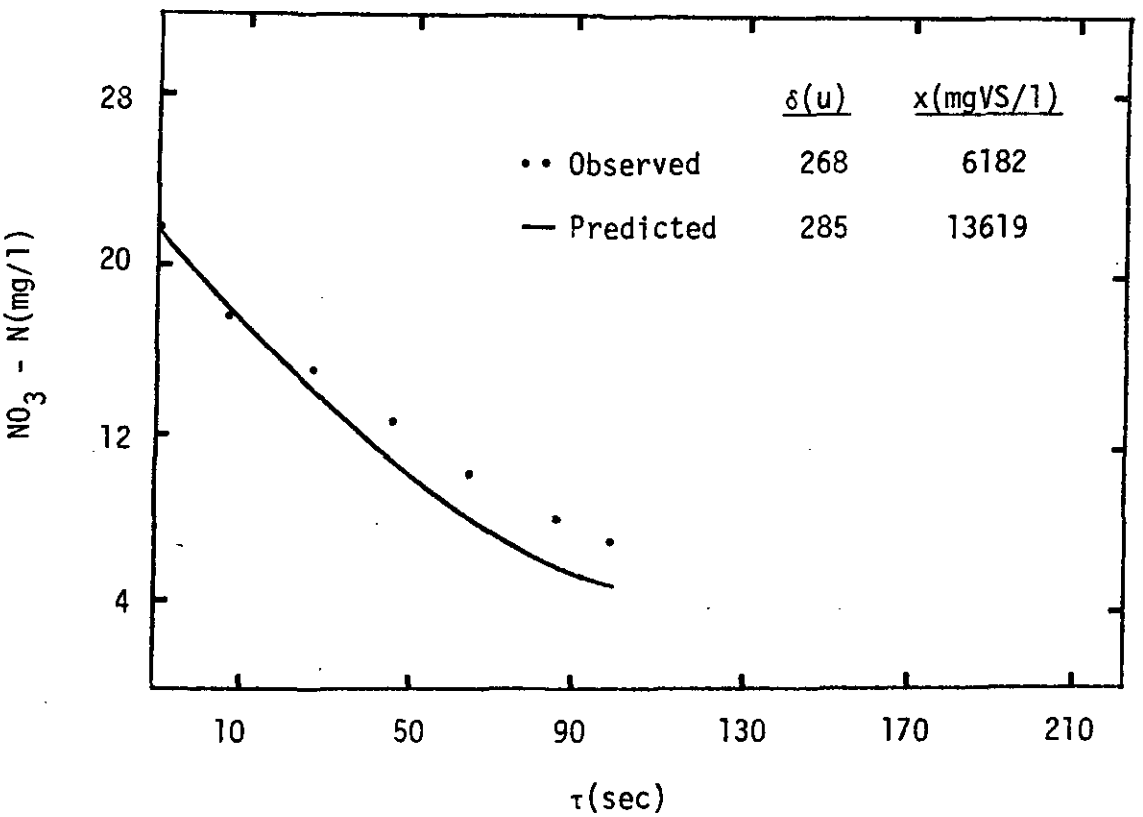
28
20
12
4
NO_3 - N(mg/l)
δ(u)
x(mgVS/l)
•• Observed
268
6182
— Predicted
285
13619
10
50
90
130
170
210
τ(sec)

Figure A3.

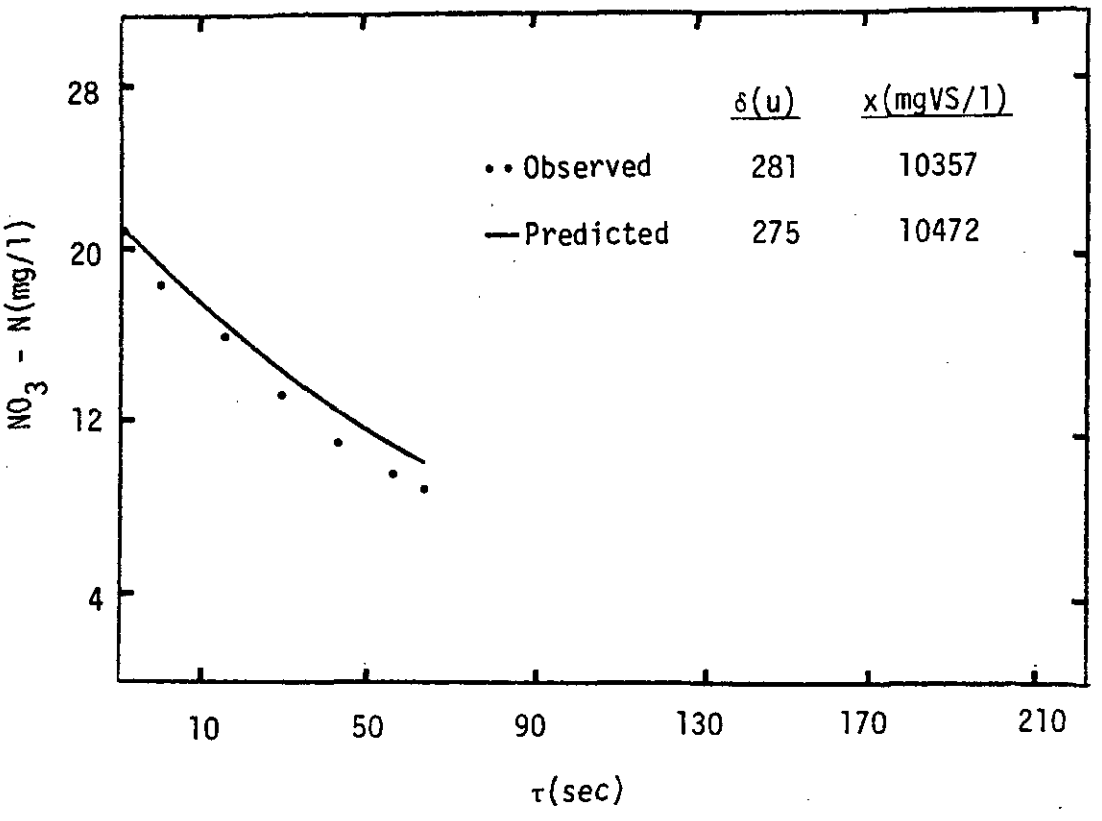
28
20
12
4
NO_3 - N(mg/l)
10
50
90
130
170
210
τ(sec)
δ(u)
x(mgVS/l)
•• Observed
281
10357
— Predicted
275
10472

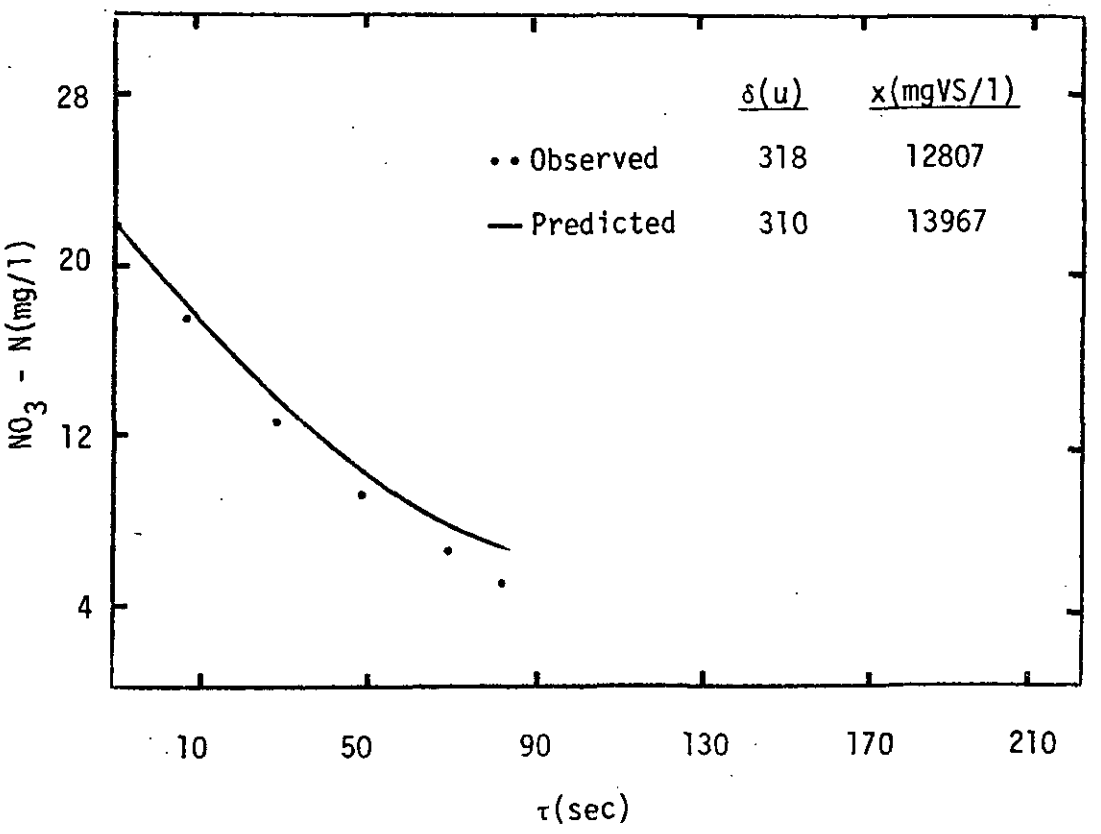
28
20
12
4
NO_3 - N(mg/l)
10
50
90
130
170
210
τ(sec)
δ(u)
x(mgVS/l)
•• Observed
318
12807
— Predicted
310
13967

Figure A4.

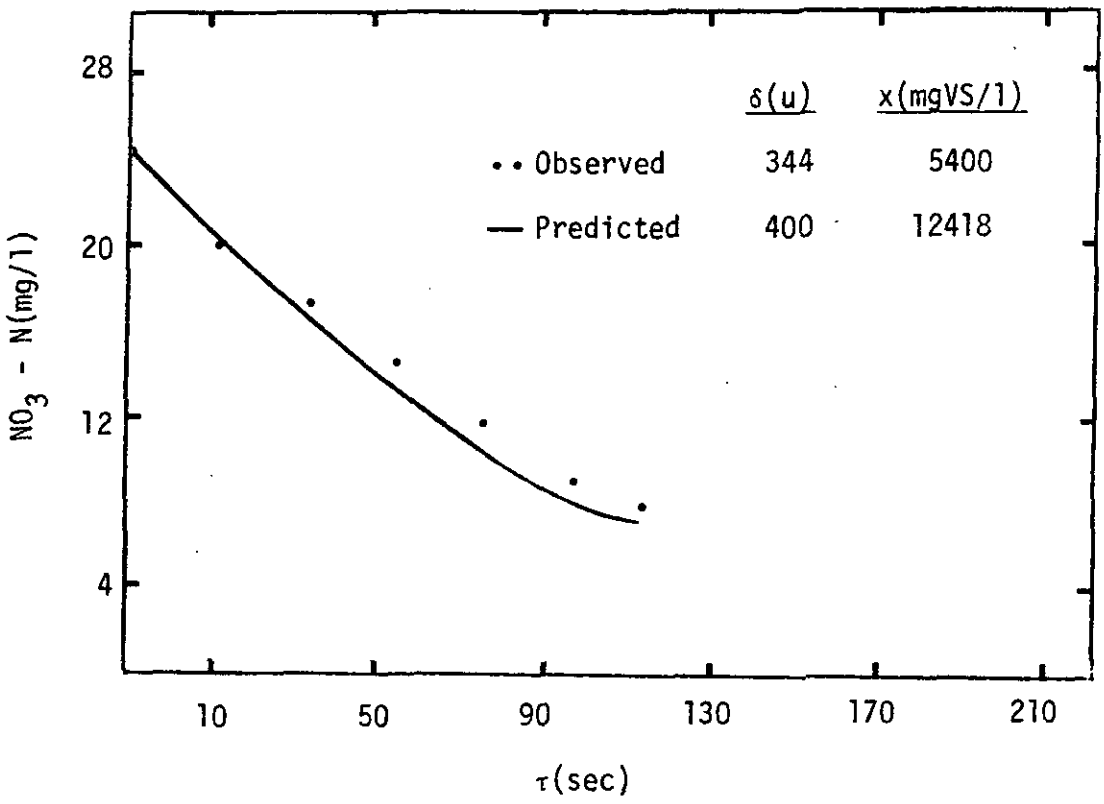
28
20
12
4
NO_3 - N(mg/l)
δ(u)
x(mgVS/l)
•• Observed
344
5400
— Predicted
400
12418
10
50
90
130
170
210
τ(sec)

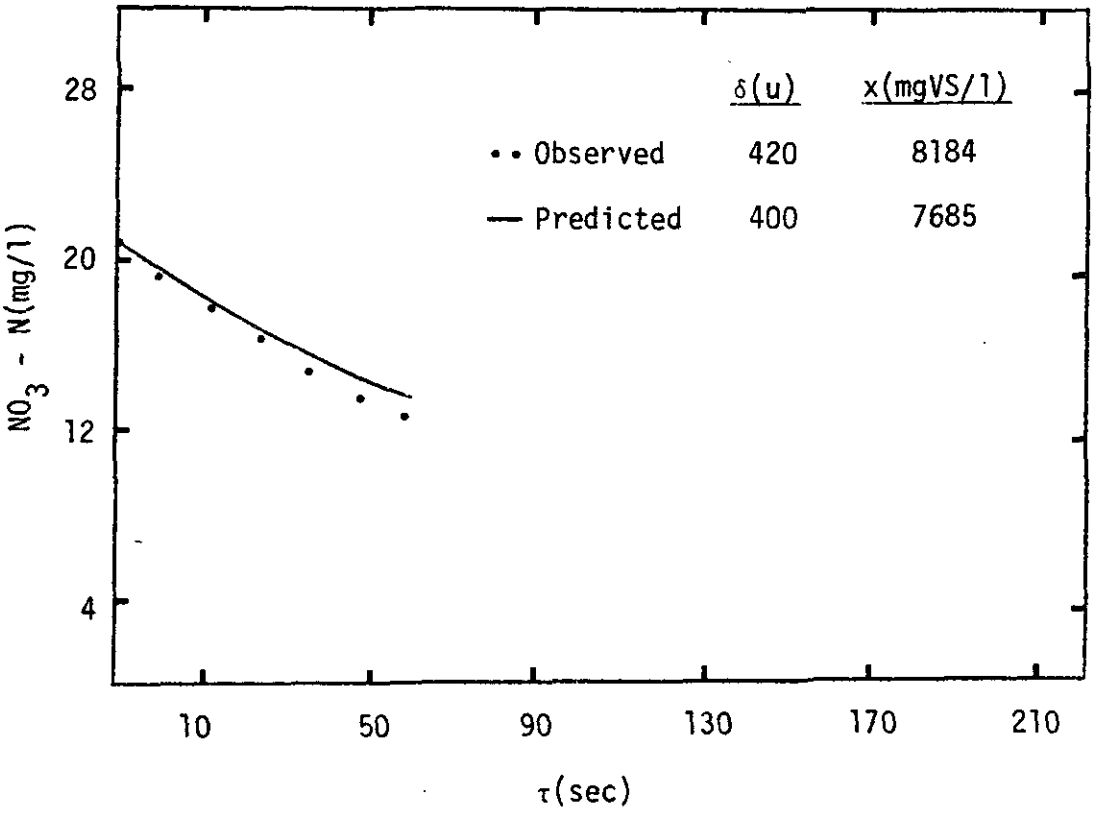
28
20
12
4
NO_3 - N(mg/l)
δ(u)
x(mgVS/l)
•• Observed
420
8184
— Predicted
400
7685
10
50
90
130
170
210
τ(sec)

Figure A5.

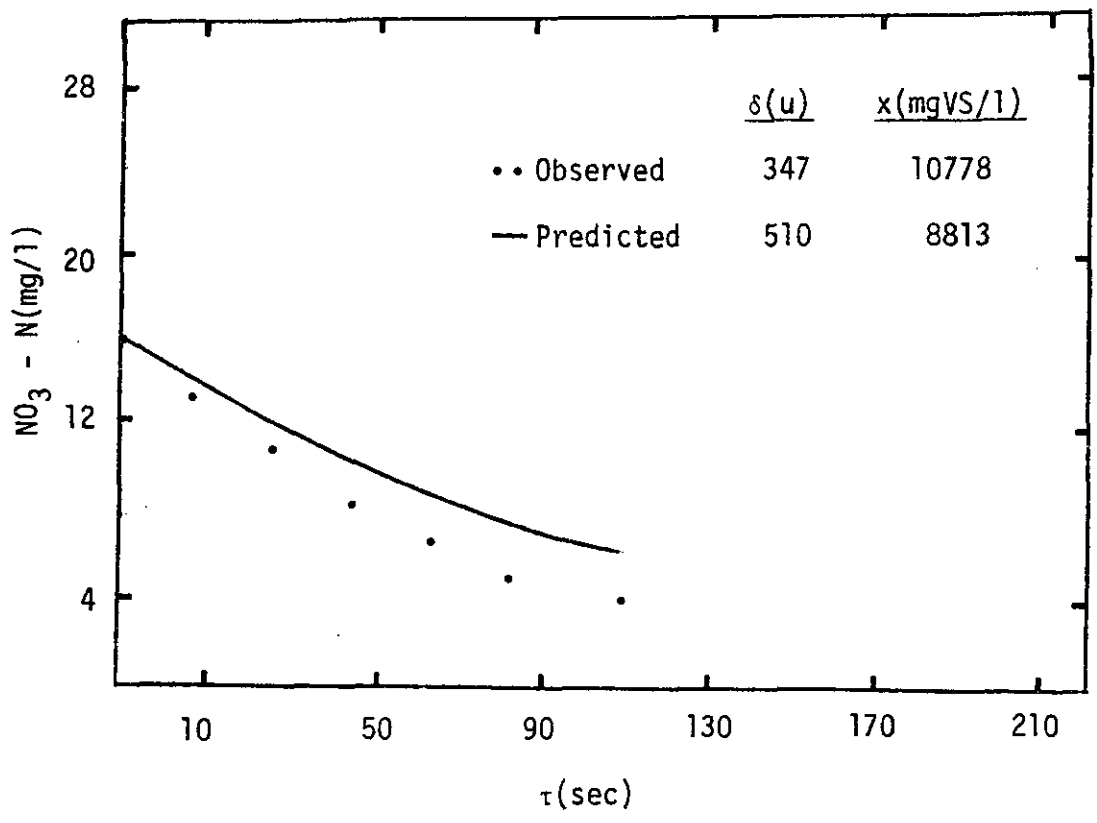
δ(u)
x(mgVS/l)
•• Observed 347 10778
— Predicted 510 8813
28
20
12
4
NO_3 - N(mg/l)
10
50
90
130
170
210
τ(sec)

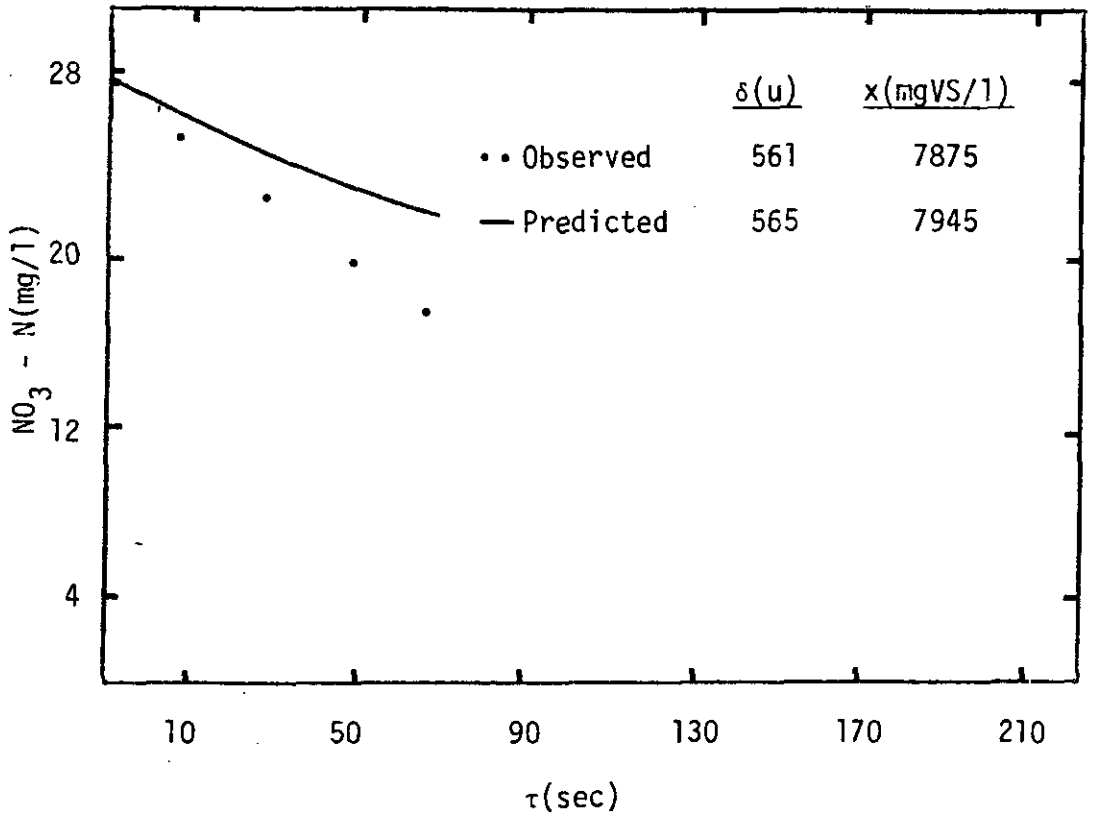
δ(u)
x(mgVS/l)
•• Observed 561 7875
— Predicted 565 7945
28
20
12
4
NO_3 - N(mg/l)
10
50
90
130
170
210
τ(sec)

Figure A6.

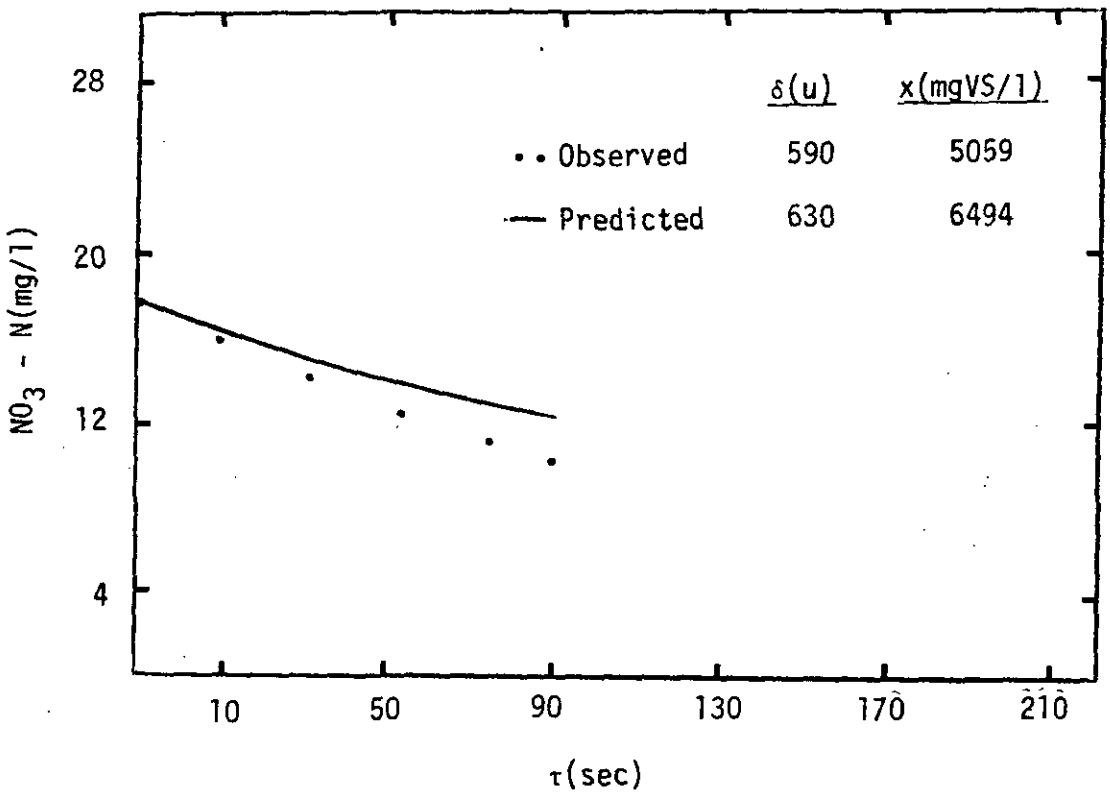
28
20
12
4
NO_3 - N(mg/l)
δ(u)
x(mgVS/l)
•• Observed
590
5059
— Predicted
630
6494
10
50
90
130
170
210
τ(sec)

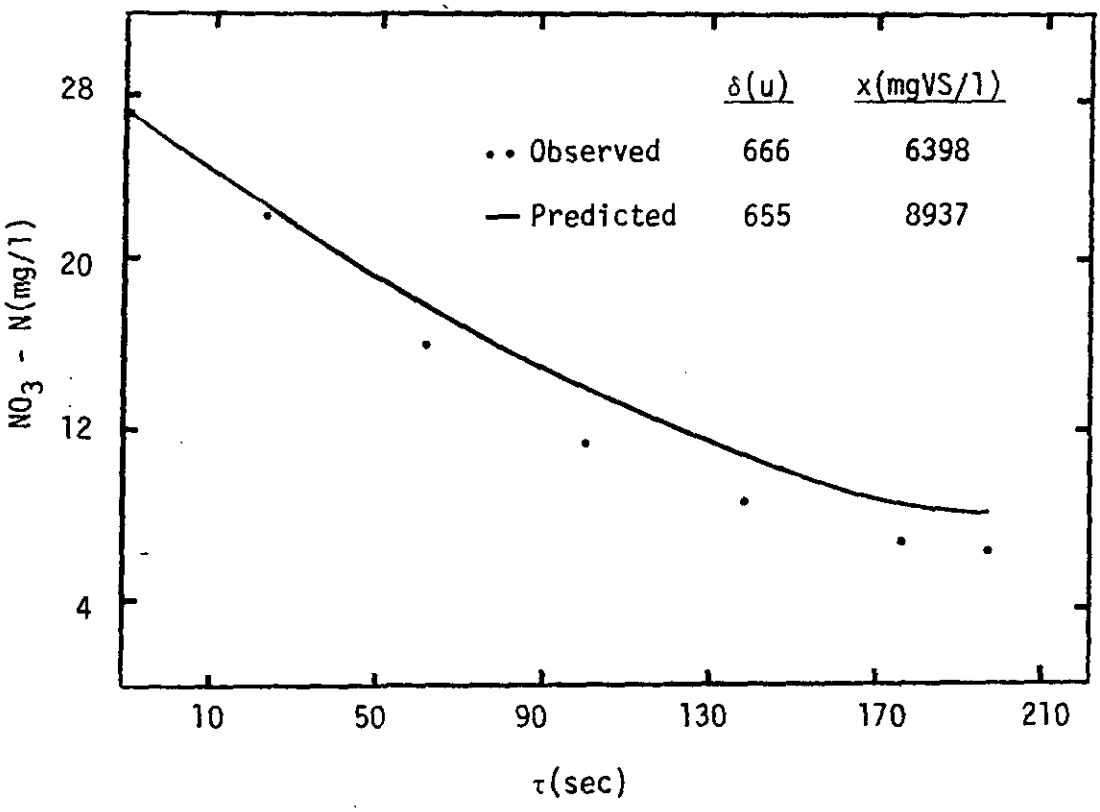
28
20
12
4
NO_3 - N(mg/l)
δ(u)
x(mgVS/l)
•• Observed
666
6398
— Predicted
655
8937
10
50
90
130
170
210
τ(sec)

Figure A7.

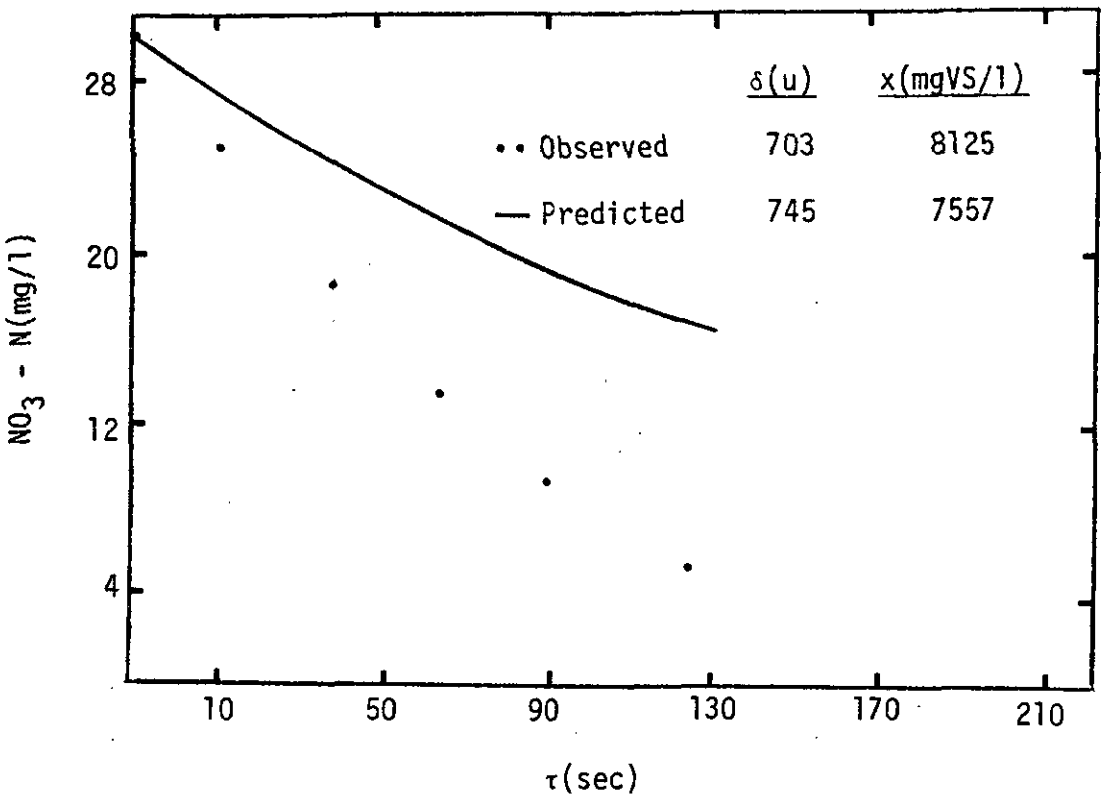
δ(u)
x(mgVS/1)
•• Observed 703 8125
— Predicted 745 7557
28
20
12
4
NO_3 - N(mg/1)
10
50
90
130
170
210
τ(sec)

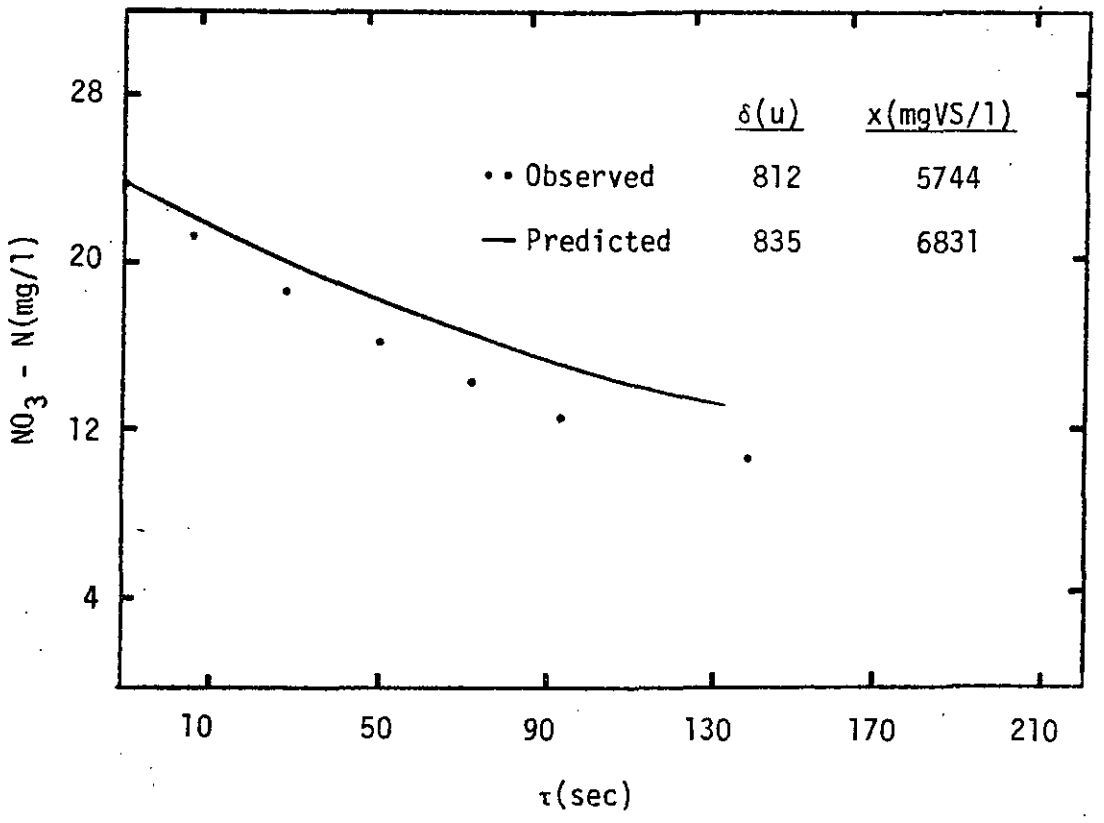
δ(u)
x(mgVS/1)
•• Observed 812 5744
— Predicted 835 6831
28
20
12
4
NO_3 - N(mg/1)
10
50
90
130
170
210
τ(sec)

Figure A8.

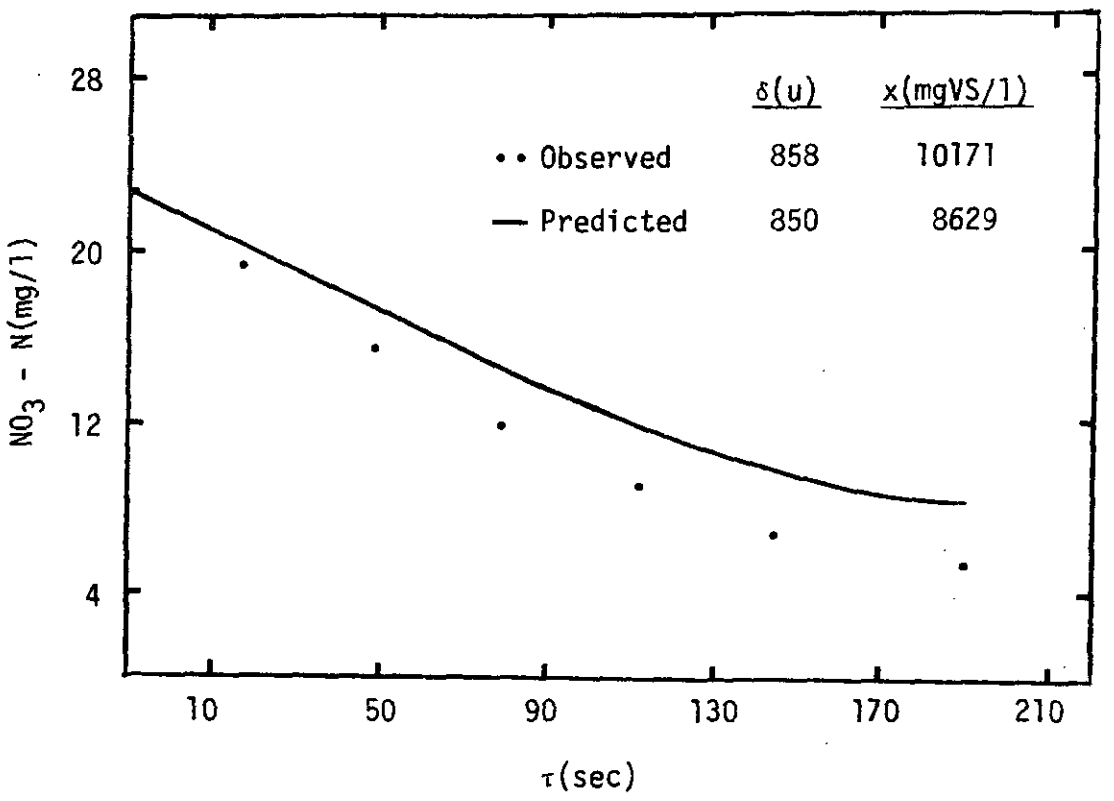
δ(u) x(mgVS/1)
•• Observed 858 10171
— Predicted 850 8629
28
20
12
4
NO_3 - N(mg/1)
10 50 90 130 170 210
τ(sec)

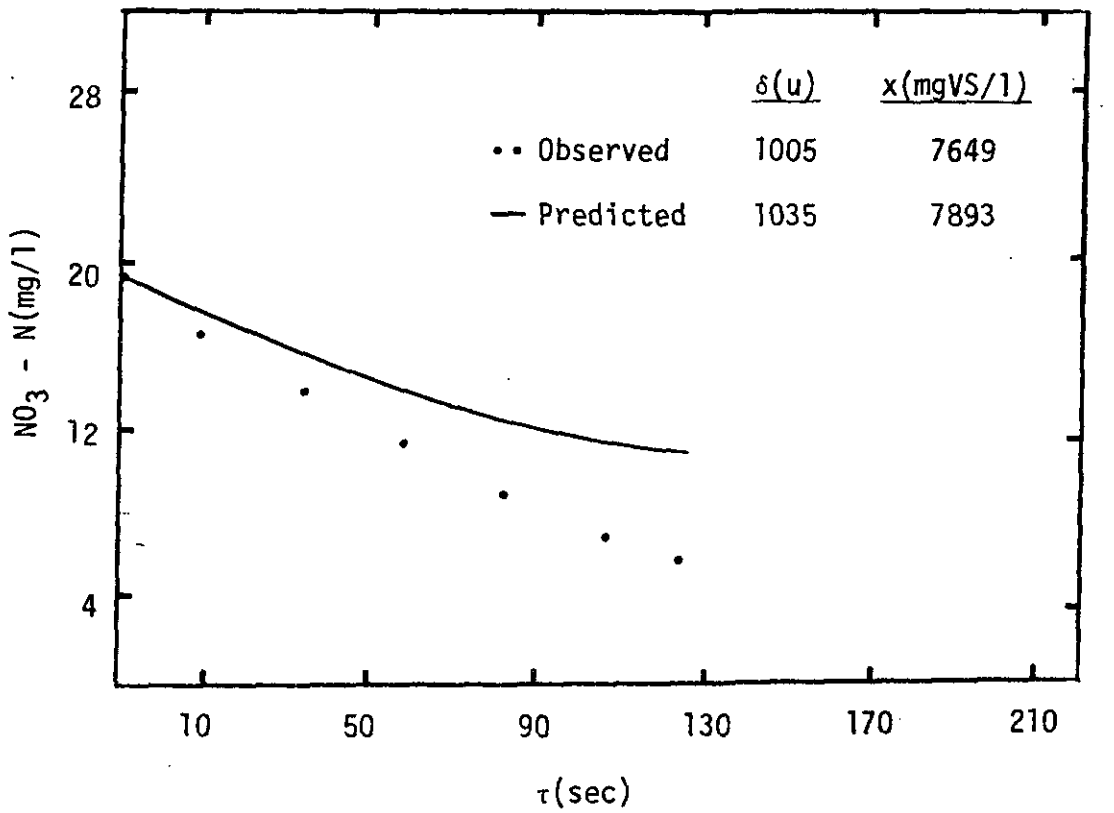
δ(u) x(mgVS/1)
•• Observed 1005 7649
— Predicted 1035 7893
28
20
12
4
NO_3 - N(mg/1)
10 50 90 130 170 210
τ(sec)

Figure A9.

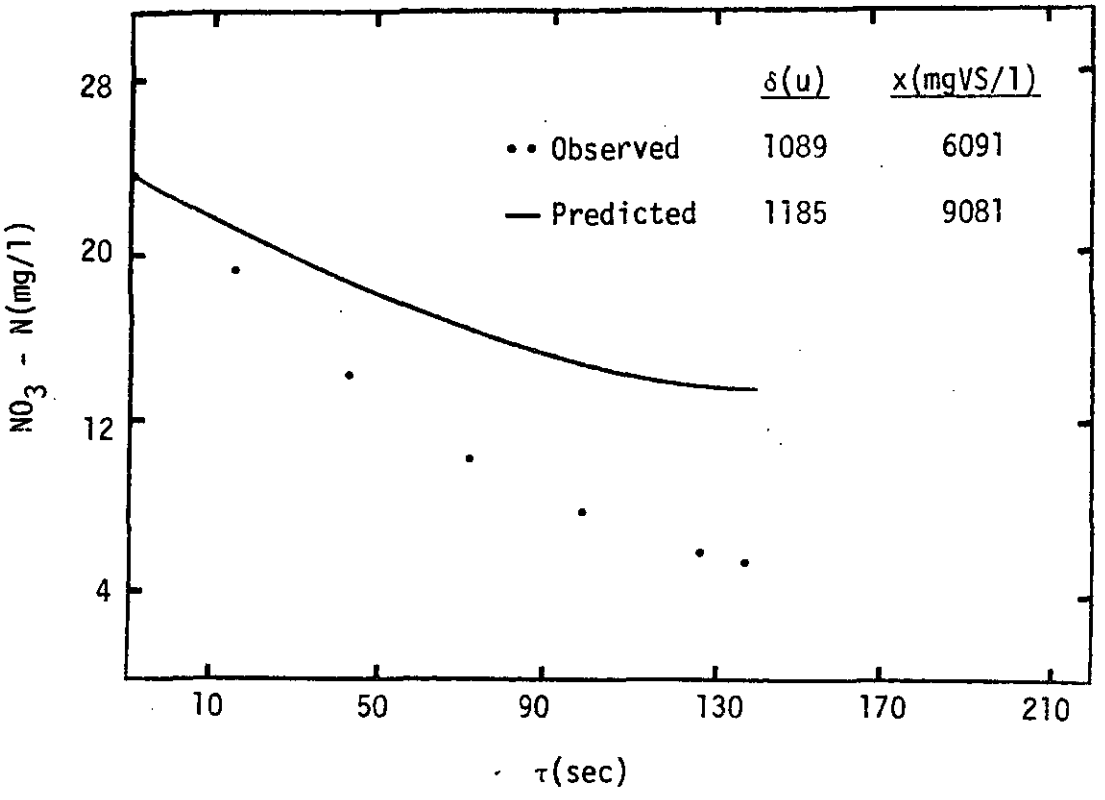
δ(u)
x(mgVS/1)
•• Observed 1089 6091
— Predicted 1185 9081
28
20
12
4
NO_3 - N(mg/1)
10
50
90
130
170
210
τ(sec)

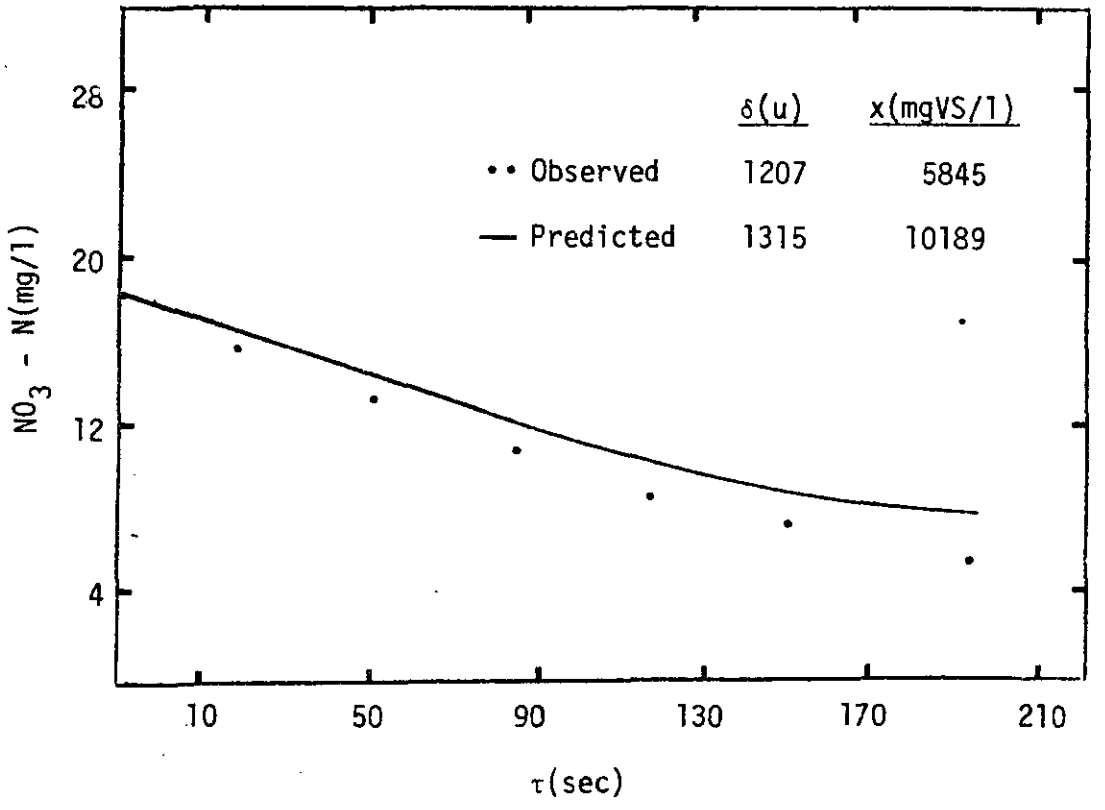
δ(u)
x(mgVS/1)
•• Observed 1207 5845
— Predicted 1315 10189
28
20
12
4
NO_3 - N(mg/1)
10
50
90
130
170
210
τ(sec)

Figure A10.